## [ur] DIMENSIONS

The Journal of Undergraduate Research in Natural Sciences and Mathematics

California State University, Fullerton



## 12th Edition

## [ur] DIMENSIONS

The Journal of Undergraduate Research in Natural Sciences and Mathematics

California State University, Fullerton

Spring 2010

## Marks of a CSUF Graduate from the College of Natural Sciences and Mathematics

## GRADUATES FROM THE COLLEGE OF NATURAL SCIENCES AND MATHEMATICS:

Understand the basic concepts and principles of science and mathematics.

Are experienced in working collectively and collaboratively to solve problems.

Communicate both orally and in writing with clarity, precision and confidence.

Are adept at using computers to do word processing, prepare spreadsheets and graphs, and use presentation software.

Possess skills in information retrieval using library resources and the Internet.

Have extensive laboratory/workshop/field experience where they utilize the scientific method to ask questions, formulate hypotheses, design experiments, conduct experiments, and analyze data.

Appreciate diverse cultures as a result of working side by side with many people in collaborative efforts in the classroom, laboratory and on research projects.

In many instances have had the opportunity to work individually with faculty in conducting research and independent projects. In addition to the attributes of all NSM students, these students generate original data and contribute to the research knowledge base.

Have had the opportunity to work with very modern, sophisticated equipment including advanced computer hardware and software.

**DIMENSIONS:** The Journal of Undergraduate Research in Natural Sciences and Mathematics is an official publication of California State University, Fullerton. Dimensions is published annually by CSUF, 800 N. St. College Blvd., Fullerton, CA 92834. Copyright ©2010 CSUF. Except as otherwise provided, Dimensions: The Journal of Undergraduate Research in Natural Sciences and Mathemaics grants permission for material in this publication to be copied for use by non-profit educational institutions for scholarly or instructional purposes only, provided that 1) copies are distributed at or below cost, 2) the author and Dimensions are identified, and 3) proper notice of the copyright appears on each copy. If the author retains the copyright, permission to copy must be attained directly from the author.

**About the cover:** Black is a seemingly forgettable tinge. In print media, however, ebony is a combination of cyan, magenta, yellow and key. These four colors can coalesce in various mixtures to create a range of colors. The cover of this journal is esteemed by the bright colors that make up black, as well as black itself. A beaker holds the liquid colors molded into an assortment of symbols that represent the math and science present within this journal. Traveling along the beaker's side, the sloshing liquid plunges into a sea of color where math and science is rampant and overflowing. Among the brilliant flush of color is an undercurrent of black bringing to light the idea that the effort put into the journal is often overlooked. Nonetheless, the labor exerted by authors, editors and scientists alike is there and recognized just as ebony is always distinguished as an individual color.

**BIOLOGICAL SCIENCES** 

Biographies

Investigation of class I integron presence and subsequent variable region characterization of 15 clinical isolates from Buenos Aires, Argentina By: Jun Kim and Jeffrey Mercado	5
Infulence of Anthropogenic Noise on Song Syructure in <i>Calypte</i> Hummingbirds By: <b>Sarah English</b>	10
The Effects of Thermal Stress on Filtration Rates of Non-native <i>Crassostrea gigas</i> and Native Ostrea lurida Oysters  By: <b>Patricia Gonzalez</b>	e 22
Characterization of <i>Thermotoga maritima</i> ADP-Glucose Pyrophosphorylase glgC2 K26A Altered Protein By: <b>Sang Lee</b>	29
Exploring the Relationship Between the California Chemistry Diagnostic Test (CCDT) and American Chemical Society (ACS) Course Final Exam and Course Grade  By: <b>Liz Michicoff</b>	39
A New Identification Method For The Tephra Layers Of The Wilson Creek Formation Using Geochemical And Statistical Methods By: <b>Nathan Diaz</b>	52
Minor and Trace Element Glass Composition of late Pleistocene Tephra Layers from the Wilson Creek Formation, Mono Lake, California, by Using Instrumental Neutron Activation By: <b>Daniel Lee</b>	59 1
Probable Discovery of a New Uranium Mineral, Consolidated Tungsten Mine Skarn, Tulare County, California By: <b>Shayda Nikjoo</b>	e 70
A Re-sampling Approach for the Comparison of Two Random Curves with an Application in Neuronal Data Analysis By: <b>Suzette Puente</b>	80
Relations Involving the Fibonacci Numbers By: <b>Jairo Aguayo</b>	87
On <i>k</i> th roots in the Symmetric Inverse Monoid* By: <b>Troy Cannon, Carlos Hernandez, and Luis Torres</b>	103
Relay Coverage Studies for the International Lunar Network By: <b>Lynette Zamora</b>	117

130

## Acknowledgements

Executive Editor

Amber Shah

Editors

Ernesto Casillas, Biology
Julie Yang, Chemistry/Biochemistry
Jade Brush, Geology
Carol Kempiak, Mathematics

Advisor

**Dr. Rochelle Woods**, Assistant Dean for Student Affairs

Graphic Design

**Brian Bouskill**, Layout Editor **Sean Ngo**, Cover Designer

Graphic Design Advisor **Arnold Holland**,

Associate Professor

College of the Arts

**Dr. Joseph H. Arnold, Jr.**, Dean **Andi Sims**, Assistant Dean for Student Affairs

College of Natural Sciences and Mathematics

Dr. Steven Murray, Dean

Dr. Mark Filowitz, Associate Dean

**Dr. Robert Koch**, Chair Department of Biological Science

**Dr. Maria Linder**, Chair Department of Chemistry/Biochemistry

**Dr. David Bowman**, Chair Department of Geological Sciences

**Dr. Paul De Land**, Chair Department of Mathematics

**Dr. James M. Feagin**, Chair Department of Physics

Special Thanks To

**President Milton A. Gordon** and **Dean Steven Murray** for their support and dedication to Dimensions.

## Investigation of class I integron presence and subsequent variable region characterization of 15 clinical isolates from Buenos Aires, Argentina

JUN KIM1, JEFFREY MERCADO1, DANIELA CENTRONa

Department of Microbiology, Parasitology, and Immunology, School of Medicine, University of Buenos Aires, Buenos Aires, Argentina.

1J.K. and J.M. both contributed equally to this work

**ABSTRACT** - In recent years the prevalence of multi- resistant clinical bacteria has been a cause of great concern to hospitals all across the world. Past literature suggests the investigation of integron structures should lead to a greater understanding of the epidemiological patterns associated with the decreased antibiotic susceptibility of clinical bacteria. Hence, this study analyzed the presence of class I integrons and their variable regions in 15 clinical isolates from Buenos Aires using PCR amplification and NCBI Blast sequence matching. Of the 15 isolates of various Enterobacteriaceae, 60% were positive for the class I integron. We received 38 previously cultured isolates that were then sequenced and analyzed, 26% contained a segment encoding for the aac(6')-lb and the 21% of occurrence for the aadA1 gene cassette. Several studies have concluded that integron bearing isolates have a significant association with multi-resistance, and this conclusion is supported by these findings.

**INTRODUCTION** - In recent years the prevalence of multi- resistant bacteria has been a cause of great concern to hospitals all across the world. Bacterial infections account for the greater part of secondary medical complications experienced by patients while under hospital care. Since the development and introduction of penicillin, antibiotics have been the primary weapon against the threat of bacterial infections. Selective pressures exerted on bacteria via the progressive use of antibiotics have led to the evolution of novel mechanisms, in addition to two other existing mechanisms, for the acquisition of genes conferring resistance to antibiotics; specifically resistance to aminoglycosides, trimethoprim, chloramphenicol, and beta-lactams [3]. The

integron and gene cassettes are a recombination system that is present on plasmids and transposons, allowing for horizontal and lateral dissemination of many antibiotic resistance genes amongst bacterial species [4]. This mechanism consists of a site-specific integrase enzyme encoded by the int1 gene, an adjacent attl site of recombination and a common promoter region, Pant, is used to express inserted gene cassettes in the integron structure. The gene cassettes can exist in two forms: free covalently closed circular molecules or, inserted in the integron structure as linear molecules. Gene cassettes contain an ORF and a recombination site designated attC site (or 59 base elements) containing imperfect inverted repeats with two 7bp core regions, the core site (GTTRRRY) and the reversed core site (RYYY-AAC) [2, 4, 5]. The promoter region is essential for the expression of integrated genes within cassette structures because most gene cassettes lack their own promoter region [4, 5].

Hence, gene cassettes involved in this system are quite successful at disseminating. The integrases' ability to mediate recombination is an essential component for dissemination. The integrase mediated recombination in the form of excision or integration of gene cassettes can occur between variable site interactions, either attC/attC or attl/attl or attl/attC, increasing the probability of recombination occurrences [3]. This genetic platform for site-specific recombination was discovered in the 1980's when the sequencing of antibiotic resistant genes revealed identical flanking sequences, indicating same site cassette insertion on a common molecular structure [3].

Later this genetic platform consisting of a 5' conserved segment, encompassing the int1 gene, attl site, and a promoter region Pant, along with a 3' conserved segment, inclusive of a gacEΔ1 antiseptic resistance gene, a sul1 sulphonamide resistance gene, and a orf5 open reading frame of unknown function, was designated as "integron" by Stokes and Hall in 1989 [3, 4]. Currently, many classes of integrons across different regions of the world have been identified with the class I integron as the most commonly occurring throughout the bacterial kingdom [5]. Recent studies are focusing on measuring frequencies of class 1, 2, and 3 integrons and their components –specifically, the mobile elements known as gene cassettes – for the purpose of understanding their epidemiology [4].

In this study we examined 15 strains of different bacterial species for the presence of int1 gene. This was accomplished by using PCR with primers which specifically recognized the int1 sequence. Upon verification of int1 gene presence, PCR was again used to identify the existing gene cassettes and determine the orientation of these gene cassettes held within the variable region of the integron structure [5]. In addition, a chart of resistance gene cassette primers constructed from sequencing data for selected strains were used as tools to guide the process of variable region characterization.

**RESULTS** - Sequence analysis for gene cassette frequency to guide variable region characterization. In total, 38 sequences were edited via BioEdit software and identified using NCBI Blast software. Out of the 38 sequences, 26% contained a segment of nucleotides encoding for the aac(6')-lb protein, which reduces susceptibility to kanamycin, amikacin, and tobramicin (Table 1). Other cassettes such as aadA1 encoding for the aad(3") protein which reduces susceptibility to estreptomicin and espectinomicin had a 21% frequency of occurrence. The last cassette that appeared in significant frequency was the aadA2 cassette, which was detected in 11% of the 38 sequences charted. The majority of the 38 sequences were 800bp in length, and had moderate to good nucleotide certainty.

STRAIN	GENES
Klebsiella pneumonia	aac(6´)-lb
Klebsiella pneumonia	aac(6´)-lb
Klebsiella pneumonia	aacC1 and aacCA1
Acinetobacter baumannii	aad1
Eromonas salmonicida	aadA
Aeromonas salmonicida	aadA
Acinetobacter baumannii	aadA1
Uncultured bacterium plasmid pSp7	aadA1
Eschericia coli	aadA2
Salmonella enerica	aadA2
Salmonella enteric	aadA2
Escheichia coli	aadB and aadA2
Arcanobacterium pyogenes	aadB, aadA1, cm1a6
Klebsiella pneumonia	bla OXA-48
Klebsiella peumoniae	catB3
Aeromonas sobria	catB3 and dfrB4
Klebsiella pneumonia	intl1
Klebsiella pneuomoniae	intl1 and aac(6´)´lb
Acientobacter baumanni	intl1 and aac(6´)′lb
Acientobacter baumanni	intl1 and aac(6´)′lb
Acinetobacter baumannii	intl1 and aac(6´)-lb
Acinetobacter baumannii	intl1 and aac(6´)-lb
Salmonella enteric	intl1 and aac(6´)-lb
Salmonella enteric	intl1 and aac(6´)-lb
Acinetobacter baumannii	intl1 and aacC1
Vibrio cholera	intl1 and aadA1
Vibrio cholera	intl1 and aadA1
Pesudomonas aeruginosa	intl1 and aadA6
Pseudomonas aeruginosa	intl1 and aadA6
Pseudomonas aeruginosa	intl1 and aadA6 and attl
Klebsiella oxytoca	intl1 and blaVIM-2
Acinetobacter baumannii	intl1 and org11 and aac(6´)-lb
Enterobacter aerogenes	oxa9
Klebsiella pneumonia	streptomycin 3´´ adenylytransferase
Pseudomonas aeruginosa	vlvim-2 and aac(6')-lb

Table 1. List of Genes contained within identified strains through Sequence Analysis

PRIMERS	SEQUENCES (5' TO 3')	SOURCE
Sulpro	gcc tga cga tgc gtg ga	Le´vesque et al, 1995
3´CS	aag cag act tga cct ga	Le´vesque et al, 1995
aac(6′) R	gtg ttc gct cga atg cc	Ramírez et al
aac(6′) F	gaa gaa gca cgc ccg ac	Ramírez et al
TniR	ttc agc cgc ata aat gga g	Ramírez et al

Table 2. PCR Primer Pairs

STRAIN	int1		PRIMER	PAIR	
(Strain no.)	(+/-)	(Sulpro / 3´CS)	(Sulpro / aac(6)´1b-r)	(aac(6)'1b-f / 3´CS)	(Sulpro / tnic-r)
E709	(+)	2kb	1kb	1,5kb	0kb
CF706	(+)	2kb	1kb	2,5kb / 1,5kb	0kb
CF704	(+)	2kb	0kb	Χ	0kb
E707	(+)	2kb	0kb	Χ	0kb
E706	(+)	2kb	0kb	Χ	0kb
PAC717	(+)	2kb	0kb	X	0kb
E1008	(+)	0kb	0kb	0kb	0kb
E708	(+)	0kb	0kb	2,5kb	0kb
K506	(+)	0kb	0kb	0kb	0kb
K508	(-)	X	Χ	X	X
K507	(-)	Χ	Χ	Χ	X
E1009	(-)	X	Χ	X	X
E710	(-)	X	Χ	X	X
CF705	(-)	Χ	Χ	X	X
E711	(-)	Χ	X	Χ	X

**TABLE 3**. PCR amplification products. X, absent

# **Integron detection and variable region characterization.** Of the 15 strains of various Enterobacteriaceae isolates, 60% were positive for the integron structure. PCR for primers of the inti1 gene revealed one amplicon of 1000bp and an additional 1400bp segment on one out of 9 integronpositive isolates [1]. In addition, PCR with primers Sulpro and 3'CS showed 6 segments approximately of 1600 to 2000bp in length. Amongst these 6 positives amplicons, there were two strains of C. freundii, 3 strains of other E. cloacae. Of these 6 iso-

lates, 2 segments of 1000bp were shown by a PCR with primers Sulpro and aac(6)'-lb. Only one of the three isolates giving no product with primers Sulpro and 3' CS gave a product with the aac(6')-lbf and 3'CS primer set. In contrast, the 2 positive isolates from the Sulpro and aac(6')-lb primer set showed various segment lengths with the aac(6')-lbf and 3'CS primer set. The specific segment lengths were 1500bp, 2500bp, and 1500bp respectively (Table 3). The attempt to identify a possible linkage to transposon Tn402 in these isolates was unsuccess

ful. The 9 integron-positive isolates were all negative when using the Sulpro and TnicR primer set.

**DISCUSSION** - Continued investigation into variable region characterization of class 1 integron structures is necessary in building the existing knowledge of gene cassette frequencies. Such information is a vital part in determining overall epidemiological patterns of dissemination. Recent studies have shown that bacterial isolates of gram-negative integron-positive strains have an alarmingly high probability of multi-drug resistant capabilities [1]. Unfortunately, in contrast to the 6 integron-negative isolates, 33% had susceptibility profiles that showed multiple resistances to antibiotics and only 22% of integron-positive isolates showed multi-resistance susceptibility profiles. Due to the small sample size for this experiment we were unable to accurately represent the general population of bacterial species. However, this study was only an investigation into the process of variable region characterization commonly performed to understand epidemiological patterns of distribution amongst other reasons. Despite reports of low gene expression within cassette structures, the rate of expression leading to reduced antibiotic susceptibility is concerning [5]. Ideally, discovering the underlying geographic epidemiological patterns of distribution is the ultimate goal. This information will be essential for constructing a system of preventive measures designed to mitigate the ongoing development of potentially fatal strains of bacteria.

The integron structure is the most recent mechanism to be discovered and thus there is still much to be explained.

Currently there is no explanation as to the origin of gene cassettes. What is known is that they exist as free circular structures or as linear structures within a plasmid or transpose [3]. Although this study does not explore the origin of gene cassettes, it outlines the basic process by which new cassettes are classified. Since the integration of gene cassettes are site-specific (i.e. confined to the variable region) detection of these cassettes can be accomplished with a high degree of accuracy. Full characterization of the variable region within integron-positive

strains was not explored in this study. The time limitation restricted how far in the characterization process this study would cover.

## **METHODS AND MATERIALS**

**Bacterial Strains and Plasmids.** Clinical bacteria from three different hospitals were collected in Buenos Aires, Argentina, in 2008. The 15 strains included *Enterobacter cloacae* (E707, E711, E709, E1009, E1008, E708, E710, E706), *Citrobacter freundii* (CF704, CF705, CF706), *Klebsiella pneumonia* (K506, K507, K508), and pAC717 were used for this study.

**Growth Conditions.** Clinical Isolates were cultured on Mueller-Hinton Agar medium plates at 37°C with low humidity.

**Sequences Analysis.** A total of 38 clinical isolates from pervious clinical samples were sequenced through BioEdit, and analyzed using NCBI Blast software program. The genes found in the clinical isolates assisted in the selection of primers (Table 1).

**DNA Extraction.** Resistant bacteria were grown in 3-5 ml of LB Broth overnight at 37°C, 200rpm. The next day, 3ml of culture were centrifuged at 6000 rpm at room temperature for 5 min. Then, the supernatant was removed and the pellet once resuspended in 500µl of 0.1XSSC Buffer was centrifuged at 6000 rpm for 5 minutes. Supernatant was again removed and the pellet was resuspended in 500µl of lysis buffer (10mM tris-HCL [pH 8], 2.5 mg/ml of lizozime) and 0.1mg/ml of RNAsa A. Incubation occurred at 37° C for 60 min. Next, 500µl of phenol: chlorophorm at a 1:1 ratio was added and tubes were centrifuged (4,000 rpm) at room temperature for 10 min. Supernatant was removed and placed into new tubes with the addition of 50µl of 3M sodium acetate [pH 4.8], 1ml of 100% ethanol, and mixed by inverting tubes, then centrifuged at room temp for 20 min at max speed (14000rpm). Tubes were left open for 30 min to allow ethanol to evaporate and then pellet was resuspended in 200µl of sterile water. Aliquots of 100µl of each sample at 10ng/µl concentration were prepared for PCR use.

## **Quantifying DNA extracted using Spectro- photometer.** A 1/100 dilution of each sample DNA extract was prepared by adding 5µl of DNA to 495µl of water. Each dilution was analyzed using a Spectrophotometer. Final concentration of each sample of DNA extract was calculated using absorption and ratio values provide by the Spectrophotometer.

**PCR amplification.** PCR amplification occurred via 25.03μl volumes containing 13μl of sterile water, 5μl of buffer (1X (1.5mM MgCl2)2), .75μl of each primer stock solution (0.1–1.0μM), .4μl of dNTPs (0.2mM each dNTP), .13μl of taq polymerase ((5u/μl)), and 5μl of template DNA (<0.5μg/50μl). The thermocycler was set to: 1-94°C 5min, 2-94°C 1min, 3-52°C for 30secs, 4-72°C for 1 to 5min depending on the fragment size, 5- repeat steps 2 to 4 30 times, 6-72°C 5 to 10min depending on the fragment's size, and 7-14°C forever.

**Gel Electrophoresis.** Amplified product of each sample underwent electrophoresis at 109 V for 40 min on a 1% agarose gel prepared with 10µl of ethidium bromide (5mg/1ml) using TBE buffer.

### **REFERENCES**

- 1. P. Martinez-Freijo, et al. (1998) Class I integrons in Gram-negative isolates from different European hospitals and association with degreesed susceptibility to multiple outlibility to multiple outlibility to multiple
- ciation with decreased susceptibility to multiple antibiotic compounds. Journal of Antimicrobial Cemotherapy. 42, 689-696.
- 2. L. Poirel, et al. (2001) Characterization of Class 1 Integrons from Pseudomonas aeruginosa

That Contain the blaVIM-2 Carbapenem-Hydrolyzing b-Lactamase Gene and of Two Novel Aminoglycoside Resistance Gene Cassettes. Antimicrobial Agents and Chemotherapy, 45, 546-552.

- 3. Recchia, G. D., Hall, R. M. (1995) Gene cassettes: a new class of mobile element. Microbiology, 141, 3015-3027.
- 4. Chang, C. Y., Chang, L. L., Chang, Y. H., Lee, T. M., Chang, S. F. (2000) Characterization of drug resistance gene cassettes associated with class 1 integrons in clinical isolates of Escherichia coli from Taiwan, ROC. J. Med. Microbiol. 49, 1097-1102.

ACKNOWLEDGMENTS - This work was supported by LA Basin Minority Health and Health Disparities International Research Training Program (MHIRT) 5T37MD001368-13 (National Center on Minority Health and Health Disparities, National Institutes of Health). We thank Marcelo Tolmasky, Daniela Centron, and Paula Aquiro for many discussions and the School of Medicine at University of Buenos Aires for the use of their instrumentations.

## Infulence of Anthropogenic Noise on Song Syructure in Calypte Hummingbirds

## SARAH ENGLISH & DR. ANNE HOUTMAN

Department of Biological Science, College of Natural Science and Mathematics, California State University Fullerton, 800 N State College Boulevard Fullerton, CA 92831-3599

**ABSTRACT** - Anthropogenic noise (noise pollution) may affect how hummingbirds use song for mate attraction and territory defense. My study focuses on the structure of Anna's Hummingbird (Calypte anna) complex song and Costa's Hummingbird (Calypte costae) simple song in areas of contrasting noise levels. Recordings were collected in Anza Borrego State Park in Imperial County, CA and at Boyd Deep Canyon Research Station in Riverside County, CA during the Spring of 2007 and 2008. Recordings of Calypte hummingbirds found in these areas were analyzed for structural and temporal changes in amplitude, frequency, syllable and bout duration, and complexity, and these measures were compared between natural and high anthropogenic noise levels. It was predicted that Anna's Hummingbirds would sing shorter syllables and longer, less complex bouts and that Costa's Hummingbird would sing longer syllables and shorter bouts. However, it was found that Anna's Hummingbirds sang with a higher peak frequency, slightly louder amplitude, and slightly longer A syllables and Costa's Hummingbirds sang louder amplitude songs in high noise conditions. It was unexpected that Calypte hummingbirds would respond to anthropogenic noise in the same way as passerines. Hummingbirds have high metabolic demands and the frequency of the loudest parts of their song is already higher than the frequency of the loudest parts of anthropogenic noise, so it was not seemingly necessary for them to sing louder or higher frequency. This similar behavior between songbirds and non-songbirds could aid in the understanding of the function of song in all birds that use song for mate attraction and territory defense similar to hummingbirds.

in anthropogenic noise, for example, from traffic, power lines, air conditioners, construction and maintenance, or residential noise. Increasing noise may be a problem for animals that depend on acoustic communication for survival and reproduction.

There are well-documented effects of noise on many animal populations across many species such decreased reproductive success and exposure to predators. Southern California has one of the highest rates of urbanization in the United States and anthropogenic noise may have a significant effect on wildlife as the state's population continues to grow (Wood and Yezerinac, 2006). For example, the Lark Sparrow in California has lower species diversity and decreased breeding density along highways (Slabbekoorn and Ripmeester, 2008). Habitat fragmentation may also increase species' exposure to noise (USDT-FHA, 2006).

Sources of noise can be natural or anthropogenic. Natural noise would include sounds like running water, air passing over vegetation, rain, or other animals vocally communicating. Anthropogenic noises include things like cars, lawn mowers, construction, and other noises from residential areas (Brumm, 2004a, Brumm and Slabbekoorn, 1965).

Hummingbirds may have specific challenges with increasing sources of anthropogenic noise because of metabolic restrictions and the existing characteristics of their song. Anna's Hummingbird BMR is 67% higher than was expected compared to other

songbirds, so they don't have as much energy to spare on activities like unnecessary singing and physical activity (Weathers and Stiles, 1988). It has been found that canaries sing more when they are in good body condition and after feeding (Ward et al., 2003). Hummingbirds must spend a considerable amount of time feeding in order to keep their metabolism working properly. They can't spend more energy devoting more time to singing in loud environments because it could decrease their body condition and lead to health and reproduction success problems. Generally, only male hummingbirds sing for the purposes of territory and resource protection or mate attraction, but singing is energetically costly for any songbird. Time spent singing is also less time spent doing other things like feeding and patrolling territory (Ward et al., 2003).

The functions of song have been well documented in passerines, but less is known about the structure and function of song in hummingbirds. Both male Anna's Hummingbirds (Calypte anna) and Costa's Hummingbirds (Calypte costae) use dive displays unique to each species to attract females (Slabbekoorn and Smith, 2002a), which is another source of precious energy being devoted to reproductive fitness. If competition with noise is high when Calypte hummingbirds are trying to sing, then competition among males is increased.

Anna's Hummingbirds and Costa's Hummingbirds males sing in the breeding season from approximately January to July. Calypte males hold territories and protect them by perching, singing, chasing, and diving. The frequency of hummingbird song is significantly higher than songbirds and their song is also quieter. It does not have as much volume (which translates into amplitude) as the songs of passerines, which sing within the lower frequency range of most ambient noise. Neighbors can sneak onto a male's territory for food or mating if the protecting male can't hear or see them. In noisy conditions, it is much easier for neighbors to sneak onto other territories and more difficult for each male to hold a territory without intruders.

Anna's Hummingbirds (Calypte anna) can be found year-round in southern California, in a broad range of habitats from coastal regions to deserts. They are prevalent in residential and remote wild areas in the region and are well known for visiting and defending artificial feeders. Anna's Hummingbird males exhibit a complex song type consisting of three syllables (Baptista and Schuchmann, 1989; Baptista and Matsui, 1979; Steen and Houtman, 2006) (Figure 1a). These syllables are referred to as A, B, and C. There is a general pattern to male Anna's Hummingbird song: ABCC, though it does vary occasionally depending on the individual, and this entire pattern is often repeated a number of times in a bout. The A syllable has four elements, the B syllable has two elements, and the C syllable has one element, and each of these elements also varies in duration between individuals based on the frequency of the loudest part of the syllable and the duration of each individual syllable. Males either sing all A songs or more complex songs of mixed A, B, and C syllables. A-only songs are referred to as simple songs, as compared to complex mixed songs.



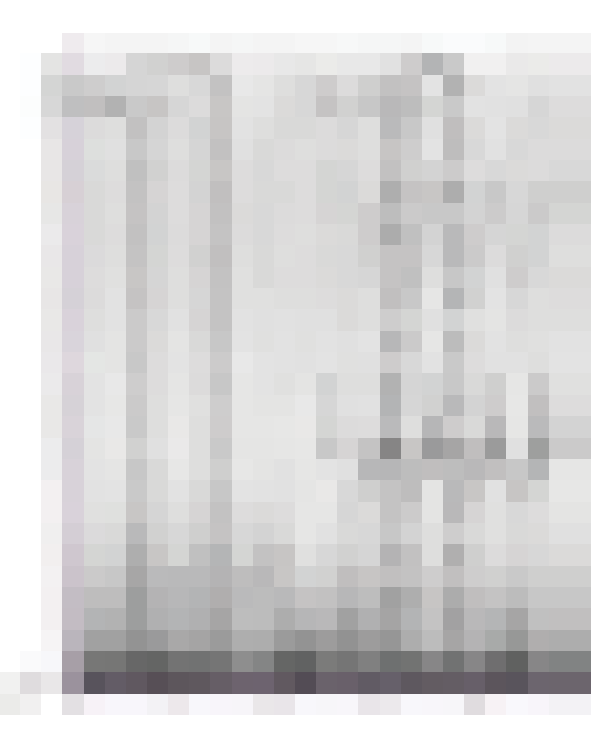
**Figure 1a**. Spectrogram showing Anna's Hummingbird song with background and individual A, B, and C syllables outlined.

It is believed that complex songs are more costly to produce than simple song types because muscular function and brain function are of higher demand (Garamszegi et al., 2006). Anna's Hummingbird song generally has a minimum frequency of approximately 2kHz and a maximum frequency of approximately 2kHz, and the loudest part of Anna's Hummingbird song is generally around 11kHz (Steen and Houtman, 2006) (Figure 1b).

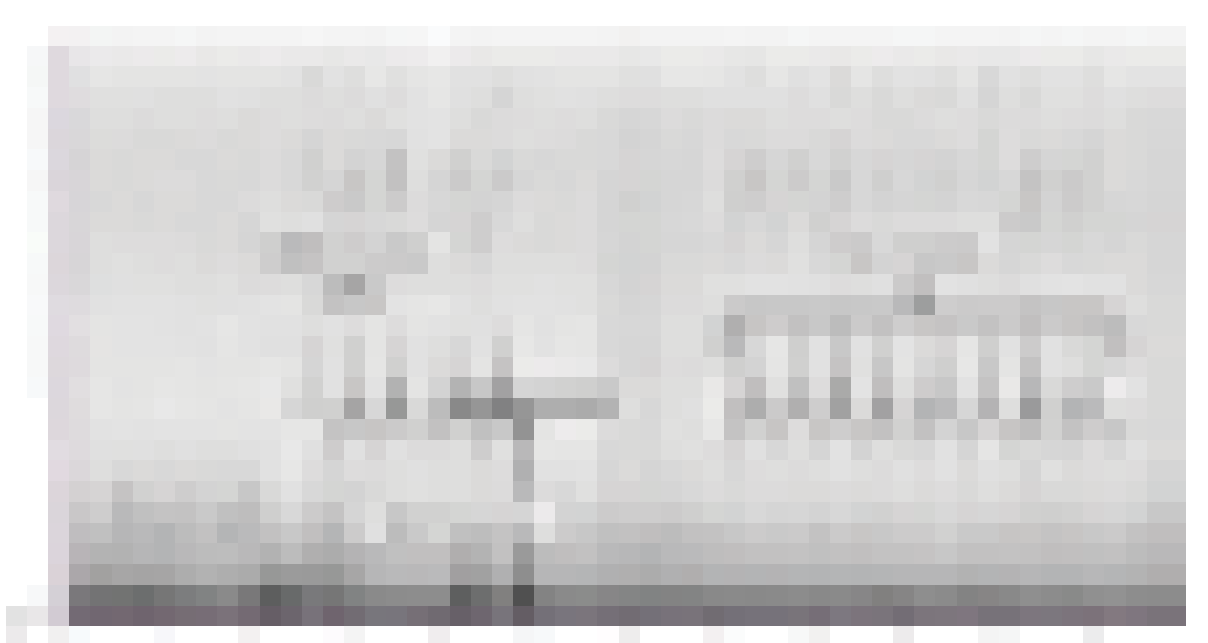


Figure 1b. Spectrogram showing Anna's Hummingbird song with syllable and bout duration defined and an example of peak frequency measurement.

Costa's Hummingbird (Calypte costae) also prefers southern California desert habitats, and often migrates to higher elevations in the winter, so they are harder to find year-round. They are usually assumed to be less aggressive than Anna's Hummingbird in relation to establishing territories and protecting artificial feeders, but they use the same methods of perching, singing, chasing, and diving for mate attraction and territory defense. Costa's Hummingbird males exhibit a simple song consisting of only one syllable type that can be repeated any number of times in a bout (Figure 2a). Each syllable is referred to as a song and there are four elements within each song. Costa's Hummingbird song has a minimum frequency of approximately 7kHz and a maximum frequency of approximately 12kHz, and the loudest part of their song is higher than Anna's Hummingbird at 11kHz (Williams and Houtman, 2008) (Figure 2b).



**Figure 2a.** Spectrogram showing Costa's Humming-bird song with background and a single syllablev



**Figure 2b.** Spectrogram showing Costa's Hummingbird song with syllable and bout duration defined and an example of peak frequency measurement.

The frequency of anthropogenic noise is generally below 4kHz and is loudest below 2kHz (Wood and Yezerinac, 2006; Slabbekoorn, 2004; Brumm and Slater, 2006). The loudest part of hummingbird song is above this 4kHz threshold for both these Calypte species. Studies of passerines (a group of true songbirds) have shown that this group alters the frequency of the loudest part of their song to be above this 4kHz threshold, though the lowest parts of passerine song can be at a low frequency that does interfere with anthropogenic noise. When song interferes with other sources of noise, there is less propogation of the song's sound and there is the potential invasion of territory from other males or less effective attraction of females to the singing bird's territory. Keeping song inside a narrow bandwidth, or frequency range, may increase amplitude of the song and transmission distance of the signal (Slabbekoorn et al., 2002b) and could be something that hummingbirds, which are not true songbirds, may do in a similar noise situation.

Though these changes have been documented in songbirds, hummingbirds are not on the same clade as songbirds, but use song for similar purposes and live in the same environments (Gahr, 2000). Documenting how Calypte hummingbirds change their song in response to the same pressures is one of the major objectives of this study. Song learning evolved independently three times, splitting into

groups of songbirds, parrots, and hummingbirds, that all use song for the same basic functions, though the groups are not so closely related. Swifts are most closely related to hummingbirds, and they don't learn or exhibit complex song types (Gahr, 2000; Wood and Yezerinac, 2006). Like songbirds, Anna's Hummingbirds learn the syllable types, frequency, rhythm and syntax of their complex songs from parents and neighboring males, meaning that there is easily a geographical population shift of song characteristics.

Slabbekoorn's studies of Great Tits have shown that these songbirds raise the frequency of their song in the presence of ambient noise and sing shorter notes in high ambient noise conditions. This study paired urban and forest birds in many major cities across Europe and found that the urban birds in every pair sang with a higher minimum frequency and a shorter first note. The forest birds also consistently sang more song types and there was no shift in peak frequency or in maximum frequency in either location. It seems that in loud, urban areas, song types that are not likely to be heard by neighbors are dropped (Slabbekoorn and den Boer-Visser, 2006; Brumm, 2006).

Song Sparrows and chaffinches (Brumm and Slater, 2006; Slabbekoorn and Ripmeester, 2008; Patricelli and Blickley, 2006) also sing at higher minimum fre

quencies in high noise conditions and concentrate more energy in higher frequencies of the song's notes, and the rest of the song was consistent in energy. This suggests that these songbirds choose to sing song types that fit into the current noise conditions (Wood and Yezerinac, 2006).

Some birds do not necessarily shift their whole song to a higher minimum frequency. They instead sing less notes with lower frequencies, so overall their song is at a higher average frequency (Patricelli and Blickley, 2006). Zebra finches do regulate the amplitude of their song. They sing louder in response to playback of white noise, but the trade-off of higher amplitude could be a lower song rate (Cynx et al., 1998). House Finches sing at higher frequencies and adjust temporal characteristics of their song in noisy environments (Fernandez-Juricic et al., 2005; Slabbekoorn and Ripmeester, 2008; Patricelli and Blickley, 2006; Brumm and Slabbekoorn, 1965).

It is possible that hummingbirds are unable to alter their song in response to changes in noise levels, in which case anthropogenic noise could have a negative effect on hummingbirds' reproductive success. In order to be successful in a noisy environment, hummingbirds could avoid the noise by altering amplitude, frequency, or timing of their song to be in-between the loudest parts of ambient noise. The latter would not be reasonable in areas with constant noise, but would be advantageous in areas with intermittent noise, for example, next to a roadway. Rush hour traffic could be competing most

with birds in the morning and in the late afternoon. If Hummingbirds simply avoided noise by moving their territories, then other population dynamics like male-male interactions would change.

The Lombard effect has been documented in humans and other species like nightingales and the Blue-Throated Hummingbird (Pytte et al., 2002; Slabbekoorn and Ripmeester, 2008). The Lombard effect is a form of short-term regulation where the subject's message gets louder when they are in louder areas (Brumm and Todt, 2002). An example of this is how nightingales increase the amplitude of their song in high noise conditions (Brumm, 2004b; Brumm and Slabbekoorn, 1965). Male nightingales sing louder when around other males, and when in quiet spaces, sing more low frequency notes (Brumm, 2004a).

Species relying on vocal communication could use the Lombard effect to increase transmission distance of the signal, which is called a signal-to-noise ratio. Ambient noise interferes with the signal-to-noise ratio, (Slabbekoorn, 2004) and it has been found that zebra finches and nightingales seem to assess noise conditions and then transmit a signal. This regulation mechanism allows energy to be saved for more complex song, more repetition of one song type (Brumm and Slabbekoorn, 1965), or singing more often (Cynx et al., 1998; Brumm, 2004a; Brumm and Todt, 2002). It is unknown if hummingbirds have this regulation mechanism, but it is possible that they would sing either more often in quiet times, or louder in noisier times.

I predict that peak frequency will not change in high noise conditions in either Calypte species because both species have song that is above the frequency of the loudest parts of anthropogenic noise. I also predict no change in average amplitude of either species' song because of hummingbirds' high metabolic rates and strict energy demands. It does not seem that they would have the extra energy to expend in singing louder (Table 1).

	Summary of Predictions	
	Anna's Hummingbird	Costa's Hummingbird
	(Calypte anna)	(Calypte co <mark>stae)</mark>
Peak Frequency	No Change	No Change
Average Amplitude	No Change	No Change
Duration of syllable/song	Decrease (Shorter)	Increase (Longer)
Duration of bouts	Increase (Longer)	Decrease (Shorter)
Complexity	Decrease	N/A

**Table 1.** Summary of predictions for each measured song feature for both Calypte species.

I predict that Costa's Hummingbird will sing longer individual songs in the presence of noise in order for the sound to propagate further because the frequency of their song is fairly high relative to most other sounds and they are much quieter than other hummingbirds and songbirds. In contrast, I predict Anna's Hummingbirds will sing shorter individual syllables in the presence of noise because the loudest part of their song is closer to the frequency of anthropogenic noise, and shorter sounds will propagate farther.

I predict that Costa's Hummingbird bout durations will be shorter in high noise conditions because the individual syllables are longer and this limits how much energy can be devoted to song at one time. I expect Anna's Hummingbird song bouts to possibly be longer in noisy areas due to energy distribution. If Anna's Hummingbirds are singing shorter syllables, they can sing for longer amounts of time and at the same time increase or decrease the complexity of their song.

I predict that Anna's Hummingbird song complexity will decrease in the presence of anthropogenic noise. This means that they will sing more A-only songs and less songs of mixed syllables. I expect more simplicity because of the Lombard effect. Less complex noises travel through air better and will reach neighbors that are farther away.

My measures will focus on individual syllable/song duration and the duration of the entire song bout, as well as average amplitude and peak frequency in both species. I will also measure the complexity of Anna's Hummingbird song. Use of behavioral territory defense cues, such as dive displays will be documented, since hummingbirds could modify the timing of their song when anthropogenic noise levels are highest. Recordings of Anna's Hummingbird and Costa's Hummingbird songs will be analyzed for background noise levels and then correlated with each of these structural song features.

**METHODS** - **LOCATION** - Multiple species of hummingbirds are residents of southern California habitats, from desert to coastal regions. Anza Borrego State Park in Imperial and San Bernardino Counties and UC Riverside's Boyd Deep Canyon Research Station – Palm Desert in Riverside County, CA (Figure 3) are ideal locations to study the effects of anthropogenic noise on Anna's Hummingbirds and Costa's Hummingbirds because there are both constant and temporary noises, and there are also areas with no anthropogenic noise pollution. These are also areas in which both species are abundant during the breeding season. Recordings were taken during two breeding seasons - starting January 2007 and January 2008 and ending near June 1, 2007 and 2008.



**Figure 3.** Map schematic of locations where hummingbirds were recorded in both 2007 and 2008. The pins are locations where many recordings were taken, most of which were in The Springs at Borrego Golf Course and Palm Canyon Campground at Anza Borrego State Park, and College of the Desert and Boyd Deep Canyon Research Center at Palm Desert.

**RECORDING** - Anna's Hummingbirds and Costa's Hummingbirds have slightly different behaviors regarding singing, making it important to observe the birds long enough to find the perch from which they sing the most. As birds were found, their locations were mapped, and GPS coordinates and ambient temperature were recorded. Notes were taken about the perches from which each bird sang. Recording equipment was set up near the perch to record song a set distance from the perch for recordings with the possibility of an amplitude measurement.

To record song, a unidirectional Sennheiser K6/Me-64 was attached to a studio boom tripod, which could be adjusted to position the end of the microphone as close as possible to the perch without the disturbing the bird. The microphone was connected to and powered by a Marantz PMD660 digital recorder. The

microphone height and boom angle were adjusted to get within a meter of the perch if possible. The person operating the recorder sat at the bottom of the tripod out of view, so as to not discourage the bird from returning to the perch between song bouts.

Recording was complete when at least two full song bouts were recorded. Notes were taken of observations during singing, including whether the bird was facing the microphone, whether it was interrupted by another noise, whether it was chasing before it sang, and what sources of noise, like cars, were on the recording.

**SOUND ANALYSIS** - We analyzed the song of male Anna's Hummingbirds and Costa's Hummingbirds with Raven Pro 1.3 software, developed by Cornell University, to determine whether they alter song parameters (frequency, amplitude, duration, and complexity) in response to high anthropogenic noise conditions. Every recorded track was split into bouts for analysis. A bout is defined by at least five seconds of silence between each song (Steen and Houtman, 2006). The background noise sampled for each bout was the time from the beginning of the track to immediately before each bout began, up to the five seconds long. Every measurement included was between the frequencies of 2kHz and 24kHz because of restrictions of the microphone and reliability of the sound quality between these two frequencies.

Since all recordings were not taken with the exact same distance from the bird to the microphone, all amplitude measures were standardized to 1 meter. The actual amplitude measures from Raven were in microPascals, and with this transformation were converted to decibels and standardized across recordings so they could be compared. The measures could not be compared before the transformation because amplitude is a measure of loudness that takes into account the effect of propogation and sound degradation. Each measure was converted to decibels using the following formula: dB=20\*log(RMS) where RMS is the average amplitude measure including minimum and maximum amplitude values (Fernandez-Juricic et al., 2005).

RMS was reported as  $\mu$ Pascals in Raven, so the formula dB=20 $\mu$ Pa was also applied to each RMS measure to transform every measure into decibels (Brumm and Slater, 2006). Each decibel measure was then transformed to 1 meter distance with the following formula: L1m=20\*logd + Ld where the sound level at 1 meter equals 20 multiplied by the log of the distance d in meters plus the sound level recorded at d distance (Brumm, 2004b).

Measures of the average amplitude of background noise were split into categories of natural and high levels of anthropogenic noise. The levels were determined by measuring all collected recordings and then splitting the range in half. All bouts whose background average amplitude measured louder than the middle amplitude were considered high noise conditions, and all bouts whose average amplitude measured quieter than the middle amplitude were considered low noise conditions.

Measures of peak frequency, average amplitude (RMS), and duration of bouts and individual syllables were compared across noise conditions. Additionally, Anna's Hummingbird song complexity based on syllable types was measured and compared across noise conditions.

A Mann-Whitney U Test was performed for each feature, comparing natural and high noise conditions with a p-value less than 0.05 indicating significance. The birds were separated by species and breeding season, creating four sets of data.

To determine that five seconds is enough time to measure accurate background noise amplitude, standard noise recordings of only background noise were analyzed for amplitude and correlated with the background amplitudes measured from the song recordings. To get standard noise recordings, 1 minute of ambient noise was recorded in each of the four major directions (North, South, East, West) (Slabbekoorn, 2004) and five seconds of noise was randomly selected out of each recording. These selections were analyzed for RMS amplitude like the song recordings and the values had a positive correlation (R2=0.509).

To determine that my background RMS amplitude measures taken from Raven were accurate to real-time, I took recordings of Anna's Hummingbird and Costa's Hummingbird playbacks and compared them to actual sound pressure levels. I set up the microphone in the same manner that my field recordings were taken, set a speaker 1 meter away, and recorded playback, at the same time reading measures from a sound pressure meter at the same position as the microphone. I analyzed the RMS amplitude from Raven in the same manner as my field recordings and positively correlated them with the RMS amplitude recorded by the sound pressure meter (R2=0.507).

**RESULTS** - I found that Anna's Hummingbird males from the 2007 season do not change average amplitude, syllable duration, bout duration, or song complexity but do increase peak frequency in high noise conditions (Table 2). Anna's Hummingbird males from the 2008 season do not change duration of B or C syllables, peak frequency, bout duration, or complexity but do sing louder and sing longer A syllables.

	Song	A Syllable	B Syllable	C Syllable	Peak	Bout	Complexity
	Amplitude	Duration	Duration	Duration	Frequency	Duration	(value 0.0-
	(dB)	(sec)	(sec)	(sec)	(kHz)	(sec)	1.0)
2007 Anna's	p=0.09	p=0.14	p=0.32	p=0.30	*p=0.03	p=0.45	p=0.25
	n1=9	n1=9	n1=8	n1=8	n1=9	n1=8	n1=9
	n2=8	n2=8	n2=7	n2=8	n2=8	n2=7	n2=8
	u=50	u=47	u=32	u=37	u=56	u=29	u=43
	avg=68.55	avg=1.21	avg=1.02	avg=0.39	avg=9.81	avg=3.12	avg=0.74
	±1.31	±0.004	±0.01	±0.002	±0.55	±0.02	±0.02
2008 Anna's	*p=0.01	*p=0.01	p=0.12	p=0.12	p=0.16	p=0.50	p=0.07
	n1=5	n1=5	n1=4	n1=4	n1=5	n1=4	n1=5
	n2=5	n2=4	n2=4	n2=4	n2=4	n2=4	n2=4
	u=23	u=19	u=12	u=12	u=14	u=8	u=16
	avg=77.08	avg=1.29	avg=0.83	avg=0.40	avg=6.76	avg=8.70	avg=0.20
	±0.96	±0.03	±0.08	±0.003	±0.59	±0.81	±0.03
	Song	Song			Peak Fre-	<b>Bout Duration</b>	
	Amplitude	Duration			quency	(sec)	
	(dB)	(sec)			(kHz)	p=0.26	
2007 Costa's	p=0.24	p=0.08			p=0.42	n1=10	
	n1=11	n1=11			n1=11	n2=6	
	n2=6	n2=6			n2=6	u=36	
	u=40	u=47			u=35	avg=9.46	
	avg=61.52	avg=4.74			avg=10.04	±0.71	
	±1.47	±1.80			±0.31	p=0.36	
2008 Costa's	*p=0.001	p=0.08			p=0.18	n1=8	
	n1=8	n1=8			n1=8	n2=7	
	n2=7	n2=7			n2=7	u=31	
	u=54	u=40			u=36	avg=9.52	
	avg=67.37	avg=2.08			avg=9.53	±1.62	

**Table 2.** Summary of Mann-Whitney U-Test p-values and significance for each feature test of background against high noise conditions with average value for all conditions  $\pm$  standard error. \* = significant difference (p<0.05)

Costa's Hummingbird males from the 2007 season do not change average amplitude, peak frequency, or bout duration. They do seem to sing longer songs but without a significant p-value (p=0.07). Costa's Hummingbirds from the 2008 season do not change song duration, peak frequency, or bout duration but also do sing louder songs.

Background RMS amplitudes were measured between 56 decibels and 89 decibels with an average of approximately 65 decibels in the 2007 season and between 52 decibels and 83 decibels with an average of approximately 70 decibels in the 2008 season. Some studies suggest that natural noise conditions are background noise levels of 48-62 decibels (Pytte, et al., 2002). In 1997, California published data that suggests that most species are disturbed in some way as background noise levels reach 60 decibels (TransSafety, Inc., 1997). As investigation into noise pollution continues, the standard level of noise that disturbs animals becomes clearer.

**DISCUSSION** - Anna's Hummingbirds and Costa's Hummingbirds have much higher metabolic rates than passerines. Their metabolic processes are pushed to the extreme and they must operate at their maximum metabolic rate throughout the entire day. Their small size and high metabolism demand constant feeding and could limit the amount of energy they have to devote to song and dive displays. Passerines have the potential to sing louder and expend energy in order to be heard, but not being able to sing louder may force hummingbirds to find other ways to be heard by neighbors and defend their resources.

Anna's Hummingbirds do respond to high anthropogenic noise conditions in the same way as passerines. This result was unexpected for many reasons. First, it was not believed that hummingbirds had any necessity to sing higher pitched songs. Anna's Hummingbird song is fairly close to the loudest parts of anthropogenic noise, so moving it farther away may mean that sound propagates farther. They may also be saving energy by singing higher in pitch because they don't have to sing louder or longer to be heard.

Costa's Hummingbirds also respond to high noise

conditions in some of the same ways as passerines. In the 2007 season, they sang longer songs, which allows the sound to propagate farther. They sang louder songs in the 2008 season, which was not expected because of the already high frequency and metabolic restrictions. Also, Costa's Hummingbird song in general is not as loud as Anna's Hummingbird or passerine song in natural noise conditions.

Not being heard by neighbors means that males are less likely to be able to hold distinctive territories. In high noise conditions, males cannot maximize their territory size (Brumm, 2004b; Brumm and Slabbekoorn, 1965) and are likely to be involved in more male-male interactions because of male intrusion (Slabbekoorn and den Boer-Visser, 2006). Some of the major factors that urban birds, or birds in high noise conditions, face that could potentially have an impact on song characteristics and song propagation are light, heat, chemical exposure, non-native vegetation, and changes in diet (Slabbekoorn and Ripmeester, 2008).

It has been speculated that the amplitude of ambient noise that disturbs songbirds' breeding biology is 60dB (James, 2006; TransSafety, Inc, 1997). A California construction project anticipated traffic diversions to temporarily increase background noise in a particular area by 3-4 decibels. This area was home to the endangered Least Bell's Vireo and because 60 decibels of noise is slowly becoming a standard level of disturbing noise, the project took other measures to decrease the noise in the detour area so as not to disturb the birds (TransSafety, Inc, 1997).

The possible consequence of raising the frequency of song too far is a reduction in mating success per male (Slabbekoorn, 2004). By raising frequency, they are seemingly heard by farther neighbors, but females must be able to hear the higher frequency song in order for males to have successful matings. Females still have to be able to hear chick calls and dive displays (Brumm and Slabbekoorn, 1965), which are in the range of 6-8kHz. This may interfere with some background anthropogenic noise, and males that sing at higher frequencies may be perceived as less aggressive (Patricelli and Blickley, 2006).

It is unknown exactly what frequencies hummingbirds hear and respond to. It is quite obvious that they hear in the 4-10kHz range, but whether they can hear above 24kHz, which is the highest frequency response of a studio-quality microphone is also unknown. Another possible factor is how low in frequency hummingbirds can hear. This is also unknown and if song changes in high noise conditions for territory defense, then ambient noise could be less of a factor in changing song features. Just like humans, there are limits to what frequencies hummingbirds can hear and if some of the humancreated noise in the low frequencies is not heard, then they may not be affected as significantly as if they could hear a wide range of frequencies (Pytte, 2002).

Speciation is possible if females discriminate against certain song types or characteristics (Patricelli and Blickley, 2006; Brumm and Slabbekoorn, 1965). This would in turn create reproductive isolation and decrease reproductive fitness of any single male, and would also increase male-male interactions. There would eventually be a population-level shift of song characteristics if juveniles hear song differently in high noise conditions because the noise would block and decrease the quality of learning song (Wood and Yezerinac, 2006; Slabbekoorn and Ripmeester, 2008). The effectiveness of young-age learning and genetic factors may also leave an impact on how much potential a bird has to use a regulation mechanism to make song characteristics favorable in high noise conditions (Brumm, 2006) and how aggressive a bird is in a male-male interaction (Brumm, 2004a). Male songbirds are more aggressive and more successful at holding a territory against a male with similar song (Slabbekoorn and Smith, 2002a).

There is a trade-off in singing louder. Higher amplitude of song could alert predators in the area, which if were done by juveniles that are not able to escape, would decrease the size of the population itself (Cynx et al., 1998; Slabbekoorn and Ripmeester, 2008). Singing louder could also mean that the song rate decreases (Fernandez-Juricic et al., 2005; Patricelli and Blickley, 2006). Song rate and other song characteristics could be perceived by females as an indication of male quality, which would in turn

increase or decrease the chances of the male being reproductively successful (Oberweger and Goller, 2001; Brumm, 2004a).

It was shown that particularly high amounts of singing decreased nightingales' body mass. Nightingales had to rest to avoid syringeal exhaustion (Thomas, 2002; Patricelli and Blickley, 2006). Besides a tradeoff with amplitude, there is also a trade-off between fighting fatigue from singing and transmitting a signal that is likely to be heard by neighbors (Brumm and Slater, 2006). The degree of beak opening has been shown to positively correlate with frequency and other vocal tract movements do change song characteristics in songbirds (Hoese et al., 2000). If singing loudly wasn't costly, the function of bird song may have been drastically different (Brumm, 2004a). Singing is not only costly in birds. For example, frogs and insects that sang regularly used 5-30 times the amount of oxygen as their resting respiratory rate (Thomas, 2002).

It has also been previously found that chaffinches sing longer bouts of the same song type, suggesting that repetition increases the chances that the signal will be received by neighbors, and singing one song type promotes fatigue. Switching song types after a long bout of one type creates a balance between fatigue and signal transmission success (Brumm and Slater, 2006). These and the above-mentioned pressures on song characteristics leave the possibility of speciation in urban areas where background noise is high (Slabbekoorn and den Boer-Visser, 2006).

Finding unexpected responses to anthropogenic noise in Calypte hummingbirds has profound effects on how we understand the function of song in this group. The similarities to passerines, though they are not the most closely related group to humming-birds gives even more significance to the function of song in birds. Avoiding encroachment on birds' territories in terms of noise can have lasting effects on population dynamics, though there is encouragement in the possible plasticity of a population's song structure in response to noise.

## **REFERENCES**

Baptista, L. F., and M. Matsui. Feb. 1979. The source of the divenoise of the Anna's hummingbird. The Condor **81**(1):87-89.

Baptista, L. F., and K. L. Schuchmann. 1989. Song learning in the Anna hummingbird (Calypte anna). Ethology 84:15-26.

Brumm, H., and H. Slabbekoorn. 1965. Acoustic communication in noise. Advances in the Study of Behavior, ed. D. S. Lehrman, R. A. Hinde, E. Shaw 35:151-209.

Brumm, H., and D. Todt. 2002. Noise-dependent song amplitude regulation in a territorial songbird. Animal Behaviour 63:891-897.

Brumm, H. Feb. 2004a. Causes and consequences of song amplitude adjustment in a territorial bird: a case study in nightingales. Annals of the Brazilian Academy of Sciences 76(2):289-295.

Brumm, H. 2004b. The impact of environmental noise on song amplitude in a territorial bird. Journal of Animal Ecology 73:434-440.

Brumm, H. Dec. 2006. Animal communication: city birds have changed their tune. Current Biology 16(23):R1003-R1004.

Brumm, H., and P. J. B. Slater. 2006. Ambient noise, motor fatigue, and serial redundancy in chaffinch song. Behav Ecol Sociobiol 60:475-481.

Cynx, J., R. Lewis, B. Tavel, and T. Hanson. 1998. Amplitude regulation of vocalizations in noise by a songbird, Taeniopygia guttata. Animal Behavior 56:107-113.

Fernandez-Juricic, E. et al. Dec. 2005. Microhabitat selection and singing behavior patterns of male house finches (Carpodacus mexicanus) in urban parks in a heavily urbanized landscape in the western U.S. Urban Habitats 3:1(49-69).

Gahr, M. 2000. Neural song control system of hummingbirds: comparison to swifts, vocal learning (Songbirds) and nonlearning (Suboscines) passerines, and vocal learning (Budgerigars) and nonlearning (Dove, Owl, Gull, Quail, Chicken) monpasserines. The Journal of Comparative Neurology 426:182-196.

Garamszegi, L., M. Zsolt, J. Moller, A. Pape. 2006. Avian song complexity is associated with high field metabolic rate. Evolutionary Ecology Research 8:75-90.

Hoese, W., J. Podos, N. C. Boetticher, S. Nowicki. 2000. Vocal tract function in birdsong production: experimental manipulation of beak movements. The Journal of Experimental Biology 203:1845-1855.

James, R. A. 2006. California innovation with highway noise and bird issues. http://72.14.253.104.search?q=cache:onahjriwvbUj:r espositories.cdlib.org/cgi

Oberweger, K., and F. Goller. 2001. The metabolic cost of bird-song production. The Journal of Experimental Biology 204:3379-3388.

Patricelli, G. L., and J. L. Blickley. 2006. Avian communication in urban noise: causes and consequences of vocal adjustment. The Auk 123(3):639-649.

Pytte, C. L., K. M. Rusch, M. S. Ficken. Oct. 2002. Regulation of vocal amplitude by the Blue-Throated hummingbird, Lampornis clemenciae. Animal Behavior 66:703-710.

Slabbekoorn, H., and T. B. Smith. 2002a. Bird song, ecology, and speciation. Phil. Trans. R. Soc. Lond. B 357:493-503.

Slabbekoorn, H., J. Ellers, T. B. Smith. 2002b. Birdsong and sound transmission: the benefits of reverberations. The Condor **104**(3):564-573.

Slabbekoorn, H. Dec. 2004. Habitat-dependent ambient noise: consistent spectral profiles in two african forest types. Journal of Acoustical Society of America **116**(6):3727-3733.

Slabbekoorn, H., and A. den Boer-Visser. Dec. 2006. Cities change the songs of birds. Current Biology 16:2326-2331.

Slabbekoorn, H., and E. A. P. Ripmeester. 2008. Birdsong and anthropogenic noise: implications and applications for conservation. Molecular Ecology 17:72-83.

Steen, L., and A. M. Houtman. 2006. The song of the male Anna's hummingbird, *Calypte anna*, in southern California. Poster Presentation at Animal Behavior Society 43rd Annual Meeting Snowbird, Utah, 12-16.

Thomas, R. J. 2002. The costs of singing in nightingales. Animal Behavior 63:959-966.

TransSafety, Inc. 1997. California study addresses issues of roadway noise control for the benefit of endangered songbirds. Road Engineering Journal, http://www.usroads.com/journals/p/rej/9710/re971003.htm.

U.S. Department of Transportation Federal Highway Administration. 2006. Synthesis of noise effects on wildlife populations. http://www.fhwa.dot.gov/environment/noise/effects/preface.htm.

Ward, S., J. R. Speakman., P. J. B. Slater. 2003. The energy cost of song in the canary, *Serinus canaria*. Animal Behavior 66:893-902.

Weathers, W. W., and G. F. Stiles. 1988. Energetics and water balance in free-living tropical hummingbirds. The Condor 91:324-331.

Williams, B. R., and A. M. Houtman. 2008. Song of Costa's hummingbird Calypte costae. The Auk 125(3):663-669.

Wood, W. E., and S. M. Yezerinac. 2006. Song sparrow (Melospiza melodia) song varies with urban noise. The Auk **123**(3):650-659.

**ACKNOWLEDGEMENTS** - I thank the SCERP program (UMEB DBI #0602922) and Drs. Bill Hoese, Darren Sandquist, Danielle Zacherl and Sean Walker. Dr. Anne Houtman was my wonderful mentor. CSUF Biology Department, Undergraduate-Faculty Award, CSUF Associated Students and NSF provided funds. Fellow lab and cohort members provided help in the field.

## The Effects of Thermal Stress on Filtration Rates of Non-native Crassostrea gigas and Native Ostrea lurida Oysters

PATRICIA GONZALEZ, SARA PFREMMER, SHANNON CROSSEN, ANTHONY GARCIA, BRYAN WHITE, WILLIAM HOESE, AND DANIELLE ZACHERL

Department of Biological Science, College of Natural Science and Mathematics, California State University Fullerton, 800 N State College Boulevard Fullerton, CA 92831-3599

**ABSTRACT** - Introduced species pose problems worldwide as they can displace native organisms that provide unique ecosystem functions. Successful establishment of non-natives can be related to their ability to out-compete native species. In southern California protected waters, the non-native filter-feeding oyster Crassostrea gigas may compete with the native Ostrea lurida for food and space. Crassostrea gigas is larger and has a higher thermal tolerance (Brown et al. 2004) which may give it a competitive advantage over O. lurida. We studied the effects of temperature on filtration rates of both oysters and hypothesized that C. gigas would filter at faster rates per body weight than O. lurida, particularly following exposure to higher temperatures. We tested our hypothesis by exposing both oyster species to a simulated 3-hour low tide at air temperatures of 10, 20, 30 and 40 °C, temperatures characteristic of the study region. We returned oysters to individual jars (n=5 per treatment) with water containing single-celled algae (~2x10^9 cells/ mL) at 20 °C, the average water temperature of local oyster habitat. We sampled water from each jar after two hours, measured the algal concentrations using a spectrophotometer, and determined filtration rates. Non-native oysters filtered more algae per gram wet body weight than natives (Two-way ANOVA, p=0.027) but exposure to different aerial temperatures did not affect filtration rates (p>0.05). While both species cope with extreme temperatures in southern California, C. gigas's higher feeding rates may make this introduced species a better competitor for food, possibly providing an ecological advantage over the native O. lurida.

**INTRODUCTION** - Ostrea lurida, commonly known as the Olympia oyster, is native to the west coast of North America, with a geographical range fr<mark>om</mark> Sitka, Alaska to Baja California, Mexico (Baker, 1995). Fossil and shell midden data indicate that O. lurida was once abundant in the states of California, Oregon and Washinton (Baker, 1995) with populations remaining stable until the 1930s (Hopkins 1931, Bonnot 1935, Baker 1995, Conte 1996). The decline of this species began with the utilization of oysters by Native American Indians (Bonnot 1935, Elsasser & Heizer 1966) and other humans impacts, such as over-harvesting (Galtsoff 1929, Baker 1995) and pulp mill pollution, which affected oyster reproduction and survival (White et al. 2009). In an effort to alleviate harvesting pressure on the native oyster, the Japanese oyster Crassostrea gigas was introduced to serve the fishing industry in 1964. A native to the coast of south-east Asia and Japan, this oyster has now established populations in southern California (Nehring, 2006). Oyster farmers noted the extreme tolerance of the oysters and became interested. Knowing the thermal flexibility of this non-native oyster, growers introduced this oyster to 64 additional countries (Ruesink et al. 2005).

Both species of oyster thrive in estuarine habitats but have different thermal tolerances. A previous study on oyster thermotolerance conducted by Brown, Biden and Stokel (2004) found that C. gigas could endure higher air temperatures than that of O.lurida at 34 oC and 30 oC respectively. Both species also feed on phytoplankton by filtering water through their gills. The non-native species, C. gigas has smaller gill openings than the native species,

O. lurida, making the non-natives more efficient at filter feeding nanoplankton while the natives must feed on larger particles (Elsey, 1993). While the optimal filtering temperature for O. lurida is unknown, a member of the same genus, Ostrea edulis, performs maximum filtration at 30 oC (Haure et al., 1998), more than 10 oC higher than C. gigas, which reaches maximum filtration at 19 oC (Bougrier et. al, 1995). These findings suggest that C.gigas may be better adapted to the Upper Newport Bay estuary where the average water temperature is 20 oC, as found by preliminary water measurements.

In addition, the shell lengths of the two species of oyster are also distinct. The shell length of the largest caught Olympian oyster in the 1970's was approximately 80 mm. The body size of C. gigas is larger than that of O. lurida, ranging from 80-200 mm (Nehring, 2006). Both differences in thermal tolerance and shell size are causes for concern because of the possibility that the non-native oysters may out-compete the native oyster for resources.

In this study the filtering rates of the two oyster species, O. lurida and C. gigas, were measured in order to investigate their relationships with thermal stress. We hypothesized that the non-native species, C. gigas would have higher filtering rates at higher temperatures. The field research question addressed how the two different shells between the species would affect the internal temperature of the oyster over a full tidal cycle. The shell of O.lurida has a high surface area to volume ratio, as a result of its small size, which may cause more fluctuations in internal body temperature than the larger C. gigas whose surface area to volume ratio is smaller. It was therfore hypothesized that the internal body temperature of O. lurida would vary more than C. gigas.

**METHODS** - To establish a research question and research site, a tour of Newport Bay, California USA was taken. During this tour salinity, temperature, and clarity of water were measured and recorded for a total of six sites throughout the bay. Surveys of oyster populations within this area were done on three sites: Castaways, Coney Island, and Newport Wall to determine the abundance and availability of

the two oyster species. Castaways was chosen as the site for oyster collection; due to the abundance of both species of oysters there.

A total of 30 C. gigas and 30 O. lurida oysters were collected during low tide. The relative tidal height and cobble substrate from which they were collected at were also consistent. The size of the O. lurida oysters collected was kept relatively consistent, but varied among C. gigas. These oysters were brought back into the lab and scrubbed to detach any other filtering organisms and fouling on the shells. The oysters were separated according to species and placed in two plastic tubs filled with prepared seawater. Seawater was prepared using Instant Ocean brand seawater mix. A formula of 38 g of Instant Ocean per L of de-ionized water was used each time seawater was made for a salinity of 34 ppt. Both tubs were initially placed in a 20 C incubator until the experimental temperature changes began.

After an overnight incubation period, the oysters were taken out of the tubs and placed in labeled weighing boats where they were exposed to air temperatures, simulating a low tide. Oysters from both species were then moved into one of four different incubators to begin the experimental temperature changes. Three of the treatment groups were subject to a change in air temperature from 20°C to either 10°C, 30°C, or 40°C. The control group did not experience temperature change and remained at 20°C. Incubators were programmed to gradually increase or decrease from 20°C to the designated temperature treatment. After being exposed to temperature treatments for 3 hours, the three experimental incubators returned to the initial temperature of 20°C.

The oysters were then placed into individual 1 L jars filled with 34 ppt seawater and algae. In order to account for the different filtering rates due to size between O. lurida and C. gigas, each jar of C. gigas was filled with 500 ml of seawater, and each jar of O. lurida was filled with 100 ml of seawater. Once the oysters were placed into the water-filled jars, a concentrated amount of micro-algae was diluted into the water. A concentration of 2 billion cells per milliliter was kept constant in all of the jars. The jars

were placed in incubators at 20 C for two hours. One and two hours after Oysters were placed in the incubators, samples of seawater were taken from each jar and the absorbency was measured using a Beckman DU-50 spectrophotometer at 490 nm.

The filtration or clearance rate (CR), for the oysters of each species was determined by subtracting the final concentration in a single jar (FC) from the initial concentration (IC) in cells/mL and dividing it by the run time (T) in minutes. This was then multiplied by the volume (V) of solution in each jar in milliliters as seen in Formula 1 (Coughlan, 1969).

Formula 1.

$$CR = [IC (cells/ml) - FC (cells/ml)] * V (ml)$$
 $T (minutes)$ 

To rule out differences in clearance rate caused by the settling rate of the microalgae, a control jars were implemented. One control jar consisting of microalgae and seawater, but no oyster was placed in each incubator to monitor the settling rate. In order to compensate for differences caused by soiling by the oysters, a second type of control jar containing seawater and an oyster but no food was placed in each incubator. The settling and soiling rates were determined by subtracting the final concentration (fc) from the initial concentration (ic) in each jar and dividing this by time (t). These values were then incorporated into the clearance rate formula as seen in Formula 2 (Coughlan, 1969).

Settling/soiling rate = 
$$\frac{\text{ic (cells/ml)} - \text{fc (cells/ml)}}{\text{t (minutes)}}$$

## Formula 2.

$$CR = [IC (cells/ml) - FC (cells/ml)] - (settling rate + soiling rate) * V(ml)$$

$$T (minutes)$$

In order to investigate the effect of oyster shell type on internal temperatures, the internal shell temperatures of both species were recorded over a full tidal cycle. Internal shell temperatures were recorded using Ibutton thermo-loggers that were inserted between two oyster shells sealed with epoxy. These 'robo-oysters' were programmed using a palm pilot to measure the internal temperature every 20 minutes. Three O. lurida and three C. gigas robo-oysters were epoxied to the Southeast facing side of Newport Wall located inside of the Newport Dunes boat launch in Newport Bay, California USA. Oysters were positioned vertically, half-way up the wall 13.70 cm apart from each other. The robo-oysters were deployed at 5:00 a.m. and after one full tidal cycle, the data was downloaded on a palm pilot.

Robo-oysters were also used in the laboratory feeding experiment to record the internal shell temperatures of each species within the incubators. One robo-oyster of each species was placed in the four incubators. Only one O.lurida

robo-oyster was deployed in the 20 C incubator due to a malfunction in a C. gigas robo-oyster. In addition to the robo-oysters, thermo-loggers within each incubator recorded air temperature every 30 minutes. All thermo-loggers recorded temperatures before, during and after the experimental temperature changes.

A two-way ANOVA was used to analyze the laboratory clearance rate data. A MANOVA was used to analyze the temperature data collected by robooysters in the field.

**RESULTS** - The filtering rates of native and non-native oysters were significantly different, when body weight and non-feeders were factored into the filtering rate. A two-way ANOVA revealed that temperature did not affect filtering rates (p=0.248), nor did temperature and species combined (p=0.562). What did affect filtering, however, was species type. This effect is in favor of the non-native species C. gigas which on average at any given temperature treatment filtered more cells per minute per wet body mass (p=0.027). This effect is most clearly seen in the extreme temperatures, such as in the 10 oC and 40 oC treatments (Fig. 1)

In the field, the robo-oysters recorded temperatures over a full tidal cycle (Fig. 2). The lowest recorded temperatures occurred in the early morning when tidal height was between 1 and 2 ft, the low temperatures ranged from 18 to 20 oC. The highest temperatures were recorded near noon when tidal height was at around 3 ft. There were small significant differences between species between 21:41 and 1:41 when tidal height was highest. However, a MANOVA test did not confirm any overall difference between the two types of robo-oysters.

In the laboratory, the temperature changes of the robo-oysters that were deployed in each temperature treatment were similar to those found in the field. In the 10 and 30 oC incubators, both species of oyster remained at the air temperature as it moved to the experimental temperature and back (Fig. 3). In the 20 oC incubator, the one species of robo-oyster that was available consistently recorded temperatures near the 20 oC air temperature. The

C.gigas robo-oyster in the 40 oC incubator did not change temperatures with the air because of a malfunction, but O. lurida did follow the same temperature increase as the air. Overall, the temperatures of both species of robo-oyster were relatively consistent with the air temperature in the incubator.

DISCUSSION - The filtration rates between the two species are not significantly different among temperature treatments, but they are significantly different between species. These differences are best seen at the lowest (10 oC) and highest (40 oC) temperature treatments. This may be related to the fact that the non-native oyster C. gigas is tolerant to higher temperatures than the native O. lurida oyster. The implications of this finding are that if air temperatures continue to rise, as climate change theory suggests, the non-native C. gigas may be able to continually filter more than O.lurida, after air exposure of up to 40 oC. From the collected filtration data and analysis, it may be concluded that C.gigas does filter more than O.lurida overall, particularly at temperatures of 10 and 40 oC. Figure 3 demonstrates the temperature changes that occurred inside the incubators and it can be compared to Figure 2 above it which shows actual field temperatures. These two graphs demonstrate that the temperature changes in the incubators mirrored those seen in the field, with a gradual increase over time.

The robo-oyster data from the field also yielded significant results. The temperatures recorded by the robo-oysters appear to have a regular rise and fall, peaking near 12:00. A factor that is likely to have affected this pattern, is the change in tidal height throughout the day. In the early morning around 5:00, the oysters are assumed to have been out of water and exposed to air because the tidal height falls between 1 and -1 ft. It is at this time that the lowest temperatures are recorded, and it may be because the sun is not out to warm the air or water. Similarly, when tidal height is at 3 ft around 12:00 the oysters may still be exposed to air which will have been warmed by the sun. This could explain the rapid rise in temperatures around this time (Fig 2). Also, at 21:00 to 3:00 temperatures are relatively low and tidal height is high at 5 ft which could

have cooled the oysters. Despite the differences at a few points in time, both species of oyster follow the same pattern in temperature change and there is little deviation between the two species which is contrary to our hypotheses that the internal body temperature of O.lurida would vary more than that of C. gigas. The robo-oyster data has been widely accepted to be reliable and accurate, but a future study will test this by comparing the robo-oyster data to that taken from live oysters in the field and in a laboratory setting.

Although we did not find evidence to support our hypothesis that shell type would affect the internal body temperatures of the selected native and non-native oysters, we did find that there are some interesting differences in their filtration rates at different temperatures. It may be concluded that the higher thermal tolerance of the non-native C. gigas has allowed it to filter more at higher temperatures possibly giving it a competitive advantage over the native O. lurida.

### **REFERENCES**

Baker, P. 1995. Review of ecology and fishery of the Olympia oyster, Ostrea lurida, with annotated bibliography. J. Shellfish Res. 14:501518

Bonnot, P. 1935. The California oyster industry. Calif. Fish Game 21:6580

Bougrier, S., P. Geairon, J.M. Deslous-Paoli, C. Bather & G. Jonquikres. 1995. Allometric relationships and effects of temperature on clearance and oxygen consumption rates of Crassostrea gigas (Thunberg). Aquaculture. 134: 143-154

Browne H.M., A. Briden, T. Stokell, F. J. Griffin and C.N. Cherr. 2004. Thermotolerance and Hsp70 profiles in adult and embryonic California native oysters, *Ostreola conchaphila* (Carpenter, 1857). Journal of Shellfish Research. 23(1):135-141.

Conte, F. 1996. California oyster culture. University of California Davis. Department of Animal Science 2:17

Coughlan, J. 1969. The Estimation of Filtration Rates From the Clearance of Suspensions. Marine Biol. 2:356-358.

Elsasser, A. and R. Heizer. 1966. Excavation of two northwestern California coastal sites. Report of the University of California Archeological Survey 67:1151

Elsey, C.R. 1935. On the structure and function of the mantle and gill of Ostrea lurida and Ostrea gigas. Soc. Can. Trans. 79(5):131-160

Galtsoff, P. S. 1929. Oyster industry of the Pacific coast of the United States. Appendix VIII to Report of the U.S. Commissioner of Fisheries for 1929. Bur. Fish. Doc. 1066:367400

Haure, J., C. Penisson, S. Bougrier and J.P. Baud. 1998. Influence of temperature on clearance and oxygen consumption rates of the flat oyster Ostrea edulis: determination of allometric coefficients. Aquaculture: 169: 211-224

Hopkins, A. 1931. The effects of sulfite waste liquor on the oyster (Ostrea lurida). Bull. Bur. Fish. 48:125160

Nehring, S. (2006): NOBANIS – Invasive Alien Species Fact Sheet – *Crassostrea gigas*. – From: Online Database of the North European and Baltic Network on Invasive Alien Species - NOBANIS www.nobanis.org, Date of access 7/2/2009 Ruesink, J. L., H. S. Lenihan, A. C. Trimble, K. W. Heiman, F. Micheli, J. E. Byers & M. C. Kay. 2005. Introduction of non-native oysters: ecosystem effects and restoration implications. Atom. Rev. Ecol. Evol. Syst. 36: 643-689

White, J., J.L. Ruesink, and A. C. Trimble. 2009. The nearly forgotten oyster: Ostrea lurida Carpenter 1864 (Olympia oyster) history and management in Washington State. J. Shellfish Res. 28: 1-6

**ACKNOWLEDGEMENTS** - We would like to thank Drs. Danielle Zacherl and Jayson Smith for their guidance and help in constructing and completing this research project. We would also like to thankAllison Degrassi, Tyler Flisik, Andy Fredell and Kim Walker. This project was made possible by the Southern California Ecosystems Research Program, NSF-DBI-UMEB 0602922.

## **APPENDIX**

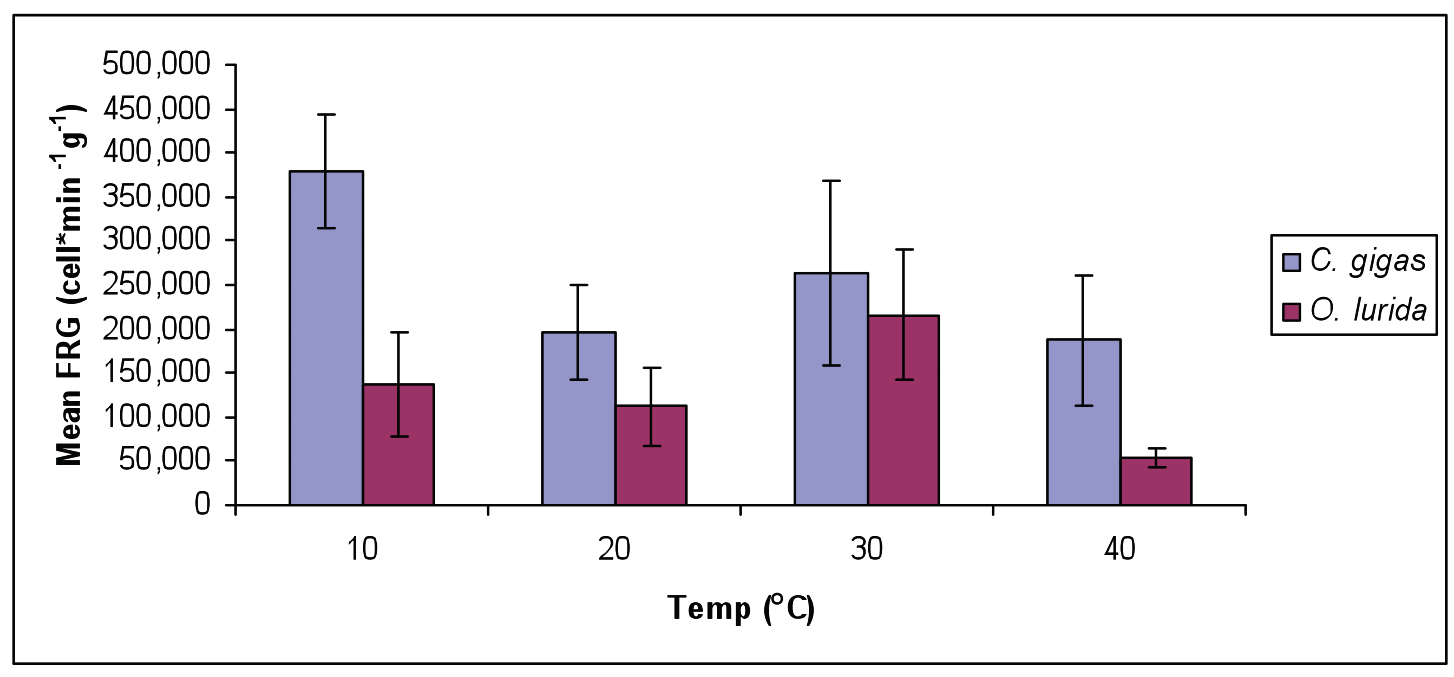


**Figure 1.** Mean + SE of filtration rates (cells\*min-1 g wet body weight-1), excluding non-feeding oysters, for the four temperature treatments. There is no significant difference among temperature treatments (two-way ANOVA, p=0.248) or for the temperature and species interaction (p=0.562) but there was a significant difference between species (p=0.027).

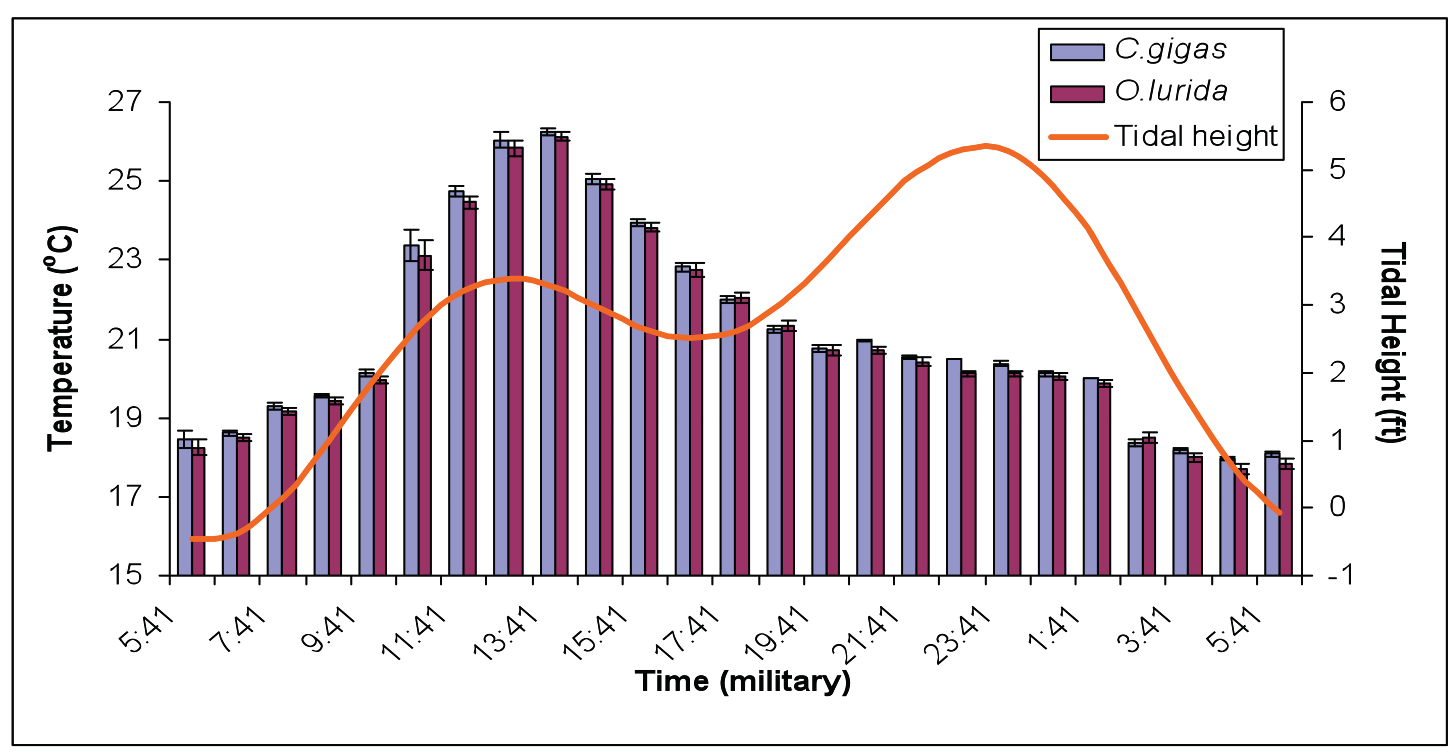


**Figure 2.** Mean + SD of hourly internal body temperatures of robo-oysters in Newport Bay, California USA. Internal body temperatures were significantly different over time (MANOVA, p=0.003) but not differ between species (p=0.827). When tidal height is < 2 ft, represented by the black dashed line, robo-oysters are exposed to air.

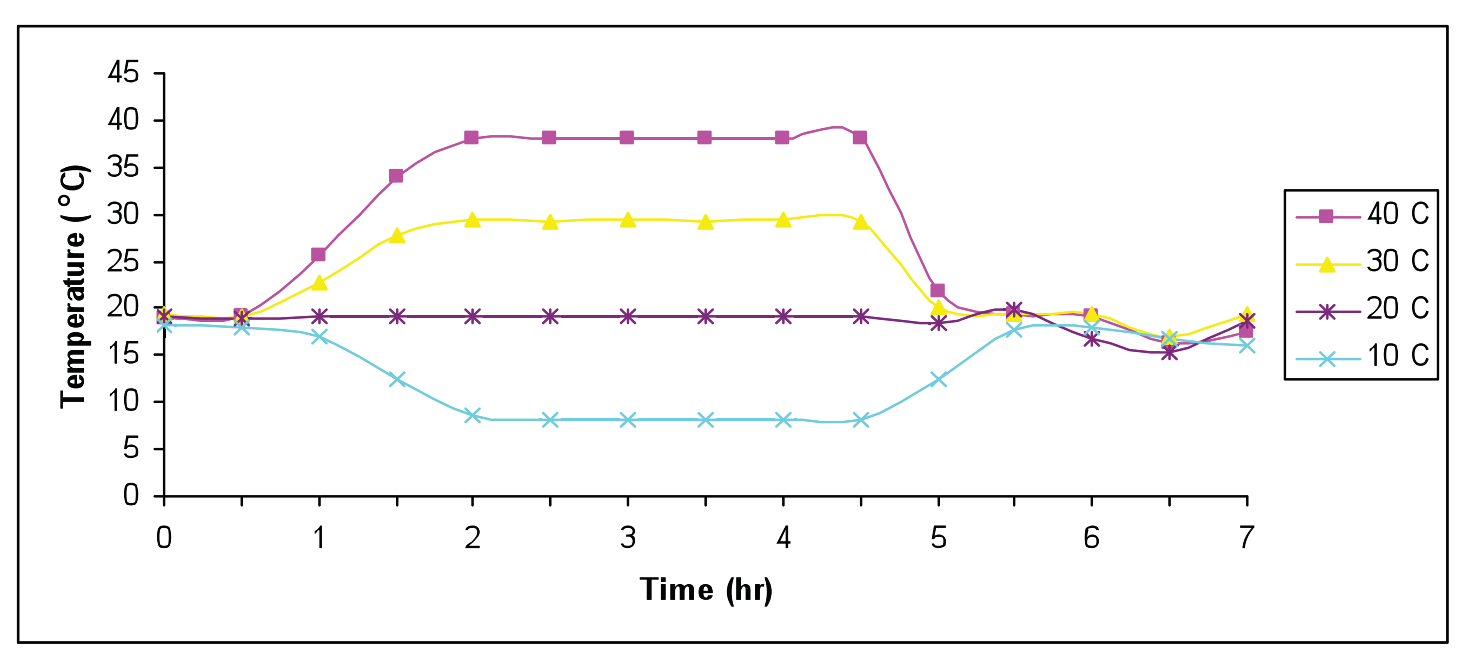


**Figure 3.** Experimental aerial temperatures (oC) inside the four incubators as recorded by the thermologgers. Temperatures changed according to experimental design, in simulation of a tidal cycle.

## Characterization of *Thermotoga maritima* ADP-Glucose Pyrophosphorylase glgC2 K26A Altered Protein

## **SANG LEE**

Research Advisor: Dr. Christopher R. Meyer Chemistry and Biochemistry Department California State University Fullerton

**INTRODUCTION** - Starch is a polysaccharide carbohydrate consisting of a large number of glucose molecules joined together by glycosidic bonds. Starch is produced by all green plants as an energy storage. In plant, carbon dioxide is able to convert into glucose through the process of carbon fixation. The glucose molecules produced through photosynthesis can then be stored as polysaccharides (starch) for later use. Starch is the most important carbohydrate in the human diet and is contained in such staple foods as rice, wheat, maize (corn), potatoes and cassava.

Starch is a polysaccharide carbohydrate consisting of a large number of glucose molecules joined together by glycosidic bonds. Starch is produced by all green plants as an energy storage. In plant, carbon dioxide is able to convert into glucose through the process of carbon fixation. The glucose molecules produced through photosynthesis can then be stored as polysaccharides (starch) for later use. Starch is the most important carbohydrate in the human diet and is contained in such staple foods as rice, wheat, maize (corn), potatoes and cassava.

Thermotoga maritima (T.ma) is a rod shaped thermophilic bacterium, first isolated from geothermal marine sediments with an optimum growth temperature of 80°C. This bacterium metabolizes many simple and complex carbohydrates including glucose, sucrose, starch, cellulose, and xylan (Conners et al., 2006). Both cellulose and xylan have great potential as renewable carbon and energy sources. ADPG PPase catalyzes the rate-limiting reaction in starch and glycogen biosynthesis in both plants and bacteria (Ballicora et al., 2003 and Bal

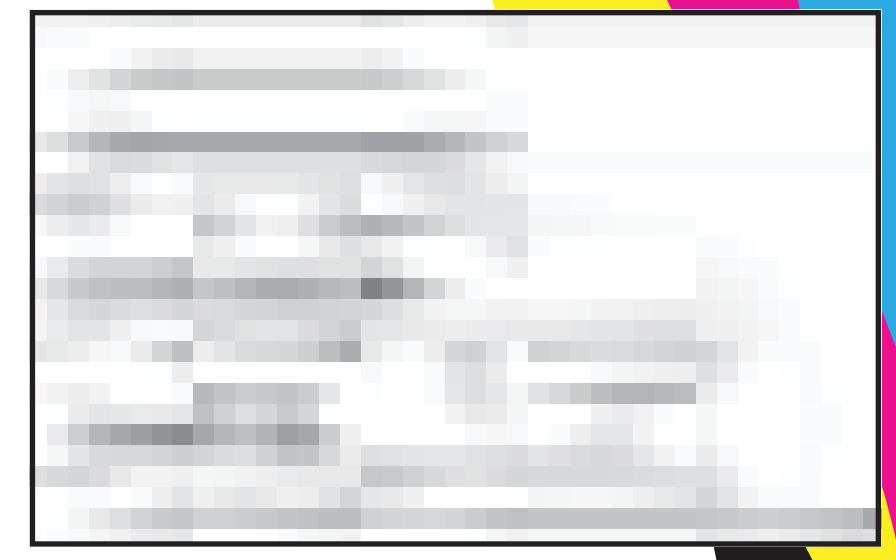
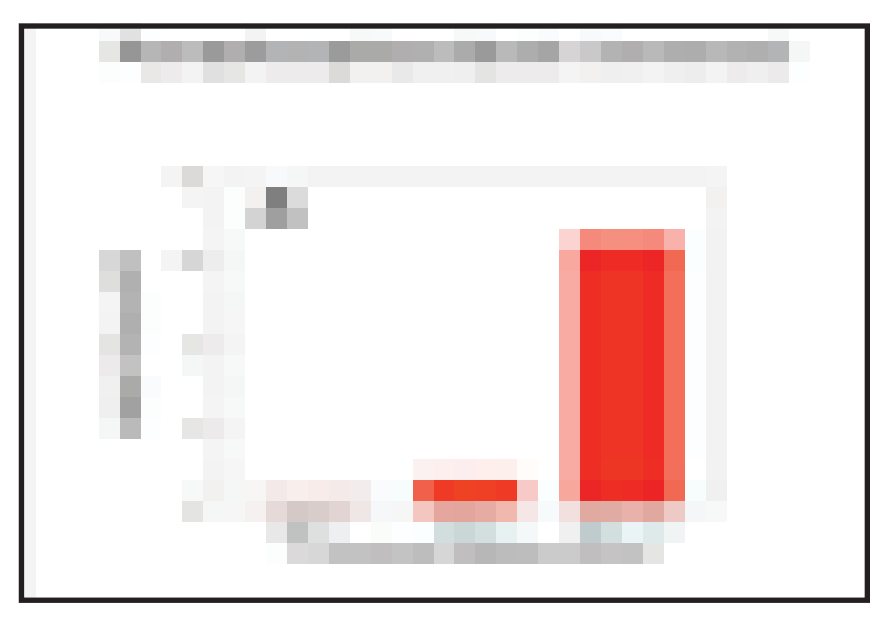


Figure 1. Starch Biosynthesis Pathway- 1) ADP-glucose pyrophosphorylase (ADPG PPase, E.C. 2.7.7.27) - ADPG PPase catalyzes the conversion of glucose-1-phosphate (G1P) and adenosine triphosphate (ATP) to ADPG and pyrophosphate (PPi) in the presence of Mg2+ (Ballicora et al 2003). This step requires energy in the form of ATP. 2) Glycogen(starch) synthase – The enzyme starch synthase then adds the ADP-glucose via a 1.4-alpha glycosidic bond to a growing chain of glucose residues, liberating ADP and creating amylase.

3) Branching enzyme- starch branching enzyme introduces 1.6-alpha glycosidic bonds between these chains, creating the branched amylopectin.

licora et al., 2004). Increasing the rate of this key step in plants and bacteria would be beneficial for the food, chemical, and pharmaceutical industries since starch and glycogen act as starting materials for synthesis of products from these industries. The ADPG PPase from T. ma is likely to be able to withstand high temperatures without succumbing to thermal denaturation. This trait would be beneficial for a variety of industrial applications. Transgenic plants expressing an engineered bacterial ADPG PPase gene can increase starch production for the production of bioethanol, alleviating dependence on vanishing oil reserves.

T. ma has two genes, glgC1 and glgC2, that encode for ADPG PPase. The diverse glgC1 and glgC2 proteins have pl values of 9 and 5, respectively, and exhibit a number of sequence differences compared to other characterized ADPG PPases (figure 3.). In accord with bioinformatics predictions, we have shown that glgC1 is inactive while glgC2 exhibits low activity and is not responsive to allosteric effectors.



**Figure 2.** Pyrophosphorolysis (Reverse) – Activity of glgC1, glgC2, and glgC1 and glgC2 complex measured with ATP.

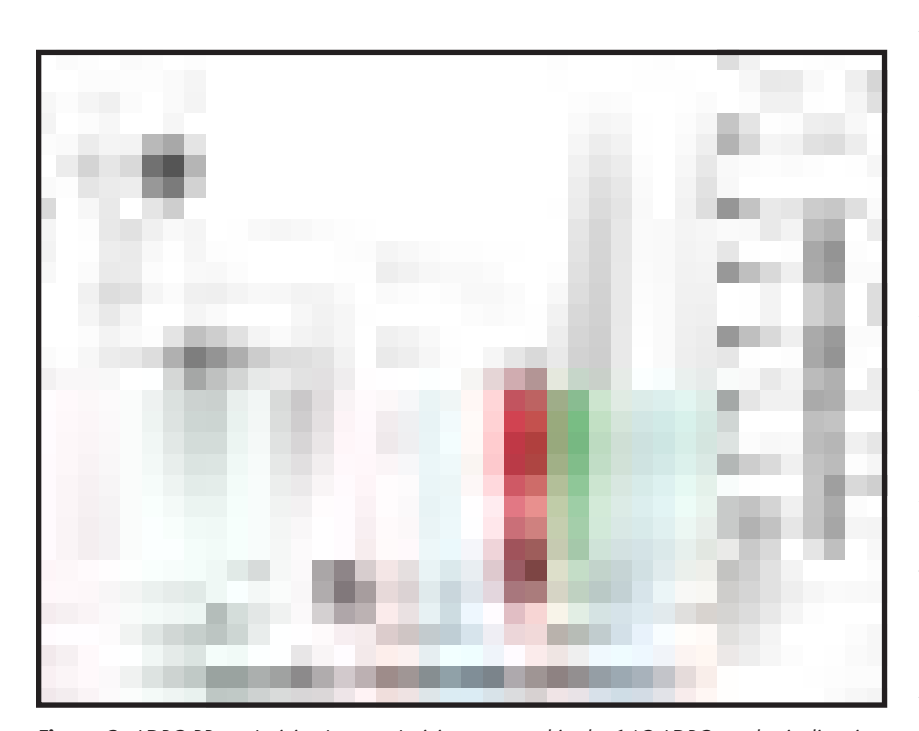


**Figure 3.** ADPG PPase Activity Assay – Activity measured in the 14C-ADPG synthesis direction in the absence and presence of 2 mM F6P, FBP, and Pyr.

However, when purified glgC1 and -2 preparations were combined, a ~20-fold stimulation in the ADPG synthesis direction was observed; further, the combined ADPG PPases are activated by FBP (Refer to figures above). *T.ma* glqC1/C2 *in vitro* complex is proving to be a unique enzyme, in comparison to other ADPG PPases, owing to its thermotolerant enzymatic properties, its putative heterotetrameric subunit assembly, and unique regulation. To probe the nature of the glgC2 active site, the K26A protein was generated and purified. This Lysine 26 position mutated with an alanine was created to evaluate whether this specific amino acid is responsible in part for any of the unique characteristics such as catalytic activity or allosteric regulation associated with His6-glgC2 and to determine its effects on the kinetic parameters for substrate and co-factors. The N-terminus of ADPG-PPase is believed to be responsible for the allosteric regulation of substrate binding to the active site.  $S_{0.5}$  and  $V_{max}$  values for ATP, Mg<sup>2+</sup>, and G1P were calculated. The His<sub>6</sub>glgC2 K26A kinetic data will be compared to the wild-type.

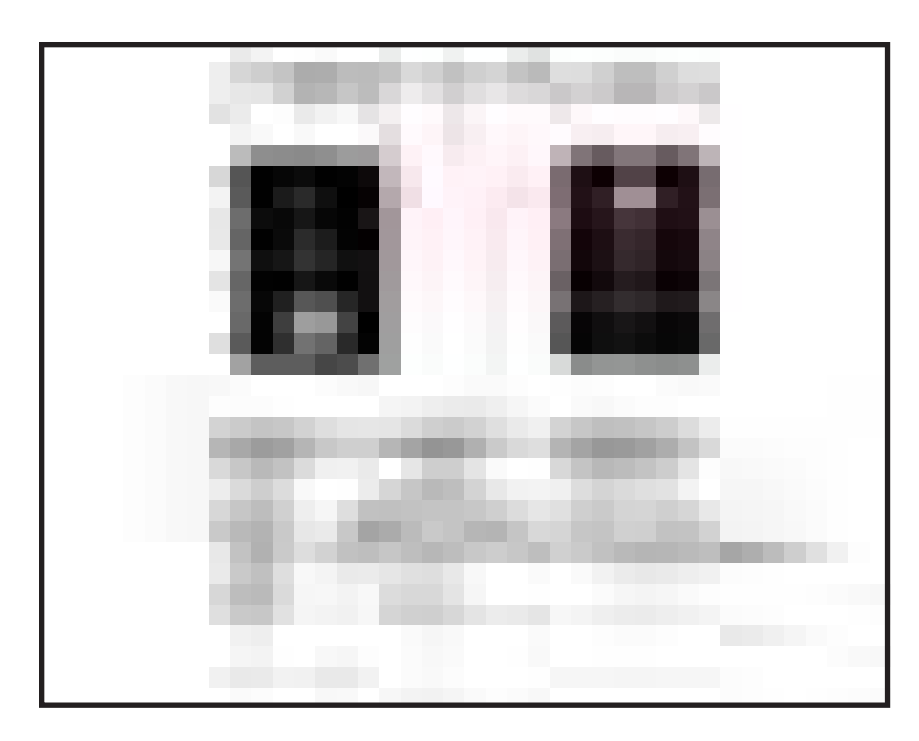


**Figure 4.** Regulation of ADPG-PPase - Activators and inhibitors are different in each different organism. Activators and Inhibitors for Thermotoga maritima will be determined through the experiment.

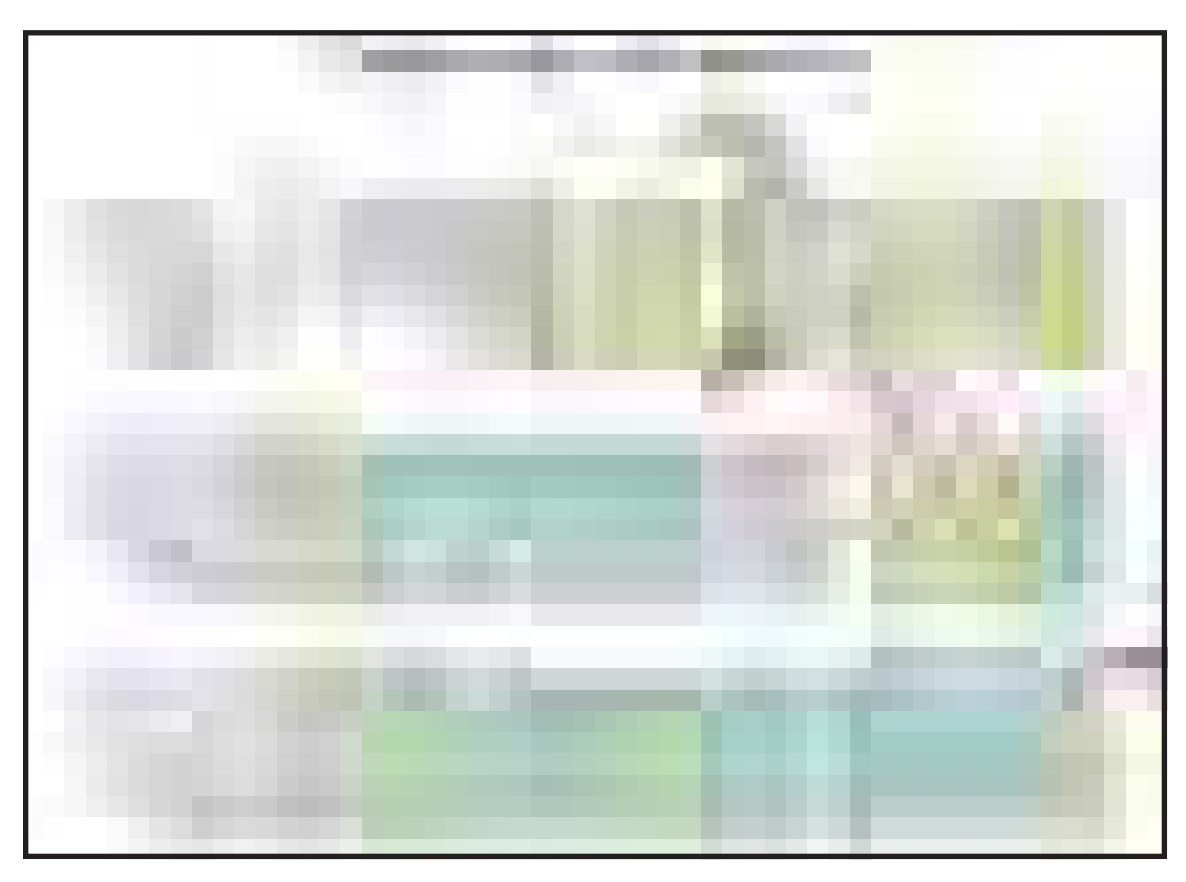
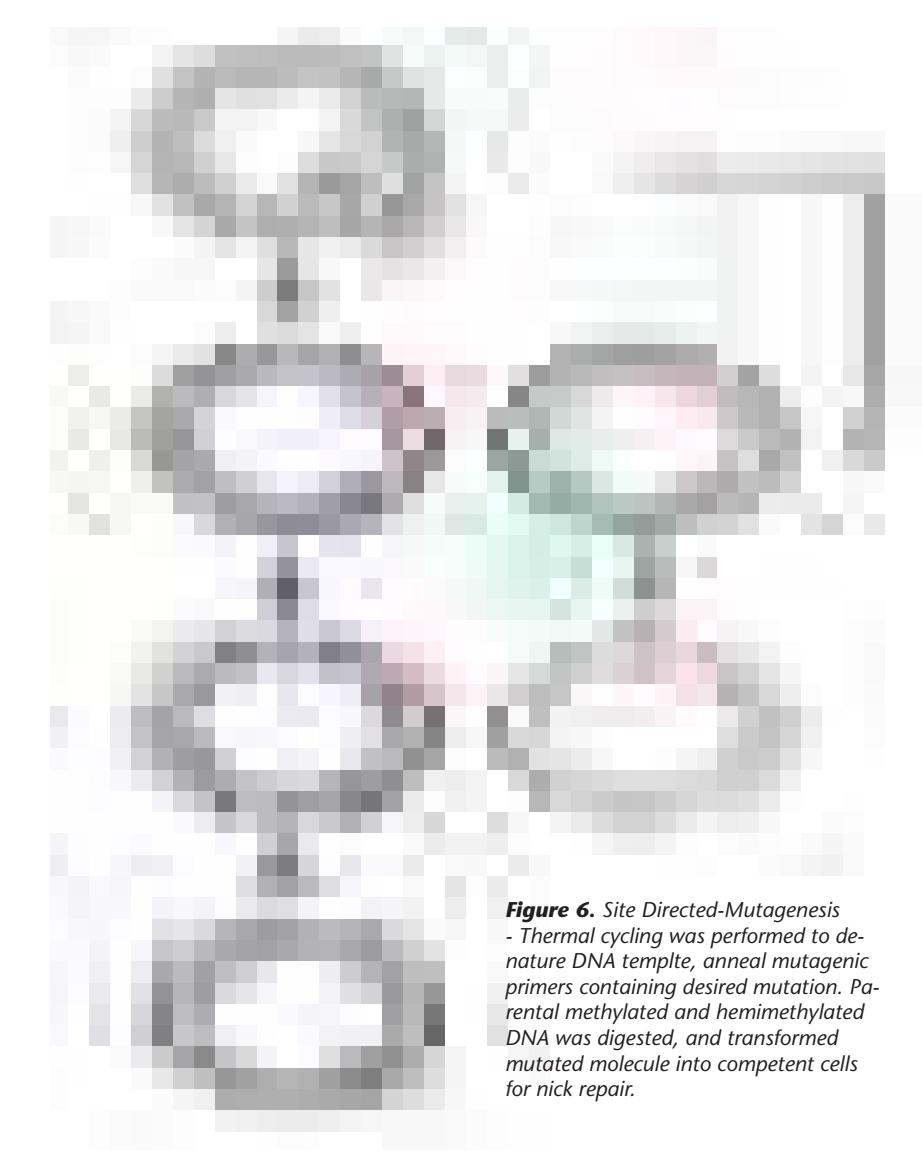


**Figure 5.** Amino acid sequence alignments for the N-terminal region of ADPG PPases from Agrobacterium tumefaciens, Rhodobacter sphaeroides, Rhodospirillum rubrum, Thermus thermophilus, T. maritima glgC1, and T. maritima glgC2. Black arrows point to amino acid residues (positions 33, 35, 108, 135, and 189) essential for allosteric regulation, catalysis, and binding of ATP and G-1-P molecules. Red arrow points to lysine residue position 26 which found to be essential for catalysis.in Thermotoga maritima glgC2

## **METHOD** - Site-Directed-Mutagenesis

Plasmid DNA containing glq-C2 gene was inserted into pMH-1 vectors (Novagen, Madison, WI), then transformed into EA345 (glgC-) cell line with XL-1 Blue competent cells. By using pMH-1 vector, plasmid DNA was transformed. 1µL of pMH-1 DNA was added to a 1.5 mL microfuge tube containing 50 µL of XL1-Blue, EA345 (glgc-) (Stratagene, La Jolla, CA) cells. The tubes were mixed gently and allowed to sit on ice for 30 minutes. The cells were heat-shocked in a 42°C water bath for 45 seconds and immediately placed back on ice for 2 minutes to allow the cells for restoration. 450 uL of LB media was added and the cells were incubated in a shaker at 37°C for one hour. 150 uL of each reaction was placed on an LB plate containing 50 ug/mL ampicillin and incubated overnight at 37°C.

Plasmid DNA containing glg-C2 gene was inserted into pMH-1 vectors (Novagen, Madison, WI), then transformed into EA345 (glgC-) cell line with XL-1 Blue competent cells. By using pMH-1 vector, plasmid DNA was transformed.  $1\mu L$  of pMH-1 DNA was added to a 1.5 mL microfuge tube containing 50  $\mu L$  of XL1-Blue, EA345 (glgc-) (Stratagene, La Jolla, CA) cells. The tubes were mixed gently and allowed to sit on ice for 30 minutes. The cells were heat-shocked in a 42°C water bath for 45 seconds and immediately placed back on ice for 2 minutes to allow the cells for restoration. 450 uL of LB media



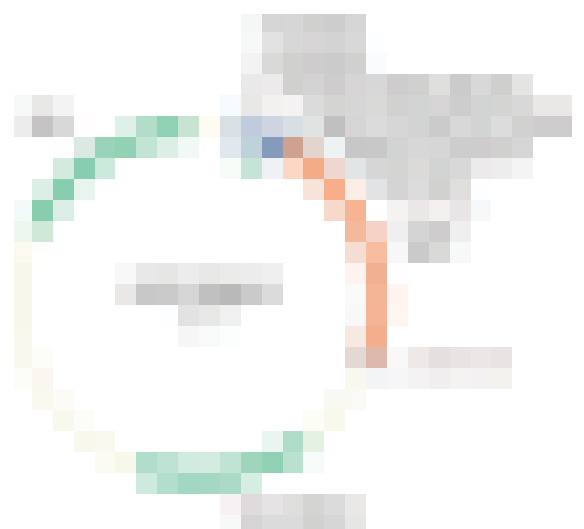


**Figure 7.** pSE420 glgC2 - T. ma glgC2 was directionallycloned into the Ncol and HindIII sites of pSE420. T. ma glgC2 in pMH1

was added and the cells were incubated in a shaker at 37°C for one hour. 150 uL of each reaction was placed on an LB plate containing 50 ug/mL ampicillin and incubated overnight at 37°C.

## Inoculation of His<sub>6</sub>-glgC<sub>2</sub> K26A

First, K26A glycerol stock was prepared and obtained from storage in the - 70 °C freezer. Ampicillin was added to 100  $\mu$ g/mL into each of four 5-mL tubes of LB media. Each tube was inoculated with a sterile pipet tip that was dipped in the glycerol stock and dropped into the tube. The cultures were allowed to incubate in a shaker at 37°C for 16-18 hours.

## Large-scale growth/ Arabinose Inducing

Two 1 L of TB media were prepared and autoclaved for 20 minutes. Ampicillin was added to 100  $\mu$ g/mL to each 1 L of TB media. Ten ml of overnight culture LB was added into each 1 L of TB media. Two 1 L of TB media flasks

were placed into a 37 0C shaker for 2-3 hours by checking O.D at 600 nm. The value of O.D should be approximately between 0.6-0.8. Arabinose was added to 0.15% per 1 L of TB media. Cultures were induced at room temperature for 16 - 18 hours.

## Harvesting 1L Cell Cultures

After 16-18 hours of induction, flasks were removed from the shaker. 500 mL plastic bottles with O-rings were obtained, balanced by filling evenly using a transfer pipette with the culture from the flask until they are exactly balanced. The bottles were placed into the centrifuge rotor SLA- 3000 and centrifuged at 7,000 rpm for 30 minutes. The pellets of cells were collected and placed into a 50 ml conical tube that was pre-weighed. After collecting entire pellet from each bottle, 50 ml conical tubes were weighed and recorded. The 50 ml conical tube was quick frozen in liquid nitrogen and placed in -70°C freezer.

### Sonication

The sonicator machine (Sonics® Vibra CellTM VCX 500) was used to break and open the membrane s of the cells harvested and weighed from above. The cells were resuspended in 1X sonication buffert (50 mM HEPES, 5 mM EDTA, 10 mM MgCl2, 5 mM DTT, pH 7.5) to a dilution of 1:2 (cell: 2X Sonication buffer), containing 0.5 mM dithiothreitol (DTT). The cells were then sonicated two times using Program 5 set at 3 seconds of sonication and 3 seconds of rest. The sonicated cells were spun in a F13 rotor at 7000 RPM for 30 minutes. An aliquot of 300 µl of sample was taken and labeled as "Crude" sample, and stored in the -70°C freezer.

## Heat Step/Upsalt

After the "Crude" was obtained, 2.0 M ammonium sulfate was added to a final concentration of 50 mM for protein precipitation. Then, the sample was heated in a 65°C water bath using a 250 mL Erlenmeyer flask for 10 minutes. After heating, the samples were spun again using the F13 rotor at 9,000 rpm for 30 minutes. A 300 µl aliquot of sample was collected and labeled as "Heat." After spinning, the supernatant were poured into a graduate cylinder to measure the volume. According to the volume of the supernatant, the calculated volume of NaCl for

a concentration of 300 mM using the M1V1=M2V2 formula was poured into the graduated cylinder.

## Nickel Affinity Column Chromatography

Next step of purification was preceded by packing a nickel column with nickel-sepharose resin. After the column is packed, 40 ml of lysis buffer was used to equilibrate the column. At this time, Syringe was used to release all of lysis buffer. After equilibration, the sample was loaded to the column, flown through the column, and collected as waste. After the all of the samples have flown through, 80 ml of wash buffer was added into the column. When wash buffer has flown through the column, 10 ml of the 100, 200, and 300 mM of imidazole was used to bind to His<sub>6</sub>-tag, and release the proteins from the column and collected 0.5 ml of 50 fractions.

## Spectrophotometer (protein)

After all of the 50 nickel fractions were collected, the absorbance of each fraction was measured with a Beckman UV spectrophotometer at a wavelength of 280 nm. A quartz cuvette which was rinsed with 70% ethanol and water was used for spectrophotometry reading. The 100 mM imidazole was used to blank the spectrophotometer. At a wavelength of 280 nm, the amino acids with aromatic side chains such as phenylalanine, tryptophan, and tyrosine may be detected. The higher levels of proteins can be observed by the peaks detected in the spectrophotometric profile. Fractions containing proteins were chosen and analyzed with SDS-PAGE to determine the purity of the protein.

## SDS-PAGE Analysis

Sodium dodecyl sulfate polyacrylamide gel electrophoresis (SDS PAGE) is a biochemical technique used to determine purity, size, and approximate quantity of protein. Sodium dodecyl sulfate will act as a detergent by denaturing the proteins allowing the gel to separate the proteins via size. The SDS-PAGE was prepared by adding 10% resolving gel (1.5 M Tris-HCl (pH 8.8), 30% acrylamide, 10% SDS, water, 10% ammonium persulfate, TEMED) and 10% stacking gel (1.0 M Tris-HCl (pH 6.8), 30% acrylamide, 10% SDS, water, 10% ammonium persulfate, and TEMED). The SDS PAGE apparatus was assembled, then a 1X electrophoresis tank buffer

(25 mM Tris, 192 mM glycine (pH 8.8) was poured into the apparatus. The samples were chosen from the previous part were loaded onto the SDS-PAGE gel. After running of the gel, fractions which have most concentrated protein can be determined by bands on the gel.

### Concentration

A 25 ml conical tube with membrane was obtained. The tube was centrifuged with ddH2O for 1 minute to clean up the membrane. The fractions that have most concentrated protein were obtained and poured into 25ml conical tube. The tube was counter balanced with water contained tube. The tubes were centrifuged for 10 minutes at 6000 RPM. When the level of sample gets 500 µl, Hepes (50 mM Hepes pH 7.5, 0.1 mM DTT) was added to wash 300 mM NaCl. This process was preceded for three times to make it pure. After the whole process is done, 300- 500 µl was obtained inside of membrane and labeled as "Peak". The sample was frozen quickly, and kept in -70°C freezer.

## **Bradford Assay**

The Bradford assay is a dye-binding assay. The blue dye binds to primarily basic and aromatic amino acid residues, especially arginine. A standard curve was established by using increasing amounts of bovine serum albumin (0-18 µg) and plotting the µg of the sample versus the absorbance of the sample. Protein dye from BioRad was used to measure the absorbance of each sample. From the graph, an equation was established that allowed unknown protein concentration determinations to be made. Dilutions were made for crude, heat, and pure samples. All absorbance readings were taken using a Beckman DU -640 spectrophotometer at a wavelength of 595nm.

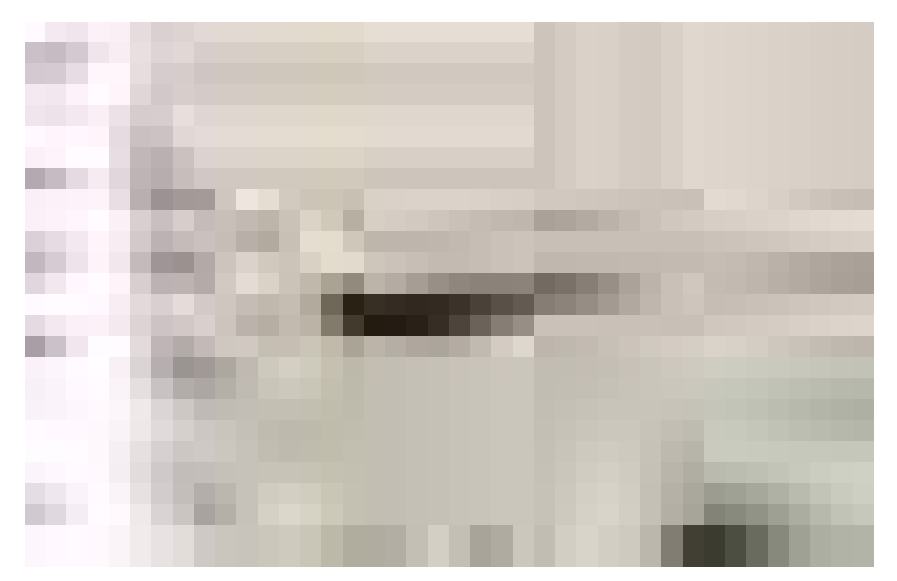
## The Purification process SDS PAGE Gel

The "Purification process SDS-PAGE" gel was run in order to determine the purity of protein in those three samples. The concentrations of Crude, Heat, and Peak give the best resolution on the gel are 18  $\mu$ g, 8  $\mu$ g, and 3  $\mu$ g, respectively. The dilution for each sample was made, and calculated the volume of each sample according to the concentration of best resolution. Most protocols are similar to SDS-

PAGE gel, except the number of samples. For this specific gel, peak sample should have one band to prove that purification was done successfully.

## <sup>14</sup>C- glgC2 Saturation Assay

The activity of T.ma His-glqC2 was determined by performing an enzyme assay in the starch synthesis direction. The assay was done under different conditions. One was done by having FBP activators, while others do not, in order to compare. Others were done by using ATP and G1P as the substrates reacting under the presence of magnesium by monitoring the reaction, to form the product ADPglucose and releasing pyrophosphate. In order to perform the assay, a premix (500mM HEPES, 10 mg/ml BSA, 200 mM MgCl<sub>2</sub>, and 11.3 mM G1P, pyrophosphatase) was prepared to be added to each assay tube. Radioactive substrate [14C] G1P was used to measure the formation of [14C] ADPG. To make the reaction driving forward, pyrophosphatase was added to the mixture and to ensure the reaction would not proceed in the reverse direction. Each reaction tube was filled with 130 µl of the premix. The reaction was initiated by adding 10 µL of diluted enzyme to the premix, vortexed the solution, and allowed to incubate for 10 minutes in a 37°C water bath. Reactions were then terminated after the ten minutes by placing each assay tube into boiling water for exactly one minute. To make sure that no unreacted [14C] G1P would interfere with the results, a 1:5 dilution of the alkaline phosphatase stock was made and 20 µl of the solution was added to each assay tube. The samples were incubated in a 37°C water bath for 2 hours. After the incubation step, 100µl of the reaction mixture was blotted onto 3cm circle pieces of DE-81 filter paper. The filter paper is positively- charged and allows for binding of the negative product [14C] G1P, which will outcompete the substrate for binding. The 3cm circle pieces of paper were then dried in an 800C oven for 15-20 minutes. The dried filter paper samples were then transferred to labeled scintillation vials. Then, 5mL of Ultima Gold Liquid scintillation mixture was added to each vial for quantification purposes. Radioactive emission was quantified by using a Beckman LS6500 liquid scintillation counter using a three-minute counting period. The radioactive CPM counts were then



converted appropriately using standard [14C] G1P stock to enzyme activity units U/ml. The activity units were then plotted and the resulting plot was analyzed.

**Figure 8.** SDS-PAGE analysis gel of His<sub>6</sub>-glgC<sub>2</sub> K26A. Five select fractions from the spectrophotometric profile were analyzed to determin protein purity. Lane 1) BioRad low molecular weight marker, lane 2) nickel fraction #4, lane 3) fraction #7, lane 4) fraction #9, lane 5) fraction #11, and lane 6) fraction #13. His<sub>6</sub>-glgC<sub>2</sub> K26A is shown at 47 kDa.

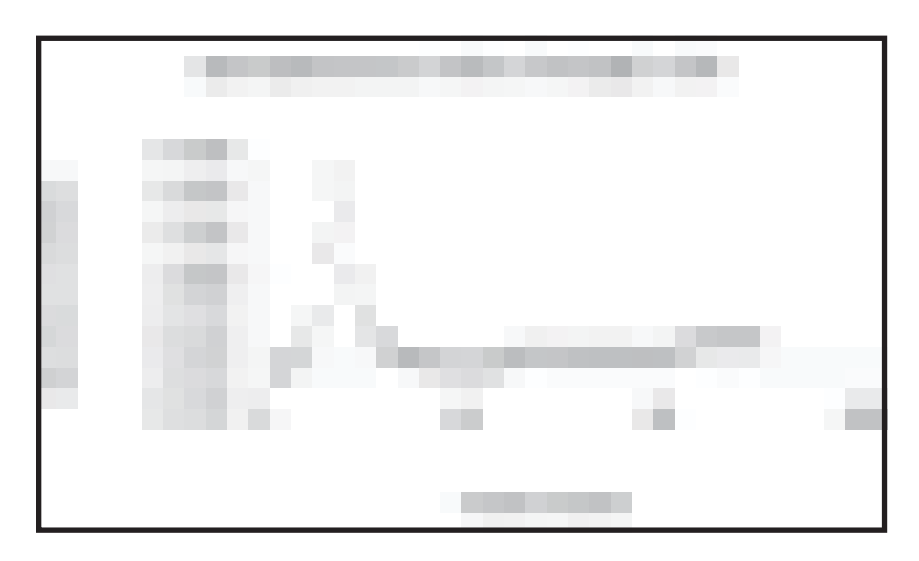


**Figure 9.** Spectrophotometric profile of His6-glgC2 K26A. Fractions #4,7,9,11 and 13 were chosen to identify the purity of protein according to the curve of graph as shown.

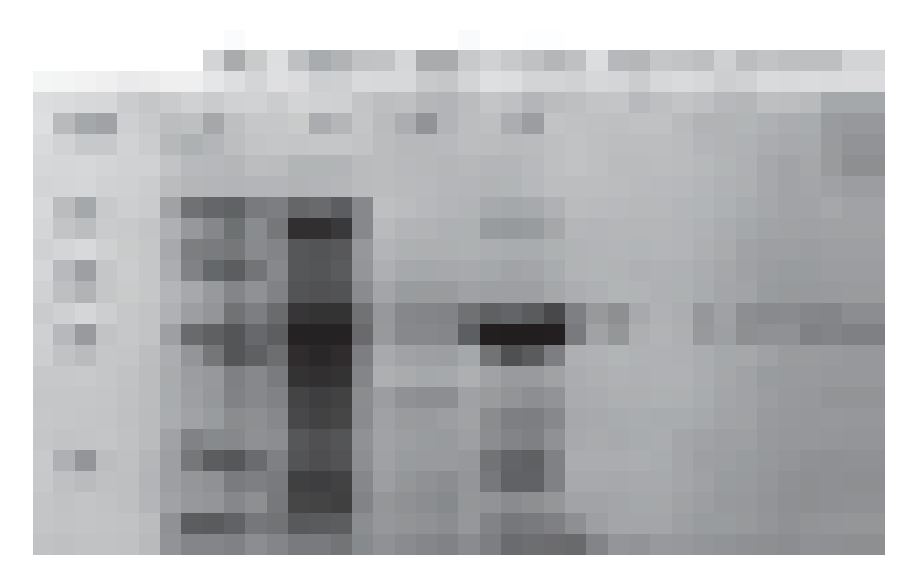


**Figure 10.** SDS-PAGE of His6-glgC-2 K26A protein purification of using nickel affinity chromatography. Lane 1) BioRad molecular protein marker, lane 2) crude (18 μg), lane 3) heat (8 μg), and lane 4) pure His6-glgC2 K26A (3 μg).

	T. maritima	glgC1 & glgC2 Kinetics Sumn	nary	
Enzyme	ATP (mM)	Mg (mM)	G1P (mM)	Vmax (Units/mg)
Liizyiile	AIF (IIIVI)	ivig (IIIIvi)	GTF (IIIIVI)	villax (Offics/frig)
		Assays at 37°C		
T.ma His <sub>6</sub> -glgC2	$5.39 \pm 0.38  (1.6 \pm 0.10)$	$18.66 \pm 0.34  (4.7 \pm 0.30)$	$0.42 \pm 0.067 (1.0 \pm 0.10)$	3.13 ± 0.13
T.ma native glgC2	$5.37 \pm 0.57$ (2.1 ± 0.30)	$18.86 \pm 0.42 \ (6.70 \pm 0.80)$	$0.69 \pm 0.31 \ (1.0 \pm 0.26)$	$5.39 \pm 0.44$
T.ma His <sub>6</sub> -glgC1/C2	2.15± 0.18 (1.22 ± 0.14)	$4.43 \pm 0.58 (1.84 \pm 0.44)$	NA	13.10 ± 0.47
T.ma native glgC1/C2	NA	NA	NA	NA
T.ma His <sub>6</sub> -glgC2 D244N	$9.1 \pm 1.1 \ (2.6 \pm 0.5)$	19.5 ± 1.4 (4.1 ± 0.7)	1.97 ± 1.17 (1.0 ± 0.19)	$0.013 \pm 0.002$
Rs.r wild-type	$4.1 \pm 0.2 \ (2.0 \pm 0.1)$	$7.1 \pm 0.3 \ (6.0 \pm 0.7)$	$0.30 \pm 0.09$ (1)	86.2 ± 5.4
Rs.r. D274N	$4.2 \pm 0.2 \ (2.0 \pm 0.1)$	$9.0 \pm 0.2 \ (9.9 \pm 1.8)$	$0.28 \pm 0.05 \ (1.6 \pm 0.3)$	$0.22 \pm 0.01$
T.th wild-type	$0.34 \pm 0.02 (1.19 \pm 0.07)$	$2.67 \pm 0.09 \ (3.02 \pm 0.26)$	$0.06 \pm 0.01 \ (1.0 \pm 0.12)$	62.6 ± 1.5
Enzyme	ATP (mM)	Mg (mM)	G1P (mM)	Vmax (Units/mg)
Litzyille	All (IIIIVI)	ivig (illivi)	dir (illivi)	villax (Offics/frig)
		Assays at 75°C		
T.ma His <sub>6</sub> -glgC2	5.57 ± 1.24 (1.4 ± 0.31)	14.81 ± 0.16 (6.14 ± 0.35)	0.81 ± 0.31 (1.0 ± 0.21)	20.76 ± 2.43
T.ma native glgC2	9.46 ± 1.53 (1.47 ± 0.14)	$14.44 \pm 0.22 (5.68 \pm 0.53)$	0.81 ± 0.31 (1.0 ± 0.21)	20.76 ± 2.43
T.ma His <sub>6</sub> -glgC1/C2	2.3 ± 0.16 (2.2 ± 0.25)	NA	NA	35.3 ± 1.0

**Table 1.** Kinetic parameters of ADPG PPases from Rhodobacter sphaeroides, Thermus thermophilus, and Thermotoga maritima at 37 °C and 75 °C. Assays were performed in the synthesis direction in the presence of  $^{14}$ [C]-glucose-1-phosphate. When compared to the thermophile T. thermophilus (T.th), the S0.5 values for the T.ma His<sub>6</sub>-glgC2 for ATP, Mg<sup>2+</sup>, and G1P were 15-, 7-, and 7-fold higher, respectively. The  $V_{max}$  (U/mg) for His<sub>6</sub>-glgC2 was 20-fold lower than the Vmax for T. th. The native glgC2 protein showed similar kinetic comparisons. A T.ma D244N mutation was introduced via site-directed mutagenesis (SDM), analogous to the Rs.r D274N. The altered T.ma D244N protein showed a 240-fold reduction in enzyme activity which is comparable to the 392-fold reduction observed for Rs.r D274N.

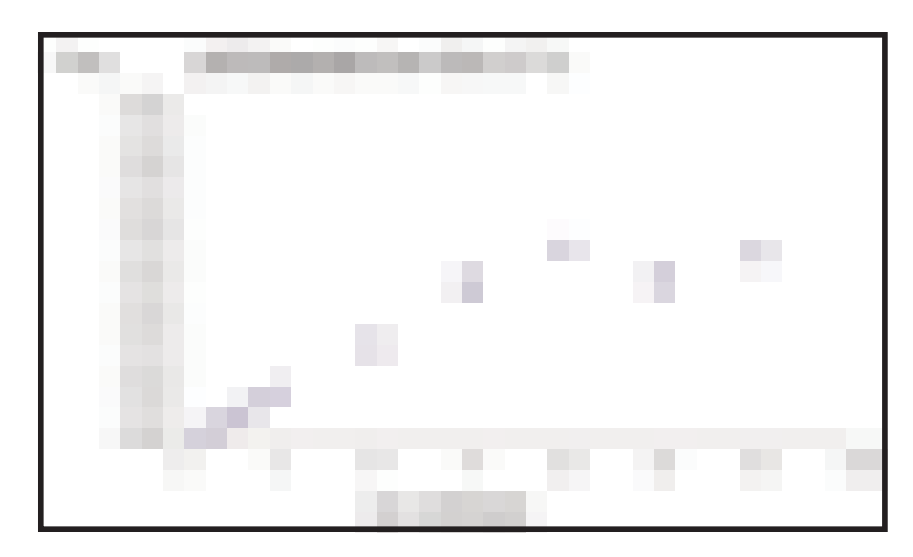


**Figure 11.** His6-glgC2 K26A ATP saturation assay. His6-glgC2 K26A 14[C]-G1P synthesis assays were conducted at 37°C with increasing concentrations of ATP. The estimated Vmax was measured at 0.03 +/- 0.003U/mg and the S0.5 value at 9.22 +/- 1.34 mM. The His6-glgC2 K26A was saturated at approximately 20 mM ATP.

**DISCUSSION** - According to the previous study of E.coli, genes of E.coli contain LAGGR region and KPAK region which are responsible for allosteric regulation and catalytic activity, respectively (Refers to figure 5). The multiple amino acid alignment (figure 5) shows that all genes contain lysine at same row within KPAK region, except glgC1. For glgC2 gene, lysine is placed at position 26. As previous study mentioned about catalytic activity on KPAK region, we decided to mutate lysine position 26 by replacing alanine to determine the effects of catalytic activity. Since alanine is not likely to affect its 3-Dimensional conformation from mutation, alanine was chosen to replace lysine position 26.

Primer was created for mutation, and codon was then mutated to replace lysine to alanine. Primer was designed as 5'-ACG GAG AGA ATA GCG GCA CCT GCG GTT CCT-3' (Lys to Ala, bold), and Reverse primer is to be 5'-AGG AAC CGC AGG TGC CGC TAT TCT CTC CGT-3'. As shown in primers, GCA is mutated to TGC by site-directed mutagenesis. Through the site directed-mutagenesis, plasmid (pMH-1) was inserted into EA345 cell line. Protein was expressed by using cell line. Site-directed mutagenesis was performed and accomplished completely and E.coli was successfully transformed.

According to the purification process SDS-PAGE gel (figure 10), the peak sample has one thick band to represent the size of protein which is 47 kDa. Through the purification process SDS-PAGE gel, the purification and expression of the His6-glqC2 altered K26A protein was successfully completed with a yield of 0.3 mg of pure protein. Three substrates, MgCl2, ATP and G-1-P were used to perform kinetic parameter. The Km value for MgCl2 saturation plot remained the same as for WT 18.6 mM. The Km for ATP sat plot changed from 5.33 mM in WT to 9.22 mM in altered protein (K26A). The estimated Vmax was measured at 0.04+/- 0.17 U/mg and the  $S_{0.5}$  value at 5.23+/- 0.18 mM. The His<sub>6</sub>-glgC2 K26A was observed to not saturate with up to 3 mM G1P. The Vmax value decreased for the altered protein (K26A) 0.035 U/mg compared to WT 3.3 U/mg. According to this comparison, this indicates approximately 100 folds differences. With data we obtained, we are able to conclude that mutating

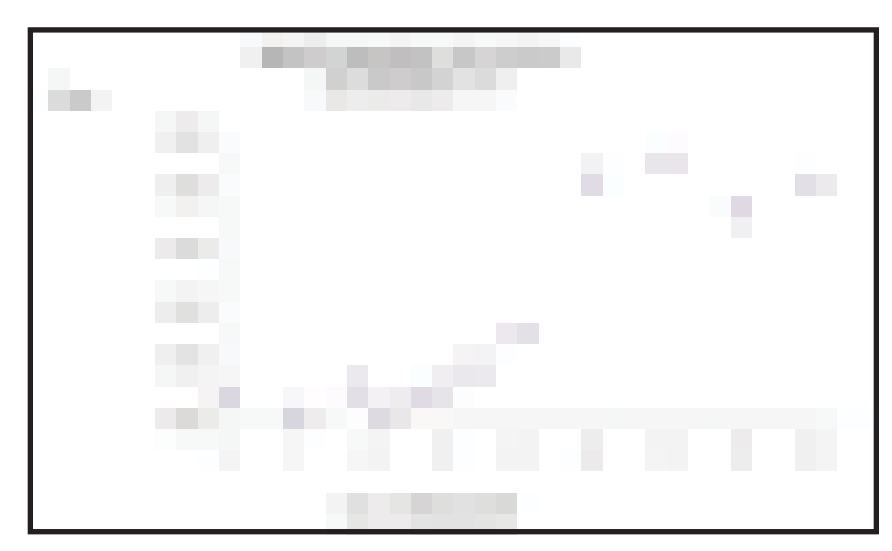


**Figure 12.** His6-glgC2 K26A Mg2+ saturation assay. His6-glgC2 K26A 14[C]-G1P synthesis assays were conducted at 37°C and 20 mM ATP with increasing concentrations of Mg2+. The estimated Vmax was measured at 0.04 +/- 0.004 U/mg and the S0.5 value at 18.8+/- 1.3 mM. The His6-glgC2 K26A saturated at approximately 30 mM MgCl2.



**Figure 13.** His6-glgC2 K26A G1P saturation assay. His6-glgC2 K26A 14[C]-G1P synthesis assays were conducted at 37°C, 20 mM ATP, and 30 mM MgCl2 with increasing concentrations of G1P.

lysine position 26 to alanine has an effect on catalytic activity by comparing to wild type glgC2. Since the altered K26A protein has the effect on catalytic activity, the K26A enzyme could be used as a tool to determine if an altered glgC1 subunit was capable of catalytic activity in complex.

In further experiments, K26A saturation assay with FBP should be analyzed and compared with other three substrates. According to figure 3, complexed glgC1 and glgC2 has high activity with FBP than glgC1 or glgC2 alone. Complex glgC1 and glgC2 should be used to determine its catalytic activity, and also in the presence of FBP. Comlpexed glgC1 and glgC2 should be analyzed the activity with all substrates, and determine also the effect of combined altered protein K26A and glgC1 gene.

### **REFERENCES**

Belanger, A. E., Hatfull, G. F.1999. Exponential-phase glycogen recycling is essential for growth of Mycobacterium smegmatis. J. Bacteriol. 181: 6670-6678.

Boeck, B., Schinzel, R. 1998. Growth dependence of alpha-glucan phosphorylase activity in Thermus thermophilus. Res. Microbiol. 149: 171-176.

Bonafonte, M. A., Solano, C., Sesma, B. Alvarez, M., Montuenga, L., Garcia-Ros, D., Gamazo, C. 2000. The relationship between glycogen synthesis, biofilm formation and virulence in Salmonella enteritidis. FEMS Mirobiol. Lett.191: 31-36.

Eydallin, G., Viale, A. M., Moran-Zorzano, M., Munoz, F. J., Montero, M., Boroja-Fernandez, E., Pozueta-Romero, J. 2007. Genome-wide screening of genes affecting glycogen metabolism in Escherichia coli K-12. FEBS Lett. 581:2947-2953.

Jackson, D. W., Suzuki, K., Oakford, L., Simecka, J. W., Hart, M. E., Romeo, T. 2002. Biofilm formation and dispersal under the influence of the global regulator csrA of Escherichia coli. J. Bacteriol. 184: 290-301.

Schoemaker, J. M., Clark, J. M., Saukkonen, J. J. 1981. Characterization of polysaccaride accumulation in a cell division defective mutant of Escherichia coli 15T-. J. Gen. Microbiol. 123: 323-333.

Smith, A.M. 2008. Prospects for increasing starch and sucrose yields for bioethanol production. Plant J. 54:546-558.

Tao, H., Bausch, C., Richmond, C., Blattner, F. R., Conway, T. 1999. Functional genomics: expression analysis of Escherichia coli growing on minimal and rich media.

J. Bacteriol. 181: 6425-6440.

Wang, T.L. 1998. Starch: as simple as A, B, C? Journal of Experimental Botany 49(320):481-502.

**ACKNOWLEDGEMENTS** - First, I'd like to thank Dr.Meyer for giving a chance to join and letting me work in his lab. It was such a precious time for me to build up my career in science field. Lastly, I want to thank Erick and Dr.Mikiko for helping me through the experience.

## Exploring the Relationship Between the California Chemistry Diagnostic Test (CCDT) and American Chemical Society (ACS) Course Final Exam and Course Grade

### LIZ MICHICOFF

Chemistry 495. Advisor: Dr. Barbara L. Gonzalez Department of Chemistry and Biochemistry California State University Fullerton

**ABSTRACT** - Before entering the first general chemistry course, CHEM 120A, at California State University Fullerton, students are required to take the California Chemistry Diagnostic Test (CCDT) as a placement exam to determine the student's potential for success in the course. At the end of the semester, the students are given the American Chemical Society (ACS) exam for the first course in general chemistry as a final exam to track their progress in chemistry. The results of these tests and final grades were recorded from Fall 2006 to Spring 2008 and were analyzed to characterize any relationships between CCDT, ACS, and final grade results. Course grades were coded on a twelve-point scale with a grade of F assigned a code of 0 and a grade of A+ a code of 12. Binary coding was used to signify success in the course, which is defined as attaining a grade of C or better. SPSS™ software was used to perform the following analyses: correlation matrix, linear and logistic regression. The results show that there is a statistical significance between the CCDT score and ASC exam (r = 0.44,  $p \le 0.05$ ), CCDT score and the course grade (r = 0.31,  $p \le 0.05$ ), as well as the ACS exam and the course grade (r = 0.70, p  $\leq$  0.05). The results also show that there is a statistically significant linear relationship between the CCDT and ACS exam, as well as CCDT and the final grade in the course. The CCDT can be used to predict the outcomes on the ACS exam and the final grade in the course. Furthermore, the threshold scores for the CCDT that predicts 50% and 70% probability of success in the course are 11.8 and 18.5, respectively, and those of the ACS at the same percent of success are 33.3 and 38, respectively. This study can be used to help predict the success of a student in CHEM 120A us-

ing the CCDT and ACS scores.

**INTRODUCTION** - It is understood that approximately 66% of individuals who obtain degrees in chemistry go into the chemical industry field, 26% go into academic institutions, 7% are employed by the government, and approximately 1% go into nontraditional fields such as science writers, specialists, and technical librarians (Crawford, 2005). Chemistry is becoming an ever changing major. For over fifty years, scientists have been continuously discovering and observing molecules as advancements in equipment and technology have progressed. Researchers have also made advancements in the medical field. This includes the treatment and cure of diseases such as measles and polio, as well as pre-natal care for women during their months of pregnancy (Medical Changes From 1945, 2009). These scientists, researchers, and possibly even doctors all have a background in chemistry.

There are many majors besides chemistry that must take general chemistry courses. These include biochemistry, chemistry, geology, physics, and mechanical engineering. Other degrees require units spent in a laboratory along with its corresponding physical science class (Degree Listing Selection Results, 2009). In knowing this information, it is safe to say that the general chemistry course consists of students who have aspirations to become involved in fields other than science.

Because the science, technology, engineering, and mathematics programs are so rigorous, the

students often feel overwhelmed at the intimidating courses that they must take in order to attain their degree. A study done by the UNO Institutional Research program followed 4,356 science, technology, engineering, and mathematics (STEM) students between the semesters of Fall 2005 and Fall 2007. They stated that 192 students began as chemistry majors. By the end of the study, fourteen of the students switched majors for another STEM major, 12 students switched to a non-STEM major, and 49 students dropped out all together (Stem Retention Study, 2008).

During the first few days of class, students at California State University Fullerton (CSUF) are required to take the California Chemistry Diagnostic Test (CCDT) as a placement exam to determine how prepared the student is for the first course in college general chemistry. Students who score less than the threshold are encouraged to take an introductory chemistry course to help them. At the end of the semester, students are given a final exam created by the American Chemical Society (ACS). This is used to compare the performance of local students to national norms. The most recent data shows that the national norms for the CCDT and the ACS exams are scores of 20.0 and 40.0 for the 50th percentile and 24.0 and 47.0 for the 70th percentile, respectively (American Chemical Society, 2009).

The following study analyzed 240 CHEM120A general chemistry students with matched CCDT and ACS scores, as well as course grade from Fall 2006 to Spring 2008. The data were compiled using Excel™ and binary coding was used to categorize the letter grade and success in the course. SPSS™ software was used to support the following hypotheses:

- The correlation between CCDT scores and ACS
   Final Exam score is statistically significant.
- The correlation between CCDT scores and Course Grade is statistically significant.
- The linear relationship between CCDT and ACS
   Final Exam score is statistically significant.
- The linear relationship between CCDT and Course Grade is statistically significant.
- The logistic regression between success in course and CCDT score can predict success in course.

 The logistic regression between success in course and ACS Final Exam score can predict success in course.

**METHODS** - This study was conducted at California State University Fullerton. The subjects of the analyses included 240 of the total 2400 CHEM 120A General Chemistry students from Fall 2004 to Fall 2008. Students from the larger sample were selected for the study if there were matched CCDT and ACS scores, as well as the course grade for CHEM 120A. Each student was given the CCDT prior to enrollment in the first course in general chemistry. The 55 minute test consists of 44 multiple choice questions covering compounds and elements, states of matter, reactions of matter, structure of matter, periodic properties, solutions, qualitative concepts in thermodynamics and kinetics, measurements and lab skills (Russell, 1994).

At the end of the semester, students are then given the ACS final exam for the first semester of general chemistry. Instructors may count the ACS final as the final exam for the course. The ACS final exam is administered in 120 minutes and consists of multiple choice questions covering atomic structure, molecular structure and bonding, stoichiometry, states of matter and solutions, energetic, dynamics, equilibrium, electrochemistry and redox, descriptive chemistry and periodicity, and laboratory chemistry, much like the CCDT.

The ACS, CCDT, and final course grades were compiled using Excel<sup>™</sup>. Course grades were coded on a twelve-point scale, assigning a grade of F to 0 and a grade of A+ to 12. Binary coding was used to signify the students' success in the course, which is defined as attaining a grade of C or better. One was the code for success in the course, while zero was the code for failure to complete the course with a minimum grade of C.

Once the data were coded, a series of analyses were performed to better understand what the data show. The first analysis that was performed was a correlation matrix using SPSS<sup>TM</sup> software. This enabled a relationship between each variable to be calculated and examined. The value that was

reported is the Pearson correlation coefficient. This value shows the relationship between the two pieces of data. A linear regression was also performed in order to calculate an equation that relates the CCDT score to the ACS and Course Grade. The linear regression equation can be used to predict the dependant variable, the ACS and Course Grade, by using the known independent variable, the CCDT score. The  $r^2$  value shows how strong the relationship is between the dependent and independent variables (GraphPad Software, 1999). This means that the amount of variance in the dependent variable is explained by the  $r^2$  in the independent variable. A binary logistic regression was executed to assess the probability of success in the course if a student gets a certain score on the ACS or CCDT. This logistic regression does not assume a normal distribution because the data is based on a binary distribution, it obeys Pascal's rule.

**REVIEW OF LITERATURE** - Before performing an analysis such as this, it is important to become familiar with the history and past studies that utilized the analyses and data items that will be used. The following information will define the purpose of placement tests, how the parameters of the California Chemistry Diagnostic Test were formed and validated, and how it is used in colleges and universities in California. The literature presented is from primary sources, in the form of journal articles and technical reports.

Placement tests are used to, as it states in the title, help place a student in the appropriate course based on their prior knowledge. Students who do not do well on these placement tests are recommended to take remedial courses to learn or relearn the material required for the more advanced course they wish to be in. Students who pass the tests show that they are prepared to take the college level courses. Placement tests help advisors and instructors verify that students are ready for college level work in the particular subject (American Diploma Project Network, 2007).

Before the CCDT was created and used as a diagnostic test, universities had created their own way to better help their students succeed in their stud-

ies. Researchers at the University of Toledo created the Toledo Chemistry Achievement Test, an exam based on questions from high school level chemistry exams that were mainly mathematical, to go along with the Iowa Aptitude Test given at the beginning of the first semester of general chemistry (Hovey, 1958). The results of the study state that there was a higher correlation between the combined scores of the two tests and the course grade or ACS exam (Hovey, 1958). In doing so, they were able help and advise students to take remedial courses to increase their probability of success in the course.

Years after the Toledo placement had been studied, researchers wanted to see how students would test and be placed after taking a diagnostic exam that tested something other than mathematical skills. One such way was to use the Group Assessment of Logical Thinking (GALT), a test that helps to assess how well a student uses reasoning skills to answer questions (Bunce, 1993). This test was mainly used to see if the students were logically ready to understand the information in the course by having them chose which answer they think is correct and to be able to chose the correct rationale for that response (Bunce, 1993). The results of the study show that the GALT can be used to help place students in the correct courses based on how they use reasoning skills to answer questions.

Universities have been concerned with students not doing well and being ill-prepared to take college level chemistry. In 1942, F.D. Martin from the University of Purdue summarized the data that was obtained on campus for a study that looked at why students struggle with freshman chemistry. In this review, Martin looked at the relationships between the student's failure in chemistry and the failure in another subject area, such as English or mathematics (Martin, 1942). The results show that a student who did not take chemistry in high school may be in need of more assistance than an individual who did take the high school level course. When their second semester chemistry grades are compared, there is no significant difference in the two individual scores (Martin, 1942). Thus, the first semester of chemistry lays down the fundamentals that will be used for the general chemistry sequence and that

once a student takes the first course, the student will be ready for the information in the second.

Chemistry Department members from a number of California Universities, community colleges, and high schools came together to create a diagnostic exam that would help advise them to take chemistry courses in which they are more likely to be successful. The committee acknowledged that the main grouping of information that is taught in the first semester of general chemistry are compounds and elements, states of matter, reactions of matter, structure of matter, periodic properties, solutions, qualitative concepts in thermodynamics and kinetics, and laboratory skills (Russell, 1994). The final product resulted in a test consisting of 44 multiple choice questions, 37 of them dealing directly with chemistry and the remaining seven being mathematics based (Russell, 1994). Two versions of the test were given to universities and colleges. The resulting means had less of a difference than the researchers had expected (Russell, 1994). The committee discovered that the reason for the unexpected results was because students come into the general chemistry courses after taking preparatory chemistry courses (Russell, 1994). The skills needed to complete and do well on this diagnostic test depend on previous knowledge of the subject and are not transferred from one subject to another (Russell, 1994). This further shows that students who take chemistry prerequisites will gain the knowledge that is needed for the upper-division chemistry courses. Once the test was validated, the title of California Chemistry Diagnostic Test (CCDT) was given to the exam, and the ACS Division of Chemical Education Examinations Institute collected data so the Universities would be able to compare their results to the national norms (Russell, 1994). In doing so, individual institutions can adjust the pass/fail score on the test as need be.

The CCDT is now used in many institutions. Students are given the test prior to delving into the course material. Research has shown that this test is useful for predicting the performance of a student choosing to gain a higher education (Georgakakos, 1997). The validity and reliability of the CCDT is continuously tested by ACS to assure that there is

a correlation between the results of this test and the success of the students in a General Chemistry course. For example, in a study done at Glendale College, the standard error of the test was 0.12 for 4,023 students (Karpp, 1995). The low error means that this placement exam is valid in its purpose as a diagnostic exam.

The CCDT is also used at California State University Fullerton (CSUF). It has been shown that approximately 20% of students enrolled in the first semester of general chemistry fail the course and 65-70% earn a grade of C or better (McFate, 1999). Students who score below 50% are advised to take a remedial course in order to gain a better understanding of the material in the general chemistry courses (McFate, 1999). The CCDT score results at CSUF are used to see if a student will pass the course or not. It is not used to predict the grade they will receive.

The idea of diagnostic exams has progressed since they were initially formulated. One of the main goals of colleges and universities is to assist their students in taking the appropriate courses that will help them succeed. Research has shown, through trial and error, that students can be better advised in which courses they would be better suited for based on the results of their diagnostic tests. The CCDT was created by using samples of past exams which were math based, chemistry based, or logic based. Researchers have found that a more reliable exam is that which contains both math and chemistry questions, because it tests the prior knowledge of the student to better advise them.

**RESULTS** - The data from 240 subjects was compared to the national norms of both the California Chemistry Diagnostic Test (CCDT) and the American Chemical Society (ACS) exams. These results are shown for the 50th and 70th percentile. The percentile states that 50% of the subjects who took the CCDT answered more than 18 questions correctly, compared to the national norm of 20. Also for the CCDT, 70% of the subjects answered more than 22 questions correctly, compared to the national norm of 24. When comparing the ACS exam results, 50% of the subjects answered more than 41 questions

correctly compared to 40. Additionally, 70% of the subjects answered more than 45 questions correctly compared to the national norm of 47 correct answers (Table 1). The national average and the average of the subjects were also compared. The national average of the CCDT was 20.45 compared to the subject average of 19.28 questions answered correctly. The national average of the ACS exam was 40.35 compared to the subject average of 40.63 questions answered correctly (Table 2).

A correlation matrix was compiled to determine if there was a statistically significant correlation between the CCDT, ACS, and Course Grades. The r-value, or the correlation coefficient, of each comparison shows how strongly the two variables are related. The correlation coefficient of the CCDT-ACS relationship is 0.44, giving a moderate strength. The correlation coefficient for the CCDT-Course Grade relationship is 0.31, giving a low strength. The correlation coefficient for the ACS-Course Grade relationship is 0.70, giving a high strength. Each of these strengths are reasonable for the Social Sciences. Each of these relationships is statistically significant because they each have a value of  $p \le 0.05$ , which means that the results have less than 5% probability of occurring due to chance (Table 3).

	Subject	Results	National	Norms
50 <sup>th</sup> Percentile	CCDT	ACS	CCDT	ACS
70 <sup>th</sup> Percentile	18.0	41.0	20.0	40.0
	22.0	45.0	24.0	47.0

**Table 1**. Results from 240 subjects between Fall 2006 and Spring 2008 compared to national norms for California Chemistry Diagnostic Test and American Chemical Society exams for 50th and 70th percentile. CCDT norms were taken from 1997 test results. ACS norms were taken from 2002 test results.

CDT-ACS Data Set	CCDT	ACS
Average All Subjects	19.28	40.63
National Average	20.45	40.35
_		

**Table 2.** Average of 240 subjects compared to national average on CCDT and ACS exams. CCDT averages were taken from 1997 test results. ACS averages were taken from 2002 test results.

	ACS	Course Grade	
CCDT	*r=0.44	*r=0.31	
ACS		*r=0.70	
*Significant	$p \leq 0.05$		

**Table 3.** Correlation Matrix showing significance of r-value, and p-value between ACS, CCDT, and Course Grade.

A linear regression was performed using the CCDT and ACS exam scores of 240 subjects. During the analysis, the CCDT score is the dependent variable and the ACS score is the independent variable. A linear equation was derived from the data, ACS = 0.83CCDT + 24.5, r2 Linear = 0.19 (F=58.294, df=1, p≤0.05; See Figure 1). The r2-value shows that 19% of the variance in the ACS score can be accounted for when using the equation. The slope value of 0.83 is close to one, showing that the independent variable can better predict the dependent variable. At the same time, the ACS score does not fully depend on the CCDT score attained. A student can improve their grade on the ACS exam throughout the semester.

A linear regression was performed using the CCDT scores and Course Grade of 240 subjects. The Course Grade was coded on a twelve-point scale, assigning a grade of F to 0 and a grade of A+ to 12 (See Table 4). During the analysis, the CCDT score is the dependent variable and the Course Grade (CG) is the independent variable. A linear equation was derived from the data, CG = 0.19CCDT + 2.18, r2 Linear = 0.094 (F=24.37, df=1, p≤0.05; See Figure 1). The r2-value shows that 9.4% of the variance in the Course Grade can be accounted for when using the equation. The slope value of 0.19 is not close to one, showing that the independent variable is not a good predictor of the dependent variable.

Letter Grade	Numerical Value
A+	12
А	11
A-	10
B+	9
В	8
B-	7
C+	6
С	5
C-	4
D+	3
D	2
D-	1
F	0



**Figure 1.** Linear regression line that shows the relationship between the California Chemistry Diagnostic Test score and the American Chemical Society final exam score.



**Figure 2.** Linear regression line that shows the relationship between the CCDT scores and the Course Grade.

**Table 4.** Key shows the coding for letter grades used in analysis

A binary logistic regression analysis was also performed on the data. The logistic regression analysis aids in the prediction of success in the course based on the students' score on the ACS exam. The success in the course is coded using the binary values, one and zero. By using the data between the between Fall 2006 and Spring 2008 semesters, a score of 33.3 on the ACS final exam will give a 50% probability for success in the course, where a score of 38 would give a 70% probability (See Figure 3).

A binary logistic regression analysis was also used to help predict the success of the student in the course based on the score attained on the ACS exam. The success in the course is coded using the binary values, one and zero. By using the data between the between the Fall 2006 and Spring 2008 semesters, a score of 11.8 on the ACS final exam will give a 50% probability for success in the course, where a score of 18.5 would give a 70% probability (See Figure 4).

### **CONCLUSIONS AND DISCUSSION**

Research Question 1

*Is there a statistically significant correlation between:* 

- the California Chemistry Diagnostic Test (CCDT) score and the American Chemical Society Final Exam?
- the CCDT score and the Course Grade?

The data from these analyses showed that there was a statistically significant correlation between the CCDT, ACS, and Course Grades. The relationships are statistically significant because each test yielded a p value that is less than or equal to 0.05. This means that the investigator is 95% confident that the results have a significant relationship that is not due to chance (Gay, 2006). The effect sizes of the analyses were illustrated by the r-value. The r-value of each comparison shows how strongly the two variables are related. Educational research interprets correlation coefficients, or r-values, to show the following relationships: a coefficient of lower than +.35 or -.35 yields a low relationship, a coefficient of between +.35 and +.65 or -.35 and -.65 yield a moderate relationship, and a coefficient higher than +.65 and -.65 yield a high relationship (Gay, 2006). Based on this convention, the correlation coefficient of r=0.44 for the CCDT-ACS relationship was classi

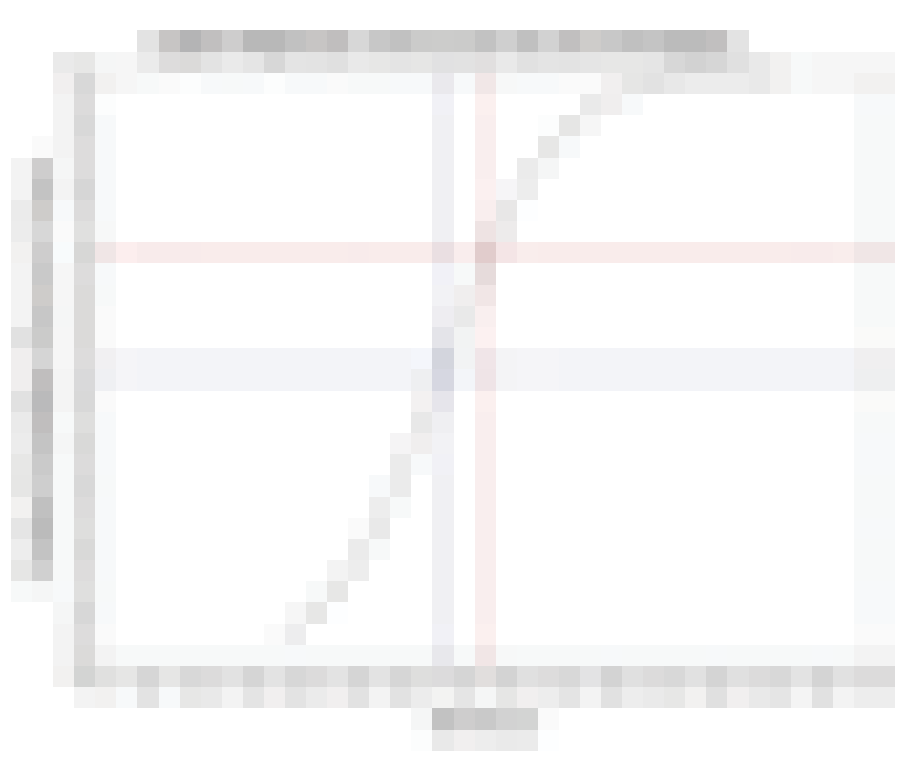


**Figure 3**. Logistic Regression of ACS scores that show 50% or 70% probability of success in the course, where success in the course is defined as a grade of C or better. The 50% and 70% probability of success were associated with a score of 33.3 and 38, respectively, on the ACS final exam.



**Figure 4.** Logistic Regression of CCDT scores that show 50% or 70% probability of success in the course, where success in the course is defined as a grade of C or better. The 50% and 70% probability of success were associated with a score of 11.8 and 18.5, respectively, on the CCDT placement exam.

fied as moderate. The correlation coefficient for the CCDT-Course Grade relationship is 0.31, indicating a low effect size. The correlation coefficient for the ACS-Course Grade relationship is 0.70, indicating a high effect size. Natural sciences do not accept low strength results because the factors within a test are highly controlled. Social sciences accept the fact that there are many variables that go into the results of an analysis that are unable to be controlled, and will therefore accept a lower r-value. Given a large data pool of 240 subjects, the low r-value can be accepted as a viable relationship (Gay, 2006).

The two exams that were used in this study, CCDT and ACS, are both released by the same organization. The main use for ACS exam is to track what the student has learned in the course, while the CCDT is used for diagnostic purposes. The CCDT score and the Course Grade have a low r-value strength because there are many variables in how different instructors assign Course Grades that do not have an impact on how the CCDT scores are assigned. Likewise, the ACS and CCDT have a moderate strength because one test is taken at the beginning of the semester while the other is taken at the end, when the student has gained more knowledge in the subject. The Course Grade and the ACS exam have a strong correlation because both variables show that the student has become more knowledgeable in the subject area.

### **RESEARCH QUESTION 2**

Is there a statistically significant linear relationship between CCDT and:

- ACS Final Exam?
- Course Grade?

The linear relationship between the CCDT scores and ACS exam scores are shown to be statistically significant. This is determined by looking at the F-value, df-value, and p-value. The values are as follows: F=58.294, df=1, and p≤0.05. The F-value explains the amount of variance in the relationship. The value for this relationship is F=58.294, which means that this relationship is statistically significant. The value for the degrees of freedom is df=1, which shows the number of independent variables present in the relationship. In this case, the CCDT can be

used to predict the ACS exam score, making it the only independent variable present in the relationship. The p≤0.05 shows that the analyst is 95% confident that the results are not due to chance. The slope of the equation of the relationship was calculated to be 0.83. A slope value of 1.00 would yield a perfect relationship (Gay, 2006). Because the slope of the CCDT score and ACS exam is close to 1.00, this relationship can be declared statistically significant and that the independent variable can better predict the dependent variable. The r2-value shows how well one variable will predict another (Gay, 2006). The r2-value for this analysis was found to be 0.19, which means that 19% of the variance in the ACS score can be accounted for when the equation is used and the rest is due to chance. In knowing this information, one can say that the CCDT score can help predict the ACS exam result. At the same time, the ACS score does not depend solely on the CCDT score attained because a student can become more knowledgeable in the subject and score higher than the predicted value of the ACS exam.

The linear relationship between the CCDT scores and Course Grades are shown to be statistically significant. This is determined by looking at the F-value, df-value, and p-value. The values are as follows: F=24.37, df=1, and p≤0.05. The F-value explains the amount of variance in the relationship. The value for this relationship is F=24.37, which means that this relationship is statistically significant. When compared to the F-value from the previous relationship, this value is lower which makes it not as significant of a relationship. The value for the degrees of freedom is df=1, which shows the number of independent variables present in the relationship. In this case, the CCDT can be used to predict the ACS exam score, making it the only independent variable present in the relationship. The p≤0.05 shows that the analyst is 95% confident that the results are not due to chance. The slope of the equation of the relationship was calculated to be 0.19. The low value of the slope shows that the CCDT is not an accurate predictor of the Course Grade. There are too many variables in how instructors assign the Course Grade that do not have an impact on how the CCDT scores are assigned, such as the inclusion

of the scores earned from homework, laboratory work, and quizzes. The r2-value for this analysis is 0.094. This shows that 9.4% of the variance in the Course Grade can be accounted for when using the equation, and that the rest is due to chance. A low r2-value shows that the independent variable used will not accurately predict the independent variable, but it is a statistically significant relationship when looking at other values given by the analysis.

### **RESEARCH QUESTION 3**

Is there a statistically significant logistic relationship between course success and:

- ACS Final Exam?
- CCDT?

In looking at these relationships, it is important to remember that a logistic relationship assumes a binomial rather than a normal distribution. The logistic regression analysis was used to calculate the scores needed in order to have a 50 and 70 percent probability of passing the course. When looking at the ACS Final Exam and course success, the number of questions a student must answer correctly to have a 50% chance of success is 41.0 compared to the national norms of 40.0, and to have a 70% chance of success a student must answer 45.0 guestions correctly, compared to the national norms of 47.0. Similarly, in order to have a 50% chance of success in the course, a student must answer 18.0 questions correctly on the CCDT compared to the national norm of 20.0, and to have a 70% chance of success, a student must answer 22.0 questions correctly compared to the national norm of 24.0. If a student scores lower than the 50th percentile, the probability the student will pass the class is less than 50%. It should be noted that the national norms that are given in this analysis are not recent, because ACS has not yet released that data for the 2006 CCDT.

**IMPLICATIONS** - Based on the findings from this study, there are statistically significant relationships between the CCDT, ACS exam, and the Course Grade. The computed subject 50th and 70th percentile norms for the CCDT, 18.0 and 22.0 respectively, and that of the ACS exam, 41.0 and 45.0 respectively, were compared to the National 50th

and 70th percentile norms, 20.0 and 24.0 for the CCDT and 40.0 and 47.0 for the ACS. Also, the subject mean scores for the CCDT and the ACS exam were calculated to be 19.28 and 40.63 respectively, compared to the national mean scores for the CCDT and the ACS exam being 20.45 and 40.35. In evaluating these results, CSU Fullerton should use the percentile norms of the university rather than the national norms. If the University were to use the reported national norms as determining factors in letting students into CHEM 120A, a large number of students would be denied the opportunity to take general chemistry. In addition, the CCDT and ACS subject mean scores are comparable to the ACS reported values, but are below the 50th percentile. This implies that students going into the chemistry undergraduate program at CSU Fullerton do not have as strong of a background in the subject when compared to the rest of the nation.

The linear and logistic regression analyses that were performed on the data set also put into motion new questions and concerns. The study showed that the relationships between the data were statistically significant. This being said, future research may show that the CCDT can be used to help advise CSUF students when necessary. The equations calculated from the linear regressions performed on the CCDT, ACS relationship and CCDT, Course Grade relationship may help to predict the Course Grade as well as the probability of success for each individual student taking the course.

### **REFERENCES**

American Chemical Society. (2009) *National Norms*. Retrieved October 2, 2009, from ACS website: http://chemexams.chem.iastate.edu/stats/national\_norms.cfm

American Diploma Project Network. (2007). Aligned *Expectations?* A Closer Look At College Admissions and Placement Tests. Washington, DC: Achieve, Inc.

Bunce, Diane M. and Hutchinson, Kira D. (1993) The Use of the GALT (Group Assessment of Logical Thinking) as a Predictor of Academic Success in College Chemistry. *Journal of Chemical Education*, 70(3), 183-187.

Crawford, Philip W. (2005). Chemistry *Career Options*. Retrieved September 16, 2009, from Southeast Missouri State University: Crawford Homepage Website: http://cstlcsm.semo.edu/crawford/careers.html

Degree Listing Selection Results. (2009). Retrieved September 16, 2009, from California State University Fullerton Website: http://www.fullerton.edu/catalog/Academic\_Programs/degree\_listing/degree\_listing.asp

Gay, L.R., Mills, Geoffrey E., and Airasian, Peter. (2006). *Educational Research: Competencies for Analysis and Applications*. Upper Saddle River, New Jersey: Pearson Education, Inc.

Georgakakos, John H. (1997). Using the California Chemistry Diagnostic Test and Other Student Background Factors to Predict Grades and Success in General Chemistry I. Retrieved from ERIC database.

GraphPad Software. (1999) *Linear Regression*. Retrieved October 23, 2009 from http://www.curvefit.com/linear\_regression.htm.

Hovey, Nelson W. and Krohn, Albertine. (1958) *Predicting Failures in General Chemistry*. Journal of Chemical Education, 35(10), 507-509.

Karpp, Edward R. (1996). <u>Paths To Success, Volume III. Validating The California Chemistry Diagnostic Test for Local Use.</u> Glendale, CA: Research study done at Glendale Community College. (ERIC Document Reproduction Service No. ED384402d).

McFate, Craig and Olmsted, John. (1999). Assessing Student Preparation through Placement Tests. *Journal of Chemical Education*, 76(4), 562-565.

Martin, F.D. (1942). A Diagnostic and Remedial Study of Failures in Freshman Chemistry. *Journal of Chemical Education*, (19)6, 274-277.

Medical Changes From 1945. (2009). Retrieved September 16, 2009, from History Learning Site: History of Medicine Website: http://www.historylearningsite.co.uk/medical\_changes\_from 1945.htm

Russell, Arlene A. (1994). A Rationally Designed General Chemistry Diagnostic Test. *Journal of Chemical Education*, 71(4), 314-317.

### **Appendix:** Data set used for analyses.

ID	Semester	CCDT	ACS	Course
		Score	Score	Grade
392494519	F 06	22	53	8
800743072	F 06	17	51	7
802597377	F 06	14	50	7
802479626	F 06	18	41	8
899569396	F 06	10	34	6
892774639	F 06	13	37	6
802548271	F 06	17	42	5
892333774	F 06	16	41	7
801374265	F 06	16	40	7
802810002	F 06	17	25	0
800788796	F 06	18	33	4
892626458	F 06	21	51	8
801912882	F 06	16	36	7
892326026	F 06	20	42	9
801390030	F 06	14	42	4
802400457	F 06	17	47	9
801455338	F 06	15	36	7
892447814	F 06	12	24	3
801881772	F 06	13	37	8
892507203	F 06	14	37	8
892309030	F 06	16	35	5
802628834	F 06	18	47	8
892581695	F 06	12	34	4
892594110	F 06	15	31	5
802663815	F 06	15	43	8
892774431	F 06	16	54	12
892325515	F 06	14	45	9
802170829	F 06	18	44	5
800204786	F 06	17	54	4
801865304	F 06	19	36	7
801417684	F 06	17	28	5
802560698	F 06	17	43	6
802842476	F 06	13	43	1
801424474	F 06	18	29	7
899547897	F 06	18	27	3
892329590	F 06	24	41	6
802350397	F 06	15	39	10
802242917	F 06	14	35	6
800517245	F 06	21	51	7
892572546	F 06	20	46	6
802938167	F 06	16	45	4
802364810	F 06	15	31	5

	892471699	F 06	12	35	8
	800849432	F 06	15	30	4
;	892755307	F 06	18	56	12
	892704073	F 06	21	54	9
	892711037	F 06	17	36	3
;	892699281	F 06	13	35	4
;	801187873	F 06	23	62	12
	892282476	F 06	13	45	8
	802786996	F 06	12	44	8
;	892676297	F 06	15	19	0
;	800048068	F 06	12	31	4
;	802450668	F 06	13	32	1
	802831438	F 06	20	50	12
	802876185	F 06	17	47	10
	897011375	F 06	22	60	12
	897468351	F 06	18	63	12
	803137611	F 06	21	61	12
:	892646613	F 06	24	66	12
:	892498809	F 06	19	44	8
;	802242610	F 06	16	44	8
	899639017	F 06	17	44	8
:	899800056	F 06	21	53	8
:	801799065	F 07	22	35	
;	805512571	F 07	28	56	11
	803259993	F 07	16	53	11
;	800732208	F 07	30	51	10
	805339892	F 07	30	57	10
	892448564	F 07	18	50	12
;	803210418	F 07	23	57	8
	802577296	F 06	17	53	8
	892579368	F 06	19	50	8
:	802597575	F 06	21	45	8
	802657981	F 06	16	46	7
	801210634	F 06	15	44	7
	801458027	F 06	19	48	7
;	892407479	F 06	18	41	7
	892662628	F 06	22	53	7
	802633263	F 06	18	56	9
	899626691	F 06	21	53	9
	800640468	F 06	18	42	5
	892714486	F 06	13	41	5
	892516311	F 06	16	46	5
	802917807	F 06	20	50	5
:	800447666	F 06	15	29	5
	801987132	F 06	15	40	5
	802838532	F 06	18	39	5

800181562	F 06	19	41	5
802319152	F 06	15	37	5
802389643	F 06	15	38	5
897062410	F 06	20	38	5
802314500	F 06	15	32	4
802464933	F 06	17	36	4
802578682	F 06	18	36	4
802504407	F 06	23	43	4
892561895	F 06	23	42	4
892765991	F 06	16	35	6
896841384	F 06	16	43	2
892476128	F 06	17	39	2
892729120	F 06	21	49	2
892718636	F 06	14		
892527508	F 06	16	39	2
802806646	F 06		30	11
		14	28	1
892684838	F 06	16	40	1
892739814	F 06	14	21	1
802558130	F 06	17	34	3
801407651	F 06	12	18	0
892692567	F 06	21	31	0
892528944	F 06	17	27	0
892539339	F 06	13	34	
892747700	F 07	25	49	8
892597352	F 07	23	39	8
892742743	F 07	29	44	7
892709478	F 07	29	44	7
801218108	F 07	20	43	7
801983214	F 07	21	43	7
892314386	F 07	27	49	7
803210079	F 07	21	52	9
892337064	F 07	18	43	9
892701293	F 07	18	40	9
805446945	F 07	29	52	5
805400579	F 07	22	32	5
803009034	F 07	23	39	5
802461830	F 07	26	43	5
805565884	F 07	20	50	5
892647942	F 07	17	44	5
803076710	F 07	22	36	5
892480039	F 07	26	38	5
892791591	F 07	14	28	4
802601328	F 07	14	22	4
802694802	F 07	21	34	4
805393634	F 07	23	33	4
802168682	F 07	18	31	4
		. •	J.	

892464470	F 07	13	27	4
803186238	F 07	17	44	6
899567424	F 07	16	40	6
892589433	F 07	27	41	6
805363082	F 07	24	49	6
805475233	F 07	25	44	6
892606229	F 07	16	46	6
802595868	F 07	19	42	6
805539657	F 07	15	35	6
800299471	F 07	22	38	6
805516416	F 07	22	41	6
892281908	F 07	22	36	2
805477171	F 07	22	36	2
892824574	F 07	19	37	1
803203272	F 07	27	25	1
805563970	F 07	20	26	1
802891424	F 07	15	36	1
805502044	F 07	18	38	3
802477182	F 07	21	38	3
802358002	F 07	26	44	3
802569020	F 07	19	28	0
805276276	F 07	17	29	0
892618844	F 07	15	31	0
801834854	S 08	40	61	11
892634908	S 08	25	46	11
892701145	S 08	20	41	11
892490251	S 08	27	54	10
892553348	S 08	22	46	10
802833533	S 08	21	55	10
892327362	S 08	21	53	12
801414582	S 08	14	39	8
802831651	S 08	17	31	8
800768335	S 08	23	37	8
892544990	S 08	25	34	8
892554577	S 08	18	34	8
802959791	S 08	22	39	7
892471897	S 08	24	42	9
803020106	S 08	24	40	9
892566258	S 08	24	46	9
805663549	S 08	16	42	5
802171025	S 08	22	33	5
899745350	S 08	16	31	4
805240108	S 08	14	29	4
801989831	S 08	23	44	6
892835687	S 08	14	28	6
892502295	S 08	22	32	6

892532755	S 08	16	22	6
802386136	S 08	23	33	6
802920009	S 08	15	29	2
801832791	S 08	14	26	2
892313081	S 08	20	32	3
805264652	S 08	21	28	0
603365409	S 08	25	48	11
892325309	S 08	17	57	11
892539909	S 08	24	42	10
803116318	S 08	30	56	12
892287962	S 08	27	55	12
805662368	S 08	14	38	8
805331618	S 08	26	46	8
800207433	S 06	16	46	U
802797753	S 08	25	45	8
805458528	S 08	16	42	8
805368198	S 08	26	43	8
800259533		25		
	\$ 08		41	7
801222357	S 08	17	44	7
803239102	S 08	16	45	7
892552605	S 08	17	42	7
892552530	S 08	19	41	7
802554600	S 08	19	43	9
802786467	S 08	24	47	9
805666252	S 08	35	52	9
892704883	S 08	34	46	9
801403155	S 08	20	41	9
802163279	S 08	31	61	9
805688892	S 08	19	35	5
892721770	S 08	23	36	5
892802927	S 08	22	33	5
899558605	S 08	13	36	5
803111608	S 08	24	38	5
805480688	S 08	22	43	5
892742834	S 08	14	42	5
892797952	S 08	15	35	5
802626176	S 08	16	27	5
801390949	S 08	20	38	4
805711371	S 08	18	36	6
801823386	S 08	17	38	6
892793324	S 08	28	39	6
802836130	S 08	18	43	6
892321910	S 08	31	48	6
896584117	S 08	14	47	6
899573588	S 08	17	37	6
803161553	S 08	29	49	6

800461501	S 08	25	52	6
892663808	S 08	17	45	6
805545324	S 08	24	49	2
803267376	S 08	23	36	1
802144774	S 08	26	32	3
805405297	S 08	15	30	3
802778019	S 08	22	51	3
892689274	S 08	22	32	3
805404498	S 08	13	25	3
805324092	S 08	18	27	0
802886846	S 08	17	27	0
803100072	S 08	21	33	0
802633511	S 08	16	37	0
802801217	S 08	16	30	0

## A New Identification Method For The Tephra Layers Of The Wilson Creek Formation Using Geochemical And Statistical Methods

**NATHAN DIAZ** 

Faculty advisor: Dr. Jeff Knott

**ABSTRACT** - The Wilson Creek (WC) Formation of the Mono Basin in eastern California consists of lacustrine silt and sand beds interbedded with 19 tephra layers. The WC family of tephra beds are intra-volcanic eruptions from the Mono Craters spanning 100 - 13 ka that have similar major -element composition, as determined by electron microprobe analysis. The WC tephra beds are found as far east as Utah and represent potential late Pleistocene marker beds for the western United States with WC-15 closely associated with the Mono Lake paleomagnetic excursion. The Wilson Creek tephra layers are distinguishable by minor and traceelement composition as measured by instrumental neutron activation analysis (INAA). In this study, minor and trace element concentrations from volcanic glass shards of 18 WC tephra layers were analyzed by laser ablation inductively-coupled-plasma mass spectrometry (LA-ICP-MS). Higher concentration trace elements are more accurate in general. Ba and Sr concentrations for WC-15 distinguish this tephra layer from the other WC tephra layers.

east of the Sierra Nevada, is a structural half-graben that contains Mono Lake and both the Inyo and Mono Craters volcanic vents (Figure 1). Exposed along Wilson Creek (WC), which flows from the Sierra into Mono Lake, is a sequence of lakebeds and intercalated 19 tephra layers ("WC-1" is youngest through the oldest "WC-19") known as the Wilson Creek Formation (Lajoie, 1968). The Mono Craters are the source of all of silicic tephra beds, except the basaltic WC-2 whose source is nearby Black Point (Figure 1) (Sarna-Wojcicki et. al., 1991; Lajoie, 1968; Wood, 1977a, b).

The WC tephra layers are tentatively found as far as Summer Lake, Oregon; Tulelake, California; the Great Salt Lake, Utah; and within the Carson Desert Basins of western Nevada (Sarna-Wojcicki et al., 1991; Benson et. al., 2003; Liddicoat, 1992). WC-15, was deposited during the Mono Lake Excursion, a paleomagnetic anomaly, which serves as a correlating stratigraphic marker for climate changes over the Northern Hemisphere (Sarna-Wojcicki et. al., 1991; Benson et. al., 2003). Thus, the ability to identify WC-15 in other areas would serve the dual purpose of identifying the Mono Lake Excursion as well.

Sarna-Wojcicki et al. (1991) described the WC tephra layers as a difficult tephrochronological problem because of the highly similar shard composition. Sarna-Wojcicki et al. (1991) suggested that shard concentrations of iron and calcium among the upper, middle, and lower tephra beds varies. Electron microprobe analysis (EMA), and instrumental neutron activation analysis (INAA), have been the

most successful geochemical analysis methods to show possible variations among the layers, such as WC-15 (Sarna-Wojcicki, 1991).

Benson et al. (2003) showed that varying concentrations of K, Sc, Co, Ba, La, Ce, Eu, Yb, and U measured by EMA and INAA distinguished WC-15 from the other WC tephra layers.

This study applies Laser Ablation Inductively
Coupled Plasma Mass Spectrometry (LA-ICP-MS) to
the problem of measuring minor and trace element
compositions of the WC tephra layer glass shards.
LA-ICP-MS is a relatively fast and accurate method
of measuring trace elements. Thus, if any differences
between the 19-tephra layers can be detected with
LA-ICP-MS, then the WC tephra layers should no
longer be held as a tephrochronological dilemma.

### **MATERIALS AND ANALYTICAL METHODS**

Materials - A total of eighteen ash samples were analyzed, representing each individual tephra layer, excluding WC-18. Samples were originally collected by Andrei Sarna-Wojcicki from a natural vertical section at Wilson Creek near 38°01′24.24″N 119°07′32.10″S. Samples were selected for collection based upon differences in layer morphology. Samples were mounted in epoxy and prepared analysis by the methods outlined by Sarna-Wojcicki et al. (2005).

Trace element analysis - Nineteen (19) samples were analyzed, a total of 47 trace elements concentrations were determined using a Hewlett-Packard 4500 quadrupole ICP-MS connected to a New Wave UP213 laser ablation system. Before and after each sample, three laboratory standards and a instrument blank were run. These served to calibrate both machine performance and the results.

Similarity Coefficient analyses - The similarity coefficient (SC) was used to statistically determine the geochemical differences between the glass shards of each tephra layer (Borchardt, 1971). Outlined by Borchardt et al. (1971, 1972) and Kuehn et al. (2006), similarity coefficients compare samples by use of oxide concentration ratios. Sarna-Wojcicki (2000) summarized that SC ratios <0.92 are con-

sidered to represent low correlation between two tephras, with SC ratios >0.97 considered to represent very strong correlation.

### **RESULTS AND DISCUSSION**

Major and Trace element geochemistry - The trace element data of the tephra layers collected by LA-ICP-MS yielded mixed results. This is best illustrated by focusing on the elements identified by Benson et al. (2003) as key to distinguishing the WC tephra layers (K, Sc, Co, Ba, La, Ce, Eu, Yb, and U). K, Ba, La, Ce, and U all had relative standard deviations (mean/standard deviation) >1.0. In contrast, Sc, Co, Eu, and Yb had relative standard deviations >1.0. Using the SC with K, Ba, La, Ce and U, yielded low (~0.70) compared to the INAA data of Benson et al. (2003) (Table 1).

The differences between the LA-ICP-MS data and the INAA data may result from (a) insufficient sampling by LA-ICP-MS. The INAA method is a bulk method and is more homogenous. Also, (b) the LA-ICP-MS data may reflect the natural variation among individual shards, which is not determinable by INAA methods. In addition, (c) those elements with high relative standard deviation are less than 10 ppm, which, again, may have greater variability. The LA-ICP-MS data do correctly demonstrate that the high silica tephra layers are subalkaline rhyolites with a characteristic Na<sub>2</sub>O + K<sub>2</sub>O content average of 8.57%. In contrast, analysis of WC-2 indicates the layer is a calc-alkaline series subalkaline basalt, with 5.25% alkalis, 9.6% Fe<sub>2</sub>O<sub>3</sub>, 6.18% MgO, and 1.62% TiO<sub>2</sub>.

Differentiating Wilson Creek tephra layers using box plots - Some variations in elemental concentrations is distinguishable among the rhyolitic tephra layers. WC-15 has relatively high concentrations of Ba and Sr compared to the other rhyolitic tephra layers (Figure 2). The Pb concentrations were unusually high whereas Rb was low in WC-14; however, it's unclear if the differences in WC-14 are real or instrumental or if they are the result of instrumental or sampling errors..

There were significant variations among elements in the Formation. WC-2 contained the highest Ba, Mn, and Sr concentration, the lowest Pb, and Rb concentrations, and an absence of Cs and U concentrations, which are indicative of a basaltic ash.

**CONCLUSIONS** - Preliminary evaluation of the LA-ICP-MS data indicates greater accuracy for higher concentration elements and that some specific elements may be useful indicators of particular WC tephra layers. This is most apparent for WC-15, which is associated with the Mono Lake excursion. Future studies should examine the impact of sample size with respect to the LA-ICP-MS. In one regard, the data collection for this study was accomplished in about 3 days, which is substantially less than the six months required for INAA.

### **REFERENCES**

Benson, L, Liddicoat, J, Smoot, J, Sarna-Wojcicki, A, Negrini, R, Lund, S, 2003. Age of the Mono Lake excursion and associated tephra. Quaternary Science Reviews 22, 135-140.

Kuehn, SC, Foit Jr., FF, 2006. Correlation of widespread Holocene and Pleistocene tephra layers from Newberry Volcano, Oregon, USA, using glass compostitions and numerical analysis. Quaternary International 148, 113-137.

Lajoie, KR, 1968. Late Quaternary stratigraphy and geologic history of Mono Basin, eastern California [Ph.D. thesis]. Berkeley, University of California, 373 p.

Liddicoat, JC, 1996. Mono Lake excursion in Mono Basin, California, and at Carson Sink and Pyramid Lake, Nevada. Geophysical Journal International 108, 442-452.

Sarna-Wojcicki, AM, 2000. Tephrochronology. In: Noller, JS, Sowers, JM, Lettis, WR (Eds.), Quaternary Geochronology Methods and Application. AGU Reference Shelf 4, American Geophysical Union, Washington, DC, 357-377.

Sarna-Wojcicki, AM, Lojoie, KR, Meyer, CE, Adam, DP, Rieck, HJ, 1991. Tephrochronologic correlation of upper Neogene sediments along the Pacific margin, conterminous United States. The Geology of North America Vol. K-2, Quaternary Nonglacial Geology: Conterminous U.S., The Geological Society of America, 117-140.

Sarna-Wojcicki, AM, Reheis, MC, Pringle, MS, Fleck, FJ, Burbank, D, Meyer, CE, Slate, JL, Wan, E, Budahn, JR, Troxel, B, Walker, JP, 2005. Tephra Layers of Blind Spring Valley and Related Upper Pliocene and Pleistocene Tephra Layers, California, Nevada, and Utah: Isotopic Ages, Correlation, and Magnetostratigraphy. U.S. Geological Survey, Professional Paper 1701.

Wood, SH, 1977a. Chronology of late Pleistocene and Holocene volcanics, Long Valley and Mono basin geothermal areas, eastern California; Final Technical Report, Contract 14-08-0001-15166, to US Geological Survey Geothermal Research Program, 55 p.

Wood, SH, 1977b. Distribution, correlation, and radiometric dating of late Holocene tephra, Mono and Inyo Craters, eastern California. Geological Society of America Bulletin, v. 88, 89-95.

**ACKNOWLEDGEMENTS** - Samples of the Wilson Creek tephra layers were provided by Andrei Sarna-Wojcicki, Elmira Wan and Dave Wahl of the U.S. Geological Survey. Hector Neff of CSU Long Beach provided assistance and access to the LA-ICP-MS. This project was funded by a grant from the Petroleum Research Fund to Jeffrey Knott.

### **APPENDIX**

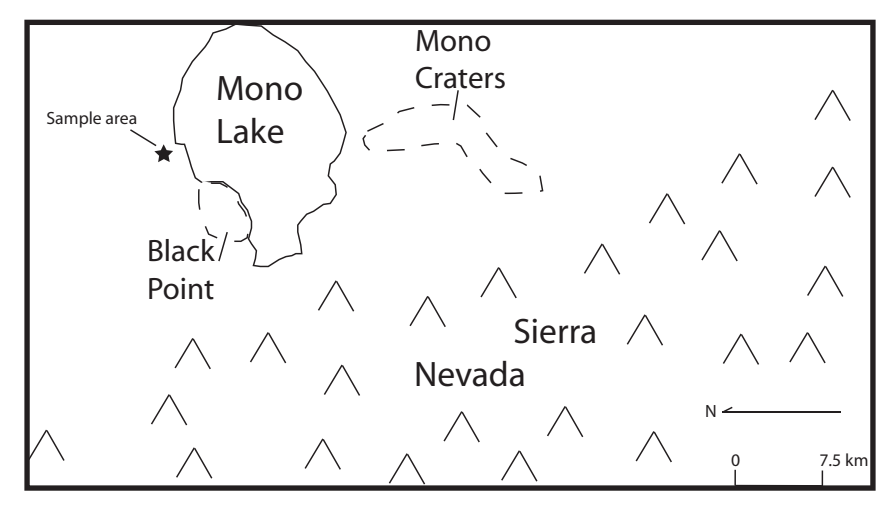


**Figure 1.** Map outlining Mono Lake, the Mono Craters, and Black Point. The star represents the location samples were obtained.

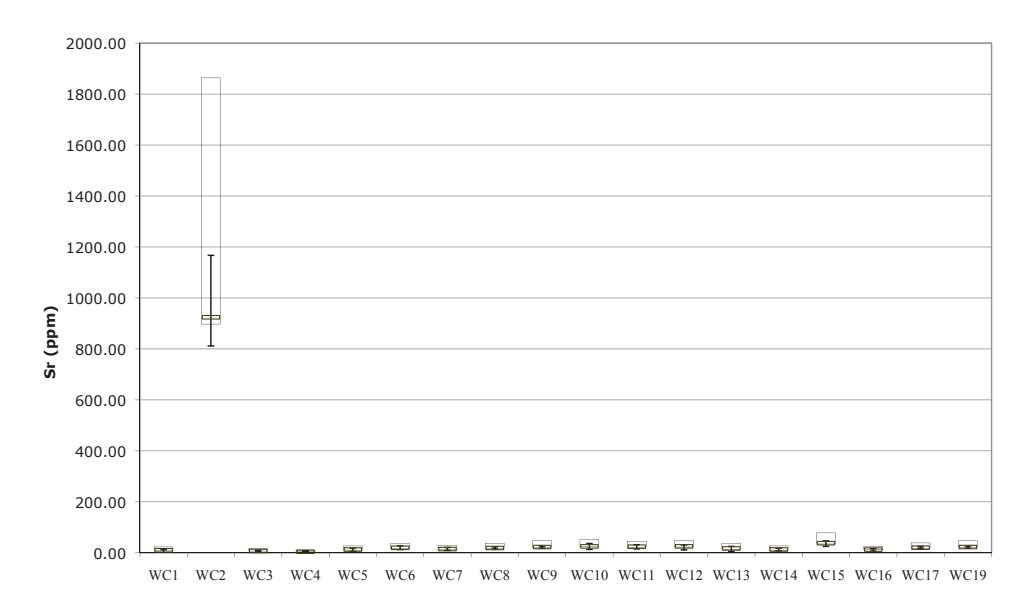


Figure 2a

Figure 2a-2d. Box plots of trace elements in the Wilson Creek tephra layers. Lower and upper quartile represent 25th and 75th percent values. The bold line contained in each box represents the median value. Whisker lines extending from each box represents the range of quantitative error.

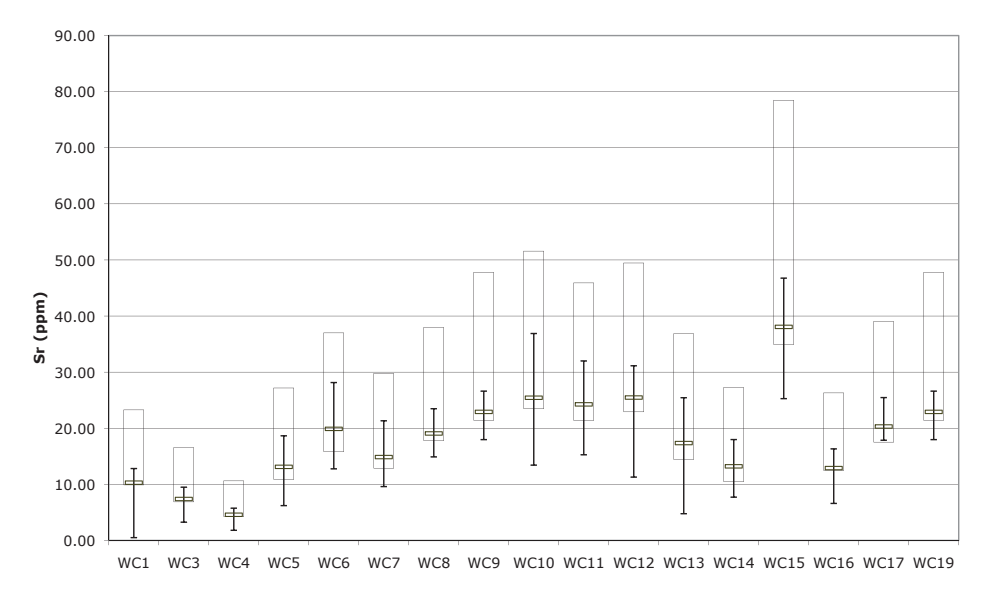


Figure 2b

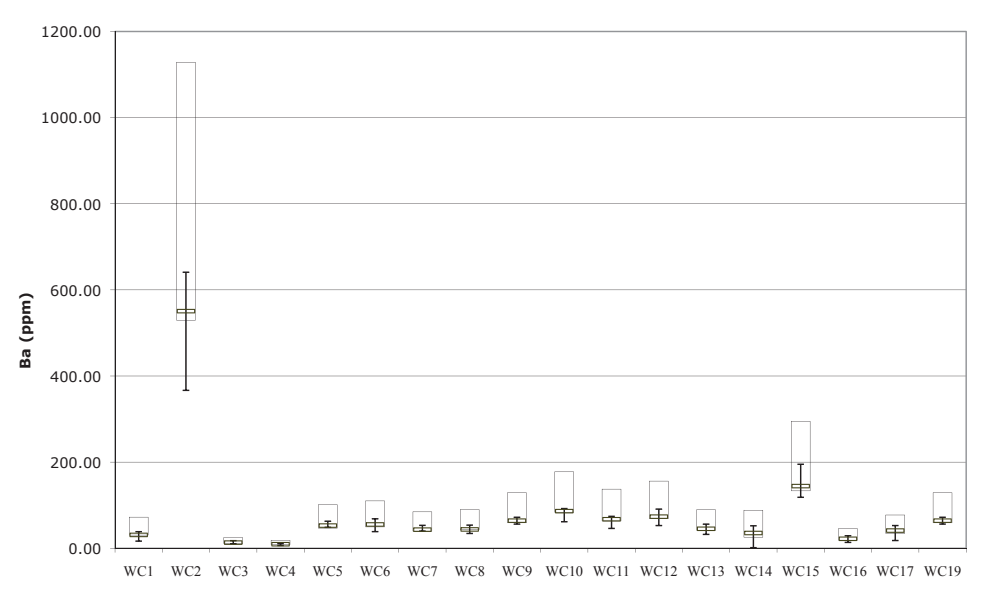


Figure 2c

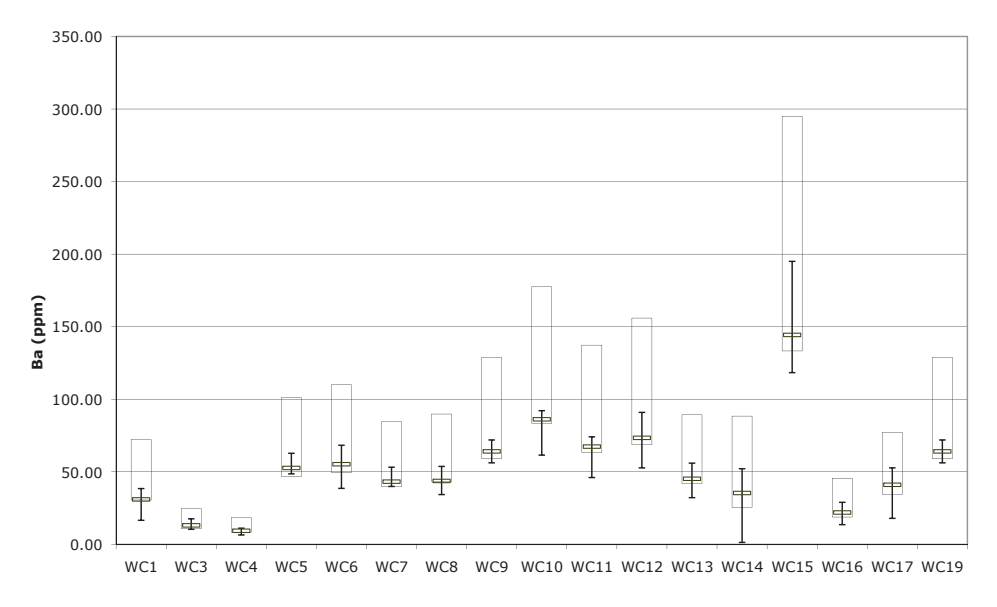


Figure 2d

Ash No.	K	Sc	Co	Ва	La	Ce	Eu	Yb	U
WC 1	4.62	1.79	0.21	35.00	19.00	42.70	0.18	2.80	6.12
WC 2	0.69	13.30	23.40	477.00	14.50	31.90	1.17	1.28	0.24
WC 3	3.68	1.69	0.13	47.00	12.40	28.50	0.14	2.94	7.28
WC 4	3.54	1.64	0.10	42.00	11.90	26.80	0.13	3.04	7.30
WC 5	3.87	1.70	0.15	88.00	19.50	39.90	0.22	2.52	6.39
WC 6	3.87	1.73	0.15	64.00	19.60	41.30	0.22	2.71	6.64
WC 7	3.82	1.70	0.15	58.00	19.50	41.20	0.20	2.62	6.60
WC 8	3.98	1.57	0.13	52.00	14.90	33.90	0.20	2.69	6.92
WC 9	3.97	1.48	0.12	86.00	16.90	33.90	0.23	2.51	6.22
WC 10	3.70	1.67	0.13	104.00	16.00	32.00	0.24	2.62	6.78
WC 11	3.82	1.51	0.12	85.00	14.80	30.70	0.21	2.64	6.68
WC 13	3.93	1.54	0.14	45.00	13.40	30.70	0.20	2.68	6.52
WC 14	3.78	1.53	0.16	78.00	15.60	33.20	0.22	2.58	6.39
WC 15	4.53	1.81	0.22	161.00	22.20	54.10	0.27	2.37	6.00
WC 16	3.72	2.26	0.13	40.00	12.30	23.50	0.19	2.70	8.34
WC 17	4.13	2.12	0.47	46.00	18.50	35.90	0.23	2.45	6.39
WC 19	4.60	2.03	0.22	77.00	15.80	33.50	0.26	2.42	6.49

 Table 1a.
 Average element concentrations (ppm) from EMA and INAA, reproduced from Benson et al (2003). K concentrations are in weight percent.

Ash No.	K	Sc	Co	Ва	La	Ce	Eu	Yb	U
WC 1	57236.02	13.35	0.04	33.11	18.84	46.16	0.00	0.86	6.04
WC 2	17905.38	16.15	20.52	582.13	20.11	44.49	0.29	0.18	0.38
WC 3	45926.53	0.61	10.83	12.76	11.86	26.90	0.34	1.66	5.77
WC 4	43736.29	6.97	2.07	9.37	10.82	28.09	0.00	0.15	6.78
WC 5	54639.96	11.10	5.40	45.03	15.71	41.55	0.00	0.49	4.54
WC 6	41714.11	4.18	0.33	54.86	24.28	48.09	0.12	0.50	7.05
WC 7	45834.57	4.10	2.44	40.63	17.90	40.24	0.23	0.37	5.83
WC 8	42654.34	1.61	5.12	43.61	17.20	32.22	0.34	1.81	6.16
WC 9	61527.15	17.88	30.12	96.62	15.15	34.42	0.23	10.76	5.12
WC 10	48771.78	10.48	11.62	93.86	19.58	39.52	0.13	2.20	6.64
WC 11	41816.21	7.67	8.80	66.93	16.83	35.69	0.12	3.94	7.23
WC 12	43769.71	2.91	19.32	117.57	18.12	38.95	0.12	0.77	6.29
WC 13	42036.70	3.53	1.73	42.43	13.35	28.18	1.12	2.71	5.84
WC 14	40364.65	3.12	19.56	45.57	10.76	25.55	5.79	1.89	4.54
WC 15	45654.90	3.10	1.69	134.37	22.47	46.64	0.73	2.27	8.20
WC 16	43011.81	13.19	6.83	23.63	10.16	25.21	3.41	7.32	8.94
WC 17	42948.33	3.97	10.32	44.20	16.33	34.31	2.47	2.06	7.26
WC 19	46705.31	14.83	11.68	63.08	20.18	29.40	0.86	3.53	9.90

**Table 1b.** Average element concentrations (ppm) from LA-ICP-MS analysis. Values in italics had relative standard deviation >1.0

Ash	No.	K	Ba	La	Ce	U	SC
WC	1	4.62	35.00	19.00	42.70	6.12	
WC	1	5.72	33.11	18.84	46.16	6.04	0.78
WC	2	0.69	477.00	14.50	31.90	0.24	
WC	2	1.79	582.13	20.11	44.49	0.38	0.55
WC	3	3.68	47.00	12.40	28.50	7.28	
WC	3	4.59	12.76	11.86	26.90	5.77	0.63
WC	4	3.54	42.00	11.90	26.80	7.30	
WC	4	4.37	9.37	10.82	28.09	6.78	0.64
WC	5	3.87	88.00	19.50	39.90	6.39	
WC	5	5.46	45.03	15.71	41.55	4.54	0.62
wc	6	3.87	64.00	19.60	41.30	6.64	
WC	6	4.17	54.86	24.28	48.09	7.05	0.73
wc	7	3.82	58.00	19.50	41.20	6.60	
WC	7	4.58	40.63	17.90	40.24	5.83	0.72
WC	8	3.98	52.00	14.90	33.90	6.92	
WC	8	4.27	43.61	17.20	32.22	6.16	0.75
WC	9	3.97	86.00	16.90	33.90	6.22	
WC	9	6.15	96.62	15.15	34.42	5.12	0.71
WC	10	3.70	104.00	16.00	32.00	6.78	
WC	10	4.88	93.86	19.58	39.52	6.64	0.71
WC	11	3.82	85.00	14.80	30.70	6.68	
WC	11	4.18	66.93	16.83	35.69	7.23	0.73
wc	13	3.93	45.00	13.40	30.70	6.52	
WC	13	4.20	42.43	13.35	28.18	5.84	0.78
wc	14	3.78	78.00	15.60	33.20	6.39	
WC	14	4.04	45.57	10.76	25.55	4.54	0.62
WC	15	4.53	161.00	22.20	54.10	6.00	
WC	15	4.57	134.37	22.47	46.64	8.20	0.73
WC	16	3.72	40.00	12.30	23.50	8.34	
WC	16	4.30	23.63	10.16	25.21	8.94	0.69
wc	17	4.13	46.00	18.50	35.90	6.39	
WC	17	4.29	44.20	16.33	34.31	7.26	0.77
wc	19	4.60	77.00	15.80	33.50	6.49	
WC	19	4.67	63.08	20.18	29.40	9.90	0.69
						average	0.70

**Table 1c.** Comparison by between concentrations from Benson et al. (2003) (bold), and concentrations from LA-ICP-MS data using Similarity Coefficent.

# Minor and Trace Element Glass Composition of Late Pleistocene Tephra Layers from the Wilson Creek Formation, Mono Lake, California, by Using Instrumental Neutron Activation

**DANIEL LEE** 

Faculty advisor: Dr. Jeff Knott

ABSTRACT - The Pleistocene Wilson Creek Formation is composed of interbedded mudstones and 19 tephra layers at the type locality along Wilson Creek, northwest of Mono Lake, California. These tephra layers range in age from 32,000 to 13,000 years old (uncalibrated 14C ages). The distribution of the Wilson Creek ash layers is difficult to assess because the glass shard compositions are indistinguishable from each other. A possible exception is ash bed #15, which is found as far east as Utah and is also associated with the Mono Lake paleomagnetic excursion. Single shard electron probe microanalyses (EPMA) and bulk Instrumental Neutron Activation Analyses (INAA) of the glass shards from many of the tephra layers exist in the U.S. Geological Survey Tephrochronology database. In this study, I present similarity coefficient calculations that compare both the EPMA and INAA data. Focusing on ash bed #15, the major elements measured by EPMA data show that #15 is geochemically similar to 7 other Wilson Creek ash layers, whereas #15 is distinctive by INAA-measured minor and trace elements. Ash bed #15 also has a unique light rare earth element (LaN/SmN) fractionation.

**INTRODUCTION** - The Pleistocene Wilson Creek Formation is composed of interbedded mudstones and tephra layers at the type locality along Wilson Creek, northwest of Mono Lake, California (Lajoie, 1968). The 19 tephra layers are dominantly rhyolitic with one basaltic layer (#2; Lajoie, 1968). According to Sarna-Wojcicki and others (1991), the glass shards of the Wilson Creek tephra layers are indistinguishable by major-element composition (Table 1) measured by electron probe microanalysis (EPMA)

and represents "one of the most difficult tephrochronological problems we have encountered".

The Wilson Creek ash beds are important as wide-spread time-stratigraphic marker beds in eastern California and western Nevada for the late Pleistocene (Sarna-Wojcicki and others, 1991). Wilson Creek ash bed #15 is closely associated with the Mono Lake paleomagnetic excursion (MLE), another key time-stratigraphic marker for the late Pleistocene (Benson and others, 2003). Some resolution among the various tephra layers was accomplished with minor and trace element studies using Instrumental Neutron Activation Analysis (INAA; Sarna-Wojcicki and others, 1991; Benson and others, 2003); however, a comprehensive comparison of all of the INAA data has not been done.

In this study, I took the EPMA and INAA analyses that have existed in the U.S. Geological Survey tephra database, some since the early 1980's, for the Wilson Creek Formation ash beds and compared the glass shard composition of ash beds #2 through #19 using the similarity coefficient of Borchardt and others (1972). By assembling a matrix of the similarity coefficients (Tables 1 & 2) for all of the Wilson Creek tephra layers I found that ash bed #15 is compositionally unique. To further illustrate the geochemical differences among the Wilson Creek ash beds, I plotted key elemental concentrations, such as chondrite-normalized rare-earth concentrations, to illustrate the compositional differences. My conclusions are that using a simple statistical comparison of minor and trace element concentrations measured by INAA, I was able to show that the

Wilson Creek tephra layers are statistically distinguishable.

**TEPHROCHRONOLOGY** - As described in Sarna-Wojcicki and Davis (1991), tephrochronology is the study of volcanic ash beds and tuffs to correlate and date sediments, rocks, and structures. Volcanic ash beds and tuffs are excellent stratigraphic markers because they may be laterally extensive. Thus, tephrochronology serves to provide stratigraphic and age controls for regional stratigraphic and tectonic synthesis as well as calibrating and evaluating magnetostratigraphic, isotopic and chemical age-dating methods. Tephrochronology is also an important correlative dating tool used for age control for paleoclimate and paleogeography studies. This is especially true of arid-land localities because volcanic products are more commonly preserved in these environments. The basic premise of tephrochronology is that tephra layers can consistently be discerned, physically or chemically, based on unique characteristics (Sarna-Wojcicki and Davis, 1991). When coupled with alternative dating and correlation methods, tephrochronology proves to be an effective chronostratigraphic technique.

Sarna-Wojcicki & Davis (1991) emphasize three major points for tephrochronological data evaluation: (1) the internal variability of layers needs to be defined with respect to each of the parameters used in characterization; (2) the match between correlated tephra samples needs to be compared with respect to this internal variability and with respect to the analytical error determined for each for the parameters used in the characterization; and (3) the differences between the tephra layer and other tephra layers need to be evaluated with respect to the internal variabilities of each tephra layer and the analytical errors of each for the characterizing parameters.

**BACKGROUND** - Studies of Mono Lake began as early as Russell's (1889) field guide to the Mono Lake area and included interpretations of volcanic history. Russell utilized petrographic analysis to describe the composition of ash beds and ejecta from the Mono Craters. Additionally, Russell provided an initial chronology for Mono Lake volcanic events

based on relations between sedimentary structures like paleo-water lines and volcanic deposits. Russell noted that ashes from violent eruptions could be transported aerially miles from the source resulting in deposition of the same ash miles from one another. This implied that deposits can be correlated distally.

The Wilson Creek Formation is found in the Mono Lake Tufa Reserve, which is located approximately 100 km northwest of Bishop, CA. The type locality is along the northwest margin of Mono Lake. Lajoie (1968) provides a detailed description of the stratigraphy of Mono Basin; inclusive of the Wilson Creek Formation. As described by Lajoie, the Wilson Creek Formation consists of approximately 20-50 feet of finely laminated to very thinly bedded lacustrine clayey silts intercalated with many layers of volcanic ash. The Wilson Creek Formation was deposited during the last major high stand of Lake Russell.

Various exposures of the Wilson Creek Formation can be correlated throughout Mono Basin based on distinctive ash beds within the formation. Apart from the basaltic ash layer (#2), the ash layers consist of rhyolitic debris. Debris is white to light tannish pink, silt to fine sand in size, and composed of predominantly glass shards. Coarser material is silvery gray and predominantly consists of pumice fragments. Lajoie (1968) used x-ray fluorescence techniques to determine origins of tephra layers by means of trace element ratios (Rb:Sr:Zr). Results indicated that the Mono Craters were the source of Wilson Creek Formation ashes. Furthermore, Lajoie (1968) proceeded to radiocarbon date ostracod samples from Wilson Creek Formation that yielded age ranges between 22,900 and 12,500 yrs. B.P. placing ashes in the late Pleistocene.

Working outside of the Mono basin in western Nevada, Davis (1978) identified phenocryst characteristics shared between the Carson Sink Bed and the Walker Lake Bed and correlative potassium concentrations in the Salt Wells Member and Carson Sink Bed. Davis (1978) presumed the source of the Carson Sink Bed was Mono Basin. Sarna-Wojcicki and others (1991) stated that the Carson Sink bed correlates with Wilson Creek #15 based on EMA

shard composition and relation to the MLE. Subsequently, Sarna-Wojcicki analyzed the Wilson Creek beds for minor and trace element chemical composition (unpublished). Interpretation of the resulting data has been virtually untouched for nearly twenty years.

Benson and others (2003) presented selected EPMA and INAA analyses of the Wilson Creek tephra layers along with Davis' Carson Sink bed. Concentrations of K, Sc, Co, Ba, La, Ce, Eu, Yb, and U were provided. Visually, the concentrations of #15 were different from the other tephra layers with only a few exceptions. However, the concentrations of these specific elements were similar between #15 and the Carson Sink bed.

**METHODS** - Andrei Sarna-Wojcicki and Ken Lajoie collected samples of the 19 tephra layers exposed in a vertical stratigraphic section at Wilson Creek during in the 1970's. Glass shards were separated from these tephra layers and analyzed for major-element composition using an electron microprobe (Table 1). Table 2 presents the similarity coefficients between each of the 24 samples. INAA data are presented in Table 3 and similarity coefficients calculated using INAA data (Table 4). The equation elected for this study is

$$d(A,B) = \frac{\sum_{i=1}^{n} R_i}{n}$$

where

d(A,B) = d(B,A) = similarity coefficient for comparison between sample A and sample B
i = element number
n = number of elements
Ri = XiA/XiB if XiB≥XiA; otherwise XiB/XiA,
XiA = concentration of element i in sample A, and

XiB = concentration of element i in sample B.

Data was inserted into a Microsoft Excel spreadsheet from which tables and graphs were generated. Metz and Mahood (1985) showed that Rb, Mn, Ca, Fe, Y and Nb varied over time in the Long Valley caldera system leading up to the Bishop Tuff eruption. Graphs depicting rare-earth element distribution

and fractionation have also been shown to be useful for correlating tephra layers (Izett, 1981). In this study, I normalized the rare-earth elements using chondrite values of Boynton (1984 in Rollinson, 1993)

Thirteen petrogenetically significant elements (Sc, Mn, Fe, Rb, Cs, La, Ce, Sm, Tb, Yb, Lu, Hf, and Th) were chosen because they have sufficient compositional variability to allow discrimination of individual intra-source tephra. An effort was made to use the same elements used by Sarna-Wojcicki and others (1984) and Knott and others (2007) since these studies showed that these particular elements were of sufficient variability and concentration to be useful.

**RESULTS** - The similarity coefficients for majorelement concentrations measured by EPMA range from 0.8185 to 0.9934; omitting Ash #2 because of its basaltic composition (Table 2). The minimum threshold for replicate analyses of tephra layers is a similarity coefficient of 0.93 (Sarna-Wojcicki and others, 1984). Focusing on ash bed #15, based on the similarity coefficient matrix constructed from EPMA data, ash bed #15 is geochemically similar to seven other Wilson Creek ash beds (#6; #7; #13; #16; #17, #19, E) in terms of major element composition. The similarity coefficients between #15 and these seven ash beds range from 0.9391 to 0.9639, well above threshold described by Sarna-Wojcicki and others (1984).

The similarity coefficients for INAA-measured trace and minor element concentrations range from 0.8160 to 0.9862 (Table 3). Ash bed #15's similarity coefficients to the other tephra layers range from 0.8331 to 0.9226. These values are below the minimum threshold, denoting that ash bed #15 is geochemically distinct from other ashes. The highest similarity coefficient of 0.9226 is between #15 and #5.

**DISCUSSION** - The major-element EPMA similarity coefficients are inadequate for differentiating among the Wilson Creek tephra layers, therefore, minor and trace elements must be used. Are these useful to distinguish ash bed #15? Using the INAA

similarity coefficients narrows the correlation to 15 and 5 (similarity coefficient = 0.9226). Plotting the chondrite normalized rare-earth elements (Figure 1) shows that the rare-earth pattern is similar in general, but there are differences in the La and Ce concentrations. Figure 2 of LaN/SmN versus SmN better illustrates the fractionation differences in these light rare-earth elements.

I also constructed a Mn vs. Rb graph (Figure 3) similar to the graph used by Metz and Mahood (1985). Unlike the precursor to the Bishop Tuff eruption, the Mono Lake ash layers do not show a temporal progression of Mn and Rb concentrations. However, included in this graph is Davis' Carson Sink bed, which plots near #15. Completing a full minor and trace element similarity coefficient calculation shows that the similarity coefficient between the Carson Sink bed and #15 is 0.9598 (Table 5). Correlation of these two ash beds by the similarity coefficient is consistent with the conclusions of Sarna-Wojcicki and Davis (1991) and Benson and others (2003).



**Figure 1**. Rare-earth element diagram of Wilson Creek ash beds #5 and #15. Gd was not determined for #15.

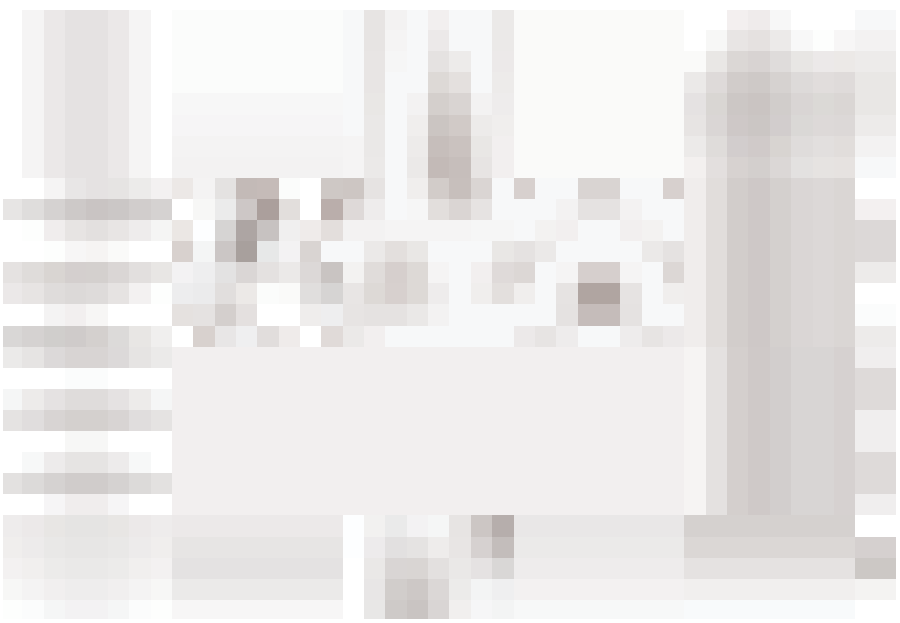


**Figure 2.** Light rare-earth fractionation of Wilson Creek ash layers. Note that #15 is an outlier from the other tephra layers.



Figure 3. Mn vs. Rb graph of Wilson Creek ash Layers. Note that # 16 is an outlier.

**CONCLUSION** - Major-element analyses is ineffective for distinguishing subtle differences in geochemical fingerprinting of the Wilson Creek ash layers; whereas, minor/trace element analyses are effective for characterizing these ash beds. Similarity coefficient matrices and graphical data show that it is possible to correlate distal ash beds and differentiate intra and inter-source ashes. Ultimately, these results lead to the conclusion that to distinguish among the Wilson Creek tephra layers minor and trace element data must be gathered. Time-of-Flight, laser ablation, inductively-coupled plasma, mass spectrometry (TOF-LA-ICP-MS) is a likely analytical tool for these types of future analyses.

### **REFERENCES**

Benson, L., Liddicoat, J., Smoot, J., Sarna-Wojcicki, A., Negrini, R., and Lund, S., 2003, Age of the Mono Lake excursion and associated tephra: Quaternary Science Reviews, v. 22, p. 135-140.

Borchardt, G.A., Aruscavage, P.J., and Millard, H.T., 1972, Correlation of Bishop Ash, a Pleistocene marker bed, using instrumental neutron activation analysis: Journal of Sedimentary Petrology, v. 42, p. 301-306.

Davis, J.O., 1978, Quaternary tephrochronology of the Lake Lahontan area, Nevada and California: Nevada Survey Archeological Research Paper 7, 137 p.

Izett, G.A., 1981, Volcanic Ash Beds: Recorders of upper Cenozoic silicic pyroclastic volcanism in the western United States; Journal of Geophysical Research, v. B11, p. 10,200-10,222.

Knott, J.R., Sarna-Wojcicki, A.M., Montanez, I.P. and Wan, E., 2007, Minor and Trace Element Analysis of Volcanic Glass Shards (Bishop Ash Bed and related tephra layers) by Solution Inductively Coupled Plasma-Mass Spectrometry: Quaternary International, v. 166, p. 79-86.

Lajoie, K.R., 1968, Quaternary stratigraphy and geologic history of the Mono basin, eastern California [Ph.D. Dissertation thesis]: Berkeley, California, University of California, Berkeley.

Metz, J.M., and Mahood, G.A., 1985, Precursors to the Bishop Tuff eruption: Glass Mountain, Long Valley, California: Journal of Geophysical Research, v. 90, n. B13, p. 11,121-11,126.

Rollinson, H., 1993, Using Geochemical Data: Evaluation, presentation and interpretation: New York, Pearson/Prentice-Hall, 352 p.

Russell, I.C., 1889, Quaternary history of Mono Valley, California: Eighth Annual Report of the U.S. Geological Survey, p. 261-394.

Sarna-Wojcicki, A.M., Bowman, H.R., Meyer, C.E., Russell, P.C., Woodward, M.J., McCoy, G., Rowe, Jr., JJ., Baedecker. P.A., Asaro, F., Michael, H., 1984, Chemical analyses, correlations, and ages of upper Pliocene and Pleistocene ash layers of east-central and southern California; U S Geological Survey Professional Paper 1293, 40 p.

Sarna-Wojcicki, A.M., and Davis, J.O., 1991, Quaternary tephrochronology, in Morrison, R.B., ed., Quaternary nonglacial geology; Conterminous U.S., Volume K-2: The Geology of North America: Boulder, Colorado, Geological Society of America, p. 93-116.

Sarna-Wojcicki, A.M., Lajoie, K.R., Meyer, C.E., Adam, D.P., and Reick, H.J., 1991, Tephrochronologic correlation of upper Neogene sediments along the Pacific margin, conterminous United States, in Morrison, R.B., ed., Quaternary nonglacial geology; Conterminous U. S., Volume K-2: The Geology of North America: Boulder, Colorado, Geological Society of America, p. 117-140.

Sample Number	Date	SiO2	Al203	Fe2O3	MgO	MnO	CaO	TiO2	Na20	K20
KRL7982-02	T50-1	50.29	18.66	9.60	6.18	0.14	8.27	1.62	4.03	1.22
KRL7982-03	T44-4	76.72	12.95	0.94	0.01	0.04	0.60	0.04	4.04	4.66
KRL7982-03	T44-4	76.61	13.08	0.96	0.02	0.06	0.58	0.04	3.97	4.69
KRL7982-04L	T49-4	77.50	12.71	0.87	0.01	0.04	0.55	0.04	3.85	4.43
KRL7982-04L	T49-4	77.02	12.87	0.99	0.03	0.04	0.63	0.03	3.91	4.48
KRL7982-04L	T49-4	77.00	13.03	0.88	0.01	0.04	0.57	0.04	3.93	4.49
KRL7982-04U	T49-5	76.91	12.96	0.96	0.02	0.05	0.59	0.03	3.94	4.55
KRL7982-04U	T49-5	77.40	12.59	0.95	0.01	0.05	0.56	0.04	3.87	4.54
KRL7982-04U	T49-5	76.76	13.08	0.93	0.02	0.04	0.59	0.04	3.97	4.58
KRL7982-05	T44-5	76.67	12.93	0.98	0.03	0.04	0.60	0.05	3.83	4.87
KRL7982-06	T49-6	76.75	12.87	0.96	0.03	0.04	0.65	0.06	3.80	4.86
KRL7982-07L	T49-7	76.73	12.94	1.04	0.03	0.02	0.61	0.06	3.82	4.76
KRL7982-08		76.68	13.00	0.97	0.02	0.03	0.64	0.05	3.84	4.77
KRL7982-09	T44-6	76.78	12.89	0.94	0.03	0.02	0.59	0.06	3.92	4.78
KRL7982-10	T44-7	76.52	13.08	0.93	0.03	0.04	0.60	0.05	3.91	4.85
KRL7982-11L	T44-8	76.76	13.01	0.92	0.02	0.03	0.63	0.04	3.89	4.70
KRL7982-11U	T45-1	76.81	12.97	0.95	0.03	0.03	0.60	0.05	3.84	4.72
KRL7982-13	T45-2	76.49	13.18	0.94	0.03	0.03	0.60	0.06	3.94	4.73
KRL7982-14	T50-3	76.58	13.06	1.00	0.03	0.04	0.65	0.05	3.88	4.71
MONO-15	T40-3	76.86	12.90	0.91	0.04	0.03	0.63	0.07	3.81	4.76
KRL7982-16	T45-3	76.66	13.17	0.83	0.03	0.02	0.68	0.07	3.91	4.64
KRL7982-17	T50-4	76.61	13.14	0.87	0.03	0.04	0.68	0.05	3.77	4.79
KRL7982-19B	T45-4	76.37	13.29	0.83	0.04	0.02	0.71	0.07	3.88	4.79
KRL7982-E	T50-2	76.77	12.99	0.98	0.05	0.04	0.66	0.06	3.69	4.76

Table 1. EPMA data for the Wilson Creek tephra layers

ш	0.3140	0.9032	0.9005	0.9473	0.9910	0.9724	0.9582	0.9691	0.9363	0.9117	0.9420	0.9700	0.9581	0.9464	0.9319	0.9356	0.9212	1	
19B	0.3172	0.8468	0.8548	0.8751	0.9201	0.8967	0.8891	0.9071	0.8868	0.8670	9088.0	0.9151	0.8879	0.9527	0.9890	0.9223	_		
17	0.3129	0.9109	0.9193	0.9507	0.9346	0.9100	0.9653	0.9211	0.9624	0.9321	0.9565	0.9273	0.9639	0.9151	0.9331	<del>-</del>			
16	0.3147	0.8563	0.8647	0.8850	0.9307	0.9068	9668.0	0.9170	0.8961	0.8773	9068.0	0.9239	0.8982	0.9631	_				
15		0.8846	0.8943	0.9181	0.9541	0.9391	0.9254	0.9520	0.9254	0.9102	0.9237	0.9503	0.9155	-					
4	0.3140	0.9301	0.9268	0.9784	0.9553	0.9444	0.9897	0.9331	0.9702	0.9366	0.9726	0.9372	<b>—</b>						
13	0.3143	0.9207	0.9257	0.9542	0.9751	0.9732	0.9448	0.9915	0.9629	0.9163	0.9605	<b>—</b>							
110	0.3104	0.9490	0.9506	0.9929	0.9475	0.9454	0.9826	0.9599	0.9934	0.9434	<del></del>								
111	0.3098	0.9743	0.9841	0.9368	0.9167	0.9028	0.9462	0.9145	0.9466	_									
10	0.3117	0.9468	0.9560	0.9871	0.9412	0.9395	92260	0.9576	_										
60	0.3104	0.9224	0.9282	0.9543	0.9770	0.9733	0.9429	-											
80	0.3124	0.9378	0.9347	0.9844	0.9593	0.9428	<b>,</b>												
07L	0.3136			0.9515	0.9712	_													
90	0.3121		0.9054	0.9461	<b>—</b>														
9	0.3109		0.9439	_															
040		0.9900	<b>—</b>																
03	0.3104	-																	
05	-																		
	07	03	040	05	90	07L	80	60	10	11	110	13	14	15	16	17	19B	ш	

 Table 2.
 Similarity Coefficients (Si, Al, Fe, Ca, Ti) calculated from electron microprobe.

Sample	R	×	Š	M	윤	S	Rb ds	ķ	Zr	Sb	ຽ	Ba	La	ల
KRL679 IV(1)*	2.68	4.62	1.79	358	0.73	0.21	182	[<75]	[150]	0.91	6.13	<35	19.0	42.7
KRL7982-2	2.22	69.0	13.30	643	4.45	23.40	17	815	pu	0.18	0.24	477	14.5	31.9
KRL7982-3	2.80	3.68	1.69	371	99.0	0.13	197	21	71	1.02	6.51	47	12.4	28.5
KRL7982-4U	2.83	3.54	1.64	371	69.0	0.10	195	pu	88	1.03	6.70	42	11.9	26.8
KRL7982-4L	2.72	3.84	1.62	369	99.0	0.09	192	pu	81	1.09	6.58	34	11.3	25.4
KRL7982-5	2.59	3.87	1.70	310	99.0	0.15	175	pu	06	06.0	5.80	88	19.5	39.9
KRL7982-6	2.72	3.87	1.73	323	0.70	0.15	181	pu	83	0.88	5.93	64	19.6	41.3
KRL679 II H-1*	2.49	4.46	1.70	307	0.70	0.17	171	[110]	[<150]	0.91	5.86	58	19.2	42.4
KRL7982-7L	2.57	3.82	1.70	312	69.0	0.15	177	pu	91	0.85	5.90	28	19.5	41.2
KRL7982-8	2.77	3.98	1.57	352	0.67	0.13	189	pu	9/	0.94	6.83	52	14.9	33.9
KRL7982-9	2.68	3.97	1.48	335	0.65	0.12	174	<30	[<130]	0.98	5.92	98	16.9	33.9
KRL7982-10	2.79	3.70	1.67	351	89.0	0.13	184	pu	[<140]	1.13	6.95	104	16.0	32.0
KRL7982-11U	2.71	4.00	1.52	349	99.0	0.12	178	[<30]	74	1.00	6.16	81	14.9	31.8
KRL7982-11L	2.76	3.82	1.51	348	99.0	0.12	179	[<30]	[<140]	1.05	6.29	85	14.8	30.7
ash 12 N.A.	not	analyzed	pa											
KRL7982-13	2.75	3.93	1.54	358	99.0	0.14	184	[<30]	77	1.04	6.25	45	13.4	30.5
KRL7982-14	2.76	3.78	1.53	351	0.67	0.16	176	[<30]	[<140]	1.07	90.9	78	15.6	33.2
KRL MONO-15*	2.65	4.53	1.81	327	0.65	0.22	179	[<75]	117	0.95	6.35	161	22.2	54.1
KRL7982-16	2.75	3.72	2.26	362	0.58	0.13	215	pu	74	1.1	8.00	40	12.3	23.5
KRL7982-17	2.70	4.13	2.12	338	0.61	0.47	197	pu	98	1.05	6.89	46	18.5	35.9
ash 18 N.A.	not	analyzed	þ											
KRL 679 IIB-19*	2.63	4.60	2.03	355	0.62	0.22	196	[<75]	129	1.06	7.26	77	15.8	33.5
LD-10 (JOD)*	2.67	4.42	1.87	333	0.64	0.20	183	[<75]	111	1.08	89.9	164	20.8	45.7
KRL7982-19B	2.65	3.84	1.73	324	0.58	0.17	195	pu	64	1.07	6.83	75	15.9	31.0
KRL7982-E	2.59	4.17	1.73	324	0.64	0.15	172	31	85	96.0	6.20	177	21.9	45.1
KRL679-409C*	2.36	4.50	1.88	309	0.57	0.14	175	[<75]	126	1.07	6.63	137	18.1	39.1

 Table 3. INAA data for the Wilson Creek tephra layers. (PART 1)

Sample	Z	Sm	3	9	g L	Š	Е	d V	3	Ŧ	Ta	丰	5
KRL679 IV(1)*	21	4.42	0.18	4.30	29.0	4.40	0.43	2.80	0.41	4.04	2.21	19.8	6.12
KRL7982-2	16	3.69	1.17	3.38	0.47	2.67	pu	1.28	0.20	2.44	1.01	<del></del>	0.24
KRL7982-3	15	4.29	0.14	4.07	0.72	4.81	0.47	2.94	0.44	4.06	2.39	19.9	7.28
KRL7982-4U	4	4.36	0.13	4.69	0.73	4.82	0.45	3.04	0.46	4.15	2.43	19.6	7.30
KRL7982-4L	4	4.18	0.12	4.40	0.73	4.78	0.46	2.97	0.45	4.08	2.37	19.8	7.45
KRL7982-5	17	4.36	0.22	4.20	0.63	4.10	0.39	2.52	0.39	3.89	1.99	18.7	6.39
KRL7982-6	20	4.56	0.22	4.07	99.0	4.36	0.43	2.71	0.40	4.05	2.09	19.8	6.64
KRL679 II H-1*	20	4.34	0.20	pu	0.65	4.16	0.41	2.67	0.40	4.15	2.01	19.2	5.79
KRL7982-7L	18	4.41	0.20	4.21	99.0	4.49	0.41	2.62	0.40	4.02	2.03	19.7	09.9
KRL7982-8	15	4.29	0.20	3.80	99.0	4.43	0.42	2.69	0.40	4.04	2.19	19.6	6.92
KRL7982-9	15	3.99	0.23	3.99	09.0	4.04	0.39	2.51	0.38	3.53	1.95	18.8	6.22
KRL7982-10	15	4.14	0.24	3.94	09.0	3.97	pu	2.62	0.40	3.88	2.11	19.5	6.78
KRL7982-11U	14	4.00	0.21	4.08	0.62	4.12	0.40	2.58	0.39	3.69	2.06	18.6	6.47
KRL7982-11L	15	4.02	0.21	3.92	0.64	3.67	0.41	2.64	0.40	3.78	2.05	18.3	89.9
ash 12 N.A.	not	analyzed	pa										
KRL7982-13	4	4.08	0.20	3.90	0.64	4.30	0.42	2.68	0.40	3.86	2.10	18.7	6.52
KRL7982-14	16	4.06	0.22	3.84	0.64	4.29	0.40	2.58	0.38	3.87	2.02	18.9	6.39
KRL MONO-15*	18	4.02	0.27	pu	0.58	3.80	0.37	2.37	0.36	3.90	1.96	19.9	6.00
KRL7982-16	12	3.57	0.19	3.68	0.59	3.98	0.41	2.70	0.41	3.80	2.30	22.7	8.34
KRL7982-17	15	3.58	0.23	4.24	0.59	4.05	0.39	2.45	0.37	3.80	2.06	21.4	6.39
ash 18 N.A.	not	analyzed	þá										
KRL 679 IIB-19*	15	3.39	0.26	pu	0.55	3.75	0.36	2.42	0.37	3.81	2.22	20.8	6.49
LD-10 (JOD)*	19	3.86	0.27	pu	0.59	3.99	0.39	2.45	0.34	3.93	2.01	20.2	6.17
KRL7982-19B	13	3.23	0.23	3.60	0.51	3.50	pu	2.30	0.35	3.55	5.09	20.2	7.27
KRL7982-E	18	3.90	0.27	3.37	0.55	3.76	0.39	2.21	0.32	3.69	1.89	18.9	6.30
KRL679-409C*	17	3.34	0.24	3.30	0.55	3.69	0.38	2.33	0.35	3.54	1.84	19.3	00.9

 Table 3. INAA data for the Wilson Creek tephra layers. (PART 2)

	KRL 679	IIB-19*	0.8739	0.8724	0.8558	0.8574	0.8771	0.8687	0.8600	0.8692	0.9123	0.9067	0.9281	0.9080	0.9010	0.8963	0.9137	0.8895	9006.0	0.9585	-	
	KRL7982 KRL7982 KRL 679	-17	0.8912	0.8622	0.8455	0.8478	0.9018	0.8929	0.8845	0.8935	0.9025	0.9128	0.9175	0.8987	0.8923	0.8851	0.9022	0.9081	0.8976	_		
	KRL7982	-16	0.8347	0.8798	0.8705	0.8786	0.8201	0.8250	0.8160	0.8215	0.8682	0.8411	0.8784	0.8630	0.8683	0.8806	0.8525	0.8222	<b>—</b>			
1	KRL	MONO-15*	0.9113	0.8514	0.8331	0.8421	0.9226	0.9180	0.9111	0.9191	0.8837	0.9067	0.9020	0.8952	0.8905	0.8830	0.9004	<del></del>				
	KRL798 KRL679 II KRL7982 KRL798 KRL798 KRL7982 KRL7982-KRL7982- KRL7982 KRL7982 KRL	-14	0.9186	0.9072	0.8928	0.8978	0.9387	0.9219	0.9246	0.9293	0.9594	0.9661	0.9606	0.9788	0.9728	0.9660	<del></del>					
	. KRL7982	-13	0.9127	0.9347	0.9193	0.9261	0.9154	0.9108	0.9089	0.9115	0.9587	0.9368	0.9552	0.9701	0.9805	_						
	KRL7982	111	0.9091	0.9174	0.9023	0.9093	0.9203	0.9121	0.9122	0.9166	0.9585	0.9508	0.9571	0.9845	<b>—</b>							
	KRL7982-	110	0.9066	0.9069	0.8922	0.8992	0.9277	0.9090	0.9099	0.9155	0.9534	0.9642	0.9579	<b>—</b>								
	KRL7982	-10	0.9228	0.9234	0.9104	0.9089	0.9284	0.9240	0.9205	0.9283	0.9660	0.9408	-									
	KRL798	2-9	0.9002	0.8767	0.8628	0.8701	0.9371	0.9133	0.9177	0.9206	0.9299	-										
	KRL798	2-8	0.9307	0.9361	0.9256	0.9244	0.9189	0.9315	0.9239	0.9311	-											
	KRL7982	٦٢-	0.9634	0.8941	0.8802	0.8748	0.9782	0.9862	0.9830	-												
	KRL679 II	#- +-	0.9591	0.8870	0.8765	0.8685	0.9730	0.9759	-													
	KRL798	2-6	0.9709	0.8963	0.8816	0.8773	0.9646	<b>—</b>														
	KRL798	2-5	0.9422	0.8815	0.8663	0.8621	-															
	KRL679 KRL798 KRL7982 KRL7982 KRL798	4	0.8889	0.9699	0.9762																	
	KRL7982	-4n	0.9078 0.8930	0.9750	-																	
	KRL798	2-3	0.9078	<b>,</b>																		
	KRL679	IV(1)*	-															*			*	
			KRL679 IV(1)*	KRL7982-3	KRL7982-4U	KRL7982-4L	KRL7982-5	KRL7982-6	KRL679 II H-1*	KRL7982-7L	KRL7982-8	KRL7982-9	KRL7982-10	KRL7982-11U	KRL7982-11L	KRL7982-13	KRL7982-14	KRL MONO-15*	KRL7982-16	KRL7982-17	KRL 679 IIB-19*	

Table 4. Similarity Coefficients calculated from INAA.

	0.9598	
19.9	20.2	
3.90	3.93	
0.36	0.34	
2.37	2.45	
0.58	0.59	
4.02	3.86	
54.1	45.7	
22.2	20.8	
6.35	89.9	
179	183	
0.65	0.64	
327	333	
1.81	1.87	
KRL MONO-15*	Carson Sink	
	† 1.81 327 0.65 179 6.35 22.2 54.1 4.02 0.58 2.37 0.36 3.90 19.9	15*         1.81         327         0.65         179         6.35         22.2         54.1         4.02         0.58         2.37         0.36         3.90         19.9           1.87         333         0.64         183         6.68         20.8         45.7         3.86         0.59         2.45         0.34         3.93         20.2

**Table 5.** Selected elemental concentrations for ash bed #15 and the Carson Sink bed. Fe is measured by EPMA and is in weight %. All other concentrations are in parts per million. SC is similarity coefficient.

### Probable Discovery of a New Uranium Mineral, Consolidated Tungsten Mine Skarn, Tulare County, California

### SHAYDA NIKJOO

California State University, Fullerton Department of Geological Sciences Faculty Advisor: Dr. Diane Clemens-Knott

**ABSTRACT** - A calcsilicate rock collected from the area surrounding a Jurassic quartz diorite pluton located in the Sierra Nevada batholith contains four grains of what is likely to be a new uranium mineral. Electron microprobe analyses of the four grains are consistent with the formula CaUSi<sub>3</sub>O<sub>8</sub>(OH)<sub>2</sub>. This mineral forms blades that appear to radiate outward from grains of uraninite (UO<sub>2</sub>) or metastudtite (UO<sub>4</sub>.2H<sub>2</sub>O). The host rock contains an abundance of wollastonite (CaSiO<sub>3</sub>) and turquoise-blue fluorapatite [Ca<sub>5</sub>(PO<sub>4</sub>)<sub>3</sub>F], implying hydrothermal metamorphism involving a F- and H<sub>2</sub>O-rich fluid. The host rock also contains the rare Ba-K feldspars celsian (BaAl<sub>2</sub>Si<sub>2</sub>O<sub>8</sub>) and hyalophane [(K,Ba)Al(Si,Al)<sub>3</sub>O<sub>8</sub>], which are known to form in low- to medium-grade hydrothermal metamorphic environments (Moro et al., 2001). Deposition of new bismuth-bearing phosphates and the rare zeolite, brewsterite-Ba [(Ba,Sr)Al<sub>2</sub>Si<sub>6</sub>O<sub>16</sub>•5(H<sub>2</sub>O)], elsewhere in the Consolidated Tungsten Mine skarn have been attributed to the latest stages of hydrothermal metamorphism (Berekian, 2008). Taken together, these results suggest that high-magnification (e.g. x1500 to x4500) examination of grain boundaries and cracks in hydrothermally altered rocks may lead to the discovery of a variety of new minerals, ultimately improving our understanding of element mobility in low temperature, fluid-rich environments.

INTRODUCTION - The Consolidated Tungsten Mine (CTM) skarn located in the western Sierra Nevada Mountains contains a variety of unusual mineral assemblages. Previous research led to the discovery of six new bismuth- and rare earth element-bearing phosphates present as bacteria-sized "nanominerals" in a single garnet-quartz-epidote

rock (Berekian, 2008). These findings suggest that thorough examination of other rock types in this deposit might lead to the discovery of additional new minerals.

This study focuses on the mineralogy of a single quartz-wollastonite-calcite rock (sample MM100-Af-13) from the CTM skarn that contains a variety of feldspars, minor diopside, grossular garnet, and distinctive turquoise fluorapatite (Fig. 1). This bright white rock type is rare relative to other rock types in the CTM waste piles, the source of virtually all samples studied by Berekian (2008). High magnification examination of grain boundaries and cracks led to the discovery of several uranium-rich grains that did not appear to match the chemistry of any known U-rich minerals. The purpose of this research is to assess whether this is a new U-rich mineral and to describe its association with the relatively rare cesium- and barium-rich feldspars. The discovery of a new mineral may lead to an improved understanding of uranium geochemistry and of the low temperature, fluid-rich phase of mineralization that characterized the final stage of the CTM skarn formation.

**BACKGROUND** - Located in Tulare County in the western foothills of the Sierra Nevada Mountains, the Consolidated Tungsten Mine (CTM) skarn formed around a Jurassic quartz diorite pluton (Clemens-Knott and Saleeby, 2005) that intruded into interbedded carbonate and siliciclastic sediments of the Kings Sequence (Fig. 2; Saleeby and Busby-Spera, 1992). This reduced skarn is dominated by calcite, quartz, garnet, epidote, and pyroxene, with lesser wollastonite, barite, scheelite, feldspar, and

zircon, and exhibits variable retrograde alteration (Berekian, 2008; Newberry, 1980). Tungsten-bearing skarns, like the CTM skarn, are typically associated with calc-alkaline intrusions emplaced relatively deep in the crust (Robb, 2005). The nearby Chickencoop Canyon deposit contains barium-rich feldspars and U-rich mineral phases that are similar to the mineralogy of the CTM skarn (Walstrom and Dunning, 2003).

Skarns are formed by the metasomatic, or hydrothermal alteration, replacement of carbonate and silicate minerals by calc-silicate minerals during either contact or regional metamorphism (Einaudi et al., 1981). Contact metamorphism, which formed the CTM skarn, occurs when a body of magma intrudes into preexisting rocks releasing heat and fluids into the surrounding rocks, while regional metamorphism occurs during mountain-building events when a large area is heated and deformed. Skarns contain multiple phases where early recrystallization occurs at high temperatures (stage 1) creating anhydrous minerals, which are later overprinted in stage 3 by hydrous minerals that form at lower temperatures during cooling (Fig. 3; Corbett and Leach, 1998). There are two types of skarns, prograde and retrograde. Retrograde skarns, like the CTM skarn, are dominated by hydrous mineral phases that formed in stage 3, a low-temperature period characterized by complex reactions and the precipitation of precious metals. Metal precipitation is related to decreasing temperatures of the ore fluids, fluid mixing, and/or neutralization of the ore fluids by carbonate reactions (Robb, 2005).

METHODS - Sample MM100-Af-13 was collected from mine tailings of the CTM skarn (Berekian, 2008) and was analyzed petrographically prior to microanalysis. Microanalytical work was conducted at the California Institute of Technology with help from Dr. Ma Chi, Research Scientist and Analytical Facility Manager. First, the scanning electron microscope (SEM) was used to analyze the rockforming minerals, to explore grain boundaries and mineral inclusions at an extremely high magnification (x1500 to x4500), and to locate uranium-rich grains. Preliminary compositions determined by the SEM guided our decision regarding which elements

were to be targeted using the electron microprobe. The electron microprobe was used subsequently to determine more accurate and precise chemical analyses of the uranium-rich grains.

The SEM and electron microprobe utilize similar technologies. Both instruments produce a beam of high-energy electrons that focus on an approximate 1-micron spot of interest within the thin section. The electron beam excites electrons in the target atoms causing the atoms to move to higher orbitals. However, the electrons are not stable in those orbitals and rapidly decay back to their previous orbitals, emitting the absorbed energy as X-rays. Each element emits a characteristic suite of X-rays, having specific wavelengths and relative abundances. Energy-dispersive X-ray spectrometers (EDS) on each instrument collect the X-ray information, which is then sent to a software program called INCA. INCA is responsible for the measurement and calibration functionality and converts the energy spectrum into an analysis of the identity and abundance of each atom in the target mineral. INCA presents the data in both weight percent and atomic percent abundances. Ratios of atomic abundances were compared to those of known U-bearing minerals listed in the Athena Minerals database (http://athena. unige.ch/athena/mineral/mineral.html). When no match was found within the Athena database, the atomic abundances were used to construct possible electronically neutral chemical formulas. One complication in this procedure is that not all elements (e.g., carbon, hydrogen, and typically oxygen) can be analyzed using these instruments. Oxygen content, however, was measured with the electron microprobe; this uncommon analytical strategy was chosen due to the possible presence of multiple oxygen-bearing units (e.g., O<sup>2-</sup>, OH<sup>-</sup>, H<sub>2</sub>O).

**RESULTS** - In addition to quartz and wollastonite, MM100-Af-13 contains a variety of rare feldspars. The feldspar chemical analyses were determined by the SEM and the relative atomic abundances of Ba-Na-K and Ba-Ca-K are displayed on ternary plots (Fig. 4). The most abundant feldspar analyzed is celsian (BaAl<sub>2</sub>Si<sub>2</sub>O<sub>8</sub>) (Fig. 5). Celsian is a rare, Ba-rich feldspar that forms during low- to medium-grade hydrothermal metamorphism, consistent with the

petrogenesis of the CTM skarn (Moro et al., 2001; Berekian, 2008). One grain each of hyalophane [(K,Ba)Al(Si,Al)<sub>3</sub>O<sub>8</sub>], an intermediate Ba-K feldspar, and calciocelsian were also analyzed. The calciocelsian contained small amounts (<1.32 atomic %) of calcium and sodium, making it essentially a bariumrich orthoclase (Fig. 5B). These feldspars are found intergrown with quartz, which together appear to pseudomorph an unidentified large mineral grain that has grown within a finer groundmass called a porphyroblast. Further characterization of this texture is required to better understand the apparent reaction relationship.

Four crystals of a uranium-rich mineral were found along grain boundaries and along cracks within fluorapatite, wollastonite, and feldspar crystals (Fig. 6). These U-rich grains form blades or needles, ~5-20 microns long, that radiate as sunbursts from crystals of uraninite (UO<sub>2</sub>) and possibly metastudtite (UO<sub>4</sub> • H<sub>2</sub>O) (Fig. 7). The formation of needles or sheets is typical for oxidation and hydration products of uraninite (Hazen et al., 2009). Six analyses of the microprobe oxide percent abundances of the grains of interest define an average composition (Table 1) that is unlike all recognized uranium-calciumsilicate minerals (Table 2). This average composition is consistent with the proposed chemical formula CaUSi<sub>3</sub>O<sub>8</sub>(OH)<sub>2</sub> (Table 2), though use of Raman spectrometry is required to determine the presence and abundance of hydroxyl in this new phase and to confirm the possible association with metastudtite. Interestingly, this possible new mineral is similar in composition to the "unnamed" mineral noted by Burns and Finch (1999) (Table 2), with the exception of the H<sub>2</sub>O stoichiometry.

**DISCUSSION** - The proposed chemical formula does not correspond to any uranium-bearing minerals listed in the Athena database (Table 2) or named in Burns and Finch (1999). In order to confirm that this is indeed a new mineral, however, the structure of the mineral must be determined and the presence of hydroxyl needs to be confirmed. Both types of analysis require larger grains; thus, colleague Dr. Ma Chi will wait until larger grains of the same minerals have been located before embarking on the next phase of research.

Many observations support formation of this uranium-rich mineral during the low-temperature, hydrothermal stage 3 of skarn development (Corbett and Leach, 1998). First, the associated celsian and hyalophane are thought to form in low temperature hydrothermal environments (Essene et al., 2005). Second, though the stability of the rare zeolite brewsterite-Ba has not been calibrated. no natural zeolites are known to be stable above 250°C (Chipera and Apps, 2001). The presence of crack-filling brewsterite-Ba suggests that associated minerals found in cracks and along grain boundaries formed at similarly low temperatures. Third, uranium-bearing accessory minerals, including uraninite and metastudtite, are thought to crystallize from reducing hydrothermal fluids (Burns and Finch, 1999). Fourth, hydration of uranium oxides forms a variety of chemically complex uraniumbearing minerals, the number of which may have increased over time as Earth's atmosphere began oxidizing and hydrothermal environments became more diverse (Hazen et al., 2009). Many of these secondary minerals grow as crystals radiating from the original uranium oxide, similar to the sunburst texture observed in MM100-Af-13.

**CONCLUSIONS** - These results confirm the hypothesis that high magnification examination of grain boundaries and cracks in the CTM skarn may lead to the discovery of new minerals (Berekian, 2008). The specific mineral discovery described in this study contributes to our growing understanding of element mobility and recrystallization in low temperature fluid-rich environments and expands our understanding of uranium mineralogy.

72

#### **REFERENCES**

Berekian, B.J., 2008, A Mineralogical Study of the Consolidated Tungsten Mine Skarn, Tulare County, California: CSUF M.Sc. Thesis, p. 103.

Burns, Peter C., and Finch, Robert, 1999, Uranium: Mineralogy, Geochemistry, and the Environment: Washington D.C., Reviews in Mineralogy, vol. 38. p. 92-137.

Chipera, S. J. and Apps, J. A., 2001, Geochemical stability of natural zeolites. In Bish, D.L. and Ming, D.W., Eds., Natural zeolites: Occurrence, properties, applications, p. 1-67, Reviews in Mineralogy and Geochemistry, Mineralogical Society of America, Washington, DC.

Clemens-Knott, Diane, and Saleeby, J., 2005, Geochronologic Constraints on Early Cretaceous Deposition of Nonmarine Sediments and Volcanics, and Synplutonic Deformation, Western Sierra Nevada Batholith, CA, GSA Abstracts with Programs.

Corbett, G.J., and Leach T.M., 1998: Southwest Pacific Gold-Copper Systems: Structure, Alteration, and Mineralization: Special Publication 6, Society of Economic Geologists, p. 238.

Deer, W.A., Howie, R.A., and Zussman, J., 1992, An Introduction to the Rock-Forming Minerals: England, Pearson Education Limited, second edition.

Einaudi, M.T., Meinert, L.D., and Newberry R.J., 1981, Skarn Deposits: Economic Geology 75th Anniversary Volume, p. 317-391.

Essene, E.J., Claflin, C.L., Giorgetti, Giovanna, Mata, P.M., Peacor, D.R., Arkai, P., and Rathmell, M.A., 2005, Two-, Three- and Four-feldspar Assemblages with Hyalophane and Celsian: Implications for Phase Equilibria in BaAl2Si2O8-CaAl2Si2O8-NaAlSi3O8-KAl-Si3O8: European Journal of Mineralogy, vol. 17, p. 515-535.

Hazen, Robert M., Ewing, Rodney C., and Sverjensky, Dimitri A., 2009, Evolution of Uranium and Thorium Minerals: American Mineralogist, vol. 94, p. 1293-1311.

Moro, Maria C., Cembranos, Maria L., and Fernandez, Agustina, 2001, Celsian, (Ba,K)-Feldspar and Cymrite From Sedex Barite Deposits of Zamora, Spain: The Canadian Mineralogist, vol. 39, p. 1039-1051

Pierre Perroud. "Athena Mineralogy." 2005, Web. 11 November 2009.

Robb, Laurence, 2005, Introduction to Ore-Forming Processes: Blackwell Publishing, p. 108-117.

Saleeby, J.B., and Busby-Spera, C., 1992, Early Mesozoic Tectonic Evolution of the Western U.S. Cordillera. In Burchfiel, B.C., Lipman, P.W., and Zoback, M.L., Eds., The Cordilleran Orogen: Conterminious U.S.: Geological Society of America, The Geology of North America, Boulder Colorado.

Walstrom, Robert E., and Dunning, Gail E., 2003, The Baumann Prospect, Chickencoop Canyon, Tulare County, California: The Mineralogical Record, vol. 34, p. 159-166.

**ACKNOWLEDGEMENTS** - Proud acknowledgment of the 2008 FDC Faculty-Student Research Grant and the California Federation of Mineralogical Societies, Inc. for funding, Dr. Diane Clemens-Knott, whose exceptional knowledge and support made this project possible, to Dr. Ma Chi from the California Institute of Technology, and Beverly Berekian for help conducting the research.

Pages 75-79 not displayed due to online digital upload size restrictions. Please contact *Dimensions* editorial staff for original copy of *Dimensions Journal 2010*.

	0	Al <sub>2</sub> O <sub>3</sub>	SiO <sub>2</sub>	FeO	CaO	$P_2O_5$	UO <sub>2</sub>	$Ce_2O_3$
	Oxide %	Oxide %	Oxide%	Oxide%	Oxide %	Oxide %	Oxide %	Oxide%
Analysis 11	2.963	0.121	31.954	0.245	9.288	0.083	43.773	0.000
Analysis 12	4.694	0.040	31.776	0.281	8.979	0.138	45.782	0.000
Analysis 13	5.723	0.191	30.848	0.151	9.106	0.029	45.250	0.000
Analysis 18	4.091	0.167	30.469	0.019	8.612	0.093	45.164	0.148
Analysis 22	6.550	0.000	30.404	0.000	8.468	0.177	46.020	0.085
Analysis 23	2.280	0.042	30.337	0.000	9.217	0.179	47.604	0.008
Average								
Composition								
(n=6)	4.384	0.094	30.965	0.116	8.945	0.117	45.599	0.040
Standard								
Deviation	1.619	0.077	0.722	0.128	0.334	0.059	1.255	0.063

 Table 1. Electron microprobe data and calculated average composition of unknown uranium mineral.

			11.6:	
Mineral Name	Chemical Formula	U:Ca	U:Si	U:O
Ursilite	$(Mg, Ca)_4(UO_2)_4(Si_2O_5)_5(OH)_6(H_2O)_{15}$	1:1	2:5	2:27
Unnamed	$Ca_2(UO_2)_2(Si_2O_5)_3*10H_2O$	1:1	1:3	2:29
Uranophane Group				
Uranophane	$Ca(UO_2)_2(SiO_3OH)_2(H_2O)_5$	2:1	1:1	2:15
Weeksite Group				
Haiweeite	$Ca(UO_2)_2[Si_5O_{12}(OH)_2](H_2O)_{4.5}$	2:1	2:5	2:22.5
Metahaiweeite	$Ca(UO_2)_2[Si_5O_{12}(OH)_2](H_2O)_n (n<5)$	2:1	2:5	2:<23
Proposed Mineral	CaUSi <sub>3</sub> O <sub>8</sub> (OH) <sub>2</sub>	1:1	1:3	1:10
i i oposeu minerai	Ca031308(011)2		1.3	1.10

Table 2. Names, formulas, and calculated atomic ratios of all known uranium-calcium-silicate minerals (Burns and Finch, 1999) compared to unknown mineral (this study).

# A Re-sampling Approach for the Comparison of Two Random Curves with an Application in Neuronal Data Analysis

#### **SUZETTE PUENTE**

Advisor: Dr. Sam Behseta

ABSTRACT - In a considerable number of neurophysiological studies, neuronal spiking data is acquired through multiple conditions. These data are typically obtained during the performance of experimental tasks with a large number of trials. Complex statistical methods are needed to summarize the outcomes of such experiments in a way that they can be considered for further scientific inquiry. In this project, we develop nonparametric permutation tests for two groups of Bayesian curves fitted to neuronal histograms of spiking intensities in order to statistically calibrate their differences. We show that our permutation tests are quite sensitive in detecting such differences both locally, within a small window of time, and globally over the entire range of the experimental time frame.

1. INTRODUCTION - This paper is motivated by a neurophysiological study of a group of neurons recorded from the primary motor cortex (M1) area of a Macaque monkey during the performance of a sequential task of reaching a set of five targets that were arranged horizontally on a touch sensitive screen. The targets were numbered 1 to 5 from left to right and would be illuminated prior to the monkey reaching for them (Matsuzaka, Picard, & Strick, 2001). The animal was trained to contact the target within 800 ms of its appearance. In the case of errors or no response, the trial was repeated. The process of target display, contact, and new target display was repeated continuously for a large number of trials (e.g. more than 3000) per day. The animal was trained to respond to the visual stimuli under two experimental scenarios, thereafter referred to as experimental modes. In both modes, the reaching task was highly practiced by the monkey (more

than 2 years). This long-term training allowed the scientists to fully investigate the emergence of M1 properties in the presence of highly practiced tasks (Matsuzaka, Picard, & Strick, 2001). In the first mode of the experiment, a sequence of targets would appear on the screen in a repeating order. For example, the monkey would have to respond to the repeating triplets of 2-3-4 targets. In the second mode, targets would appear in a pseudo-random order. Single neurons from M1 were recorded over the course of more than a year. In both modes, a 100 ms delay separated a response and the appearance of the next target. This short delay prevented the animal from initiating voluntary responses. The neuroscientists delayed the appearance of the next target after a correct response by 400 ms. At times that the monkey made a correct response during this delay, a new target did not appear and the task was incremented to the next target in the sequence. Therefore, a highly trained monkey did perform the correct sequence in the repeating mode without visual cues to guide their movements. Consequently, for each selected neuron, spiking data in both modes were recorded.

An interesting scientific question then emerged as to examine the firing patterns of a group of selected neurons when recorded under the two modes described above. A series of analyses related to this experiment are reported in Behseta & Kass (2005) and Kass, Ventura, & Cai (2003). Neuronal data are acquired by discretizing continuous functions (curves) fitted to the Peri Stimulus Time Histogram (PSTH) of spike recordings. In this paper, we develop a permutation-based statistical inferential tool that would allow the scientists to compare the spike

patterns of the studied neurons in the two modes at any given subinterval of the experimental time window.

**2. METHODS** - *2.1. Smoothing Neuronal Histograms*. In a typical neurophysiological experiment such as the one described in section 1, microelectrodes are inserted between the cortex and the white matter of the monkey's brain to record the spike activity of a single neuron while the monkey is performing the various stages of the experimental task (i.e. the process of reaching for the target). Consequently, two types of data are being collected: 1) neuronal data, consisting of spiking occurrences, and 2) behavioral data, reflecting the animal's responses to the experimental stimuli. By combining the two datasets, scientists seek interesting spike patterns in correlation with behavioral responses. The main focus of this paper is the analysis of neuronal data. Utilizing the graphical tools known as raster plot and the PSTH, one can study neuronal data in conjunction with the behavioral responses (see Figure 1).

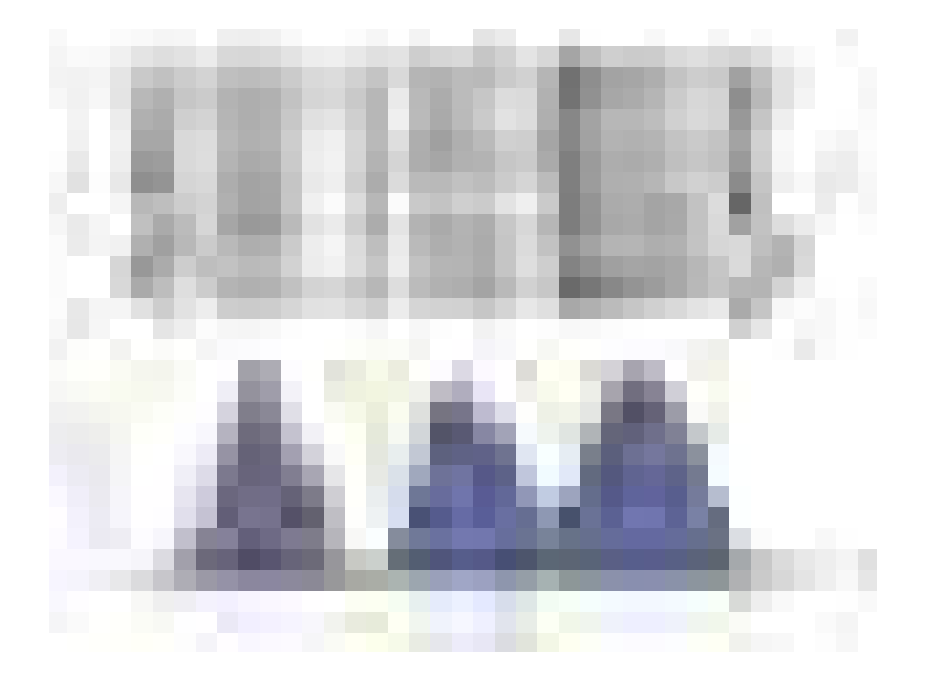


Figure 1. An example of a raster plot (top) and a PSTH (bottom) for spike recordings of a single neuron over all trials. Each row in the raster plot represents a trial. Tick marks are spiking times. The triangles on the raster plot mark the time the monkey reached the target. The horizontal axis is the experimental time. The vertical axis is the firing rate obtained via dividing the total spiking occurrences in each bin by the number of trials. The curve fitted on the PSTH is obtained via BARS.

Each row in the raster plot (shown in Figure 1) represents a trial and times at which a spike occurred are indicated by a tick mark. In our analysis, an experimental window of 300 milliseconds (ms) was considered. This time window begins at 200 ms prior to reaching a target (i.e., hitting a 3 in the 2-3-4 triplet), all the way to 100 ms after the target reach. By slicing the window of 300 ms into slices of 10 ms, and through pooling the spike occurrences within each bin, we create the PSTH plots shown in the lower part of Figure 1. An advantage of PSTH is that one can look for peaks and troughs of overall spike occurrences against time. Since the number of trials in the two modes could be different, it is necessary to make the spike recordings of one bin in the random mode comparable to its counterpart in the repeating mode. To do this, we divide the spike counts in that particular bin by the number of trials in each mode.

This transformation from spike counts to firing rates will make the comparison between the two modes meaningful.

Statistically, we find it insufficient to simply compare the two histograms. The reason for this argument is that we view each histogram as one realization of an underlying theoretical stochastic process that generates data. In other words, one can argue that if the same experiment was repeated, we will probably obtain different spike histograms. To capture the randomness of spike occurrences, we fit a statistical model to the histograms in each mode. A statistical model in this setting translates into a curve fitted to the PSTH. This mathematical procedure is known as histogram smoothing.

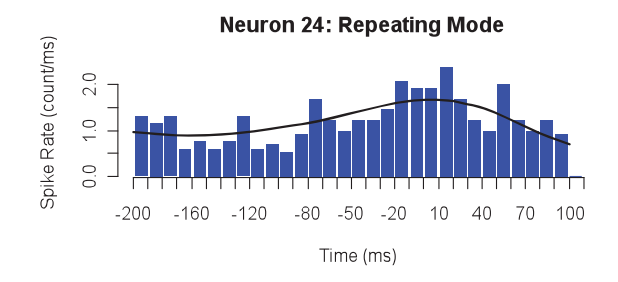
There exist a large number of smoothing technologies. The one we work with in this paper is called Bayesian Adaptive Regression Splines (BARS) (DiMateo et al., 2001, Wallstrom et al., 2001). Here, we briefly describe this complex smoothing technique: BARS utilizes data  $Y_1 \dots Y_p$  evaluated at an arbitrary time point  $t = t_1 \dots t_p$  with each  $Y_j$  assumed to depend probabilistically on some function  $f(t_j)$  through the model

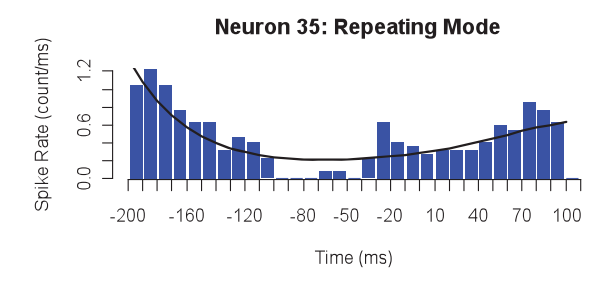
$$Y_j \sim p(y_j | \theta_j, \zeta)$$
  
 $\theta_j = f(t_j)(1)$ 

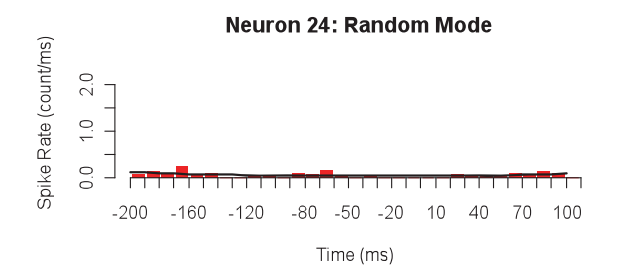
It is quite useful to let f be represented via a cubic-spline, having knots at unknown locations  $\xi_i \dots \xi_k$ . This is due to the fact that cubic-splines are quite flexible in capturing a wide range of functional forms.

Model (1), also known as the hierarchical model in statistical literature, includes a vector of auxiliary parameters  $\xi$  to indicate generality. Typically, these parameters are included in the model to represent the unavoidable noise or error associated with the neuronal recordings. We can now represent f(t) in terms of basis functions of splines or  $b_{\xi,h}(t)$  as  $f(t) = \sum_h b_{\xi,h}(t) \beta_{\xi,h}$  which would result in  $f(t_1),\dots,f(t_p)$  or the vector form  $(f(t_1),\dots,f(t_p))^T = X_\xi \beta_\xi$ , where  $X_\xi$  is the design matrix of the generalized linear model and  $\beta_\xi$  is the coefficient vector. Typically, in any curve-fitting with splines the main challenge is to choose the optimal number of knots and their positions. BARS employs a complex technology known as reversible jump Markov Chain Monte Carlo (MCMC) to sample from a posterior distribution on the knot set  $\xi$  (Green, 1995) in a Bayesian setting. This, in turn, produces samples from the posterior distribution on the space of all possible splines.

The main advantage of using BARS then is it can be used as an automatic curve fitting procedure in which both the number of knots and their locations are optimized. In figure 2, we demonstrate the fitted curves obtained by implementing BARS over the two modes of two of the selected neurons in our analysis. The top panel is the repeating mode and the lower panel is the random mode. Left panel is a neuron responding differentially to the two modes, whereas the neuron in the right side seems to respond non-differentially to the two task objectives for at least the first half of the time period.







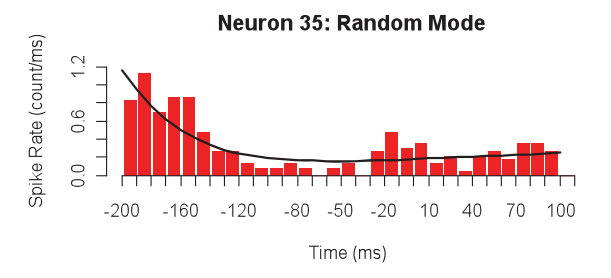


**Figure 2.** PSTH for neurons no. 24 (left panel) and no. 35 (right panel) with the corresponding BARS (fitted curves) shown in the repeating mode (top) and the random mode (bottom). Neuron 24 seems to respond differently to the task objectives in the two modes, whereas neuron 35 seems to behave similarly to the two task objectives for most of the time window.

2.2. Statistical Analysis of the Fitted Curves. The experimental window has a length of 300 milliseconds. We considered partitioning the total time into 30 bins of size 10 milliseconds each. We then fitted BARS to histograms in both modes. This resulted in two curves that may alternatively be represented as two vectors of size 30, namely,  $\hat{u}^1 = (f^1(t_1), \dots, f^1(t_{30}))$ , and  $\hat{u}^2 = (f^2(t_1), \dots, f^2(t_{30}))$ , where superscripts 1 and 2 reflect the fitted curve to the repeating mode and the random mode respectively. We are interested in making a statistical inference about the difference curve or  $\hat{u}_{obs} = \hat{u}^1 - \hat{u}^2$ . Alternatively, we can think of a set of 30 hypotheses:

$$H_0: U^1(t) = U^2(t)$$
  
 $H_a: U^1(t) \neq U^2(t)$ 

for  $t=1,\ldots,30$ , where,  $U^1(t)$ , and  $U^2(t)$  are two unknown curves at time bin t. In our neurophysiological analysis,  $U^1(t)$  and  $U^2(t)$  represent the theoretical firing rates of the two experimental modes.

We address this hypothesis testing problem via a test-statistic obtained through a permutation method. We note that the two histograms are obtained through dividing the total number of spiking occurrences in each bin by the number of trials. Let  $tr^1$  denote the number of trials in the repeating mode, and  $tr^2$  represent the number of trials in the random mode. Thus,  $tr_{tot} = tr^1 + tr^2$  is the total number of trials in both modes. In a permutation scheme (Efron, 1982), we combine the  $tr_{tot}$  many trials together, followed by randomly assigning  $tr^1$  many of them to group 1, and  $tr^2$  remaining ones to group 2. As a result of this random assignment, we essentially create two new histograms that may be individually modeled by BARS. Let us call these fitted curves to the repeat-

ing and the random mode  $u_b^1$  and  $u_b^2$  respectively. Next, we can calculate the difference curve, as represented before. That is,  $u_b = u_b^1 - u_b^2$ . Now, we repeat this procedure B times, for  $b = 1, \ldots, B$ , we obtain  $u_1, \ldots, u_B$  difference curves. For a relatively large B, and at each time bin t, we construct a distribution of all the sampled difference curves which will allow us to calculate the following re-sampling p-value:

$$p(t) = \frac{number\ of(|u_b(t)| \ge |\widehat{u_b}(t_{obs})|)}{R},$$

or the proportion of re-sampled curve differences that are as or more extreme than the observed curve difference at time-bin  $^{\it f}$ . A small value of  $^{\it p}$  may be taken as a sign of rejecting the null hypothesis of the equality of the two modes.

In addition to hypothesis testing, one can easily construct a  $(1-\alpha)\times 100\%$  confidence interval around  $\hat{u}(t)$  (see Figure 3). This is due to the fact that at time-bin t we have a distribution of re-sampled differences, or  $u_b(t)$  s. A  $(1-\alpha)\times 100\%$  re-sampling confidence interval then is easily obtained via:

$$(u_h(t, \alpha/2), u_h(t, 1-\alpha/2)),$$

where,  $u_b(t,\alpha/2)$ , and  $u_b(t,1-\alpha/2)$  represent the  $[\alpha/2]$  and  $[1-\alpha/2]$  order statistics. The sign [] indicates to round to the nearest integer.

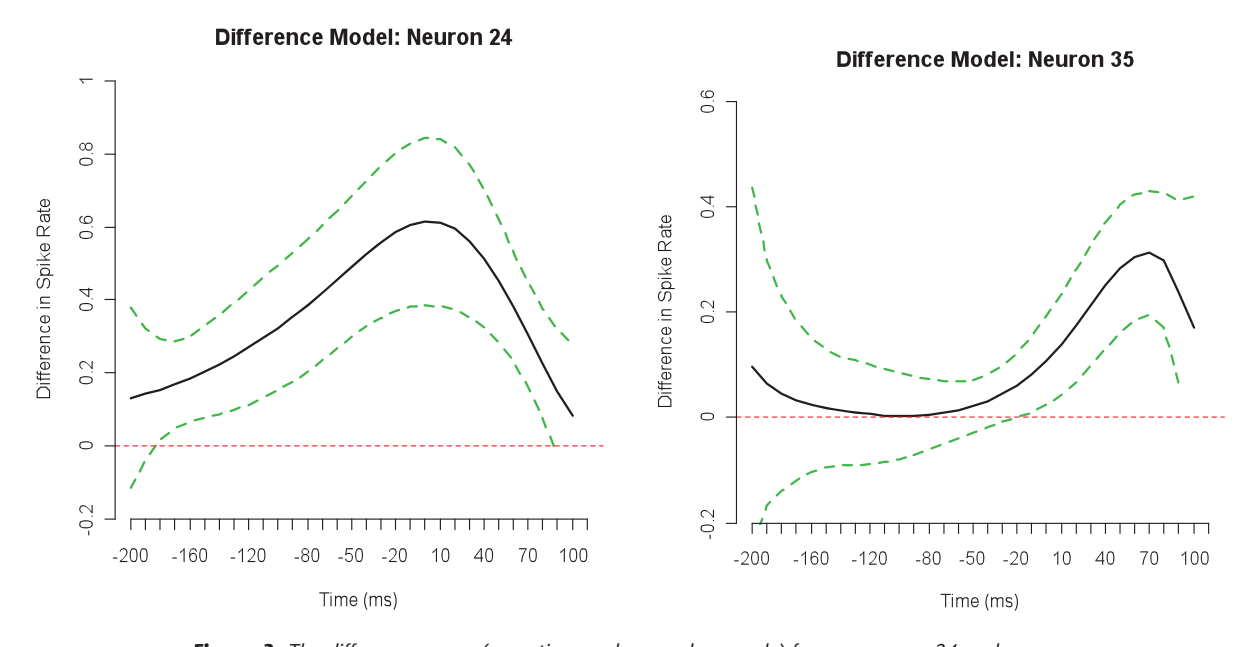


**Figure 3.** The difference curves (repeating mode – random mode) for neurons no. 24 and no. 35 are shown as the solid curves. The dashed curves above and below each difference model form its corresponding 95% confidence band. With an exception of a few time bins, the re-sampling confidence interval the neuron on the left does not cover zero, whereas the neuron on the right side does not respond differentially to the task objectives for the first half of the time period.

3. Discussion and Results - We applied our proposed method to a total of 36 neurons. Here, we present the numerical results of our analysis for neuron no. 24 and neuron no. 35 (displayed in Figure 1). As shown in Figure 3, for neuron 24, we expect to reject the null hypotheses for nearly all time bins. Only the time bins at the very beginning of the experimental time frame have a confidence interval that contains a difference of zero, or  $U^1(t) - U^2(t) = 0$ . From our permutation test, we find that bins 1 and 2 are the only bins that did not result in a rejected null hypothesis with  $p(t_1) = .282$  and  $p(t_2) = .123$ , respectively (Table 1). Thus, we can conclude that  $U^1(t_i) \neq U^2(t_i)$  for i = 3, 4,...,30, and that there is sufficient evidence to conclude that the spike rate for neuron 24 is significantly different during the repeating and repeating mode at these time points.

Neuron 35, on the other hand, is an example of a neuron in our analysis that does not behave as differentially. As shown in Figure 1, we expect to reject the null hypotheses towards the end of the experimental time window. This is also confirmed through the examination of Figure 3: the confidence bands around the difference model does not contain zero at the end of the time window. Specifically, we conclude  $U^1(t_i) \neq U^2(t_i)$  for i = 19, 20, ..., 30. The results are summarized in Table 2.

The results associated with confidence intervals were consistent with the p-values obtained with the re-sampled curves. Hence, the method used in this paper is efficient in revealing the differences in spike rate between the two experimental conditions.

The consistency between the results of the proposed confidence intervals and hypothesis testing suggests that in practice, it would be sufficient to consider only one of these statistical procedures. The forte of the re-sampling method presented here is its simplicity: there is a package for BARS that can be easily implemented in the freeware R or Matlab (Walstrom et al., 2008). We wrote the entire set of codes for this paper using the freeware R (www.r-project.org).

Bin No.	Difference	95% Confi	dence Interval	P-Value
i	$\widehat{u}(t_i) = \widehat{u}(t_i) - \widehat{u}(t_i)$	Lower Limit	UpperLimit	1 - Value
1	0.097	-0.116	0.379	0.282*
2	0.064	-0.039	0.323	0.123*
3	0.045	0.015	0.292	0.029
4	0.032	0.048	0.286	0.006
5	0.024	0.066	0.301	0.000
6	0.017	0.077	0.327	0.000
7	0.013	0.087	0.358	0.000
8	0.009	0.098	0.392	0.000
9	0.006	0.112	0.426	0.000
10	0.004	0.130	0.460	0.000
11	0.003	0.151	0.495	0.000
12	0.004	0.176	0.530	0.000
13	0.006	0.205	0.566	0.000
14	0.009	0.236	0.604	0.000
15	0.015	0.267	0.644	0.000
16	0.022	0.299	0.685	0.000
17	0.032	0.327	0.727	0.000
18	0.045	0.351	0.767	0.000
19	0.062	0.369	0.803	0.000
20	0.082	0.381	0.830	0.000
21	0.108	0.385	0.845	0.000
22	0.139	0.383	0.842	0.000
23	0.175	0.372	0.818	0.000
24	0.213	0.352	0.772	0.000
25	0.251	0.323	0.705	0.000
26	0.283	0.284	0.623	0.000
27	0.305	0.231	0.533	0.000
28	0.313	0.162	0.448	0.000
29	0.299	0.077	0.377	0.004
30	0.240	-0.018	0.320	0.083

**Table 1.** Results for neuron no. 24: The observed difference value,  $\hat{u}(t_i)$ , the confidence interval for  $\hat{u}(t_i)$ , and the p-value obtained from the permutation test. (\*) indicates the time bins that did not result in a rejected null hypothesis.

Bin No.	Difference	95% Confi	dence Interval	P-Value
i	$\widehat{u}(t_i) = \widehat{u}(t_i) - \widehat{u}(t_i)$	<b>Lower Limit</b>	UpperLimit	
1	0.097	-0.243	0.438	0.564
2	0.065	-0.168	0.298	0.574
3	0.045	-0.140	0.230	0.606
4	0.032	-0.121	0.186	0.668
5	0.024	-0.104	0.151	0.718
6	0.017	-0.094	0.129	0.780
7	0.013	-0.091	0.117	0.838
8	0.009	-0.090	0.109	0.850
9	0.006	-0.089	0.102	0.868
10	0.004	-0.085	0.093	0.922
11	0.003	-0.079	0.085	0.920
12	0.004	-0.070	0.078	0.906
13	0.006	-0.061	0.073	0.832
14	0.009	-0.050	0.069	0.730
15	0.015	-0.039	0.068	0.584
16	0.022	-0.028	0.072	0.400
17	0.032	-0.018	0.081	0.208
18	0.045	-0.008	0.098	0.108
19	0.062	0.000	0.123	0.044**
20	0.082	0.010	0.154	0.024**
21	0.108	0.024	0.192	0.016**
22	0.139	0.043	0.235	0.002**
23	0.175	0.068	0.282	0.000**
24	0.213	0.098	0.329	0.000**
25	0.251	0.131	0.371	0.000**
26	0.283	0.161	0.405	0.000**
27	0.305	0.185	0.425	0.000**
28	0.313	0.194	0.431	0.000**
29	0.299	0.171	0.427	0.000**
30	0.240	0.067	0.413	0.006**

**Table 2.** Results for neuron no. 35: The observed difference value,  $\hat{u}(t_i)$ , the confidence interval for  $\hat{u}(t_i)$ , and the p-value obtained from the permutation test. (\*\*) indicates the time bins that resulted in a rejected null hypothesis

#### **REFERENCES**

Behseta, S. & Kass, R.E. 2005. Testing equality of two functions using BARS. *Statistics in Meidcine*. 24: 3523-3534.

DiMatteo, I., Genovese, C.R., & Kass, R.E. 2001. Bayesian curve-fitting with free-knot splines. *Biometrika*. 88: 1055-1071.

Efrom, B., 1982. The Jacknife, the Bootstrap and Other Resampling Plans. Siam, Philadelphia.

Green, P. 1995. Reversible jump Markov Chain Monte Carlo computation and Bayesian model determination. *Biometrika*. 82: 711-732.

Hansen, M.H., & Kooperberg, C. 2002. Spline adaptation in extended linear models (with discussion). *Statistical Science*. 17: 2-51.

Kass, R.E., Ventura, V., & Cai, C. 2003. Statistical smoothing of neuronal data. *Network: Computation in Neural Systems*. 14: 5-15.

Matsuzaka, Y., Picard, N., & Strick, P.L. 2001. Sequence learning in monkeys. *Society for Neuroscience Abstracts.* 24: 174.

Matsuzaka, Y., Picard, N., & Strick, P.L. 2007. Skill representation in the primary motor cortex after long-term practice. *Journal of Neurophysiology.* 97: 1819-1832.

Wallstrom, G., Liebner, J., & Kass, R.E. 2008. An implementation of Bayesian Adaptive Regression Splines (BARS) in C with S and R wrappers. *Journal of Statistical Software*. 26.

#### **ACKNOWLEDGEMENTS**

I would like to thank my advisor, Dr. Sam Behseta, for introducing me to this fascinating area of statistics, as well as his generous help in the research process and always being enthusiastic about what he teaches. Additionally, I would like to thank the Louis Stokes Alliance for Minority Participation Program (LSAMP) for funding this project and Dr. Christina Goode for presenting me this research opportunity.

# **Relations Involving the Fibonacci Numbers**

#### **JAIRO AGUAYO**

Advisor: Dr. Scott Annin

Department of Mathematics, California State University, Fullerton

**Abstract** - One of the most celebrated sequences in mathematics is the sequence of Fibonacci numbers. Countless recurrence relations for these special numbers have been discovered as a byproduct of clever calculations, combinatorial reasoning, and pattern recognition. In this paper, we use various arrangements of the Fibonacci sequence into two-dimensional arrays to discover an infinite family of recurrence relations for the Fibonacci sequence. These relations are then proved by mathematical induction and the use of other well-known Fibonacci relations. We subsequently investigate some generalizations and leave the reader with some interesting avenues for further investigation.

Introduction - The sequence of Fibonacci numbers  $f_n$  is defined by  $f_1 = 1$ ,  $f_2 = 1$ , and then defining each successive number as the sum of the two previous numbers for n > 2,

$$f_n = f_{n-1} + f_{n-2}$$
.

For example,

$f_1$	$f_2$	$f_3$	$f_4$	$f_5$	$f_6$	$f_7$	f <sub>8</sub>	$f_9$	$f_{10}$	$f_{11}$	$f_{12}$	
1	1	2	3	5	8	13	21	34	55	89	144	

There are many known relations for the Fibonacci sequence. Here is a brief list of some of the most famous ones:

Cassini's Identity:

For n > 1,

$$f_{n-1}f_{n+1} - f_n^2 = (-1)^n$$
.

This identity guarantees that the difference between the product of Fibonacci numbers two apart in the sequence and the square of the one in between always has magnitude 1. This identity will play a part in proving our main result in Section 3 below. It is a particular case (r = 1) of our next result, Catalan's Identity.

Catalan's Identity:

For n > r > 0,

$$f_n^2 - f_{n+r} f_{n-r} = (-1)^{n-r} f_r^2$$
.

Here is another similar identity known as d'Ocagne's Identity: For integers m > n > 0,

$$f_m f_{n+1} - f_n f_{m+1} = (-1)^n f_{m-n}$$
.

The above formulas provide relations among different terms of the Fibonacci sequence. It is also of great interest to find a specific closed-form formula for fn. Using the relation fn = fn-1 + fn-2, there are several well-known derivations leading to the formula:

The expression arising in this formula is the famed Golden ratio. We will derive Equation (1) later as a special case of a more general sequence (Section 5).

Here are two more relations, both of which are easy to derive by an elementary induction argument for all  $n \ge 1$ :

$$f_{2n} = f_{n^2} + 2f_n f_{n-1},$$
  
 $f_{2n+1} = f_{n+1^2} + 2f_n f_{n+1}.$ 

Of course, the relations we have seen here barely scratch the surface in the extensive list of relations involving Fibonacci numbers. Many others are contained in a variety of sources [1], [2], [3], [4], and [5].

**Spatial Arrangements of the Fibonacci Numbers** - We begin by placing the Fibonacci numbers into a column. After listing all the numbers we look for an integer combination of the two previous numbers in that same column.

1	Column
1	
1	
2	<b>1</b> · 1 + 1
3	$1 \cdot 2 + 1$
5	$1 \cdot 3 + 2$
8	$1 \cdot 5 + 3$
13	$1 \cdot 8 + 5$

In the case where the Fibonacci numbers are arranged into one column, we of course recover the Fibonacci recurrence relation that we started with:

$$f_n = 1 \cdot f_{n-1} + f_{n-2} = f_{n-1} + f_{n-2}$$

Next, we place the Fibonacci numbers into two columns, from left to right, top to bottom, as shown:

	2 Columns							
1		1						
2		3						
5	<b>3</b> · 2 - 1	8	<b>3</b> · 3 -	1				
13	<b>3</b> · 5 - 2	21	<b>3</b> · 8 -	. 3				
34	<b>3</b> · 13 - 5	55	<b>3</b> · 21 -	. 8				
89	<b>3</b> · 34 - 13	144	<b>3</b> · 55 -	21				
233	<b>3</b> · 89 - 34	377	<b>3</b> ·144 -	- 55				

From the calculations seen here, it appears that we have discovered a different relation for the Fibonacci sequence when n > 4:

$$f_n = 3 \cdot f_{n-2} - f_{n-4}.$$

Similarly, when we arrange the Fibonacci numbers into three columns, left to right, top to bottom, we observe the following calculations:

	3 Columns									
1		1		2						
3		5		8						
13	<b>4</b> · 3 + 1	21	<b>4</b> · 5 + 1	34	<b>4</b> · 8 + 2					
55	<b>4</b> · 13 + 3	89	<b>4</b> · 21 + 5	144	<b>4</b> · 34 + 8					
233	<b>4</b> · 55 + 13	377	<b>4</b> · 89 + 21	610	<b>4</b> · 144 + 34					
987	<b>4</b> ·233 + 55	1597	<b>4</b> · 377 + 89	2584	<b>4</b> · 610 + 144					
4181	<b>4</b> ·987 + 233	6765	<b>4</b> ·1597 + 377	10946	<b>4</b> ·2584 + 610					

In this case, we seem to have found another recurrence relation for n > 6:

$$f_n = 4 \cdot f_{n-3} + f_{n-6}$$
.

As we continue to arrange the Fibonacci numbers into four columns, five columns, or more columns, we conjecture additional recurrence relations:

Results							
1 Column	$f_n = 1$	$f_{n-1} + f_{n-2}$	if $n > 2$				
2 Columns	$f_n = 3$	$\cdot$ $f_{n ext{-}2}$ - $f_{n ext{-}4}$	if $n > 4$				
3 Columns	$f_n = 4$	$f_{n-3} + f_{n-6}$	if $n > 6$				
4 Columns	$f_n = 7$	$\cdot$ $f_{n\text{-}4}$ - $f_{n\text{-}8}$	if $n > 8$				
5 Columns	$f_n = 11$	$f_{n-5} + f_{n-10}$	if $n > 10$				
6 Columns	$f_n = 18$	$\cdot$ $f_{n ext{-}6}$ - $f_{n ext{-}12}$	if $n > 12$				
7 Columns	$f_n = 29$	$f_{n-7} + f_{n-14}$	if <i>n</i> > 14				

Now we carefully study the recurrence relations in this table as a function of the number of columns, which we will subsequently denote by k. We find that a pattern arises from the coefficients, which are given in bold in the table. The sequence begins 1, 3, 4, 5, 11, 18, 29, .... Observe that, as with the Fibonacci sequence, each term is the sum of the two previous terms. That is, the sequence is defined by  $L_1 = 1$ ,  $L_2 = 3$ , and then defining each successive number as the sum of the two previous numbers for k > 2:

$$L_k = L_{k-1} + L_{k-2}$$
.

This is a close relative of the Fibonacci sequence, known as the Lucas sequence. For example,

$L_1$	$L_2$	$L_3$	$L_4$	$L_5$	$L_6$	$L_7$	$L_8$	$L_9$	$L_{10}$	$L_{11}$	$L_{12}$	
1	3	4	7	11	18	29	47	76	123	199	322	•••

There are numerous additional recurrence relations for the Lucas sequence, some of which also involve the Fibonacci numbers. For instance, for n > 2:

$$L_n = f_{n+1} + f_{n-1}$$
.

Many others are contained in a variety of sources [2], [3], and [5].

There is a similar closed-form formula for the Lucas sequence to that given in Equation (1) for the Fibonacci numbers:

As with Equation (1), Equation (2) is another formula that we can derive as a special case from a more general sequence (Section 5).

An Infinite Family of Recurrence Relations for the Fibonacci Sequence - Looking again at the results in the table, we see that if k denotes the number of columns, then it appears that

$$f_n = L_k f_{n-k} + (-1)^{k+1} f_{n-2k}$$
.

It turns out that this is indeed true for all n > 2k, which is our main result.

#### Theorem 1:

For every n > 2k, where  $k \ge 1$ :

$$f_n = L_k f_{n-k} + (-1)^{k+1} f_{n-2k}$$
.

Proof: We give a proof by mathematical induction on n with  $k \ge 1$  fixed.

Base Step:

We begin by showing that the formula holds whenever n = 2k + 1 and n = 2k + 2.

Let n = 2k + 1. Then we must show that  $f_n = f_{2k+1} = L_k f_{k+1} + (-1)^{k+1} f_1$ . Since  $f_1 = 1$ , this reduces to  $f_{2k+1} = L_k f_{k+1} + (-1)^{k+1}$ . To see this is true, we use the following calculation:

By the Fibonacci relation, we know that

$$f_{2k+1} = f_{2k} + f_{2k-1}$$

and

$$f_{2k} = f_{2k-1} + f_{2k-2}$$
.

Thus, after substitution for f2k:

$$f_{2k+1} = 2 \cdot f_{2k-1} + 1 \cdot f_{2k-2}$$
.

In the same way,

$$f_{2k+1} = 3 \cdot f_{2k-2} + 2 \cdot f_{2k-3}$$
  
=  $5 \cdot f_{2k-3} + 3 \cdot f_{2k-4}$   
=  $8 \cdot f_{2k-4} + 5 \cdot f_{2k-5}$ 

Continuing in this fashion, we can derive a general relation for f2k+1 as follows:

#### Lemma 2:

For every j = 0, 1, 2, ..., k-1,

$$f_{2k+1} = f_{j+2} f_{2k-j} + f_{j+1} f_{2k-j-1}$$
.

A rigorous proof of this relation is also an exercise in induction and relegated to Section 7 at the end of this paper to avoid undue distraction from the flow of the present argument.

In particular for j = k-1, we obtain

$$f_{2k+1} = f_{k+1}^2 + f_k^2.$$

By Cassini's Identity,

$$f_{2k+1} = f_{k+1}^2 + f_{k-1} f_{k+1} - (-1)^k$$
  
=  $(f_{k+1} + f_{k-1}) f_{k+1} + (-1)^{k+1}$   
=  $L_k f_{k+1} + (-1)^{k+1}$ ,

where we have used the relation  $L_k = f_{k+1} + f_{k-1}$  in the last step. This completes the argument in the case n = 2k + 1.

Let n = 2k + 2. Then we must show that  $f_n = f_{2k+2} = L_k f_{k+2} + (-1)^{k+1} f_2$ . Since  $f_2 = 1$ , this reduces to  $f_{2k+2} = L_k f_{k+2} + (-1)^{k+1}$ . To see this is true, we construct a similar calculation to that used in the n = 2k + 1 case.

By the Fibonacci relation, we know

$$f_{2k+2} = f_{2k+1} + f_{2k}$$
.

Thus,

$$\begin{split} f_{2k+2} &= 2 \cdot f_{2k} &+ 1 \cdot f_{2k-1} \\ &= 3 \cdot f_{2k-1} &+ 2 \cdot f_{2k-2} \\ &= 5 \cdot f_{2k-2} &+ 3 \cdot f_{2k-3} \\ &= 8 \cdot f_{2k-3} &+ 5 \cdot f_{2k-4} \end{split}$$

As before, we derive a general relation for f2k+2 as follows:

$$f_{2k+2} = f_{j+2} f_{2k-j+1} + f_{j+1} f_{2k-j},$$

for every j = 0, 1, 2,..., k-1. This proof is nearly identical to Lemma 2 of n = 2k + 1 case and is left to the reader. Setting j = k-1, we have

$$f_{2k+2} = f_{k+1} f_{k+2} + f_k f_{k+1}$$

$$= f_{k+1} (f_{k+1} + f_k) + f_k (f_k + f_{k-1})$$

$$= f_{k+1}^2 + f_k^2 + f_k (f_{k+1} + f_{k-1})$$

$$= f_{k+1}^2 + f_k^2 + f_k L_k$$

$$= f_{k+1}^2 + f_k^2 + (f_{k+2} - f_{k+1}) L_k$$

$$= L_k f_{k+2} + f_{k+1} (f_{k+1} - L_k) + f_k^2$$

$$= L_k f_{k+2} - f_{k+1} f_{k-1} + f_k^2$$

$$= L_k f_{k+2} + (-1)^{k+1},$$

where we have applied Cassini's Identity on the last step. This completes the argument in the case n = 2k + 2.

#### **Induction Step:**

We will assume that the formula in the main theorem holds for  $f_n$  and  $f_{n+1}$  and apply induction to show that the formula holds for  $f_{n+2}$ . That is, given that

$$f_n = L_k f_{n-k} + (-1)^{k+1} f_{n-2k}$$

and

$$f_{n+1} = L_k f_{n-k+1} + (-1)^{k+1} f_{n-2k+1}$$

we will show that

$$f_{n+2} = L_k f_{n-k+2} + (-1)^{k+1} f_{n-2k+2}.$$

We have that

$$f_{n+2} = f_{n+1} + f_n$$

$$= (L_k f_{n-k+1} + (-1)^{k+1} f_{n-2k+1}) + (L_k f_{n-k} + (-1)^{k+1} f_{n-2k})$$

$$= L_k (f_{n-k+1} + f_{n-k}) + (-1)^{k+1} (f_{n-2k+1} + f_{n-2k})$$

$$= L_k (f_{n-k+2}) + (-1)^{k+1} (f_{n-2k+2}),$$

as needed. Therefore, for every n > 2k,

$$f_n = L_k f_{n-k} + (-1)^{k+1} f_{n-2k}$$
.

Generalization of the Fibonacci Relation - We now seek to generalize the work in the previous section by considering the sequence  $J_1 = a$ ,  $J_2 = b$ , with a recurrence relation of the form  $J_n = x J_{n-2} + y J_{n-1}$  for fixed real numbers a, b, x, and y. For example,

$J_1$	$J_2$	$J_3$	$J_4$	$J_5$	$J_6$
а	b	ax+by	$a(xy)+b(x+y^2)$	$a(x^2+xy^2)+b(2xy+y^3)$	$a(2x^2y+xy^3)+b(x^2+3xy^2+y^4)$

$J_7$	$J_8$	
$a(x^3+3x^2y^2+xy^4)+b(3x^2y+4xy^3+y^5)$	$a(3x^3y+4x^2y^3+xy^5)+b(x^3+6x^2y^2+5xy^4+y^6)$	

Note, if a = b = x = y = 1, then the sequence In reduces precisely to the Fibonacci sequence fn considered earlier. Similarly, if a = 1, b = 3, and x = y = 1, we obtain the Lucas sequence Ln. In this section, we seek therefore to generalize the work above (especially Theorem 1), for the sequence In. In addition, we can also seek a closed-form formula for In that parallels Equations (1) and (2) given earlier in the paper. We now take on both of these tasks, beginning with the generalization of Theorem 1.

We use our method of arranging the sequence In into columns to derive a family of recurrence relations for the sequence Jn.

For the main result in this section, we introduce two sequences Ak and Bk defined recursively as follows:

Let  $A_1 = x$ , and for every  $k \ge 2$ ,

$$A_k = -x A_{k-1}.$$

Let 
$$B_1 = y$$
 and  $B_2 = 2x + y^2$ , and for every  $k \ge 3$ ,

$$B_k = x B_{k-2} + y B_{k-1}$$
.

For example, we can see in the table below how the  $A_k$  sequence and  $B_k$  sequence behave for the first 5 columns.

lc .	$A_k$	$B_k$
Λ.	21K	D <sub>K</sub>
1 Column	X	y
2 Columns	-x <sup>2</sup>	$2x + y^2$
3 Columns	<b>X</b> <sup>3</sup>	$3xy + y^3$
4 Columns	-x <sup>4</sup>	$2x^2 + 4xy^2 + y^4$
5 Columns	<b>x</b> <sup>5</sup>	$5x^2y + 5xy^3 + y^5$

Then we have the following theorem.

#### Theorem 3:

For every n > 2k, where  $k \ge 1$ :

$$J_n = A_k J_{n-2k} + B_k J_{n-k}.$$

Observe that if x = y = 1, we have  $A_k = (-1)^{k+1}$  and  $B_k = L_k$  for all  $k \ge 1$ . Therefore, in this case,  $J_n$ obeys the same recurrence relation that we derived for  $f_n$  in Theorem 1. Hence, if we also assume a = b = 1, Theorem 3 reduces to Theorem 1 as a special case.

We will present the proof of Theorem 3 shortly. However, let us first present some insight into how the result was obtained by considering a specific example:

If we take a = b = 1, x = 3, and y = -1 (i.e.  $J_n = 3 \cdot J_{n-2} + (-1) \cdot J_{n-1}$ ), we obtain the following sequence  $J_n$ :

$J_1$	$J_2$	$J_3$	$J_4$	$J_5$	$J_6$	$J_7$	$J_8$	$J_9$	$J_{10}$	$J_{11}$	$J_{12}$	
1	1	2	1	5	-2	17	-23	74	-143	365	-794	

As in the case of the Fibonacci numbers, we want to arrange the sequence into 1 column, 2 columns, 3 columns, and so on, to uncover the recurrence relation that satisfies the sequence  $J_n$ . We begin by listing the sequence in one column, as we did for the Fibonacci numbers.

1 Column							
1							
1							
2	<b>3</b> · 1	+ (-1)	· 1				
1	<b>3</b> · 1	+ (-1)	· 2				
-2	<b>3</b> · 2	+ (-1)	· 1				
17	<b>3</b> · 1	+ (-1)	· (-2)				
-23	<b>3</b> · (-2)	+ (-1)	· 17				

In the case where sequence the  $J_n$  is arranged into one column, we recover the recurrence relation we started with:  $J_n = 3 \cdot J_{n-2} + (-1) \cdot J_{n-1}.$ 

$$J_n = 3 \cdot J_{n-2} + (-1) \cdot J_{n-1}$$

Next, recall that when multiple columns are involved, we place the sequence from left to right, top to bottom.

	2 Columns						
1		1					
2		1					
5	<b>-9</b> · 1 + <b>7</b> · 2	-2	<b>-9</b> ⋅ 1	+ <b>7</b> · 1			
17	<b>-9</b> · 2 + <b>7</b> · 5	-23	<b>-9</b> ⋅ 1	+ <b>7</b> · (-2)			
74	<b>-9</b> ⋅ 5 + <b>7</b> ⋅ 17	-143	<b>-9</b> · (-2)	+ <b>7</b> · (-23)			
365	<b>-9</b> ⋅ 17 + <b>7</b> ⋅ 74	-794	<b>-9</b> · (-23)	+ <b>7</b> · (-143)			
1889	<b>-9</b> ⋅ 74 + <b>7</b> ⋅ 365	-4271	<b>-9</b> · (-143)	+ <b>7</b> · (-794)			

From the calculations seen in the case of two columns, we have discovered a different recurrence relation for  $J_n$ :

$$J_n = (-9) \cdot J_{n-4} + 7 \cdot J_{n-2}$$
.

3 Columns						
1			1	2		
1			5	-2		
17	<b>27</b> · 1	+ (- <b>10</b> ) · 1	-23	74		
-143	<b>27</b> · 1	+ (- <b>10</b> ) · 17	365	-794		
1889	<b>27</b> · 17	+ ( <b>-10</b> ) · (-143)	-4271	9938		
-22751	<b>27</b> · (-143)	+ (- <b>10</b> ) · (1889)	52565	-120818		
278513	<b>27</b> · (1889)	+ (- <b>10</b> ) · (-22751)	-640967	1476506		

In this case, we found another recurrence relation that the reader can use to fill in the rest of the table:

$$J_n = 27 \cdot J_{n-6} + (-10) \cdot J_{n-3}$$
.

As we continue to arrange the  $J_n$  numbers into four columns, five columns, or more columns, we can summarize our results in the table below:

Results						
1 Column	$J_n = 3$	$\cdot J_{n-2}$	+ (-1)	· <i>J</i> <sub><i>n</i>-1</sub>		
2 Columns	$J_n = -9$	$\cdot J_{n-4}$	+ (7)	$\cdot J_{n-2}$		
3 Columns	$J_n = 27$	$\cdot J_{n-6}$	+ (-10)	· <i>J</i> <sub>n-3</sub>		
4 Columns	$J_n = -81$	$\cdot J_{n-8}$	+ (31)	· <i>J</i> <sub>n-4</sub>		
5 Columns	$J_n = 243$	· J <sub>n-10</sub>	+ (-61)	$\cdot J_{n-5}$		
6 Columns	$J_n = -729$	$\cdot J_{n-12}$	+ (154)	$\cdot J_{n-6}$		
7 Columns	$J_n = 2187$	· J <sub>n-14</sub>	+ (-337)	$J_{n-7}$		

The pattern of coefficients for the  $A_k$  sequence is clear:  $A_k = -3$   $A_{k-1}$  for all  $k \ge 2$ . While the pattern for the  $B_k$  sequence is not as transparent, a little thought shows the remarkable fact that  $B_k$  obeys the same recurrence relations as the original sequence  $J_n$ :  $B_k = 3$   $B_{k-2} + (-1)$   $B_{k-1}$  for all  $k \ge 3$ . It was precisely these observations that helped us to formulate Theorem 3 in general. We now turn to its proof, which begins by stating a couple of lemmas. We will relegate their proofs to Section 7 at the end of the paper.

#### Lemma 5:

For  $k \ge 3$ ,

$$B_{k-1} J_k - B_{k-2} J_{k+1} = (-x)^{k-3} [B_2 J_3 - B_1 J_4].$$

#### Lemma 6:

For  $k \ge 2$ ,

$$B_{k-1} J_{k+1} - B_k J_k = (-x)^{k-2} [B_1 J_3 - B_2 J_2].$$

**Proof of Theorem 3:** We give a proof by mathematical induction on n with fixed  $k \ge 1$ .

Base Step:

We begin by showing that the formula holds whenever n = 2k + 1 and

n = 2k + 2. In other words, for all  $k \ge 1$  we need to show

$$J_{2k+1} = A_k J_1 + B_k J_{k+1}$$
 (3)

and

$$J_{2k+2} = A_k J_2 + B_k J_{k+2}. (4)$$

We simultaneously prove both formulas by induction on k, beginning with k = 1 for both formulas:

Considering  $J_{2k+1}$ , for k = 1 we have

$$J_3 = ax + by$$
  
=  $A_1 J_1 + B_1 J_2$ ,

which is confirmed by the values in the table at the beginning of this section.

Considering  $J_{2k+2}$ , for k = 1, we have

$$J_4 = a(xy) + b(x+y^2)$$
  
=  $xb + y(ax + by)$   
=  $A_1 J_2 + B_1 J_3$ ,

as needed.

Since we are proving the formulas for  $J_{2k+1}$  and  $J_{2k+2}$  by an "alternating" induction process, we must consider two inductive steps:

proving (3) from the formulas for  $J_{2k-1}$  and  $J_{2k}$ .

proving (4) from the formulas for  $J_{2k}$  and  $J_{2k+1}$ .

Proof of (i): Assuming for  $k \ge 2$  that

$$J_{2k-1} = A_{k-1} J_1 + B_{k-1} J_k$$
  
 $J_{2k} = A_{k-1} J_2 + B_{k-1} J_{k+1},$ 

we need to show

$$J_{2k+1} = A_k \, J_1 \, + \, B_k \, J_{k+1}.$$

By the defining relation given for  $J_n$ , we know that

$$J_{2k+1} = x J_{2k-1} + y J_{2k}.$$

Substituting our formulas for  $J_{2k-1}$  and  $J_{2k}$ , we have

$$J_{2k+1} = x [A_{k-1} J_1 + B_{k-1} J_k] + y [A_{k-1} J_2 + B_{k-1} J_{k+1}]$$
  
=  $x A_{k-1} J_1 + x B_{k-1} J_k + y A_{k-1} J_2 + y B_{k-1} J_{k+1}.$ 

By our recurrence relation for  $B_k$ ,

$$J_{2k+1} = x A_{k-1} J_1 + x B_{k-1} J_k + y A_{k-1} J_2 + J_{k+1} [B_k - x B_{k-2}]$$

$$= x A_{k-1} J_1 + x B_{k-1} J_k + y A_{k-1} J_2 + B_k J_{k+1} - x B_{k-2} J_{k+1}$$

$$= A_{k-1} [x J_1 + y J_2] + x [B_{k-1} J_k - B_{k-2} J_{k+1}] + B_k J_{k+1}.$$

From Lemma 5,

$$J_{2k+1} = A_{k-1} [x J_1 + y J_2] + x(-x)^{k-3} [B_2 J_3 - B_1 J_4] + B_k J_{k+1}.$$

Substituting values of  $J_1$ ,  $J_2$ ,  $J_3$ ,  $J_4$ ,  $B_1$ , and  $B_2$  provides us with the following,

$$J_{2k+1} = A_{k-1} [xa + yb] + (-1)^{k-3} x^{k-2} [(2x + y^2)(ax + by) - y(axy + b(x + y^2))] + B_k J_{k+1}.$$

Using  $A_k = -x A_{k-1}$ , it is easy to show that the closed form for  $A_k = (-1)^{k+1}x^k$ , so that

$$J_{2k+1} = A_{k-1} [ax + by] + A_{k-2} [x(2ax + by)] + B_k J_{k+1}$$

$$= A_{k-1} [ax + by] - A_{k-1} [2ax + by] + B_k J_{k+1}$$

$$= A_{k-1} [-ax] + B_k J_{k+1}$$

$$= -x A_{k-1} [a] + B_k J_{k+1}$$

$$= A_k [a] + B_k J_{k+1}$$

$$= A_k J_1 + B_k J_{k+1},$$

as needed.

Proof of (ii): Assuming for  $k \ge 2$  that

$$J_{2k} = A_{k-1} J_2 + B_{k-1} J_{k+1}$$
  
$$J_{2k+1} = A_k J_1 + B_k J_{k+1},$$

we need to show

$$J_{2k+2} = A_k J_2 + B_k J_{k+2}$$
.

By the defining relation given for  $J_n$ , we know that

$$J_{2k+2} = x J_{2k} + y J_{2k+1}$$
.

Substituting our formulas for  $J_{2k}$  and  $J_{2k+1}$ , we have

$$J_{2k+2} = x [A_{k-1} J_2 + B_{k-1} J_{k+1}] + y [A_k J_1 + B_k J_{k+1}]$$
  
=  $x A_{k-1} J_2 + x B_{k-1} J_{k+1} + y A_k J_1 + y B_k J_{k+1}.$ 

Using the fact that  $y J_{k+1} = J_{k+2} - x J_k$  and the relation  $A_k = -x A_{k-1}$ ,

$$J_{2k+2} = x A_{k-1} J_2 + x B_{k-1} J_{k+1} + y A_k J_1 + B_k [J_{k+2} - x J_k]$$

$$= x A_{k-1} J_2 + x B_{k-1} J_{k+1} + y A_k J_1 + B_k J_{k+2} - x B_k J_k$$

$$= x A_{k-1} [J_2 - y J_1] + x [B_{k-1} J_{k+1} - B_k J_k] + B_k J_{k+2}.$$

From Lemma 6,

$$J_{2k+2} = x A_{k-1} [J_2 - y J_1] + x (-x)^{k-2} [B_1 J_3 - B_2 J_2] + B_k J_{k+2}.$$

Substituting values of  $J_1$ ,  $J_2$ ,  $J_3$ ,  $B_1$ , and  $B_2$  provides us with the following,

$$J_{2k+2} = x A_{k-1} [b - ya] + (-1)^{k-2} x^{k-1} [y(ax + by) - (2x + y^2)(b)] + B_k J_{k+2}$$

$$= x A_{k-1} [b - ay] + (-1)^{k-2} x^{k-1} [axy - 2bx] + B_k J_{k+2}$$

$$= x A_{k-1} [b - ay] + (-1)^{k-1} x^k [2b - ay] + B_k J_{k+2}.$$

Once more, using the closed form for  $A_k = (-1)^{k+1}x^k$ , we obtain

$$J_{2k+2} = -A_k [b - ay] + A_k [2b - ay] + B_k J_{k+2}$$
  
=  $A_k [b] + B_k J_{k+2}$   
=  $A_k J_2 + B_k J_{k+2}$ ,

as needed.

#### **Induction Step:**

Now assume  $n \ge 2k + 3$ . We will assume that the formula in the main theorem holds for  $J_{n-2}$  and  $J_{n-1}$  and apply induction to show that the formula holds for  $J_n$ . That is, given that

$$J_{n-2} = A_k J_{n-2-2k} + B_k J_{n-2-k},$$

and

$$J_{n-1} = A_k J_{n-1-2k} + B_k J_{n-1-k}$$

we will show that

$$J_n = A_k J_{n-2k} + B_k J_{n-k}.$$

We have that

$$J_{n} = x J_{n-2} + y J_{n-1}$$

$$= x [A_{k} J_{n-2-2k} + B_{k} J_{n-2-k}] + y [A_{k} J_{n-1-2k} + B_{k} J_{n-1-k}]$$

$$= x A_{k} J_{n-2-2k} + x B_{k} J_{n-2-k} + y A_{k} J_{n-1-2k} + y B_{k} J_{n-1-k}$$

$$= A_{k} [x J_{n-2-2k} + y J_{n-1-2k}] + B_{k} [x J_{n-2-k} + y J_{n-1-k}]$$

$$= A_{k} J_{n-2k} + B_{k} J_{n-k},$$

as needed. Therefore, by mathematical induction we have shown that for every n > 2k,

$$J_n = A_k J_{n-2k} + B_k J_{n-k}.$$

#### Matrix Approach to the Sequence $J_n$

Next, we turn our attention to deriving a closed-form formula for the sequence  $J_n$ .

We consider the following matrix equation that describes the sequence of  $J_n$ . For every  $n \ge 2$ ,

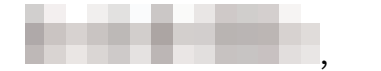
or



Applying the matrix we have

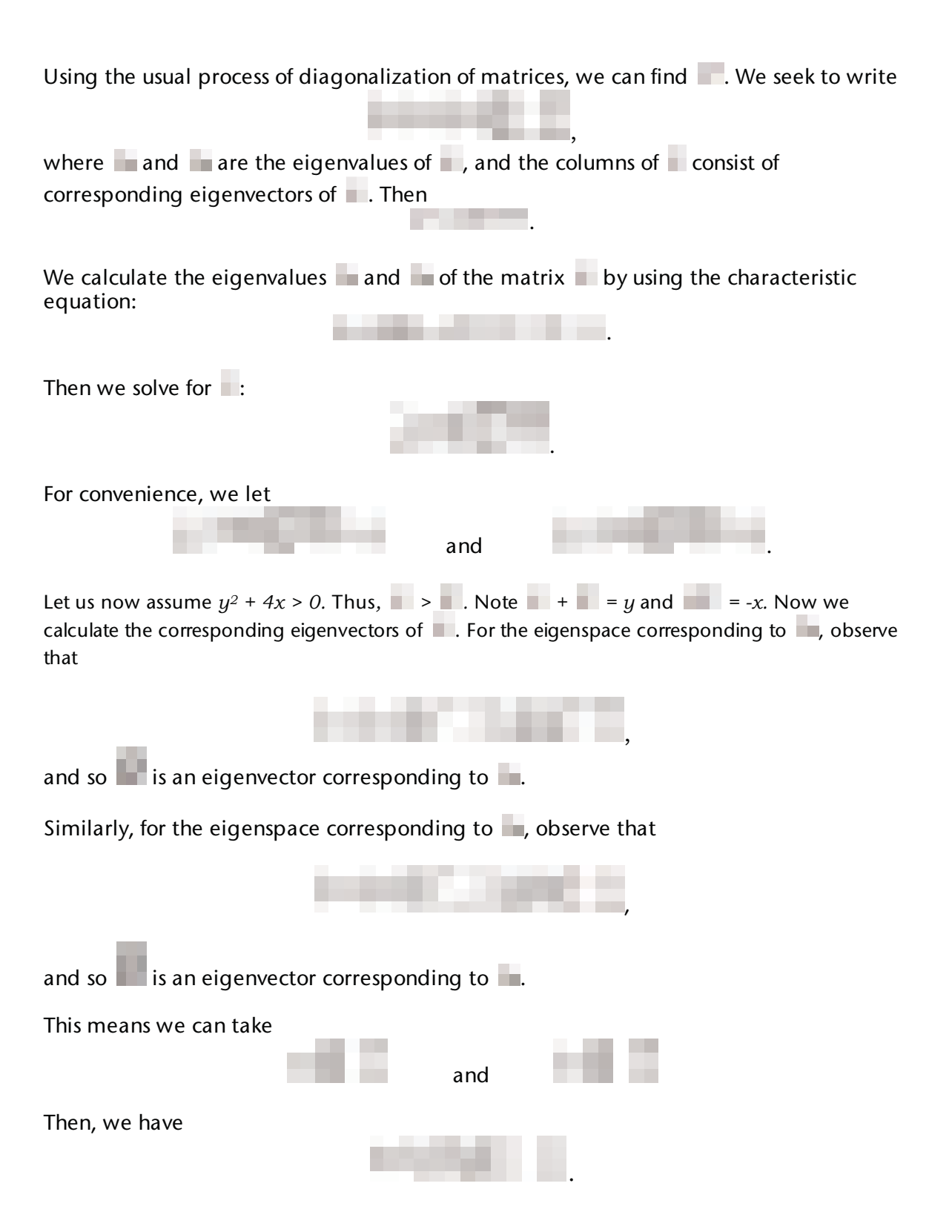


a total of r times, by left multiplication of the vector

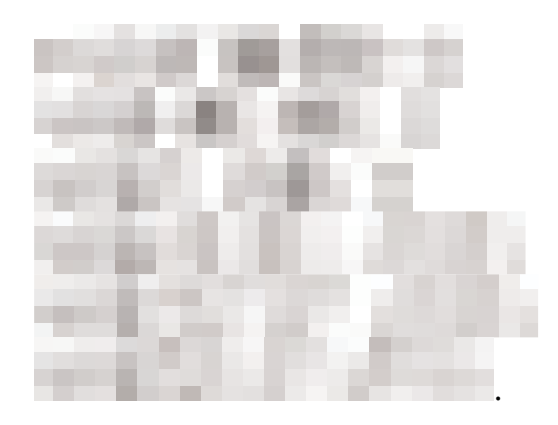


(5)

for every integer  $r \ge 1$ .



It follows that



Substituting this expression for and n = 2 into (5), we obtain:



Thus,



Therefore, setting n = r + 1, we have proved:

#### Theorem 6:

If x and y are real numbers such that  $y^2 + 4x > 0$  and and are defined as above for all  $n \ge 2$ ,



The reader can verify that the special case of Equation (1) arise by setting a = b = x = y = 1, the Fibonacci numbers. Similarly, the case Equation (2) can be derived with a = 1, b = 3, and x = y = 1, the Lucas numbers.

#### **Further Questions**

In all of the work we considered above, our recurrence relations involved only the two previous terms in the sequence in question. It is natural to extend this investigation to recurrence relations involving more terms. For instance, starting with a sequence  $J_1 = a$ ,  $J_2 = b$ , and  $J_3 = c$ , we could seek a recurrence relation of the form  $J_n = x J_{n-3} + y J_{n-2} + z J_{n-1}$  for fixed real numbers a, b, c, x, y, and z. We invite the reader to investigate arrangements of the sequence  $J_n$  into columns to look for a pattern that may reveal a new family of recurrence relations.

More generally, we ask: Is there a d-termed recurrence relation for  $J_n$  generalizing d = 2, d = 3, and so on? For example, we could begin with a recurrence relation of the form

$$J_n = \chi_d J_{n-d} + \chi_{d-1} J_{n-d+1} + ... + \chi_1 J_{n-1}$$

where  $x_1$ ,  $x_2$ ,  $x_3$ ,...,  $x_d$  are given constants and d initial terms  $J_1$ ,  $J_2$ ,  $J_3$ , ...,  $J_d$ . From here, one can seek to develop additional recurrence relations and a closed-form formula for  $J_n$ , in much the same way we have done in this paper for d = 2.

If we take a closer look at the closed-form solution of the generalized two-termed recurrence relations, can we find a ratio such as the golden ratio appears in the closed form of the Fibonacci numbers?

The proofs of the theorems given in this paper were done by induction. It is of interest to ponder whether there are other ways to prove these theorems. For example, can we use combinatorial reasoning to derive Theorems 1 and 3?

Finally, are there other forms of arrangements that we can consider to produce a new family of recurrence relations? For example, could we arrange the terms of the sequence  $J_n$  into a 3-dimensional array, rather than the 2-dimensional arrangement discussed in this paper? This is likely to lead to additional recurrence relations for  $J_n$  that depend on more than just the one parameter k we have seen in the relations in this paper. These recurrence relations are waiting for discovery, and the methods used in this paper should be useful to this end.

#### Proofs of the Lemmas Used in Theorems 1 and 3

We conclude this paper by returning to verify some of the technical results that arose in the inductive arguments in the proofs of the main results of this paper.

#### Lemma 2:

For every j = 0, 1, 2, ..., k-1,

$$f_{2k+1} = f_{i+2} f_{2k-i} + f_{i+1} f_{2k-i-1}.$$

**PROOF:** We give a proof by mathematical induction on *i*:

#### **Base Step:**

We begin by showing that the formula holds when j = 0. In this case, the proposed equation simply reads  $f_{2k+1} = f_2 f_{2k} + f_1 f_{2k-1}$ . Since  $f_1 = 1$  and  $f_2 = 1$ , this reduces to  $f_{2k+1} = f_{2k} + f_{2k-1}$ , which is the recurrence relation defining the Fibonacci numbers.

#### **Induction Step:**

By inductive hypothesis, we assume that the formula is valid with j-1 in place of j:

$$f_{2k+1} = f_{j+1} f_{2k-j+1} + f_j f_{2k+j}$$
.

Then applications of the defining recurrence relation for the Fibonacci numbers allow us to proceed as follows:

$$f_{2k+1} = (f_{j+2} - f_{j}) (f_{2k\cdot j} + f_{2k\cdot j-1}) + (f_{j+2} - f_{j+1}) (f_{2k\cdot j+1} + f_{2k\cdot j-1})$$

$$= f_{j+2} f_{2k\cdot j} + f_{j+2} f_{2k\cdot j+1} - f_{j} f_{2k\cdot j} - f_{j} f_{2k\cdot j-1} + f_{j+2} f_{2k\cdot j+1} - f_{j+2} f_{2k\cdot j-1} - f_{j+1} f_{2k\cdot j+1} + f_{j+1} f_{2k\cdot j-1}$$

$$= f_{j+2} f_{2k\cdot j} - f_{j} f_{2k\cdot j} - f_{j} f_{2k\cdot j-1} + f_{j+2} f_{2k\cdot j+1} - f_{j+1} f_{2k\cdot j+1} + f_{j+1} f_{2k\cdot j-1}$$

$$= f_{j+2} f_{2k\cdot j} - f_{j} (f_{2k\cdot j} + f_{2k\cdot j-1}) + (f_{j+2} - f_{j+1}) f_{2k\cdot j+1} + f_{j+1} f_{2k\cdot j-1}$$

$$= f_{j+2} f_{2k\cdot j} - f_{j} f_{2k\cdot j+1} + f_{j} f_{2k\cdot j+1} + f_{j+1} f_{2k\cdot j-1}$$

$$= f_{j+2} f_{2k\cdot j} + f_{j+1} f_{2k\cdot j-1},$$

as needed. Therefore, by mathematical induction we have shown Lemma 2:

$$f_{2k+1} = f_{j+2} f_{2k-j} + f_{j+1} f_{2k-j-1}.$$

#### Lemma 5:

For  $k \ge 3$ ,

$$B_{k-1} J_k - B_{k-2} J_{k+1} = (-x)^{k-3} [B_2 J_3 - B_1 J_4].$$

**Proof:** Observe:

$$B_{k-1} J_k - B_{k-2} J_{k+1} = [x B_{k-3} + y B_{k-2}] J_k - B_{k-2} J_{k+1}$$

$$= B_{k-2} [y J_k - J_{k+1}] + x B_{k-3} J_k$$

$$= B_{k-2} [-x J_{k-1}] + x B_{k-3} J_k$$

$$= (-x) [B_{k-2} J_{k-1} - B_{k-3} J_k]$$

Note that all subscripts reduced by one. Now we repeat the process k - 3 times to obtain

$$B_{k-1} J_k - B_{k-2} J_{k+1} = (-x) [B_{k-2} J_{k-1} - B_{k-3} J_k]$$
$$= (-x)^{k-3} [B_2 J_3 - B_1 J_4].$$

#### Lemma 6:

For  $k \ge 2$ ,

$$B_{k-1} J_{k+1} - B_k J_k = (-x)^{k-2} [B_1 J_3 - B_2 J_2].$$

**Proof:** Observe:

$$B_{k-1} J_{k+1} - B_k J_k = B_{k-1} J_{k+1} - [x B_{k-2} + y B_{k-1}] J_k$$

$$= B_{k-1} [J_{k+1} - y J_k] - x B_{k-2} J_k$$

$$= x B_{k-1} J_{k-1} - x B_{k-2} J_k$$

$$= (-x) [B_{k-2} J_k - B_{k-1} J_{k-1}]$$

Note that all subscripts reduced by one. Now we repeat the process k - 2 times to obtain

$$B_{k-1} J_{k+1} - B_k J_k = (-x) [B_{k-2} J_k - B_{k-1} J_{k-1}]$$
  
=  $(-x)^{k-2} [B_1 J_3 - B_2 J_2].$ 

#### **REFERENCES**

Benjamin, Arthur T.; Quinn, Jennifer J. Recounting Fibonacci and Lucas Identities. *The College Mathematics Journal*, Vol 30, No. 5, pp. 359-366, November 1999.

Dunlap, Richard A. <u>The Golden Ratio and Fibonacci Numbers</u>. World Scientific Publishing Co. Pte. Ltd., 2003.

Johnsonbaugh, Richard. <u>Discrete Mathematics</u>. 7th Edition. Upper Saddle River: Pearson Education, Inc., 2009.

Spivey, Michael Z. Fibonacci Identities via the Determinant Sum Property. *The College Mathematics Journal*. Integre Technical Publishing Co., Inc. Vol. 37, No. 4, pp. 286-289, September 2006.

Thongmoon, Montri. New Identities for the Even and Odd Fibonacci and Lucas Numbers. Int. J. Contemp. Math. Sciences, Vol. 4, No. 14, pp. 671-676. 2009.

**ACKNOWLEDGEMENTS** - Never in my life would I have thought that I would start doing research as an undergraduate. This is why I would like to thank my family and friends for being supportive and understanding of the importance of my research to me. A special thanks to Dr. Scott Annin, my professor, advisor, and friend for always steering me in the right direction.

## On kth roots in the Symmetric Inverse Monoid\*

TROY CANNON, CARLOS HERNANDEZ, LUIS TORRES

Advisor: Dr. Scott Annin

#### **Abstract**

This paper classifies elements in the symmetric inverse monoid SIM(n) that possess kth roots, for fixed positive integers n and k. This is done by classifying the so-called terminating cycles with kth roots and then combining these results with those for kth roots in  $S_n$  [2]. The proofs of these results provide procedures for constructing such roots. We also look at issues under consideration for some semigroups closely related to SIM(n).

#### 1 Introduction

In this paper, we will study roots in the familiar semigroup, the symmetric inverse monoid SIM(n), consisting of all partial one-to-one transformations of the set  $X = \{1, 2, ..., n\}$ . For example, if  $X = \{1, 2, 3, 4, 5\}$ , then the element that maps  $1 \to 3$ ,  $4 \to 1$ ,  $5 \to 2$ , and does not map 2 or 3 to anything can be denoted  $\begin{pmatrix} 1 & 2 & 3 & 4 & 5 \\ 3 & - & - & 1 & 2 \end{pmatrix}$ . Let us briefly review the relevant terminology.

The semigroup SIM(n) holds an important place in semigroup theory, particularly in the study of inverse semigroups. Inverse semigroups are "close" to groups (every group is an inverse semigroup, for example), and in fact, these semigroups are closely related to aspects of geometric and combinatorial group theory [10]. They also play an increasingly significant role in the theory of operator algebras, and other branches of mathematics as well. An inverse semigroup is a semigroup S in which, for every  $a \in S$ , there exists an unique element  $x \in S$  such that a = axa and x = xax. Such x is the unique inverse of a. In general, an element of a semigroup can have more than one inverse. Provided that each element of the semigroup has at least one inverse, we call the semigroup regular. Thus, an inverse semigroup is a regular semigroup in which each element has a unique inverse. For instance, the element  $\begin{pmatrix} 1 & 2 & 3 & 4 & 5 \ 3 & - & - & 1 & 2 \end{pmatrix}$  has an inverse, namely  $\begin{pmatrix} 1 & 2 & 3 & 4 & 5 \ 4 & 5 & 1 & - & - \end{pmatrix}$ , which is unique. Some examples of regular semigroups are bands

namely  $\begin{pmatrix} 1 & 2 & 3 & 4 & 5 \\ 4 & 5 & 1 & - & - \end{pmatrix}$ , which is unique. Some examples of regular semigroups are bands (semigroups in which every element is an idempotent), groups, and SIM(n). Some examples of inverse semigroups are commutative bands, groups, and SIM(n). It has been shown by Vagner and Preston [3] that every inverse monoid M (i.e. semigroup with identity) can be embedded in a suitable SIM(X), for some set X. That is, there exists an injective semigroup homomorphism  $\varphi: M \to SIM(X)$  for some X.

Symmetric inverse semigroups enjoy a major role in the landscape of theoretical algebra, as demonstrated by the extensive literature on the subject. An entire volume [9] was composed

<sup>\*</sup>This research was partially supported by a CURM mini-grant funded by the NSF grant DMS-0636648

in the 1990s and devoted entirely to the subject of symmetric inverse semigroups (see also [1]). There is indeed much to say. Many parallels with the development of group theory can be found, yet the territory of semigroups remains unquestionably the most challenging.

Throughout this paper, we use  $\mathbb{Z}^+$  to denote the set of positive integers. For fixed k and n in  $\mathbb{Z}^+$ , our aim is to classify the elements of  $\mathrm{SIM}(n)$  that possess kth roots. This is accomplished in our main results, Theorems 3.2 and 3.6. Before we proceed, let us develop an efficient notation to represent the elements of  $\mathrm{SIM}(n)$ . As we shall see momentarily, every element of  $\mathrm{SIM}(n)$  can be written as a permutation in  $S_n$  (possibly the identity) multiplied by a product of so-called terminating cycles (Definition 1.1 below). We will call the cycles that are in a permutation in  $S_n$  traditional cycles. Recall from basic modern algebra [4], [8], [11] that the traditional cycle  $(a_1a_2\ldots a_r)$  denotes the permutation in  $S_n$  that maps  $a_1$  to  $a_2$ ,  $a_2$  to  $a_3$ , ...,  $a_r$  to  $a_1$ . Let us now define the notion of a terminating cycle.

**Definition 1.1.** Let  $\sigma = (a_1 a_2 \dots a_t -) \in SIM(n)$  denote the partial one-to-one mapping that sends  $a_1$  to  $a_2$ ,  $a_2$  to  $a_3$ , ...,  $a_{t-1}$  to  $a_t$ , and does not map  $a_t$  to anything. We call  $(a_1 a_2 \dots a_t -)$  a terminating cycle. Define the length of  $\sigma$ , denoted  $\ell(\sigma)$ , to be t.

Our work will take advantage of the disjoint cycle (both terminating and traditional) representation of elements in SIM(n). Such expressions are uniquely determined for each element, up to the order in which the disjoint cycles appear in the product.

### 2 Preliminary Results

We begin with some basic results and terminology that will facilitate the statement and proof of our main results in Section 3.

For  $m, k \in \mathbb{Z}^+$ , we will denote the floor of  $\frac{m}{k}$  by  $\lfloor \frac{m}{k} \rfloor$  and the ceiling of  $\frac{m}{k}$  by  $\lceil \frac{m}{k} \rceil$  in what follows.

**Lemma 2.1.** Let  $m \ge k$  for some  $m, k \in \mathbb{Z}^+$ . Write m = qk + r, where  $r \in \{0, 1, 2, ..., k - 1\}$ . Then  $(a_1 a_2 ... a_m -)^k$  is a product of r terminating cycles of length  $\lceil \frac{m}{k} \rceil$  and k - r terminating cycles of length  $\lfloor \frac{m}{k} \rfloor$ .

**Proof** Note that we have  $q = \lfloor \frac{m}{k} \rfloor \geq 1$ . It is easy to see by direct computation that

$$(a_1 a_2 \dots a_m -)^k = \prod_{i=1}^r (a_i a_{k+i} a_{2k+i} \dots a_{qk+i} -) \cdot \prod_{i=r+1}^k (a_i a_{k+i} \dots a_{(q-1)k+i} -)$$

Hence,  $(a_1 a_2 \dots a_m -)^k$  consists of r terminating cycles of length  $\lceil \frac{m}{k} \rceil$  and k-r terminating cycles of length  $\lfloor \frac{m}{k} \rfloor$ .

**Example 2.2.** Let m=33 and k=7 and consider the element  $(1\ 2\ 3\ \dots\ 33\ -)^7$ . By direct calculation, q=4 and r=5. So  $(1\ 2\ 3\ \dots\ 33\ -)^7$  must have 5 terminating cycles of length q+1=4+1=5 and k-r=7-5=2 terminating cycles of length q=4. In fact,

$$(1\ 2\ 3\ \dots\ 33\ -)^7 = (1\ 8\ 15\ 22\ 29\ -)(2\ 9\ 16\ 23\ 30\ -)(3\ 10\ 17\ 24\ 31\ -)\dots$$
  
 $\dots (4\ 11\ 18\ 25\ 32\ -)(5\ 12\ 19\ 26\ 33\ -)(6\ 13\ 20\ 27\ -)(7\ 14\ 21\ 28\ -).$ 

**Lemma 2.3.** If m < k, then  $(a_1 a_2 \dots a_m -)^k = (a_1 -)(a_2 -) \dots (a_m -)$ .

Proof Trivial.

**Lemma 2.4.** A product of k disjoint terminating cycles has a kth root in SIM(n) if and only if the lengths of the cycles differ at most by 1.

**Proof of**  $\Longrightarrow$  Let  $\sigma$  be a product of k disjoint terminating cycles that has a kth root in SIM(n), such that  $\sigma = \sigma_1 \sigma_2 \dots \sigma_k = \alpha^k$ . Thus,  $\alpha^k$  consists of exactly k disjoint terminating cycles.

Case 1: Suppose  $\alpha$  is a single cycle of length m. If m < k, then  $\alpha^k$  is only a product of m disjoint terminating cycles (by Lemma 2.3), a contradiction. So  $m \ge k$ . Lemma 2.1 implies that  $\alpha^k$  produces k cycles whose lengths differ by  $\le 1$ , since  $\lceil \frac{m}{k} \rceil - \lfloor \frac{m}{k} \rfloor \le 1$ .

Case 2: Suppose  $\alpha = \alpha_1 \alpha_2 \dots \alpha_j$  for  $j \geq 2$  and  $\ell(\alpha_i) = m_i$ . If there exists an i such that  $m_i \geq k$ , then  $\alpha_i^k$  is already a product of k terminating cycles, so  $\alpha^k$  has too many terminating cycles. So for all i,  $m_i < k$ . Thus,  $\alpha^k$  consists only of cycles of length 1.

**Proof of**  $\Leftarrow$  Suppose  $\sigma$  consists of r cycles of length q+1 and k-r cycles of length q. By a suitable re-labelling of the elements of these cycles, we can write

$$\sigma = \prod_{i=1}^{r} (a_i a_{k+i} a_{2k+i} \dots a_{qk+i}) \cdot \prod_{i=r+1}^{k} (a_i a_{k+i} \dots a_{(q-1)k+i}).$$

We see that  $\sigma$  is a product of k disjoint terminating cycles whose lengths differ from each other by at most 1. By Lemma 2.1,

$$(a_1 a_2 \dots a_{qk+r})^k = \prod_{i=1}^r (a_i a_{k+i} a_{2k+i} \dots a_{qk+i}) \cdot \prod_{i=r+1}^k (a_i a_{k+i} \dots a_{(q-1)k+i}) = \sigma,$$

and so  $\sigma$  has a kth root.

**Fact 2.5.** For  $n \geq 3$ , every element of rank 1 in SIM(n) has a kth root whenever  $k \leq n-1$ .

**Proof** We prove this by cases. Every element  $\sigma$  of rank 1 has one of the following forms:

1. 
$$\sigma = (a_2 -)(a_3 -) \dots (a_n -)$$
  
2.  $\sigma = (a_1 a_2 -)(a_3 -) \dots (a_n -)$ 

Case 1: We have,

$$\sigma^k = (a_2 -)(a_3 -) \dots (a_n -) = \sigma.$$

Therefore,  $\sigma$  is a kth root of itself.

Case 2: Let

$$\tau = (a_1 a_3 a_4 a_5 \dots a_{k+1} a_2 -) (a_{k+2} -) \dots (a_n -).$$

Then,

$$\tau^k = (a_1 a_2 -)(a_3 -) \dots (a_n -) = \sigma.$$

Therefore,  $\tau$  is a kth root of  $\sigma$ .

Hence, every element of rank 1 in SIM(n) has a kth root.

**Fact 2.6.** Let  $\sigma = (a_1 a_2 \dots a_m -)$  with  $m \geq 2$ . Then  $\sigma$  fails to have a kth root in SIM(n) for  $k \geq 2$ .

**Proof** If  $\tau \in S_n$ , then  $\tau^k \in S_n$  for all  $k \in \mathbb{Z}^+$ . So  $\tau^k \neq \sigma$ . Also, if  $\tau \in SIM(n)$  with  $rank(\tau) \leq n-2$ , then  $rank(\tau^k) \leq rank(\tau) \leq n-2$  for all k, so  $\tau^k \neq \sigma$ , since  $rank(\sigma) = n-1$ . Therefore, if  $\sigma$  has a kth root, we must have  $\sigma = \tau^k$  for some  $\tau \in SIM(n)$  with  $rank(\tau) = n-1$ . In this case, it is easy to see that  $rank(\tau^k) = n-1$  if and only if  $\tau$  acts as a permutation on n-1 elements and kills the one remaining element. But this same thing is then true for  $\tau^k$  for all  $k \geq 1$ , so  $\tau^k \neq \sigma$ . Hence,  $\sigma$  has no kth root in SIM(n).

Fact 2.7. Let  $\sigma \in SIM(n)$  with  $rank(\sigma) = n - 1$ . Write  $\sigma = (a_1 a_2 \dots a_m -) \mu$  where  $\mu \in S_{n-m}$ . For  $k \geq 2$ ,  $\sigma$  has a kth root in SIM(n) if and only if  $\mu$  has a kth root in  $S_{n-m}$  and m = 1.

**Proof** Let  $\sigma = (a_1 a_2 \dots a_m -) \mu$  with  $\mu \in S_{n-m}$  (Here,  $S_{n-m}$  refers to the group of permutations on the set  $\{1, 2, \dots, n\} - \{a_1, a_2, \dots, a_m\}$ ). Assume  $\sigma$  has a kth root. This means that  $\mu$  has to have a kth root in  $S_{n-m}$  and  $(a_1 a_2 \dots a_m -)$  must have a kth root in SIM(n). From Fact 2.6, the terminating cycle with length  $m \geq 2$  fails to have a kth root. Hence, m < 2, and we have m = 1. The converse follows from the fact that  $(a_1 -)^k = (a_1 -)$  and the assumption that  $\mu = \tau^k$  for some  $\tau \in S_{n-1}$ . Thus  $[(a_1 -)\tau]^k = (a_1 -)\mu$ .

Before we state and prove our main theorems characterizing the elements of SIM(n) that possess kth roots, we need to state some definitions.

**Definition 2.8.** Fix  $k \in \mathbb{Z}^+$ . Let  $\{\sigma_1, \sigma_2, \dots, \sigma_r\}$  be a set of disjoint terminating cycles. For each positive integer i, let  $m_i$  be the number of terminating cycles in this collection of length i. Without loss of generality, assume that these cycles are arranged in order of weakly increasing length, that is

$$\ell(\sigma_1) \le \ell(\sigma_2) \le \cdots \le \ell(\sigma_r).$$

Using the Division Algorithm, write

$$m_2 + m_3 + \dots + m_{\ell(\sigma_r)} = q \cdot k + r_1, \qquad 0 \le r_1 < k.$$

If the following properties hold:

- 1.  $\ell(\sigma_1)=1$ ,
- 2.  $\ell(\sigma_{i+k-1}) \ell(\sigma_i) \le 1$ , (for all i = 1, 2, ..., r k + 1)
- 3. if  $r_1 \neq 0$ , then  $m_1 \geq k r_1$ ,

then we call  $\{\sigma_1, \sigma_2, \dots, \sigma_r\}$  an initial k-cluster.

#### Example 2.9. Consider the element

$$\sigma = (1 \ 2-)(3-)(4-)(5 \ 6 \ 7-)(8 \ 9-)(10 \ 11-) \in SIM(11).$$

Rearrange the cycles of  $\sigma$  in weakly increasing order of length. Let  $\sigma_1 = (3-)$ ,  $\sigma_2 = (4-)$ ,  $\sigma_3 = (1\ 2-)$ ,  $\sigma_4 = (8\ 9-)$ ,  $\sigma_5 = (10\ 11-)$ ,  $\sigma_6 = (5\ 6\ 7-)$ . Then  $\sigma = \sigma_1\sigma_2\sigma_3\sigma_4\sigma_5\sigma_6$ . Suppose that k = 2. We claim that  $\{\sigma_1, \sigma_2, \sigma_3, \sigma_4, \sigma_5, \sigma_6\}$  is an initial 2-cluster, according to Definition 2.8. To see this, we verify the Properties 2 and 3 as follows:

Property 2: For i = 1, 2, 3, 4, 5,

$$\ell(\sigma_{1+2-1}) - \ell(\sigma_1) = \ell(\sigma_2) - \ell(\sigma_1) = 1 - 1 = 0 \le 1$$

$$\ell(\sigma_{2+2-1}) - \ell(\sigma_2) = \ell(\sigma_3) - \ell(\sigma_2) = 2 - 1 = 1 \le 1$$

$$\ell(\sigma_{3+2-1}) - \ell(\sigma_3) = \ell(\sigma_4) - \ell(\sigma_3) = 2 - 2 = 0 \le 1$$

$$\ell(\sigma_{4+2-1}) - \ell(\sigma_4) = \ell(\sigma_5) - \ell(\sigma_4) = 2 - 2 = 0 \le 1$$

$$\ell(\sigma_{5+2-1}) - \ell(\sigma_5) = \ell(\sigma_6) - \ell(\sigma_5) = 3 - 2 = 1 \le 1.$$

Property 3: We have  $m_1 = 2$ ,  $m_2 = 3$ , and  $m_3 = 1$ . So  $m_2 + m_3 = 4 = 2 \cdot 2 + 0$ , so q = 2 and  $r_1 = 0$ . So Property 3 is vacuously true.

Hence  $\{\sigma_1, \sigma_2, \sigma_3, \sigma_3, \sigma_4, \sigma_5, \sigma_6\}$  is an initial 2-cluster.

Next, suppose k = 3. We check the properties of an initial 3-cluster:

Property 2: For i = 1, 2, 3, 4,

$$\ell(\sigma_{1+3-1}) - \ell(\sigma_1) = \ell(\sigma_3) - \ell(\sigma_1) = 2 - 1 = 1 \le 1$$

$$\ell(\sigma_{2+3-1}) - \ell(\sigma_2) = \ell(\sigma_4) - \ell(\sigma_2) = 2 - 1 = 1 \le 1$$

$$\ell(\sigma_{3+3-1}) - \ell(\sigma_3) = \ell(\sigma_5) - \ell(\sigma_3) = 2 - 2 = 0 \le 1$$

$$\ell(\sigma_{4+3-1}) - \ell(\sigma_4) = \ell(\sigma_6) - \ell(\sigma_4) = 3 - 2 = 1 \le 1.$$

Property 3: We have  $m_2 + m_3 = 4 = 1 \cdot 3 + 1$ , so q = 1 and  $r_1 = 1$ , then  $2 \ge 3 - 1$ . Therefore Property 3 holds.

Hence  $\{\sigma_1, \sigma_2, \sigma_3, \sigma_4, \sigma_5, \sigma_6\}$  is an initial 3-cluster.

Finally, suppose k = 5. Since  $\ell(\sigma_6) - \ell(\sigma_2) = 3 - 1 = 2 > 1$ ,  $\{\sigma_1, \sigma_2, \sigma_3, \sigma_4, \sigma_5, \sigma_6\}$  is not an initial 5-cluster. Note, however that since q = 0 and  $r_1 = 4$ , we have  $k - r_1 = 5 - 4 = 1 \le m_1$ , and Property 3 does hold.

**Definition 2.10.** Fix  $k \in \mathbb{Z}^+$ . Let  $\{\sigma_1, \sigma_2, \dots, \sigma_r\}$  be a set of disjoint terminating cycles. Without loss of generality, assume that these cycles are arranged in order of weakly increasing length, that is

$$\ell(\sigma_1) \leq \ell(\sigma_2) \leq \cdots \leq \ell(\sigma_r).$$

If the following properties hold:

- 1.  $\ell(\sigma_1) > 1$ ,
- 2.  $\ell(\sigma_{i+k-1}) \ell(\sigma_i) \le 1$ , (for all i = 1, 2, ..., r k + 1)
- 3. r = sk for some  $s \in \mathbb{Z}^+$ ,

then we call  $\{\sigma_1, \sigma_2, \dots, \sigma_r\}$  a regular k-cluster.

#### Example 2.11. Consider the element:

$$\sigma = (1 \ 2 \ 3-)(4 \ 5-)(6 \ 7 \ 8 \ 9-) \in SIM(9).$$

Rearrange  $\sigma$  with its cycles in weakly increasing order of length:  $\sigma_1 = (4\ 5-), \sigma_2 = (1\ 2\ 3-), \sigma_3 = (6\ 7\ 8\ 9-)$ . Suppose that k=2. Note that  $\{\sigma_1, \sigma_2, \sigma_3\}$  is not a regular 2-cluster, according to Definition 2.10, because Property 3 fails. Hence  $\sigma$  is not a regular 2-cluster.

Next suppose k = 3. Now we check the properties of a regular 3-cluster for  $\{\sigma_1, \sigma_2, \sigma_3\}$ , starting with Property 2.

Property 2: For i = 1,

$$\ell(\sigma_{1+3-1}) - \ell(\sigma_1) = \ell(\sigma_3) - \ell(\sigma_1) = 4 - 2 = 2 \nleq 1.$$

Therefore Property 2 fails.

Hence  $\sigma$  is not a regular 3-cluster, despite the fact that Property 3 does hold. Since  $\sigma$  possesses only three disjoint terminating cycles, for k > 3, the cycles comprising  $\sigma$  do not form a regular k-cluster.

#### 3 The Main Results

**Definition 3.1.** An element  $\sigma \in SIM(n)$  that can be expressed solely as a product of disjoint terminating cycles (i.e. no traditional cycles) is called a terminating element.

As we will see in Theorem 3.6, if  $\mu \in S_n$  and  $\varphi$  is a terminating element in SIM(n), then the element  $\sigma = \mu \varphi$  has a kth root in SIM(n) if and only if  $\mu$  has a kth root in  $S_n$  and  $\varphi$  has a terminating element for a kth root. So it suffices to determine when  $\varphi$  has a kth root, since the corresponding result for  $\mu \in S_n$  has been proven in [2]. In what follows, we again revert to using  $\sigma$ , rather than  $\varphi$ , for the terminating element.

**Theorem 3.2.** Let  $\sigma \in SIM(n)$  be a terminating element. Then  $\sigma \in SIM(n)$  has a kth root in SIM(n) if and only if its cycles can be arranged into a disjoint product of regular k-clusters and/or initial k-clusters.

**Proof of**  $\Longrightarrow$  Assume  $\sigma$  has a kth root. Write  $\sigma = \alpha^k$  for some  $\alpha \in SIM(n)$ . Write  $\alpha = \alpha_1 \alpha_2 \dots \alpha_t$  for some  $t \in \mathbb{Z}^+$ , where we can assume that all the  $\alpha_i$  are disjoint terminating cycles. So,

$$\sigma = \alpha_1^k \alpha_2^k \dots \alpha_t^k$$

Claim For every i, the disjoint terminating cycles of  $\alpha_i^k$  form either a regular or initial k-cluster.

**Proof** Let  $m = \ell(\alpha_i)$  and write m = qk + r,  $0 \le r < k$ . If m < k, Lemma 2.3 implies that  $\alpha^k$  consists only of cycles of length 1, so we have an initial k-cluster. Assume now that  $m \ge k$ . By Lemma 2.1,  $\alpha_i^k$  consists of r terminating cycles of length  $\lceil \frac{m}{k} \rceil$  and k - r terminating cycles of length  $\lfloor \frac{m}{k} \rfloor$ . Therefore,  $\alpha_i^k$  has exactly k disjoint terminating cycles, and since  $\lceil \frac{m}{k} \rceil - \lfloor \frac{m}{k} \rfloor \le 1$ , the cycles of  $\alpha_i^k$  satisfy Property 2 of k-clusters.

Case 1: Assume  $\lfloor \frac{m}{k} \rfloor > 1$ . Then  $\alpha_i^k$  is a regular k-cluster (apply Definition 2.10 with r = k).

Case 2: Assume  $\lfloor \frac{m}{k} \rfloor = 1$ . Then  $\alpha_i^k$  consists of  $m_1 = k - r$  terminating cycles of length 1, and  $m_2 = r < k$ . Hence q = 0 in Definition 2.8, and we have  $r_1 = r$ . So  $m_1 = k - r_1$ . Hence, the terminating cycles of  $\sigma \in SIM(n)$  can be arranged into regular and initial k-clusters.

**Proof of**  $\Leftarrow$  Assume that the terminating cycles of  $\sigma \in SIM(n)$  can be arranged into regular and initial k-clusters. It suffices to prove that a regular k-cluster and an initial k-cluster have a kth root, because the product of the kth roots of all the regular and initial k-clusters will be a kth root for  $\sigma \in SIM(n)$ .

Assume  $\sigma_1, \sigma_2, \ldots, \sigma_r$  is a regular k-cluster. Then r = sk for some  $s \in \mathbb{Z}^+$ . Since  $\ell(\sigma_{i+k-1}) - \ell(\sigma_i) \leq 1$  for all  $i = 1, 2, \ldots, r - k + 1$ , by Lemma 2.4 we can construct a kth root  $\tau_i$  for

$$\sigma_{ik+1}\sigma_{ik+2}\cdots\sigma_{ik+k}$$
 for  $i = 0, 1, 2, \dots, q-1$ .

Thus,  $\tau_0 \tau_1 \cdots \tau_{q-1}$  is a kth root of  $\sigma_1 \sigma_2 \cdots \sigma_r$ .

Next, assume  $\sigma_1, \sigma_2, \dots, \sigma_r$  is an initial k-cluster. By assumption,

$$\ell(\sigma_1) = 1$$
 and  $m_2 + m_3 + ... + m_{\ell(\sigma_r)} = qk + r_1$ ,

where  $0 \le r_1 < k$ .

Case 1: Assume  $r_1 = 0$ . Let  $\sigma_{m_1+1}, \sigma_{m_1+2}, \dots, \sigma_r$  denote the cycles of length > 1. Note that there are qk of them. Since  $\ell(\sigma_{ik+m_1+k}) - \ell(\sigma_{ik+m_1+1}) \le 1$ , by Lemma 2.4 we can construct a kth root  $\tau_i$  for

$$\sigma_{ik+m_1+1} \cdots \sigma_{ik+m_1+k}$$
 for  $i = 0, 1, 2, \dots, q-1$ .

Thus,  $\tau_0\tau_1\cdots\tau_{q-1}$  is a kth root of  $\sigma_{m_1+1}\cdots\sigma_r$ . Let  $(a_i-)$  for  $i=1,2,\ldots,m_1$  be the terminating cycles of length 1 in the cluster. Then, a kth root for the initial k-cluster is  $\tau_0\tau_1\cdots\tau_{q-1}(a_1-)(a_2-)\cdots(a_{m_1}-)$ .

Case 2: Assume  $r_1 \neq 0$ , Then  $m_1 \geq k - r_1$ . By Lemma 2.4 we can construct a kth root  $\tau_i$  for

$$\sigma_{ik+m_1-(k-r_1)+1}\cdots\sigma_{ik+m_1-(k-r_1)+k}$$
 for  $i=0,1,2,\ldots,q$ .

Thus,  $\tau_0 \tau_1 \cdots \tau_q$  is a kth root for  $\sigma_{m_1-(k-r_1)+1} \cdots \sigma_r$ .

Now, consider  $\sigma_1, \sigma_2, \ldots, \sigma_{m_1-(k-r_1)}$  all of length 1. (Note: If  $m_1 = k - r_1$ , there are no such terminating cycles to consider) write  $\sigma_i = (a_i -)$  for  $i = 1, 2, \ldots, m_1 - (k - r_1)$ . Then  $\sigma_i$  is its own kth root. Then, a kth root for the initial k-cluster is  $\tau_0 \tau_1 \cdots \tau_q(a_1 -)(a_2 -) \cdots (a_{m_1-(k-r_1)} -)$ . Hence,  $\sigma \in \text{SIM}(n)$  has a kth root.

**Example 3.3.** Let  $k \geq 3$  be arbitrary. Let  $\sigma_1 = (1-)$ ,  $\sigma_2 = (2\ 3-)$ ,  $\sigma_3 = (4\ 5\ 6\ -)$ , and  $\sigma = \sigma_1\sigma_2\sigma_3$ . Since  $\sigma$  can not be arranged into regular k-clusters and/or initial k-clusters, for all  $k \geq 3$ ,  $\sigma$  does not have a kth root ( $k \geq 3$ ) by Theorem 3.2. However,  $\{\sigma_1, \sigma_2, \sigma_3\}$  is an initial 2-cluster, so  $\sigma$  has a square root:

$$[(1-)(4\ 2\ 5\ 3\ 6-)]^2 = (1-)(2\ 3-)(4\ 5\ 6\ -).$$

**Example 3.4.** Let k=2. Let  $\sigma_1=(1\ 2\ 3\ 4-),\ \sigma_2=(5\ 6\ 7\ 8-),\ \sigma_3=(9\ 10\ 11\ 12-),\ and <math>\sigma=\sigma_1\sigma_2\sigma_3$ . Since  $\sigma$  can not be arranged into regular 2-clusters and/or initial 2-clusters,  $\sigma$  does not have a square root by Theorem 3.2. Note, however,  $\{\sigma_1,\sigma_2,\sigma_3\}$  is a regular 3-cluster so  $\sigma$  does have a cube root:

$$(1\ 5\ 9\ 2\ 6\ 10\ 3\ 7\ 11\ 4\ 8\ 12-)^3 = (1\ 2\ 3\ 4-)(5\ 6\ 7\ 8-)(9\ 10\ 11\ 12-).$$

In the preceding two examples we exhibited appropriate roots of a given element of SIM(n). These roots were easy to construct by inspection since the examples were small. More generally it would be instructive to see how to construct a kth root for an arbitrary element  $\sigma$ . Here is a more complex example:

#### Example 3.5. Does

$$(1\ 2\ 3\ 4\ -)(5\ 6\ -)(7\ 8\ 9\ 10\ 11\ -)(12\ -)(13\ 14\ 15\ 16\ -)(17\ 18\ 19\ -)(20\ 21\ -)\cdots \\ \cdots (22\ -)(23\ -)(24\ 25\ -)(26\ 27\ 28\ -)$$

have a cube root? We begin by arranging the cycles in increasing order of length by letting

$$\sigma_1 = (12 -), \ \sigma_2 = (22 -), \ \sigma_3 = (23 -), \ \sigma_4 = (5 6 -), \ \sigma_5 = (20 \ 21 -), \ \sigma_6 = (24 \ 25 -),$$

$$\sigma_7 = (17\ 18\ 19\ -)\sigma_8 = (26\ 27\ 28\ -), \ \sigma_9 = (1\ 2\ 3\ 4\ -), \ \sigma_{10} = (13\ 14\ 15\ 16\ -), \ \sigma_{11} = (7\ 8\ 9\ 10\ 11\ -)$$

and  $\sigma = \sigma_1 \sigma_2 \sigma_3 \sigma_4 \sigma_5 \sigma_6 \sigma_7 \sigma_8 \sigma_9 \sigma_{10} \sigma_{11}$ . Observe that  $\sigma$  can be arranged into one initial 3-cluster,  $\{\sigma_1, \sigma_2, \sigma_3, \sigma_4, \sigma_5\}$  and two regular 3-clusters,  $\{\sigma_6, \sigma_7, \sigma_8\}$  and  $\{\sigma_9, \sigma_{10}, \sigma_{11}\}$ . By Theorem 3.2,  $\sigma$  has a cube root. We can construct a cube root on a cluster-by-cluster basis. To construct a cube root of  $\sigma_9 \sigma_{10} \sigma_{11}$ , we build a single terminating cycle composed of the elements arising in  $\sigma_9, \sigma_{10}$ , and  $\sigma_{11}$  as follows: Interlace the elements from these three cycles, rotating between them cyclically, starting with the longest cycle,  $\sigma_{11}$ , followed by either of the shorter cycles  $\sigma_9$  or  $\sigma_{10}$ . So the pattern of interlacing takes one of the two forms:

$$\sigma_{11} \rightarrow \sigma_{10} \rightarrow \sigma_9 \rightarrow \sigma_{11} \rightarrow -$$

Oï

$$\sigma_{11} \rightarrow \sigma_9 \rightarrow \sigma_{10} \rightarrow \sigma_{11} \rightarrow -$$

We must proceed from left to right as we select elements from the same cycle through the process. Hence, we can construct either of these cube roots for  $\sigma_9\sigma_{10}\sigma_{11}$ :

(7 1 13 8 2 14 9 3 15 10 4 16 11 
$$-$$
)<sup>3</sup> =  $\sigma_9 \sigma_{10} \sigma_{11}$   
or  
(7 13 1 8 14 2 9 15 3 10 16 4 11  $-$ )<sup>3</sup> =  $\sigma_{10} \sigma_9 \sigma_{11}$ .

Next, consider the regular 3-cluster  $\{\sigma_6, \sigma_7, \sigma_8\}$ . The same interlacing process we used before will yield a single terminating cycle to serve as a cube root for  $\sigma_6\sigma_7\sigma_8$ . In this case, however, both  $\sigma_7$  and  $\sigma_8$  have the same (longest) length, so our interlacing pattern can start with either:

$$\sigma_8 \rightarrow \sigma_7 \rightarrow \sigma_6 \rightarrow \sigma_8 \rightarrow \sigma_7 \rightarrow \sigma_6 \rightarrow \sigma_8 \rightarrow \sigma_7 \rightarrow \sigma_6 \rightarrow \sigma_8 \rightarrow \sigma_7 \rightarrow -$$
or
$$\sigma_7 \rightarrow \sigma_8 \rightarrow \sigma_6 \rightarrow \sigma_7 \rightarrow \sigma_8 \rightarrow \sigma_6 \rightarrow \sigma_7 \rightarrow \sigma_8 \rightarrow -$$

So we have two possible cube roots for  $\sigma_6\sigma_7\sigma_8$ :

$$(26\ 17\ 24\ 27\ 18\ 25\ 28\ 19\ -)^3 = \sigma_6\sigma_7\sigma_8$$
 and  $(17\ 26\ 24\ 18\ 27\ 25\ 19\ 28\ -)^3 = \sigma_6\sigma_7\sigma_8$ 

Lastly, we have the initial 3-cluster  $\{\sigma_1, \sigma_2, \sigma_3, \sigma_4, \sigma_5\}$ . It turns out that numerous cube roots can be constructed. We must treat  $\sigma_1\sigma_4\sigma_5$  or  $\sigma_2\sigma_4\sigma_5$  or  $\sigma_3\sigma_4\sigma_5$  separately in like manner to that given above for the regular 3-clusters to obtain a cube root such as (20 5 23 21 6 –), where we used  $\sigma_3\sigma_4\sigma_5$ . Clearly,  $(\sigma_1\sigma_2)^3 = \sigma_1\sigma_2$  (this is true for any terminating cycles of length 1). Thus, a cube root for  $\sigma$  can be constructed by taking the product of the cube roots found for each 3-cluster above. For example,

$$(12 -)(22 -)(5\ 20\ 23\ 6\ 21\ -)(7\ 1\ 13\ 8\ 2\ 14\ 9\ 3\ 15\ 10\ 4\ 16\ 11\ -)(26\ 17\ 24\ 27\ 18\ 25\ 28\ 19\ -)$$

is a cube root of  $\sigma$ .

The reader may have noticed that  $\sigma$  will have many cube roots. In fact, it is an interesting question to consider the number of such roots, but we will not address this here. Instead, what we wish to do at present is to generalize the construction we carried out in Example 3.5 to an algorithm for producing a kth root of a terminating element when it exists. Theorem 3.6 below will address the case when  $\sigma$  contains traditional cycles.

Algorithm for constructing a kth root of a terminating element  $\sigma$ : Assume  $\sigma$  has a kth root. Arrange all (terminating) cycles of  $\sigma$  in weakly increasing order of length:

$$\sigma_1, \sigma_2, \sigma_3, \ldots, \sigma_t$$
.

Using the Division Algorithm, write  $t = d \cdot k + r$ , where  $0 \le r < k$ . By Theorem 3.2,  $\{\sigma_i\}$  can be arranged into initial and/or regular k-clusters. Since the number of k-cycles in each regular k-cluster is a multiple of k, we must have at least r cycles of length  $1, \sigma_1, \sigma_2, \sigma_3, \ldots, \sigma_r$ . Clearly, for  $i \le r$ ,  $\sigma_i^k = \sigma_i$ . So  $\sigma_i$  can serve as its own kth root for  $i \le r$ . The remaining  $d \cdot k$  cycles,  $\sigma_{r+1}, \sigma_{r+2}, \ldots, \sigma_t$  can be put into d groups of k as follows:

$$S_j := [\sigma_{jk+1+r}, \dots, \sigma_{(j+1)\cdot k+r}], \qquad j = 0, 1, 2, \dots, d-1.$$

Since the cycles  $\sigma_i$  belong to initial and/or regular k-clusters,

$$\ell(\sigma_{(j+1)\cdot k+r}) - \ell(\sigma_{jk+1+r}) \le 1,$$
 for all  $j = 0, 1, 2, \dots, d-1$ .

The proof of  $\Leftarrow$  in Lemma 2.4 exhibits a kth root for the product of the cycles in each collection  $S_j$  above, achieved by interlacing the elements in the cycles of  $S_j$ , from right to left.

**Theorem 3.6.** Let  $\sigma \in SIM(n)$  and write  $\sigma = \mu \varphi$  where  $\mu \in S_n$  and  $\varphi$  is a terminating element. Then  $\sigma$  has a kth root in SIM(n) if and only if  $\mu$  has a kth root in  $S_n$  and  $\varphi$  has a terminating cycle for a kth root.

**Proof of**  $\Longrightarrow$  Assume  $\sigma = \tau^k$  and  $\tau \in SIM(n)$ . Write  $\tau = \alpha\beta$  where  $\alpha \in S_n$  and  $\beta$  is a terminating element. So,

$$\sigma = (\alpha \beta)^k = \alpha^k \beta^k = \mu \varphi.$$

Since  $\alpha^k$  contains no terminating cycles, because  $\alpha \in S_n$ , and  $\beta^k$  contains no traditional cycles, since  $\beta$  is composed of terminating cycles, we have

$$\mu = \alpha^k$$
 and  $\varphi = \beta^k$ .

**Proof of**  $\Leftarrow$  Write  $\mu = \alpha^k$  for some  $\alpha \in S_n$  and  $\varphi = \beta^k$  for some terminating element  $\beta$ . Then

$$\sigma = \mu \varphi = \alpha^k \beta^k = (\alpha \beta)^k.$$

**Example 3.7.** Consider  $\mu = (1\ 2\ 3\ 4\ 5)(6\ 7)(8\ 9)$  and  $\varphi = (10\ 11\ 12\ 13-)(14\ 15\ 16\ 17-)(18\ 19\ 20\ 21-)$ .

$$\sigma = \mu \varphi = (1\ 2\ 3\ 4\ 5)(6\ 7)(8\ 9)(10\ 11\ 12\ 13-)(14\ 15\ 16\ 17-)(18\ 19\ 20\ 21-) \in SIM(21).$$

From ([2], Example 4), we know  $\mu$  has a cube root. The cycles of  $\varphi$  are arranged in order of weakly increasing length, and since they all have length 4, the cycles of  $\varphi$  form a regular 3-cluster. From Theorem 3.2,  $\varphi$  has a cube root. According to Theorem 3.6,  $\sigma$  has a cube root in SIM(21). Indeed, we can verify

$$[(1\ 3\ 5\ 2\ 4)(6\ 7)(8\ 9)(10\ 14\ 18\ 11\ 15\ 19\ 12\ 16\ 20\ 13\ 17\ 21-)]^3=\cdots$$

$$\cdots$$
 (1 2 3 4 5)(6 7)(8 9)(10 11 12 13-)(14 15 16 17-)(18 19 20 21-).

Note:  $\sigma$  does not have a fourth root since from ([2], Example 4),  $\mu$  does not have a fourth root.

**Example 3.8.** Consider 
$$\mu = (1\ 2\ 3\ 4\ 5)(6\ 7)(8\ 9)$$
 and  $\varphi = (10-)(11\ 12-)(13\ 14\ 15-)$ . Let  $\sigma = \mu \varphi = (1\ 2\ 3\ 4\ 5)(6\ 7)(8\ 9)(10-)(11\ 12-)(13\ 14\ 15-) \in SIM(15)$ .

From ([2], Example 4), we know  $\mu$  has a cube root. However  $\varphi$  does not have a cube root from Example 3.3 . According to Theorem 3.2,  $\sigma$  does not have a cube root. On the other hand, we see that  $\sigma$  does have a square root:

$$[(1\ 4\ 2\ 5\ 3)(6\ 8\ 7\ 9)(10-)(13\ 11\ 14\ 12\ 15-)]^2 = (1\ 2\ 3\ 4\ 5)(6\ 7)(8\ 9)(10-)(11\ 12-)(13\ 14\ 15-).$$

### 4 Further Questions

Hoping that the results just presented will inspire readers, we finish with some tantalizing questions that can expand the research further.

**Problem 4.1.** If k and n are fixed positive integers and an element of SIM(n) is chosen at random, what is the probability that the element possesses a kth root in SIM(n)?

For small values of n, we have collected some preliminary data in the case k=2. As the results suggest, the probability appears to tend toward 0 as  $n \to \infty$ , but no rigorous proof has been formulated.

n	SIM(n)	# of elements with square root	% of $SIM(n)$
1	2	2	100
2	7	4	57.14
3	34	16	47.06
4	209	83	39.71
5	1546	546	35.32
6	13327	4102	30.78
7	130922	35246	26.92
8	1441729	340797	23.64

Table 2: Precentage of elements in SIM(n) with square roots.

It is interesting to compare the results of the question for SIM(n) in the table above with those obtained in [2] for  $S_n$ . The bar graphs below suggest that the behavior in both settings are similar, but the odds are better for  $n \geq 3$  that an element chosen from  $S_n$  will have a square root than an element chosen from SIM(n).

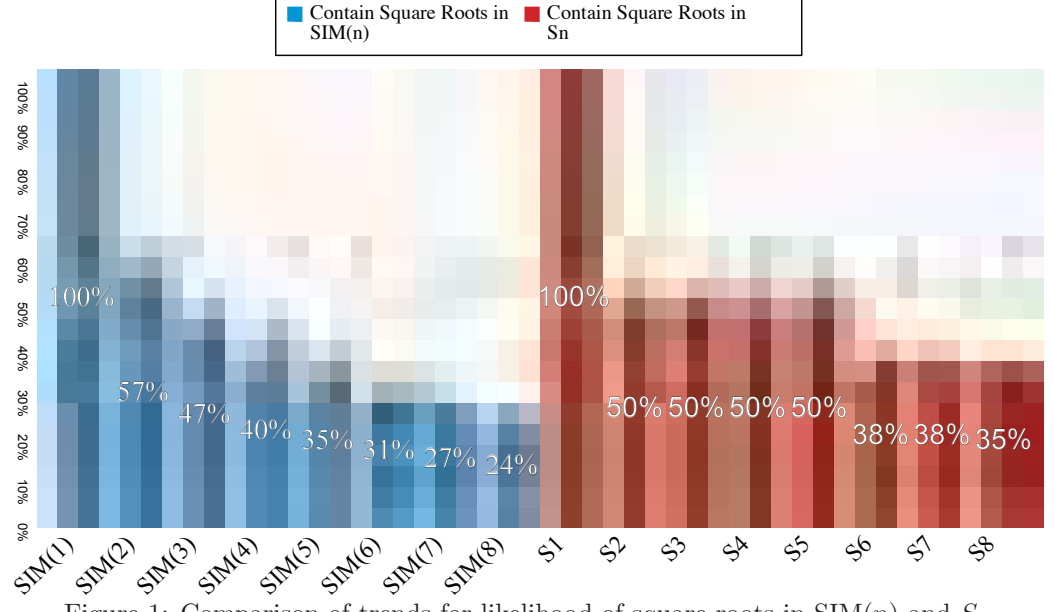


Figure 1: Comparison of trends for likelihood of square roots in SIM(n) and  $S_n$ 

**Problem 4.2.** Several notable semigroups are related to the symmetric inverse monoid, including the dual symmetric inverse monoid  $SIM^*(n)$  (see also [5] or [7]), the submonoid POI(n) [6] of

SIM(n) consisting of the collection of all partial order-preserving one-to-one mappings in SIM(n), and FTS(n), the full transformation semigroup of all functions mapping  $\{1, 2, ..., n\}$  to itself. The question of kth roots for elements in these and other semigroups remains open. Let us make a few preliminary remarks that should be helpful in studying our problem in these semigroups. We begin with  $SIM^*(n)$ .

Now,

 $SIM^*(n)$  = the semigroup of all isomorphisms between quotients of an *n*-set.

The notion of taking quotients of an n-set is perhaps best understood by considering an example. **Example 4.3.** We consider an example of an element  $\sigma \in SIM^*(8)$ . The idea is that the elements

**Example 4.3.** We consider an example of an element  $\sigma \in SIM^*(8)$ . The idea is that the elements of the set  $\{1,2,3,4,5,6,7,8\}$  are "glued" into blocks, and then the blocks are permuted by  $\sigma$ . Thus, we call  $\sigma$  a block bijection. To represent it, we can use traditional 2-line notation using vertical bars to separate the blocks, or we can draw pictures such as that shown in the figure.



Figure 2: Illustration of an element in SIM\*(8).

To "multiply" elements of this semigroup, we compose isomorphisms together. Once more, the pictures can be an invaluable aid in this process. For instance, when we square this element, we essentially draw 2 copies of it, joined in the middle line,

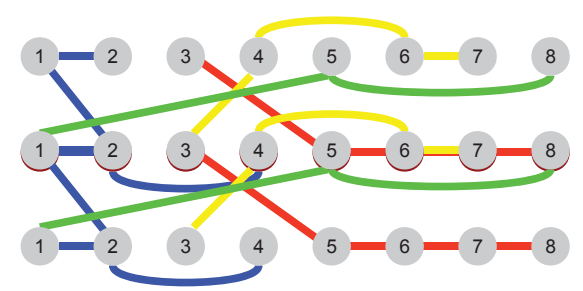


Figure 3: Illustration of how to square an element in SIM\*(8).

Once the middle rows are stacked upon each other, then the connected components of the resulting graph are constructed and the interior vertices are ignored [5]. That is, we follow the connected lines to see the end result:

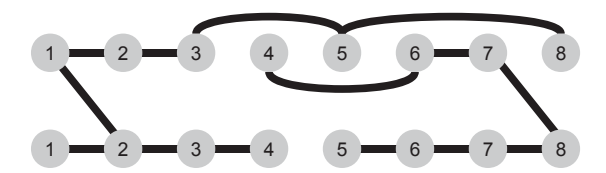


Figure 4: The result of squaring the element in Figure 2.

or equivalently,

The calculation above shows therefore that this latter element does indeed have a square root. Nonetheless, the reader can rightly see that drawing general conclusions about kth roots in this complicated semigroup is a formidable challenge.

The following are preliminary results and some relevant terminology:

**Notation:** Let  $\sigma \in SIM^*(n)$ . We define rank $(\sigma)$  by

 $r=rank(\sigma)=$  number of blocks in the domain of  $\sigma=$  the number of blocks in the range of  $\sigma$ .

Write  $Dom(\sigma)=(B_1,B_2,\ldots,B_r)$  and  $Rng(\sigma)=(C_1,C_2,\ldots,C_r)$ :

Figure 5: The block structure of an element in  $SIM^*(n)$ 

Then we say that  $Dom(\sigma)$  creates a partition of  $n: B_1, B_2, \ldots, B_r$ 

**Definition 4.4.** A trivial block bijection element is one such that each block maps to itself, that is, for some  $r \leq n$ ,

Figure 6: A trivial block bijection

**Definition 4.5.** A simple block bijection is an element  $\alpha \in SIM^*(n)$  such that the blocks of  $Dom(\alpha)$  are the same as the blocks in  $Rng(\alpha)$ . If, in addition,  $\alpha$  acts as an identity on these blocks, then  $\alpha$  is a trivial block bijection.

Conjecture 4.6. Let  $\alpha$  be a simple block bijection in  $SIM^*(n)$  consisting of r blocks. Then  $\alpha$  has a kth root in  $SIM^*(n)$  if and only if  $\sigma \in S_r$  has a kth root [2], where  $\sigma$  is the permutation in  $S_r$  induced by the simple block bijection.

Next, we turn our attention to the monoid  $\mathcal{POI}(n)$ . As noted above,  $\mathcal{POI}(n) \subseteq SIM(n)$  consists of the set of all partial *order-preserving* one-to-one mappings from  $\{1, 2, ..., n\} \longrightarrow \{1, 2, ..., n\}$ , or equivalently,

$$\mathcal{POI}(n) = \{ \sigma \in SIM(n) : \text{If } i, j \in Dom(\sigma) \text{ with } i < j, \text{ then } \sigma(i) < \sigma(j) \}$$

For example:

$$\begin{pmatrix} 1 & 2 & 3 & 4 & 5 \\ 3 & 5 & - & 1 & - \end{pmatrix} = (413 - )(25 - ) \notin \mathcal{POI}(5) \text{ but } \begin{pmatrix} 1 & 2 & 3 & 4 & 5 \\ - & 1 & - & 3 & 5 \end{pmatrix} = (43 - )(21 - ) \in \mathcal{POI}(5).$$

By considering the two-line notation, it is easy to see that  $\sigma$  belongs to  $\mathcal{POI}(n)$  if and only if the entries on the second line appear in increasing order (from left to right). So, we ask: which elements of  $\mathcal{POI}(n)$  possess kth roots? To answer this question, the following helpful observations have been made:

**Remark 4.7.** If  $\sigma \in SIM(n)$  contains a traditional cycle not equal to the identity, then  $\sigma \notin \mathcal{POI}(n)$ . So we can restrict our attention to  $\sigma \in SIM(n)$  such that  $\sigma$  is a product only of terminating cycles.

**Definition 4.8.** Let  $\sigma = (a_1 a_2 \dots a_m)$  be a terminating cycle. We say that  $\sigma$  is

- a)monotonically increasing if  $a_1 < a_2 < \cdots < a_m$
- b)monotonically decreasing if  $a_1 > a_2 > \cdots > a_m$
- c)monotonic if it is monotonically increasing or monotonically decreasing.

Remark 4.9. Every element  $\sigma \in \mathcal{POI}(n)$  is expressible as a disjoint product of monotonic cycles. Note, however, that the converse of this remark fails, since some elements that do not belong to  $\mathcal{POI}(n)$  can also be expressed as a disjoint product of monotonic cycles. As an example, take  $\sigma = (124-) \notin \mathcal{POI}(4)$ . It is monotonically increasing, but fails to be order preserving since  $\sigma(3) = 3 < 4 = \sigma(2)$ .

**Remark 4.10.** If  $\sigma = (a_1 a_2 \dots a_m -)$  is monotonic, then  $\sigma^k = (a_1 a_2 \dots a_m -)^k$  is a regular or initial k-cluster consisting of either monotonically increasing or monotonically decreasing terminating cycles.

Remark 4.11. Observe that  $\sigma \in \mathcal{POI}(n)$  might have a kth root in SIM(n), according to Theorem 3.2, but yet no kth root in  $\mathcal{POI}(n)$ . As an example, take  $\sigma = (1-)(23-) \in \mathcal{POI}(3)$ . It has a square root  $\tau = (231-) \in SIM(3) \setminus \mathcal{POI}(3)$ . We want to classify the elements that have kth roots inside  $\mathcal{POI}(n)$ .

Conjecture 4.12. Let  $\sigma = \alpha_1 \alpha_2 \cdots \alpha_l \in \mathcal{POI}(n)$  be a disjoint product of monotonic cycles. Then  $\sigma$  has a kth root  $\tau \in \mathcal{POI}(n)$  if and only if the  $\alpha_i$  can be arranged as a product of initial and/or regular k-clusters such that the difference of consecutive elements in each cycle  $\alpha_i$  has absolute value at least k.

Finally, we turn our attention to the semigroup FTS(n). As noted above, FTS(n) consists of all functions mapping  $\{1, 2, ..., n\}$  to itself, under composition of functions, or equivalently

$$FTS(n) = (\alpha : \{1, 2, ..., n\} \to \{1, 2, ..., n\}, \circ) \supseteq S_n.$$

This semigroup has the analogous result that  $S_n$  has for Cayley's Theorem. Therefore, it is natural to ask: For fixed  $k \in \mathbb{Z}^+$ , which elements of FTS(n) possess kth roots?

The situation is easy to resolve for elements of rank 1, where rank( $\alpha$ ):=|Rng( $\alpha$ )|. For instance,

$$\alpha = \begin{pmatrix} 1 & 2 & 3 & 4 & 5 \\ 3 & 3 & 3 & 3 & 3 \end{pmatrix} \in FTS(5) \text{ has rank 1.}$$

**Remark 4.13.** For every  $\alpha \in FTS(n)$  with  $rank(\alpha)=1$  we have  $\alpha^k=\alpha$  for all  $k \in \mathbb{Z}^+$ . Thus  $\alpha$  is its own kth root in FTS(n).

#### **REFERENCES**

- [1] Annin, S., Hierarchy of efficient generators of the symmetric inverse monoid, Semigroup Forum Vol. 54, pp 327-355, 1997.
- [2] Annin, S., Jansen, T. and Smith, C., On kth roots in the symmetric and alternating groups, Pi Mu Epsilon Journal, Vol.12, No.10, pp 581-589,2009.
- [3] Clifford, A.H. and Preston, G., B., "The Algebraic Theory of Semigroups," Vol. 1, American Mathematical Society, Providence, RI, 1961.
- [4] Dummit, D. and Foote, R., "Abstract Algebra," 2nd ed., John Wiley and Sons, Inc., Hoboken, NJ, 1999.
- [5] Easdown, D., East, J., and Fitzgerald, D. G., A Presentation of the Dual Symmetric Inverse Monoid, International Journal of Algebra and Computaion, Vol. 18, No. 2, pp 357-374, 2008.
- [6] East, J., A Presentation of the Singular Part of the Symmetric Inverse Monoid, Communications in Algebra, Vol. 34, pp 1671-1689, 2006.
- [7] Fitzgerald, D. G. and Leech J., Dual Symmetric inverse Monoids and Representation Theory, J. Aust. Math. Soc.64, pp. 345-367, 1998.

- [8] Hungerford, T., "Abstract Algebra: An Introduction," 2nd ed., Brooks and Cole, 1996.
- [9] Lipscomb, S., "Symmetric Inverse Semigroups", Mathematical Surveys and Monographs, Vol. 46, American Mathematical Society, Providence, RI, 1996.
- [10] Meakin, I., Groups and Semigroups: Connections and Contrasts, London Mathematical Society Lecture Note Series 340, Vol. 2, pp 357-400, 2005.
- [11] Rotman, J., "A First Course in abstract Algebra with Applications", 3rd ed., Pearson, Upper Saddle River, NJ, 2006.

**ACKNOWLEDGEMENTS** - We would like to thank Michael Dorff and the NSF for the CURM mini-grant that helped fund this research. We also would like to especially thank our advisor, Dr. Scott Annin, for his dedication and counsel in our research endeavors.

## Relay Coverage Studies for the International Lunar Network

#### LYNETTE ZAMORA

California State University, Fullerton

Faculty Advisors: James Schier and Charles H. Lee

Space Communications and Navigation Office, Space Operations Mission Directorate

NASA Headquarters, 300 E St SW, Washington, DC 20546-0001

ABSTRACT - Efforts by the U.S. and other international space agencies (Canada, France, Germany, India, Italy, Japan, the Republic of Korea, and the United Kingdom) are underway to develop and deliver instruments to the lunar surface to explore the Moon collaboratively in the next decade. A series of geophysical nodes, including four NASA landers, to be launched as early as 2017, will evolve gradually into an International Lunar Network (ILN) of six to eight elements. These geophysical monitoring stations are expected to be launched and operated by the different space organizations, but will function simultaneously as a single seismic monitoring network. ILN landing sites have not been studied but will require wide geographic separation similar to the ten high-priority landing sites, which have been identified in the NASA's Exploration Systems Architecture Study (ESAS) as locations of profound scientific value. Six among these sites are either located on the far side of the Moon, which has no direct contact with Earth, or at the lunar limb, where landers could, depending on the libration of the Moon, spend days without seeing Earth. Thus the presence of a relay satellite at the Moon will make the establishment of the ILN flexible, versatile, and global. More importantly, communication payload of the geophysical nodes, in both mass and power, will be reduced as lesser effort is required to send data to Earth via a relay satellite at the Moon. An International Lunar Relay (ILR) satellite is postulated because it requires the use of compatible communications spectrum, standards, compliances, and interoperability between the different international partners. In this article, we focus on the coverage and the telecom capabilities provided by different candidate orbit selections for the ILR. We particularly

consider stable frozen lunar orbits that can provide pole-to-pole periodic global communication coverage and at the same time excellent data throughput. Nominal S-band telecom configurations for both the geophysical stations and the ILR are assumed. Various contact and telecom metrics such as the contact frequency, duration, maximum gaps, link performance, data rates, and data throughputs will be calculated using the JPL-developed Telecom Orbit Analysis and Simulation Tool (TOAST). We will end the article with the discussion of our findings and the optimal orbit suggestions for the ILR.

INTRODUCTION - Over the next decade, the establishment of an International Lunar Network (ILN) will take place in the form of a geophysical network consisting of six to eight stations carefully positioned on the lunar surface and operating continuously for a six year lunar cycle. The goal of the ILN will be to investigate and understand the composition and structure of the deep inner core of the moon, including lunar seismic activities, lunar heat flows, and lunar interior conductivity as well as the early history of the Earth-Moon evolution. Although each space agency is responsible for launching and delivering one or more geophysical stations to the Moon's surface independently, these stations will function collaboratively as a single network to conduct experiments and collect measurements simultaneously. Since each agency operates on its own budget and schedule, the period for ILN data collection may stretch to 10 years or longer. Significant information on both the composition and structure of the moon were obtained during the previous Apollo Lunar missions. During the Apollo era, no instruments were placed on the far side of the moon

where communications between the lunar nodes and the Earth would have required a relay system. In fact, the Apollo era nodes were geographically clustered together on the moon's near side (Figure 1). Consequently, analysis of Apollo seismic data has provided only partial understanding of lunar internal structure, evolution, and behavior.



Figure 1. Locations of Apollo, Surveyor and Luna landing sites. Red lines denote the Apollo passive seismic network (stations at the A12, A14, A15 and A16 sites); black lines denote the laser retrore—flector network. The small angular distances between stations (<1200 km) limited the ability of the seismic experiment to probe the deep lunar interior [1].

For purposes of this paper, to avoid similar results as the Apollo Lunar Missions, ten candidate landing sites previously identified in the NASA's Exploration Systems Architecture Study (ESAS) [5] for their scientific values are selected for preliminary study. The locations are shown in Figure-2 and Table 1. Six among these ten landing sites, are either located on the far side of the Moon, which has no direct contact with Earth, or at the lunar limb, where it could, depending on the libration of the Moon, spend days without seeing Earth. To provide communication and navigation support to these far-side missions, the presence of an International Lunar Relay (ILR) satellite at the Moon will make the establishment of the ILN flexible, versatile,

and global. More importantly, the communication subsystem of the landed nodes will be reduced in both mass and power as lesser effort is required to send data to Earth via a relay satellite at the Moon. Thus, the presence of an ILR satellite at the Moon will allow the ILN nodes to be at any location on the lunar surface allowing new scientific studies to be conducted, thus closing the gaps and secrets of the moon.

In this article, we focus on the coverage and the telecom capabilities provided by the different orbit selections for the ILR. One class of orbits to be studied is a set of stable frozen lunar orbits that require very little trajectory maintenance while providing useable communication data. Due to the global effects of 3rd body interaction, the orbit of the ILR is subjected to Earth-Moon gravitational perturbations, causing the orbits to become unstable and too costly to maintain for a number of years. To avoid being pulled out of orbit by the global effects of 3rd body interaction, the candidate orbits of the ILR are constrained for this study to a small set of stable frozen lunar orbits. These constellations are designed to provide pole-to-pole global communication, uniform coverage, and excellent data throughput. In particular, we will find a stable orbit with the best combination of eccentricity and inclination that will meet certain coverage and telecom requirements. In the second part of the paper, we demonstrate the use of constrained optimization (optimized in a sense that their orbits are stable and require very little trajectory maintenance) to seek a constellation of relay satellites that can meet a number of mission criteria. First, we will compare and contrast the power requirements of the ILR satellite with the recurrent frequency of gaps between each satellite pass. Second, we will discuss the coverage performance of the relay satellites such as: contact frequency, percent coverage, pass duration, gaps, minimum data rates, and maximum data storage. Lastly, we will discuss why certain lunar locations require small data storage while other locations require larger data storage. We will end the paper with the discussion on the optimal ILR orbit suggestion based on the geophysical station requirements.

- **2.** Stability of Lunar Orbits In this section, we will discuss the stability of the different types of lunar orbits that can support the ILN. Particularly, we will address the advantages and disadvantages of the frequently-used circular polar orbits and the proposed frozen orbits.
- 2.1 Circular Polar Orbits Let us first begin with the introduction to the 100km circular polar orbits. These circular polar orbits are designed and used for missions that desire frequent contacts with the pole. Space agencies that have developed and used these orbits are the following: Chang-Yi I (China), Chandrayaan (India), Selene-1 (Japan), Smart 1 (Europe), and Lunar Reconnaissance Orbiter (United States). In addition, due to the orientation and altitude of circular polar orbits, these orbits can provide numerous short passes with the poles. However, since the moon rotates very slowly (27.321 days/revolution), this leads to longer gaps between passes; therefore, certain regions along the equator cannot have any contact with the user for an extended period. Moreover, as the gravitational perturbation of the moon varies along the surface, it creates an uneven gravitational pull, which forces the spacecraft out of orbit requiring constant and enormous station-keeping efforts. In fact, the continuous station-keeping efforts of these orbits can be a major burden on the mission cost. In particular, due to the high propellant demands of constant station-keeping and the rise in mission cost, the life span of these circular polar orbits is typically restricted to approximately two years. Therefore, the 100 km circular polar orbits are unsuitable for providing coverage for the 6-10 years needed for ILN.
- **2.2** Frozen Orbits The unique feature for a frozen orbit is that its orbital elements will remain relatively fixed. Thus, in the planetocentric frame, the orbit seems to stand still with very small wobbling for a number of years, while the Moon is rotating beneath it. Once a frozen orbit is found, it can provide consistent coverage and it would require little or no orbit maintenance. As the result, a frozen orbit can have much longer longevity and its coverage performance is repetitive and predictable. We narrowed our search by considering the simplified Lagrange's

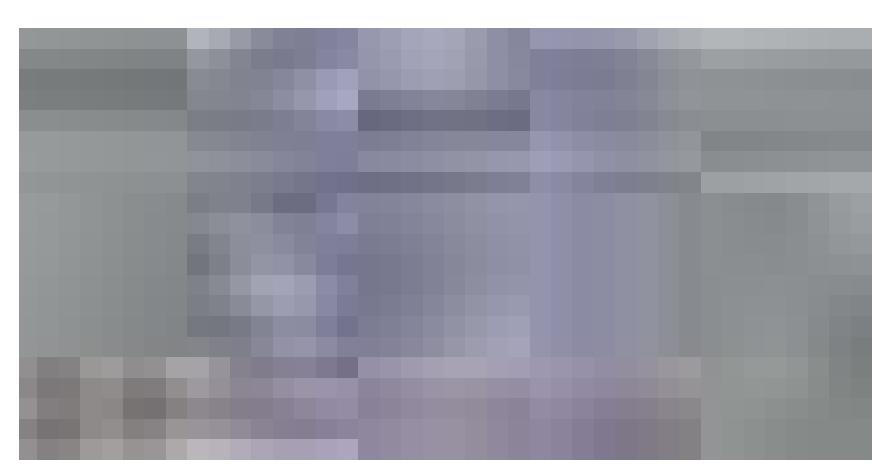


Figure 2: ESAS Top 10 Lunar Mission Sites

Landing Site	Latitude	Longitude
North Pole	89.5 N	91.0 E
Central Highlands	26.0 N	178.0 E
Aristarchus Plateau	26.0 N	49.0 W
Rima Bode	13.0 N	3.9 W
Mare Transquilitatis	8.0 N	21.0 E
Mare Smythii	2.5 N	86.5 E
Oceanus Procellarum	3.0 S	43.0 W
Orientale Basin Floor	19.0 S	88.0 W
S. Pole Aitken Basin	54.0 S	162.0 W
South Pole	89.9 S	180.0 W

**Table 1:** ESAS top ten lunar landing sites

planetary equations for the third body perturbed problem,

$$\frac{de}{dt} = \frac{15}{8} \frac{n_M^2}{n_S} e^{\sqrt{1 - e^2}} \sin^2 i \sin 2\omega \qquad (1)$$

$$\frac{di}{dt} = -\frac{15}{16} \frac{n_M^2}{n_S} \frac{e^2}{\sqrt{1 - e^2}} \sin 2i \sin 2\omega$$

$$\frac{d\omega}{dt} = \frac{3}{8} \frac{n_M^2}{n_S} \frac{1}{\sqrt{1 - e^2}} \left[ 5\cos^2 i - 1 + 5\sin^2 i \cos 2\omega + e^2 (1 - 5\cos 2\omega) \right]$$

$$+ \frac{3n_S J_2}{2a^2 (1 - e^2)^2} e \cos i \left( 1 - \frac{5}{4} \sin^2 i \right) \qquad \text{where...}$$

 $a \sim \text{semi major axis}$ 

 $e \sim$  eccentricity

 $i \sim \text{inclination}$ 

 $\omega$  ~ argument of perilune

$$n_{M} = \sqrt{\frac{GM_{E}}{a_{M}^{3}}}$$

$$n_{S} = \sqrt{\frac{GM_{M}}{a_{M}^{3}}}$$

 $G \sim$  Universal Gravitational Constant

 $M_F \sim \text{Mass of Earth}$ 

 $M_M \sim \text{Mass of the Moon}$ 

 $J_2 \sim$  Second Gravitational Harmonic

The dynamical systems in (1) are sensitive to the initial conditions. Namely, by choosing a set of stable orbits, one can force the equations to remain relatively constant for all times

$$\frac{de}{dt} = \frac{di}{dt} = \frac{d\omega}{dt} = 0$$
 (2)

Note that the right hand sides of (1) become zeros when

$$\omega = 90^{\circ} \text{ or } 270^{\circ} \text{ and } e^2 + \frac{5}{3}\cos^2(i) = 1$$
 (3)

It can be easily verified from (3) that the stable inclination will vary between 39.24° through 140.76°. Note that, when the eccentricity is equal to zero, the minimum inclination must be 39.24° or 140.76°. For elliptical orbits (non-zero eccentricity), the inclination can be higher.

To ensure that these orbital parameters (eccentricity, inclination, and argument of perilune) do in fact meet the frozen orbit conditions, we study the evolution of its dynamical system over the 20-year period and the results are displayed in Figures 3 and 4. Some important observations can be established from their dynamics. In Figure 3, we selected an orbit with semi-major axis of 6142.3 km (12-hr orbit) and an initial inclination of 39.32° for several eccentricity values ranging from 0.05 to 0.75. According to (3), the frozen condition can be met when eccentricity is near 0.05. As figure 3 displays the

obtained results, we see that indeed our constrained parameters do meet the frozen condition; while the time dynamics of  $(e\cos\omega,e\sin\omega)$  remain relatively close to its equilibrium point for small eccentricities and become quite unstable for other eccentricities. The similar behaviors of the orbits can be found in Figure 4. Here, however, we have changed the initial inclination to 51.71°, and according to (3) the stable eccentricity would be 0.60. For any other eccentricity values the orbit, once again, begins to oscillate and thus becomes unstable. In general, the closer the eccentricity and inclination values satisfy to the frozen conditions (3), the more stable the orbit becomes.



**Figure 3:**  $e\cos \omega$  vs.  $e\sin \omega$  for initial inclination 39.32°

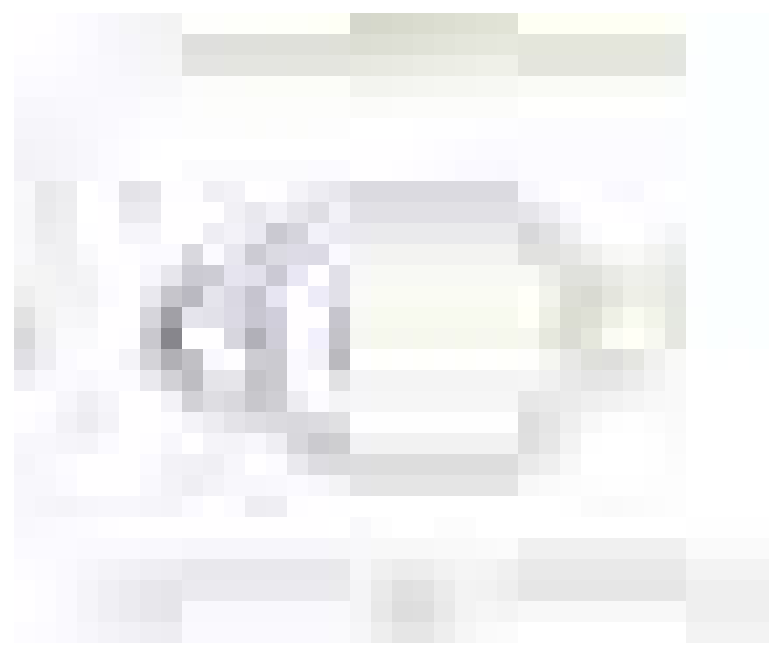


**Figure4:** ecos  $\omega$  vs. esin  $\omega$  for initial inclination 51.71°

As we observe in (3) the stable inclination is a function of eccentricity, and upo n requiring the orbiter to provide relay services for both poles, it turns out semi-major axis, , must be sufficiently high. Particularly, depending on the required elevation mask angle , the semi-major axis must satisfy (4) in order to have any contacts with both poles with each orbit. Notice that if we choose a semi-major axis that is too close to the moon's surface we lose the visibility with the poles. Thus, we must manipulate the orbit altitudes in order to maintain sight with the poles.

$$sma = \frac{1}{1 - \sqrt{1 - \frac{5}{3}\cos^{2}(i)}} \frac{R_{moon}}{\sin(i) - \cos(i)\tan(\alpha)}$$

First let us emphasize that based upon the frozen orbit condition, the lunar orbits need to be elliptical to stay frozen. As seen in figure 5, near circular stable orbits require less inclination, however, low inclination orbits cannot see the pole unless its altitude is sufficiently high.

On the other hand, the orbits with higher inclination will need high eccentricity to be stable, which forces the perilune to be closer to the surface and thus less capable of seeing the poles. Both cases require the use of (4) to calculate the proper combinations of semi-major axis and inclination. Note that the semi-major axis elevates very stiffly as the inclination increases in Figure 5. We can extract the minimum combination values of inclination and semi-major axis in order to maintain sight with the poles. For example, an orbit with an approximate 3000km semi-major axis and 40° inclination would require 0° elevation. In other words, these two combinations are sufficient to maintain contact with the poles without any required elevation. Let us now address this same issue of line of sight with the pole in a slightly different manner. In figure 6, we can physically view the relationship between the stable frozen inclination and eccentricity for the inclination between 39.24° through 140.76°. However, in figure 6, we observed a more important concept; for each selected orbit (4hr, 8hr, 12hr and 24hr), that particular combinations of inclination and eccentricity that will not only satisfy the frozen condition, but will also guarantee that these orbits are sufficiently high enough to avoid any collision between the user and the lunar surface. For example, one cannot expect the 24-hr frozen stable orbit to have the inclination beyond 63° because it forces the eccentricity to be more than 0.8 and thus the ILR will crash into the Moon. The thresholds for the maximum inclinations can be found on Figure 6. As a result, Low-Lunar Frozen stable orbits cannot be polar.

Figure 7 displays the perilunes of frozen stable (4hr, 8hr, 12hr and 24hr) orbits. The perilunes, distinguished with the circles, are those that can maintain a line of sight with the North Pole with at least 10° horizon mask. Note that the frozen stable 4-hour orbits do exist; However, due to their low semi-major axes, they will appear below the 10° horizon for landers at the North Pole. Therefore, with the right combination of inclination and semi-major axis, we can acquire a frozen stable orbit that can provide uniform pole-to-pole coverage to serve any mission with multiple requirements.

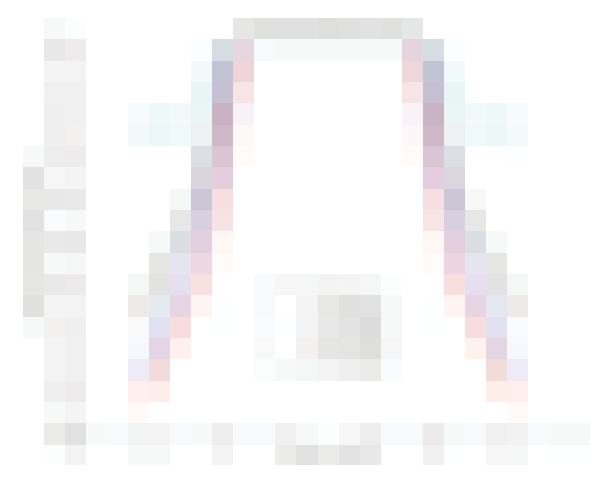


**Figure 5:** Minimum elevation and minimum semimajor axis an orbit can have in order to maintain sight with the pole

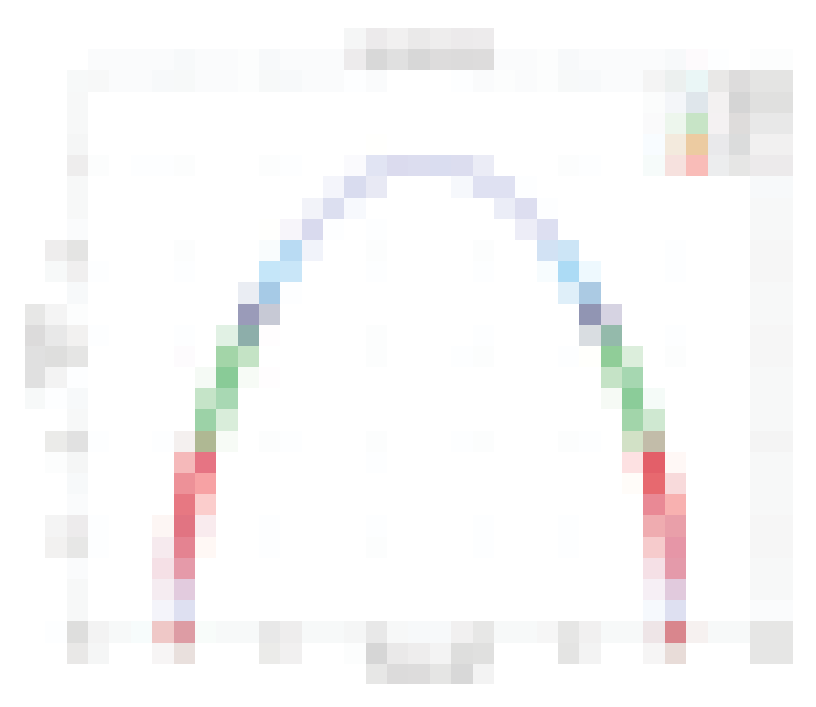


Figure 6: Low-Lunar frozen stable orbits can never be polar



Figure 7: Perilunes of frozen stable orbits (pole-to-pole coverage orbits are marked with circles)

3. ILR RELAY PERFORMANCE - In the previous section, we were able to obtain restrictions for the Keplerian orbital elements so that we can obtain the frozen stable lunar orbits that could provide a user with consistent performance for a number of years. In this section, we will compute the coverage performance of a number of frozen stable lunar orbits. As mentioned earlier, six among the ten landing sites studied have no direct contact with Earth or could spend days without seeing Earth. Thus, the presence of a relay satellite will allow the geostations to be located anywhere on the Moon and be able to contact Earth.

The next question is how much power these geostations would need to communicate with the ILR. To alleviate the lander's burden, the ILR orbit can be designed to have low altitudes. As expected, coverage of low orbits is narrow and limited to a small area. In addition, since the Moon rotates very slowly, the communication gap between the ILR and the surface user could be long. On the other hand, higher orbits provide excellent surface coverage with smaller communication gaps, but require more transmitting power from the surface user. This is the area where one would need the figures of merit of the orbits in order to perform the trade studies. The altitudes of the considered frozen stable lunar orbits are displayed in Figure 8.

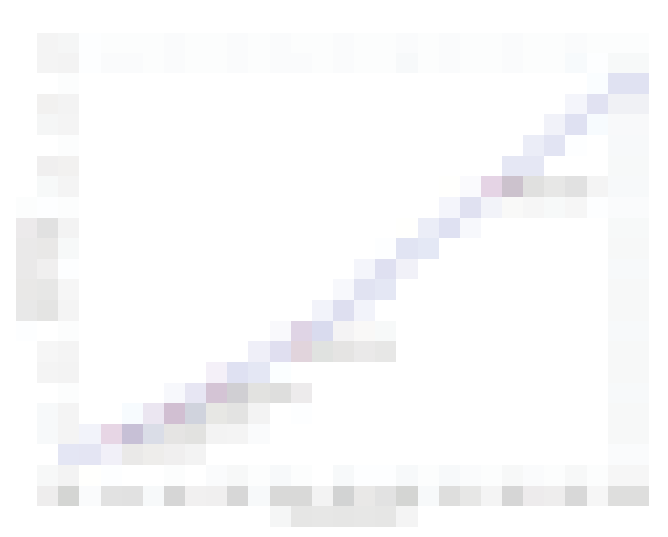


Figure 8: Semi-major axis versus Orbital period Altitude

Let us start by first addressing the number of contacts per day (Figure 9). Since the 4-hr orbit could not cover the North Pole, only the 8-hr, 12-hr and 24-hr orbits are simulated. The average numbers of contacts per month for the different orbits at 10° elevation mask are shown in Figure 9.

Note that at high eccentricities of the 8-hour and 12-hour orbits, it is clearly observed that while the South Pole receives up to three contacts per day, the North Pole receives a minimum of zero contacts per day<sup>1</sup>. For example, the orbit with eccentricity 0.6 has a maximum of three contacts and a minimum of zero contacts per day. However, recall that our goal is to find a user with the best overall uniform coverage. Although three contacts per day provide more coverage, the coverage is not uniform throughout the lunar surface.

Next, let us observe the 12-hour orbits. Even though we would expect the 12-hour orbit to provide more contacts per day opposed to the 8-hour orbit, we see fewer contacts per day. However, we also observe that the coverage for 12-hour orbits is more uniform and thus provides more consistent data return. Once again, the orbit with eccentricity 0.6 provides as low as zero contacts per day at the North Pole.

Finally, we study the behavior of the 24-hour orbits. Again, the number of contacts per day has dropped to about one; however, the overall coverage throughout the lunar surface has become more consistent. In other words, the 24-hour orbits provide the most uniform coverage behavior although only about one contact per day is obtained. Recall that the closer the eccentricity value is to one, the more elliptical the shape of the orbit. Notice that from these graphs we can observe the problem with highly elliptical orbits. Near the South Pole highly elliptical orbits provided the best coverage, however, towards the North Pole they provide the worst case scenario of surface coverage. Therefore, if we study which orbit provides uniform coverage, as expected, we would select the orbit with eccentricity value 0.1 (near circular) and according to (3) the corresponding inclination will be 39.32°. Uniform coverage is a beneficial trait, as these orbits provide the most satellite visibility and maximize the average contact per day. In fact, uniform orbits provide a high degree of symmetry; hence contribute to strong global coverage throughout the lunar surface.

Based on the overall visibility behavior found in orbits with eccentricity 0.1, we will restrict our further studies to only this selected constellation. For each orbiter, we propagate their trajectories for a total of 365 Earth days. Then for each candidate site, we calculated their view period with the orbital's constellation using 10° elevation mask angle. As a result, we computed the percentage coverage for the candidate 10 sites (Table 2). Some important observations can be extracted from Table 2. First, let us address the coverage percentages. If we look at each site individually we notice that the percent coverage increases as the orbital period increases. For example, a 100km polar orbit for the North Pole provides 10.6% coverage whereas a 24-hour orbit for the North Pole provides

**Figure 9a:** Average number of contacts per day for the 8-hr ILR orbit with 10° elevation mask



**Figure 9b:** Maximum Communication Gaps for the 8-hr ILR orbit with 10° elevation mask



**Figure 9c:** Average contacting time per day for the 8-hr ILR orbit with 10° elevation mask

<sup>&</sup>lt;sup>1</sup> For orbits with southern apolune; northern apolune orbits are symmetric.

34.6% coverage. This characteristic is expected since large semimajor axis orbits provided wider view ranges. Another observation concerns the coverage behavior of polar orbits. If we recall polar orbits are elliptical with higher ends at both the North and South Pole, thus these two sites receive the best coverage from the 100km orbit. However, let us now discuss only the behavior of the 4-hr, 8-hr, 12-hr and 24-hr orbits, which share a particular characteristic among each other. Based on the data obtain form these orbits, it suggests that there is a larger coverage in the South Pole and decreases towards the North Pole. For example, a 12-hour orbit only receives 29.6% coverage at the North Pole whereas the South Pole receives 41% coverage. This particular characteristic has to do with the placement of the perilune and apilune. As the perilune is closer to the North Pole surface, these constellations receive less coverage whereas, the distance between the orbit and the South Pole is greater, and thus has more surface area coverage. Next, let us address the contacts (hrs) and gaps (days) of these constellations. For both the contacts and gaps we have displayed the min/avg/max data. By similar reasoning as stated above, the 24-hour orbits provide the best contacts and least gaps compared to the polar or 4-hour orbits. A last note to make is that the more contact these orbits receive, the less the gaps between view periods. Figure 10 displays in details the on and off view periods of the candidate sites. As we ran these orbits for 365 Earth days, we recorded their passes and gaps. For simplicity purposes, we have displayed only the first 27 days of the data.

We now address the minimum data rates and maximum data storage (fig.12 and 13) of our constellations in order to fulfill the minimum ILN requirements. In the published report, 'Inter-

national Lunar Network Communications Working Group'[6] an estimate of ~225 Mbits/day data volume per ILN surface station is suggested. Therefore, for our stimulations we have taken the 225 Mbits/day into consideration as the minimum data volume per day and analyzed it in comparison to the number of seconds each site sees the orbiter. As a result we obtained the minimum data rate each orbit must transmit per second to meet the 225 Mbits/day. In comparison to the minimum data rate we calculated the data storage. The data storage was calculated by collecting the data rates every time there was a gap between passes. As figure 11 suggests, the less time the orbiter is in contact with the site, the more storage the site will require. Whereas, the more time the orbiter is in view of the landing site, the less data rate per second the site must transmit. For example, in an 8-hour orbit the maximum contact time (36%) is at Oceanus Procellarum, thus a minimum data rate of 8 kbps is required and a maximum data storage of 173 Mb. In figures 12 and 13, the minimum relay rates (kbps) and the maximum data storage (Mb) are displayed for all five orbits and displayed for the entire simulation time (365 Earth days). In figure 12, it is easily observed that the 100km polar orbit would require a user to transmit a larger amount of data per second, whereas a 24-hour orbit with continuous contact with each location requires less data per second. Likewise, in figure 12, we can observe that orbits such as the 100km polar and 4-hour orbits in which fewer contacts with the sites accumulate larger amounts of data stored with each pass.

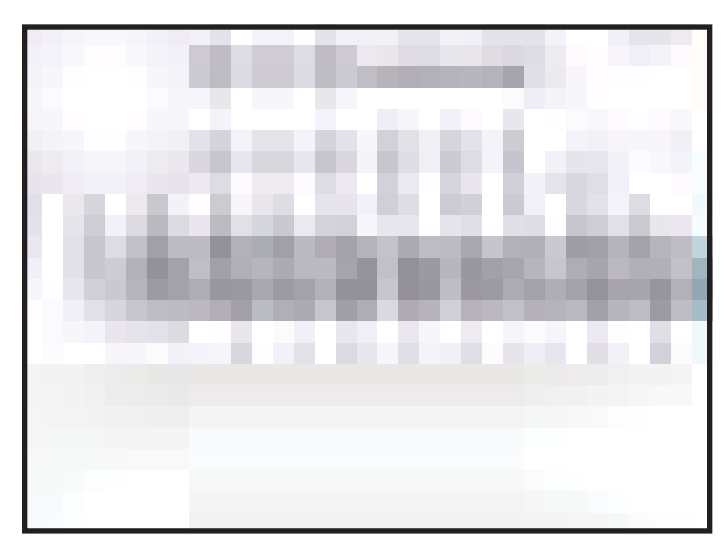
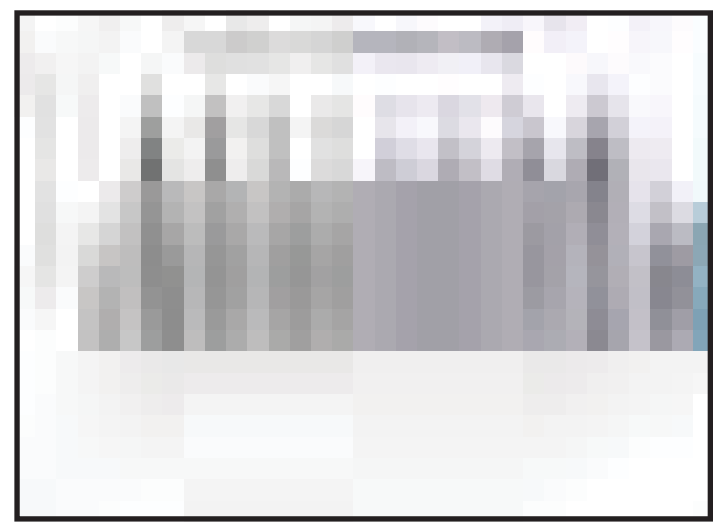


Figure 12: Minimum data required to transmit 225 Mb



**Figure 13:** Maximum data storage an orbit can accumulate between view periods.

**4. CONCLUSION** - The main goal of the article was to find a stable frozen orbit that could provide global uniform coverage, to alleviate the mass, and power requirements of the geophysical stations. In the first section we mathematically controlled the Lagrange Planetary Equations to obtain stable lunar frozen orbits of equation (2). In order to satisfy the ordinary differential equations, we assured the parameters in equation (3). Following that, we observed that low inclination and low eccentricity orbits are desirable as they yield near circular orbits. However, we soon noticed that these low inclination orbits were not in line of sight with the poles. To address this matter we controlled the orbits' elevation. This brought us to section three, where our main objective was to study the coverage performance of our stable lunar frozen orbits. We quickly noticed a very distinguishable characteristic about our chosen stable lunar frozen orbits. As seen in figure 6, these orbits can never be polar. Let us first address the findings among the 100km polar orbits. Although the 100km polar orbits only permit a limited two year life span, they do provide excellent polar coverage. However, the equatorial regions find themselves limited to about 0.1% surface coverage with an overall maximum gap time of 11 days. In reference to their data performance, the 100km surface users must transmit at least 150 kbps and supply 3.0 Gb of data storage. On the other hand, due to their low inclination, the 4-hour orbit's perilunar pole obtains no coverage. Although, as seen in section 2, the inclination and orbit elevation can be manipulated to meet these demands, the coverage would then be uneven in such a way that the North and South Poles would receive the most coverage compared to sites near the equator where less contact would be received. Therefore, in considering an optimal orbit for the ILR, we restrict our attention to only the 8, 12 and 24 hour orbits. As we first calculated the number of contacts per day (fig.9), we noticed a particular trend among our chosen orbits. In particular, we observed the behavior patterns of the orbits in respect to their selected eccentricity values. As discussed in section two, orbits with eccentricity values of 0.1 provided the best overall uniform coverage for all our suggested constellations. We therefore restricted our studies to such orbits with eccentricity 0.1 and 10° elevation

mask angle. To continue the investigation of these orbits, we studied their coverage performance and calculated the view periods (fig. 10) for a total of 365 days.

Based on the discussion in section two, we will summarize the coverage performance of only the 8hr stable frozen orbit, as it will be the suggested orbit for the ILR. In the 8-hour orbit, our findings showed that there were at least two to three contacts per day such that each contact varied between one to two hours. Both Poles and equatorial regions have very small communication gaps. The maximum number of days that a site (South Aitken Basin) goes without contact from the orbiter is six days.

Lets us now direct our attention to the data rate findings of the suggested 8-hour orbit. A quick conclusion of our data rates shows the following: The more contact between the orbiter and the site, the less data is required to transmit within each pass. Also, the less contact that the site receives, the more data storage is required by the station. To be more precise, note that the maximum data required to transmit 225 Mb/day as suggested by the ILN Communications Working Group study, would require an average of 10 kbps. Data storage of about 1471 Mb would be sufficient to store the data accumulated between view periods. Therefore, our suggested 8-hour orbit can serve both high and low demands of communication data rates.

#### **5. REFERENCES**

- [1] Cheung, Kar-Ming. & Lee, Charles H. "Deep Space Network and Lunar Network Communication Coverage of the Moon." 57th International Aeronautical Congress, 2006
- [2] Cohen, Barbara A. "The International Lunar Network (ILN) and the US Anchor Nodes Mission." NLSI Lunar Science Conference, 2008
- [3] Folta, David. & Quinn, David. "Lunar Frozen Orbits." AIAA/AAS Astrodynamics Specialist Conference, Keystone, Colorado, 2006
- [4] Final Report of the Science Definition Team for the ILN Anchor Nodes, Barbara Cohen and Joseph Veverka, co-chairs, January 2009
- [5] NASA's Exploration Systems Architecture Study Final Report, NASA-TM-2005-214062, 2005.
- [6] International Lunar Network Communications Working Group Final Report, February 2009, http://iln.arc.nasa.gov/working\_groups

Pages 128-130 not displayed due to online digital upload size restrictions. In addition photos to accompany biographies below also not displayed. Please contact *Dimensions* editorial staff for original copy of *Dimensions Journal 2010*.

## **Author Biographies**

**JUN KIM** will graduate from California State University Fullerton in the spring of 2010 with a Bachelor's Degree in biological Science. His publication focused on characterizing class 1 integrons in 15 clinical isolates found in Buenos Aires, Argentina. He conducted this research for ten weeks in Argentina during the summer of 2009 in the Minority Health and Health Disparities International Research Training Program (MHIRT). His study was also presented in January of 2010 at the CSU Program for Education and Research in Biotechnology (CSU-PERB) symposium in Santa Clara, California. He is currently conducting research on how ionic Manganese (i-Mn) increases resistance against reactive oxygen species (ROS) laboratory of Dr. Chanda Srinivasan. Jun's passion for science and serving underrepresented communities has caused a strong aspiration to one day become a compassionate physician.

**PATRICIA GONZALEZ** is a third year undergraduate biology student, concentrating in marine biology. She is currently a research scholar for the Southern California Ecosystems Research Program, funded by NSF. This paper details the results of the oyster study focusing on thermal effects on filtration rates, carried out in the summer of 2009 as part of the SCERP program. Her current research with mentor Jennifer Burnaford, is a continuation of the presented study and focuses on the effects of thermal and saline stresses on the filtration and respiration rates of Crassostrea gigas and Ostrea lurida and monitoring oyster body temperatures in Newport Bay, CA. After completing a B.S., she plans to pursue a PhD in ecology and conservation.

**JEFFREY MERCADO** will graduate from California State University Fullerton in the spring of 2010 with a Bachelor's Degree in Psychology. His publication focuses on detecting the presence of class I integrons and characterizing their variable regions in 15 clinical isolates from Buenos Aires Hospital using PCR amplification and NCBI Blast sequence matching. His research was conducted in Argentina during the summer of 2009 in the Minority Health and Health Disparities International Research Training Program (MHIRT). His study was copresented in January of 2010 at the CSU Program for Education and Research in Biotechnology (CSU-PERB) symposium in Santa Clara, California. He is currently conducting research on the protective properties of the manganese ion using a heat and paraquat stress assay to induce oxidative stress in C. Elegans within the laboratory of Dr. Srinivasan. Jeffrey's ultimate aspiration is to become a doctor for the underserved communities of California.

**SARAH ENGLISH** graduated from CSUF with her Bachelor's degree in Biological Science in the Spring of 2008 and completed her undergraduate thesis in the Spring of 2009. Her degree concentration was Biodiversity, Ecology, and Conservation and she also graduated with a Chemistry minor. She was accepted into the 2006 cohort of the Southern California Ecosystems Research (SCERP) program, led by Drs. Bill Hoese and Darren Sandquist. She has a special interest in studying the interactions between humans and animals and their environment and conservation for the future. Sarah's work as an undergraduate in Dr. Anne Houtman's lab studied the effects of human noise pollution on the song structure and behavior of two southern California hummingbird species. While at CSUF, she was the recipient of the Emeriti Memorial Scholarship and the Rachel Carson Scholarship in Conservation Biology. She is currently a general education elementary substitute teacher and is working in a Master's program in Environmental Engineering at National University in San Diego.

**SANG LEE** was born and educated in Seoul, South Korea. Soon after the eighth grade, he immigrated to the United States. Upon graduation from high school, Sang decided to pursue science at a junior college. His transfer to California State University, Fullerton has allowed him to continue his interest in Chemistry as a Biochemistry major. He has since been working in Dr. Meyer's lab on campus.

**LIZ MICHICOFF** completed her Bachelors of Arts in Chemistry in the fall of 2009 and will join her fellow graduates in the May commencement ceremonies. During her undergraduate studies, she presented her poster at the Southern California Conference for Undergraduate Research (SCUUR) in 2009. She has also been actively involved with Cal State Fullerton's student chapter of the California Science Teacher Association (CSTA) with the position of secretary. Next fall, she will be working on getting her teaching credentials to become a high school chemistry teacher, and will be furthering her education by working towards her masters in chemistry at the same time.

**SUZETTE PUENTE** is a Mathematics major, with a concentration in Probability & Statistics, and a Business Administration minor. In 2008 I was fortunate enough to be selected as a scholar in the Ronald E. McNair Post Baccalaureate Achievement Program, through which I worked on microarray data analysis with Dr. Gülhan Bourget. I also became a part of the Louis Stokes Alliance for Minority Participation Program (LSAMP) in 2009, which funded the submitted research. In the summer of 2009 I participated in Rice University's Summer Institute in Statistics, an NSF funded REU, where I worked on a project in survival analysis and studied the bias of the Kaplan-Meier Estimator. I plan to graduate in May and attend graduate school in a statistics program, starting in the Fall of 2010. I hope to one day become a professor, have a research-based career, and mentor other underrepresented students in the STEM fields.

**SHAYDA NIKJOO** graduated with honors from the California State University, Fullerton in January 2010 with a B.S. in Geological Sciences. She received a \$2000 scholarship from the California Federation of Mineralogical Societies for her research regarding the discovery of a new microscopic mineral and presented a poster at the 1st Annual Research Day for the CSUF Department of Geological Sciences in 2009, receiving 1st place for Outstanding Undergraduate Research Poster Presentation. Shayda has worked for the Department of Geological Science for the past year and intends on receiving a masters in geological sciences in the near future.

**DANIEL J. LEE** is majoring in geology and will be graduating this spring. He is a Southern California native, born in Los Angeles and raised in South Pasadena. Currently, he is interning at an environmental consulting firm and has aspirations of pursuing a master's degree in geology.

**TROY CANNON** is a senior majoring in Mathematics with a concentration on teaching. He has had the privalege of representing California State University, Fullerton at the AMS MAA Joint Mathematics Meeting during the winter of 2010. In addition to Troy's undergraduate and research studies, he is also an AVID tutor at Sunny Hills High School, a school bent on helping students prepare for their future at university. He plans on entering the Teaching Credential Program at Cal State Fullerton and becoming a high school math teacher. Troy enjoys performing experiments involving game theory mixed with chaos theory on flat pieces of cardboard and little plastic pieces.

**CARLOS HERNANDEZ** is a junior majoring in mathematics at California State University Fullerton. He is currently working with Troy Cannon and Luis Torres under the advisement of Dr. Scott Annin on analyzing algebraic semigroups. He plans to become a high school math teacher and eventually enter into a Ph.D. Program. He enjoys attempting to play the guitar, participating in his church, and occasionally playing video games.

**LUIS TORRES** started doing research with Dr. Annin in algebra during his freshman year. More recently, he has become interested in statistics and is applications to the real world. In addition to considering a pure mathematics Ph.D. program, he has thoughts of earning a masters in economics, architecture, or computer science. In his spare time he loves working out and staying fit, playing soccer, drawing and painting, reading, spending time with his family and girlfriend, Elaine, who encourages to succeed in life and attend a prestegious university and to whom he owes his inspiration and hard work.

**JAIRO AGUAYO** under the research supervision of Dr. Scott Annin, has a new fascination with the famous Fibonacci numbers. He shared this research with fellow mathematicians at the MAA's 2009 MathFest in Portland, OR and at the 2010 Joint meetings of the AMS/MAA in San Francisco, CA. While an undergraduate at CSUF, Jairo participated in various leadership positions, including the President of Math Club, the Natural Sciences and Mathematics - Inter Club Council Vice-Chair, and as the Mexican American Engineering and Sciences Pre-College Coordinator. Jairo plans to pursue his Masters degree in mathematics at CSUF, and he is also looking forward to receiving his credential to teach at the high school level.

**LYNETTE ZAMORA** is an applied mathematics major at California State University, Fullerton. She has found that working alongside her advisor Dr. Charles Lee, has been a great honor and learning experience. In this project they focused on the design of the International Lunar Relay satellite to fulfill coverage and telecom needs of the geophysical stations located on the lunar surface. During this process, Lynette received an award in Special Recognition for Undergraduate Research. She has presented her research at the following conference and meetings: The Southern California Conference for Undergraduate Research and The Joint Mathematics Meetings. Although, her internal curiosity for mathematics is in space related fields, her ultimate goal is to become a high school mathematics teacher. After graduation she plans to enter the single subject teaching credential at CSUF. She was blessed with great faculty mentors and hopes to become one to her students. Her overall goal is to encourage students to pursue a future in mathematics by giving them the motivation and skills to further their studies.

**NATHAN DIAZ** is currently attending California State University, Fullerton as an undergraduate Geology Major, and is scheduled for graduation in Summer 2010. Nathan's undergraduate thesis surrounds a volcanic deposit in Mono Basin, which is situated east of Sierra Nevada. Aside from school, and working full-time as an Emergency Medical Technician, Nathan spends his time enjoying day hikes, ocean diving, camping, and cooking.

## **Editor Biographies**

AMBER SHAH (Executive Editor) is currently an undergraduate studying biology at California State University, Fullerton. She intends to graduate having achieved a Bachelor's of Science concentrating in Molecular Biology and Biotechnology. Furthermore, Amber intends to complete a minor in Child and Adolescent Studies so that she is better prepared for her career as a pediatric oncologist. She is a part of the University Honors Program and is intrigued by its many diverse disciplines. Amber's hobbies include writing, painting and reading. After graduating from Cal State Fullerton, she will pursue medical school and fulfill her many aspirations.

BRIAN BOUSKILL (Layout Editor) A graduate student at California State University, Fullerton in the MFA program. Graduated from CSUF in 1982 and has worked as a Graphic Designer, Art Director, and Photographic Retoucher and has returned to school in order to teach Graphic Design.

> **SEAN NGO** (Cover Designer) Bworn in 1989 in Fountain Valley, California. He became an artist at a young age drawing his favorite cartoon characters, the Teenage Mutant Ninja Turtles. From that point on, his love for art grew. In 1999, Sean moved to the little state of Rhode Island. His new teachers and friends introduced him to a wide range of new art medias, including graphic design. Once he graduated from his small town high school, Sean could not wait to move back to a larger city and state. He chose CSUF due to its location of his old home in Orange County. Now he is a 3rd year studying as an Art major with a minor in Advertising. When he graduates, he hopes to be a successful artist and graphic designer.

**JULIE YANG** (Chemistry/Biochemistry) is a first year graduate student at California State University, Fullerton. She obtained a Bachelors of Science at California State University, Los Angeles and is now continuing her education to make herself into a stronger candidate for competitive PhD programs in chemical biology. Through her research in Dr. Alison McCurdy's lab she came to realize that writing and science went hand in hand and discovered that she wanted to continue doing scientific research as a career. Julie is published in *Organic Letters* and is a teaching assistant at Cal State Fullerton. Julie is currently working in Dr. Chandra Srinivasan's and Dr. Nikolas Nikolaidis research labs.

**JADE BRUSH** (Geology) is a geology major who is currently working on an undergraduate research project on the exhumation of the Chugach Mountains in Southern Alaska using zircon fission track analysis. Last summer, Jade traveled to Alaska to collect samples for her research with her thesis advisor Dr. Phil Armstrong and fellow student Mike Prior. Jade is an excited graduating senior who is looking forward toward graduate school where she will pursue a doctorate in geological science.

**ERNESTO CASILLAS** (Biology) is an 4th year student majoring in Biological Science with and emphasis on Molecular Biology and Biotechnology. He is a researcher for the Southern California Ecosystems Research Program (SCERP), an NSF-UMEB funded undergraduate research training program. He is advised by Dr. Danielle Zacherl and his research focuses on determining tissue metal loads of the marine gastropod Kelletia kelletii via ICP-MS. Ernesto will graduate in the spring of 2011 and hopes to pursue graduate school to obtain a PhD.

**CAROL KEMPIAK** (Mathematics) is currently finishing up the last semester of her mathematics degree. She is also graduating with a minor in music. Next year she hopes to be in the secondary education credential program here at CSUF, and then proceed to teach math at the high school level. Also, in the near future, she plans to attend graduate school and possibly teach at the college level.

# CHEMISTRY BIOLOGY GEOLOGY MATHEMATICS PHYSICS BIOCHEMISTRY

